Department of Physics and Astronomy "G. Galilei"

Doctoral School in Physics

Ultracold Quantum Gases: Beyond-Mean-Field Effects

Author:

Alberto Cappellaro

Supervisor:

Prof. Luca Salasnich

Vice Coordinator of the Doctoral School:

Prof. Cinzia Sada

Ph.D. Cycle XXXI

Examination date:

Part of the results of this thesis has been already published in the following papers:

- A. Cappellaro and L. Salasnich, Phys. Rev. A **95**, 033627 (2017)
  Thermal field theory of bosonic gases with finite-range effective interaction;
- A. Cappellaro, T. Macrí, G. F. Bertacco and L. Salasnich, Scientific Reports **7**, 13358 (2017)
  Equation of state and self-bound droplet in Rabi-coupled Bose mixtures;
- A. Cappellaro and L. Salasnich, Phys. Rev. A **96**, 063610 (2017)
  Finite-range corrections to the thermodynamics of the one-dimensional Bose gas;
- F. Cinti, A. Cappellaro, T. Macrí and L. Salasnich, Phys. Rev. Lett. **119**, 215302 (2017).
  Superfluid Filaments of Dipolar Bosons in Free Space;
- A. Cappellaro, T. Macrí and L. Salasnich, Phys. Rev. A **97**, 053623 (2018)
  Collective modes across the soliton-droplet crossover in binary Bose mixtures;
- A. Cappellaro, F. Toigo and L. Salasnich, Phys. Rev. A **98**, 043605 (2018)
  Collisionless Dynamics in Two-Dimensional Bosonic Gases.

Thesis Abstract

In this thesis we present a detailed investigation of the role played by quantum and thermal fluctuations in ultracold Bose gases.

We begin with a review of several important concepts and analytical tools within a functional integration formalism. We first focus on the so-called zero-range approximation for the interaction potential, by recovering the Bogoliubov results and the Landau two-fluid model from a field-theory perspective. In deriving the beyond-mean-field equation of state, we are going to show that a crucial point concerns the proper regularization of the divergent zero-point energy. Among the alternative approaches to investigate finite-temperatures Bose gases, we apply the kinetic theory to explain some recent results on the sound propagation in two-dimensional Bose gases.

We then move to consider the eventual corrections to the thermodynamics of Bose gases due to the finite-range character of the interaction potential. The coupling constants of the finite-range model are related to measurable scattering parameters through an effective-field-theory approach. The role of finite-range corrections is considered not only in three spatial dimensions but also in systems with lower dimensionalities. Our analytical predictions are in good agreement with available Monte Carlo simulations and consistent with other theoretical frames, as the Lieb-Lininger theory for one-dimensional systems.

In the third chapter, the relevance of fluctuations is investigated from an alternative point of view. Indeed, for a single-component Bose gas we have actually considered their effect as deviations of thermodynamic quantities from the mean-field and zero-range picture. In the case of collapsing Bose mixtures, we are going to show that zero-temperature fluctuations play a crucial stabilizing role against the collapse instability. Because of this peculiar mechanism, ultracold mixtures can display finite-density configurations also in free space. Inspired by recent experiments, we characterize this novel self-bound state by comparison with bright solitons, following a variational scheme. We also consider the case of binary mixtures where a coherent internal coupling is turned on.

In the last chapter, we move to deal with dipolar condensates. In particular, we are interested in beyond-mean-field effects leading to the formation of inhomogeneous ground states. In order to provide a reliable answer to the open issue of superfluid properties of these structures, we present our recent numerical investigation on the phase diagram of dipolar bosons.

Contents

List of Figures

0

INTRODUCTION AND THESIS OUTLINE

Since the first realization of a Bose-Einstein condensate (BEC) in 1995, ultracold quantum gases have been subject of an intense research effort, both theoretical and experimental. Fascinating technical advances in magneto-optical trapping provided a wide variety of different quantum fluids. From the first alkali-atoms BEC, a lot of experiments have been performed with optical lattices, multicomponent quantum fluids, strongly magnetic atoms, up to recent setups with reduced dimensionality or the implementation of synthetic dimensions; obviously, this is not even a fully comprehensive list.

Many successful theoretical studies have been based on the Bogoliubov (i.e. mean-field) framework, where the dynamics of the macroscopic wavefunction is described by the Gross-Pitaevskii equation (GPE). The GPE provides reliable results when the system is so dilute and ultracold that the true inter-atomic interaction can be replaced by a contact pseudopotential, whose strength depends on the s-wave scattering length a_s. The resulting thermodynamics description is defined universal, since only a single parameter is required to take into account the role of two-body interactions. Despite its success, recent experiments with higher densities, reduced dimensionalities or richer interactions (compared to a δ-like pseudopotential) highlight the necessity to extend the theoretical scheme based on the GPE. In other words, we need to include in our description beyond-mean-field corrections due to more complicated inter-atomic interactions. Our research activity stems from this theoretical necessity to develop an analysis of quantum gases in setups where the mean-field theory and the zero-range approximation are no more reliable.

The thesis is structured as follows: in Chap. 1 we review some important concepts concerning bosonic gases within a functional integration formalism. We address the issue of taking into account quantum and thermal fluctuations in the thermodynamic description of

condensed Bose gases. We begin by considering the simplest case of an ideal gas, where all interactions are turned off. Despite being an unrealistic situation, it provides a way to interpret Bose-Einstein condensation in terms of symmetry breaking. Moreover, we will almost immediately encounter the problem of divergences, which are accompaning us throughtout the whole thesis. Basically, infinite quantities arise because over-simplifying assumption results in unphysical situations. The absence of inter-atomic interactions surely makes the case, but also the assumption of a zero-range interaction leads to ultraviolet divergences in the theory. The problem is that a zero-range approximation for the interaction does not decay for high momenta in the Fourier space, as one should expect from a realistic two-body potential.

A relevant part of this first chapter will then be devoted in reviewing some regularization techniques to heal this unphysical divergences. First, we mention the so-called convergence-factor regularization, which is strongly linked to technical details in the construction of the many-body path integral. Thus we manage to generate the same regularizing terms appearing in second-quantization, after diagonalizing the quadratic hamiltonian through canonical Bogoliubov transformations.

We proceed by presenting the momentum cutoff and dimensional regulazation techniques, the latter being widely exploited in the following chapters. These theoretical tools are fundamental in deriving meaningful contributions for quantum and thermal Gaussian fluctuations in the equation of state. Clearly, since the physics has to be independent from the regularization mechanism, convergence-factor, momentum cut-off and dimensional regularization all leads to the same beyond-mean-field corrections.

A review of the two-fluid model from a field-theory perspective is then presented, accounting for the superfluid properties of ultracold dilute Bose gases. We introduce the phase-amplitude representation for the bosonic fields and recover the famous Landau's formula for the superfluid fraction. The condensate fraction for an interacting Bose gas is also considered, with a particular attention for the case of two spatial dimensions. We recover the important statement of Mermin-Wagner-Hohenberg theorem, preventing the occuring of true long-range order, and consequently Bose-Einstein condensation, in two-dimensional systems.

At the end of the chapter we mention an alternative approach for the investigation of

finite-temperature properties of bosonic quantum gases. In place of functional integration, dilute Bose gases can be described within the boundaries of kinetic theory. Actually, we apply this formalism in a practical case, in order to substantiate the claim about its effectiveness. Indeed, we manage to explain a recent puzzling result concerning the sound propagation in two-dimensional Bose gases by simply considering a Landau-Vlasov equation, the main equation for a collisionless theory of finite-temperature atomic gases.

In Chap. 2, we start by considering the 3d Bose gas, where the true inter-atomic interaction is replaced by a finite-range pseudopotential. It has been shown that finite-range corrections crucially modify the GPE, leading to a better agreement with Quantum Monte-Carlo (QMC) outcomes. In particular, the inclusion of finite-range effects has been proved to be relevant at higher values of the gas parameter na_s^3, where the zero-range approximation fails. Indeed, within the zero-range case, a uniform configuration does not exist above a critical value of na_s^3, since there is no control on fluctuations growth, which destroys the ordered phase. We derived the non-universal equation of state taking into account corrections up to the Gaussian level, both at zero and finite temperature. The quantum fluctuations contribution results to be strongly modified by the finite-range character of the interaction: now, the uniform configuration is not destroyed by fluctuations and the thermodynamic instability is removed as expected, since it was an artifact due to the choice of a constant potential in the momentum space. The importance of finite-range effects is confirmed by the comparison of our non-universal Gaussian theory with QMC datas concerning a 3D Bose gas made of hard-spheres, which display a good agreement with our prediction. We also underline that we have been able to connect the coupling constants of our finite-range pseudopotential to measurable parameters as the s-wave scattering length and the s-wave effective range, thanks to well-known effective-field-theory procedures.

This tools allow us to extend our theory in lower dimensions, where deviations from universality are expected to be more relevant than in the 3d case because of the fluctuations enhancement, as stated by the Mermin-Wagner-Hohenberg theorem. As in 3d, for the 1d Bose gas we were able to establish a connection between the coupling constants of the finite-range pseudopotential and the scattering parameters. The non-universal equation of state was then derived both at zero and finite temperature. At $T = 0$ K, we compare our Gaussian theory in the zero-range limit to the Lieb-Lininger model, which provides

a detailed description of the system for a whole crossover of the (zero-range) interaction strength. Compared to the mean-field, the zero-range Gaussian theory can be safely applied up to intermediate strength, while it fails in the strong-coupling limit, where one expects a Tonks-Girardeau gas. We analyze then how finite-range corrections modify measurable quantities as the sound velocity and the pressure.

For the sake of completeness, we also analyzed the 2d case, despite not being directly involved in this thesis work. Here, one has to face two main complications; first, since $d = 2$ is the lower critical dimensions, logarithmic divergences appears: they have to be explicitly renormalized. In this case, the connection between the coupling constants and the scattering theory parameters is highly non-trivial. However, with a slightly different definition of effective range, not based on the scattering theory, it is still possible to derive a non-universal equation of state. From an experimental point of view, we recall that regimes where finite-range corrections are relevant can be achieved by fixing the scattering length and increasing the density.

In Chap. 3, we begin the study of binary Bose mixture. By binary we mean a system made of atoms belonging to the same atomic species but in two different hyperfine states. Thanks to the modern experimental techniques it is even possible to switch on an internal coupling between the components, enabling the flipping of atoms from one states to the other. In this chapter, we derive the beyond mean-field equation of state for both cases. We will pay peculiar attention to the situation of a strong enough inter-component attraction. Standard mean-field calculation predicts a threshold between a stable uniform configuration and a collapsing region in the parameters space. Within this unstable phase, the system evolves towards state with increasingly higher density, up to the point where three-body recombinations kick all atoms out of the condensate and everything basically evaporates. This picture has been recently challenged by theoretical proposal describing the stabilizing action of beyond-mean-field corrections. In this framework, the mean-field attraction is counterbalanced by a fluctuation-driven repulsion and the collapse can be halted if we are not too deeply beyond the mean-field stability threshold. We review this ground-breaking proposal by showing that it is possible to obtain finite-density configuration also in absence of external trapping. It is crucial to remark that we are then in presence of a self-bound state whose existence is made possible only through the role played by quantum fluctuations.

This is not a pure theoretical proposal: during the last year, experiments in Barcelona and Florenc e confirmed the stabilization of collapsing mixtures into the self-bound droplets. Moreover, a similar theoretical explanation has been crucial to understand the formation of inhomogeneous structures in dipolar condensates, not accounted by the standard mean-field theory. Inspired by these experimental advances, in this chapter we propose a practical characterization of the quantum droplet state by comparing it to another renowned self-bound configuration in ultracold Bose gases, the bright solitons. Differently from droplets, solitons do not require beyond-mean-field corrections to be stable, but their shape is strongly dependent on the external confining potential.

Later in Chap. 3, we address the question of droplet formation in binary mixtures where an internal coupling is turned on. We compute the Gaussian correction to the zero-temperature equation of state, proving that the scenario for the droplet nucleation still holds, since a collapsing mean-field attraction can be contrasted by an effective repulsion led by fluctuations. The coupling frequency acts an additional knob to tune the stability of the self-bound configuration.

In Chap. 4 we move towards the interesting field of dipolar condensates. During the last ten years, since the Bose-Einstein condensation of Chromium in 2005, strongly magnetic atoms like Dysprosium and Erbium have played a relevant role in the atomic physics community. The interest in these system is due to the peculiar nature of dipole-dipole interaction, which is long-range and anisotropic. Within the broader context of quantum simulation, thanks to the exquisite parameters control achieved in actual experiments, they provide a reliable platform to study and probe a plethora of condensed matter theoretical model.

First, as in the previous chapters, we derive the beyond-mean-field correction due to quantum fluctuations: dipole-dipole interaction enhances this Gaussian contribution, compared to the pure zero-range case. As previously mentioned, stimulated by recent experimental results with Erbium and Dysprosium setups, in dipolar condensates it is possible to recover a picture for droplets formation similar to collapsing mixtures. Indeed, when the partial attractive character of dipole-dipole interaction dominates over short-range repulsion collapse should occur, according to mean-field calculations. However, repulsion stemming from quantum fluctuations can again stabilize the system against this instability, leading to

inhomogeneous ground-state. We focus our attention on the superfluid properties of these structures which can be elongated filaments or small disordered clusters, according to the interaction strength and densities at play. Here, we report the results of our numerical investigation performed in collaboration with F. Cinti (Johannesburg University South Africa), a leading expert on Path-Integral Monte Carlo simulations, and T. Macrí (UFRN, Brazil) whose research deals with long-range interactions in ultracold atoms and the corresponding phases.

1

BOSONIC SUPERFLUIDS AND FUNCTIONAL INTEGRATION

In this introductory chapter we are going to characterize the thermodynamic properties of the dilute Bose gas in presence of a broken-symmetry phase within a functional integration framework. According to this theoretical scheme, we initially consider an ideal Bose gas, which is exactly described by a Gaussian theory, and then move to the weakly interacting case. We calculate the one-loop thermodynamic corrections to the equation of state by assuming a zero-range interaction. A careful analysis is devoted in deriving the zero-point energy of the system, which requires a proper regularization scheme. Then, key quantities as the quantum depletion and the superfluid fraction are computed within the two-fluid model, providing a deeper insight to the coherence properties of the Bose gas in its broken-symmetry phase. At the end of the chapter, we approach the issue of sound propagation in the peculiar situation of two spatial dimensions. Differently from the rest of the chapter we apply a different theoretical framework based on kinetic theory.

The relevance of this preliminary review will be evident in the following chapters, where theoretical schemes and computational recipes are going to be generalized for bosonic gases with more complex interactions and a richer phenomenology.

1.1 The ideal Bose gas: a functional integration approach

Let us begin by considering a set of non-interacting identical bosonic particles of mass m and chemical potential μ in d-dimensions ($d = 1, 2, 3$). Within the path integral formulation of quantum statistical mechanics, atoms are described by a complex field $\psi(\mathbf{r}, \tau)$, whose non-relativistic free-theory is build upon the Euclidean action [1, 2, 3]

$$S_E\big[\psi^*, \psi\big] = \int_0^{\beta\hbar} d\tau \int_{L^d} d^d\mathbf{r}\; \psi^*(\mathbf{r}, \tau)\left(\hbar\frac{\partial}{\partial\tau} - \frac{\hbar^2\nabla^2}{2m} - \mu\right)\psi(\mathbf{r}, \tau) \tag{1.1}$$

where $\beta \equiv (k_B T)^{-1}$, k_B being the Boltzmann constant and T the temperature, while L^d is the volume enclosing the system. The chemical potential is required to implement the normalization constraint $\int dx\big|\psi(x)\big|^2 = N$ with x a $d+1$ vector defined as $x \equiv (\tau, \mathbf{r})$. By performing the integral over the whole space one rightfully recover the term μN, as expected in the grand-canonical ensemble.

The Bose statistics is implemented by imposing periodic boundary conditions [4], i.e. $\psi(\mathbf{r}, 0) = \psi(\mathbf{r}, \beta\hbar)$. By moving to the momentum space, this implies that, along the time axis, the Fourier transform becomes a series, namely

$$\begin{aligned} \psi(\mathbf{r}, \tau) &= \frac{1}{\beta\hbar}\sum_n e^{-i(\omega_n\tau + \mathbf{q}\cdot\mathbf{r})}\psi_{\mathbf{q},\omega_n} \\ \psi^*(\mathbf{r}, \tau) &= \frac{1}{\beta\hbar}\sum_n e^{i(\omega_n\tau + \mathbf{q}\cdot\mathbf{r})}\psi^*_{\mathbf{q},\omega_n}\ . \end{aligned} \tag{1.2}$$

Because of the symmetry constraint, the so-called Matsubara frequencies $\{\omega_n\}_{n\in\mathbb{N}}$ are defined as

$$\omega_n = \frac{2\pi n}{\beta\hbar}\ . \tag{1.3}$$

In the path integral approach, quantum-field-theories are naturally quantized by letting ψ assume every possible value, not just the one determined by the equation of motion. For a many-body theory aiming to derive the thermodynamic picture of the system, this translates in counting all the possible atomic configurations. All the relevant thermodynamic quantities

can then be computed by means of the partition function defined as

$$\mathcal{Z} = \int \mathcal{D}\big[\psi, \psi^*\big] e^{-S_E[\psi,\psi^*]/\hbar} \,, \tag{1.4}$$

where $S_E[\psi, \psi^*]$ is Euclidean action of the theory. The thermodynamic potential $\Omega(\mu, T)$ can be easily derived by taking the logarithm of Eq. (1.4), i.e.

$$\Omega(\mu, T) = -\beta^{-1} \log \mathcal{Z} \,. \tag{1.5}$$

It is evident that the free theory described by Eq. (1.1) leads to a Gaussian integral which can be computed analytically. Indeed, in the Fourier space, the Euclidean action reads

$$S_E[\psi, \psi^*] = -\mu\psi_0^2\, \beta\hbar L^d + \frac{1}{2} {\sum_{\mathbf{q}}}' \; {\sum_{n}}' \big(\psi^*_{\mathbf{q},n}; \psi_{-\mathbf{q},-n}\big)\; \mathcal{G}_0^{-1}(\omega_n, \mathbf{q}) \begin{pmatrix} \psi_{\mathbf{q},n} \\ \psi^*_{-\mathbf{q},-n} \end{pmatrix} \tag{1.6}$$

The subscript n obviously signals a sum over the Matsubara frequencies ω_n, while the prime means that the sum runs for every value of momentum and frequency except $\mathbf{q} = 0$ and $n = 0$. From the inverse kernel of Eq. (1.1) we can obtain $\mathcal{G}_0^{-1}$, namely

$$\mathcal{G}_0^{-1}(\omega_n, \mathbf{q}) = \beta \begin{pmatrix} -i\hbar\omega_n + \frac{\hbar^2 q^2}{2m} - \mu & 0 \\ 0 & i\hbar\omega_n + \frac{\hbar^2 q^2}{2m} - \mu \end{pmatrix} \,. \tag{1.7}$$

In the equation above, we explicity pulled out the mode ψ_0 corresponding to $\mathbf{q} = 0$ and $n = 0$, which represents a uniform and static configuration. The occurring of Bose-Einstein condensation (BEC) is related to spontaneous breaking of a $U(1)$ global gauge symmetry [5, 6]. From a theoretical point of view, one can capture the symmetry breaking physics by splitting the field as $\psi(\mathbf{r}, \tau) = v + \eta(\mathbf{r}, \tau)$, with v the uniform and static ground-state perturbed by the complex fluctuation field $\eta(\mathbf{r}, \tau)$. By reinterpreting v as ψ_0 and replacing this splitting in Eq. (1.1) we obviously recover Eq. (1.7). Within the usual framework of phase transition theory, we can interpret v (or ψ_0) as the order parameter characterising the onset of the condensation transition [6, 7].

At this point, we can perform the integral specified by Eq. (1.4) and Eq. (1.6). Gaussian

functional integration for complex fields is based on the generalized formula [3]

$$\begin{aligned}\int \mathcal{D}[v,v^*]\,\exp\Big\{-\int dx\,dx'\,v^*(x)A(x,x')v(x')+\int dx\,\big[j^*(x)v(x)+j(x)v^*(x)\big]\Big\}\\ \propto\big(\det A\big)^{-1}\exp\Big[\int dx\,dx'\,j^*(x)A^{-1}j(x)\Big]\end{aligned} \tag{1.8}$$

leading, in our case, to the following equation for the thermodynamic potential in Eq. (1.5):

$$\begin{aligned}\Omega(\mu,T,\psi_0)&=-\mu\psi_0^2\,L^d+\frac{1}{2\beta}{\sum_{\mathbf{q},n}}'\log\,\det\mathcal{G}_0^{-1}(\omega_n,\mathbf{q})\\ &=-\mu\psi_0^2\,L^d++\frac{1}{2\beta}{\sum_{\mathbf{q},n}}'\log\left[\beta^2(\hbar^2\omega_n^2+\epsilon_{\mathbf{q}}^2)\right]\,,\end{aligned} \tag{1.9}$$

with the shifted free-particle spectrum $\epsilon_{\mathbf{q}}$ defined by

$$\epsilon_{\mathbf{q}}=\frac{\hbar^2q^2}{2m}-\mu\,. \tag{1.10}$$

Strictly speaking, Eq. (1.8) also involves a term proportional to π^N which is divergent in the limit $N\to+\infty$ required by the extension of Gaussian integration to functional spaces. This further term is though independent from thermodynamic variables and can then be neglected while computing $\Omega(\mu,T)$. The summation over the Matsubara frequencies can be performed analytically by means of contour integration techniques as detailed in Appendix A, reading

$$\frac{1}{2\beta}\sum_n\log\left[\beta^2(\hbar^2\omega_n^2+\epsilon_{\mathbf{q}}^2)\right]=\frac{\epsilon_{\mathbf{q}}}{2}+\frac{1}{\beta}\log\left(1-e^{-\beta\epsilon_{\mathbf{q}}}\right)\,. \tag{1.11}$$

Thus, the structure of the thermodynamic potential is built upon three different contributions [8]:

$$\Omega(\mu,T)=\Omega_{\rm mf}+\Omega_g^{(0)}+\Omega_g^{(T)}\,. \tag{1.12}$$

In Eq. (1.12), $\Omega_{\rm mf}(\mu)$ is given by the first term of Eq. (1.9), while $\Omega_g^{(g)}$ is a purely quantum-mechanical term describing the zero-point energy of single-particle excitations; on the other

hand, the role played by temperature is encoded in $\Omega_g^{(T)}$. These contributions are respectively

$$\Omega_g^{(0)} = \frac{1}{2}\sum_{\mathbf{q}} \epsilon_{\mathbf{q}} \tag{1.13}$$

$$\Omega_g^{(T)} = \frac{1}{\beta}\sum_{\mathbf{q}} \log\left(1 - e^{-\beta\epsilon_{\mathbf{q}}}\right) . \tag{1.14}$$

In the following section we will come back to this splitting of the thermodynamic potential and analyze how interactions affect each of the above contribution. By moving to the continuum of states where we can replace series with integrals, i.e. $\sum_{\mathbf{q}} \to L^d \int d^d\mathbf{q}/(2\pi)^d$, Eq. (1.13) appears to be ultraviolet (UV) divergent. This zero-point energy divergence is not an accident confined to the ideal case, but it is instead ubiquitous within this framework. Thus, in order to obtain finite, and then reasonable, thermodynamic results, an effective regularization method is required to solve this unphysical impasse.

In the next section we are going to outline various strategy to look after this issue with particular consideration for the so-called *dimensional regularization* first developed by 't-Hooft and Veltmann [9]. Within this framework, it can be proved that the zero-point energy of single particle excitation in Eq. (1.13) completely vanishes.

The same conclusion can be achieved through a different argument borrowed from Stoof [2]. Here, we made use of a technical subtlety concerning the quantum mechanical definition of path integral. In particular, let us consider again the Euclidean free action in Eq. (1.1) with the further assumptions of dealing with bosons in a single-state labelled by its energy ϵ. Thus, the partition function simply results in

$$\mathcal{Z} = \int \mathcal{D}\big[\psi,\psi^*\big] \exp\left\{ -\frac{1}{\hbar}\int_0^{\hbar\beta} d\tau\ \psi^*(\tau)\big(\hbar\partial_\tau + \epsilon - \mu\big)\psi(\tau)\right\} . \tag{1.15}$$

Actually, this notation introduces an ambiguity in the integral over time (i.e. the temperature). Indeed, within the functional integration framework we are developing, the time axis has to be intended as discretized. As a consequence, one has to specify the correct time ordering of the fields. In Eq. (1.15) and the other ones related to it, we are not pointing out on which time slice the field $\psi^*(\tau)$ (corresponding to the operator $\hat{\psi}^\dagger$) acts. If $\psi(\tau)$ acts on the time slice τ_i, then we can choose that $\psi(\tau+\delta)$ acts on the τ_{i+1} one. In order to implement

this prescription, a $\delta \to 0^+$ is needed, translating into a factor $e^{i\omega_n 0^+}$ in the Fourier space. On the other hand, the backwards time ordering $\delta \to 0^-$ is likewise possible, leading to a factor $e^{i\omega_n 0^-}$. By performing the countour integral to remove the Matsubara sum, one can however realize that the partition functions corresponding to these different orderings differ in a factor $e^{-\beta(\epsilon-\mu)}$. In Eq. (1.6) we can introduce a Nambu spinorial structure, where the vector elements are taken at equal times. For the extremely simplified case of single-state bosons this implies that [2] (with the choice $\delta \to 0^+$)

$$\begin{aligned}
\mathcal{Z} &= \int \mathcal{D}[\psi,\psi^*] \exp\left\{ -\frac{1}{\hbar}\int_0^{\beta\hbar} d\tau d\tau' \; \psi^*(\tau+\delta) \left[\hbar\partial_\tau + \epsilon - \mu\right]\delta(\tau-\tau') \; \psi(\tau')\right\} \\
&= \int \mathcal{D}[\psi,\psi^*] \exp\left\{ -\frac{1}{\hbar}\int_0^{\beta\hbar} d\tau d\tau' \left[\psi^*(\tau+\delta),\psi(\tau')\right] \frac{\mathcal{G}^{-1}(\tau,\tau')}{2} \begin{bmatrix} \psi(\tau') \\ \psi^*(\tau'+\delta) \end{bmatrix} \right\} \\
&= e^{\beta(\epsilon-\mu)/2} \int \mathcal{D}[\psi,\psi^*] \exp\left\{ -\frac{1}{\hbar}\int_0^{\beta\hbar} d\tau d\tau' \left[\psi^*(\tau),\psi(\tau)\right] \frac{\mathcal{G}^{-1}(\tau,\tau')}{2} \begin{bmatrix} \psi(\tau'+\delta) \\ \psi^*(\tau'+\delta) \end{bmatrix} \right\}
\end{aligned} \tag{1.16}$$

where the matrix structure of the propagator reads

$$\mathcal{G}^{-1}(\tau,\tau') = -\frac{1}{\hbar}\begin{pmatrix} \hbar\partial_\tau + \epsilon - \mu & 0 \\ 0 & \hbar\partial_\tau + \epsilon - \mu \end{pmatrix} \delta(\tau-\tau') \; . \tag{1.17}$$

The factor appearing in the last line of Eq. (1.16) takes into account the change of limit and the proper time ordering. Moving to many-states systems, its logarithm generates the proper counterterm to regularize the divergence arising from Eq. (1.13). It is worth to underline that this argument can be generalized without any difficulties to an interacting system [8]. In that case, however, the choice of the interaction potential could determine an additional divergence which requires a specific treatment involving the T-matrix [2, 10].

Therefore, the thermodynamic potential of non-interacting Bose systems is given by

$$\Omega(\mu,T,\psi_0) = -\mu\psi_0^2 \, L^d + \frac{1}{\beta}\sum_{\mathbf{q}} \log\left(1 - e^{-\beta\epsilon_{\mathbf{q}}}\right) . \tag{1.18}$$

The $\mathbf{q} = 0$ contribution ψ_0 is not a free parameter of the theory. Indeed, if interpreted as the order parameter of the condensation transition, its value can be drawn from the saddle-point

equation. In other words, we have to search for its classical value by stationarizing the action in Eq. (1.1), i.e. $\delta S[\psi_0]$. This implies

$$\left(\frac{\partial \Omega_{\rm mf}}{\partial \psi_0}\right)_{\mu,T} = 0 \,, \tag{1.19}$$

where the derivative is intendend by keeping the other quantities as constants. We remind that, for non-interacting Bose gases, $\Omega_{\rm mf}/L^d = -\mu\psi_0^2$, i.e. the first term of Eq. (1.9). Within the unbroken symmetry phase, the spectrum in Eq. (1.10) must be gapped, meaning $\mu < 0$, so the only possible solution to Eq. (1.19) is $\psi_0 = 0$. On the other hand, the spontaneous breaking of a continuous symmetry is intimately connected to the occuring of a gapless mode [11]. Thus, $\mu = 0$ and the saddle-point equation is satisfied for every value of ψ_0. In order to fix a precise value, we need the equation of state connecting the chemical potential to the total number density. By deriving the thermodynamic potential with respect to the chemical potential, we get

$$n = \frac{N}{L^d} = -\frac{1}{L^d}\left(\frac{\partial \Omega}{\partial \mu}\right)_T = \psi_0^2 + \int \frac{d^d\mathbf{q}}{(2\pi)^d}\frac{1}{e^{\beta\epsilon_{\mathbf{q}}} - 1} \,. \tag{1.20}$$

From Eq. (1.19) we deduced that the critical point is characterised by $\mu_c = 0$ so, by setting $\mu = \psi_0 = 0$ in Eq. (1.20), one can easily recover the critical temperature equation for the condensation in a free Bose gas [6]:

$$n = \int \frac{d^{\mathbf{q}}}{(2\pi)^d}\frac{1}{\exp\left(\frac{\hbar^2 q^2}{2mk_BT_c}\right) - 1} \Longrightarrow k_BT_c = \begin{cases} \text{impossible Eq.} & \text{for } d = 1 \\ 0 & \text{for } d = 2 \\ \frac{\hbar^2}{2\pi\zeta(3/2)^{2/3}}n^{2/3} & \text{for } d = 3 \end{cases} , \tag{1.21}$$

where $\zeta(t)$ denotes the Riemann zeta function.

At the end of this section we mention that the result for $d < 3$ are expected because of the Mermin-Wagner-Hohenberg theorem [12, 13]: while a true long-range order is possible in $d = 3$, there is no condensate for lower dimensions since fluctuations are strong enough to destroy the ordered phase. It is important to underline that one can still have the so-called quasi-condensate in $d = 2$, meaning that phase correlation (or equivalently the two-body

density matrix) decays algebraically [2, 6].

1.2 Weakly-interacting Bose gases: the Bogoliubov theory

We now move to consider an interacting bosonic field theory. As in the previous section, within the functional integration framework, all the relevant thermodynamic quantities can be derived from the partition function. The latter is defined in Eq. (1.4) as exponential of the Euclidean action integrated over the whole set of possible system configurations, i.e. the fields describing the atoms. In the previous section we presented the extremely simplified case of a non-interacting theory. Despite its simplicity, that treatment outlined a set of different issues which are going to play an increasingly relevant role within an interacting theory, such as the necessity of proper regularization recipes for the zero-point energy.

So, the starting point is, as usual, the Euclidean action expressed in terms of its corresponding lagrangian density:

$$S_E\big[\psi,\psi^*\big] = \int_0^{\beta\hbar} d\tau \int_{L^d} d^d\mathbf{r}\; \mathcal{L}\big[\psi,\psi^*\big] \tag{1.22}$$

with

$$\mathcal{L}\big[\psi,\psi^*\big] = \psi^*(\mathbf{r},\tau)\Big(\hbar\frac{\partial}{\partial\tau} - \frac{\hbar^2\nabla^2}{2m} - \mu\Big)\psi(\mathbf{r},\tau) + \frac{1}{2}\int d^d\mathbf{r}'|\psi(\mathbf{r}',\tau)|^2 V(|\mathbf{r}-\mathbf{r}'|)|\psi(\mathbf{r},\tau)|^2\ . \tag{1.23}$$

In the equation above we assume that atoms interact via the two-body spherical-symmetric potential $V(|\mathbf{r}-\mathbf{r}'|)$. In the proceeding of this thesis we will consider Bose-Einstein condensates made of dipolar atoms where the isotropy assumption does not hold, with relevant consequences for transport quantities as the superfluid fraction.

1.2.1 The zero-range effective potential

The choice of the inter-atomic potential is crucial, since the physical description depends on the parameters we choose to model $V(r)$. First of all, one has to acknowledge that using a sort of *true* interaction potential is not a viable strategy, for a number of reasons [14, 15]. Indeed, the real interaction potential between atoms is extremely complicated to determine and, moreover, any possible error, no matter how much small, can significantly affect the

scattering properties.

However, this picture can be greatly simplified by reminding that we usually deal with dilute and ultracold atoms and, consequently, we are only interested in the low-energy physics. In this limit, for short-range potentials, universality holds: the scattering properties depends on a single parameter, the scattering length, with the potential shape playing no role in the thermodynamic picture. Moving from this observation, since the birth of many-body quantum mechanics several authors underlines the convenience of replacing the real inter-atomic potential with a pseudopotential which has the only (but crucial) constraint of reproducing the low-energy scattering properties of the system [16, 17, 18, 19].

We deal with ultracold and dilute atoms, so the usual and simplest approach consists in replacing $V(r)$ with the zero-range Fermi pseudopotential

$$V_{\mathrm{p},0}(r) = g_0\, \delta^{(3)}(r)\ . \tag{1.24}$$

Because of this choice, the Lagrangian density in Eq. (1.23) becomes local, i.e.

$$\mathcal{L}\big[\psi,\psi^*\big] = \psi^*(\mathbf{r},\tau)\Big(\hbar\frac{\partial}{\partial\tau} - \frac{\hbar^2\nabla^2}{2m} - \mu\Big)\psi(\mathbf{r},\tau) + \frac{1}{2}\, g_0\, \big|\psi(\mathbf{r},\tau)\big|^4\ , \tag{1.25}$$

and falls in the set of ψ^4-theories which are ubiquitous in physics, with a wide range of applications [3]. The connection between this effective field theory approach and the measurable quantities has to be provided by a proper choice of the coupling constants in terms of the scattering parameters.

In $d = 3$, within the zero-range approaximation specified by Eq. (1.24), the usual parametrization is obviously in terms of the scattering length

$$g_0 = \frac{4\pi\hbar^2}{m}\, a_s\ . \tag{1.26}$$

The reason behind Eq. (1.26) can be presented in terms of the two-body transition matrix, defined as [2]

$$f(\mathbf{q},\mathbf{q}') = -\frac{m}{4\pi\hbar^2}\, \langle \mathbf{q}'|\hat{T}^{(2B)}|\mathbf{q}\rangle \tag{1.27}$$

with $f(\mathbf{q},\mathbf{q}')$ being the scattering amplitude. On the other hand, in the low-energy limit

the dominant contribution to the scattering amplitude comes from partial waves with zero orbital momentum ($l = 0$), i.e. only s-waves play a relevant role in the two-body scattering processes. This implies that the scattering amplitude can be greatly simplified by taking into account the contribution of only one set of partial waves, i.e.

$$f(\mathbf{q}, \mathbf{q}') \simeq f_0(\mathbf{q}) = \frac{1}{q \cot \delta_0(q) - iq} \tag{1.28}$$

where $\delta_0(q)$ is the s-wave phase shift [20]. It can be evaluated in terms of the s-wave scattering length a_s and effective range r_s by means of

$$q \cot \delta_0(q) = -\frac{1}{a_s} + \frac{1}{2} r_s q^2 + \mathcal{O}(q^3) \, . \tag{1.29}$$

According to the equation above, the t-matrix is then given by

$$T_0(q) \simeq \left[\frac{m}{4\pi\hbar^2} \Big(\frac{1}{a_s} - \frac{1}{2} r_s q^2 \Big) + i \frac{m\, q}{4\pi\hbar^2} \right]^{-1} \tag{1.30}$$

On the other hand, from an operatorial point of view, the transition matrix obeys to the following equation [2],

$$\hat{T}^{(2B)} = \hat{V} + \hat{V} \frac{1}{E - \hat{H}_0 + i\kappa} \hat{T}^{(2B)} \, . \tag{1.31}$$

The operator $(E - \hat{H}_0 + i\varepsilon)^{-1}$ corresponds to the free propagator, as in Eq. (1.7) or Eq. (1.17), $\hat{V}$ is the interaction operator and κ has to be intended as $\kappa \to 0^+$. By considering only the s-wave contribution, Eq. (1.31) admits the following solution in the momentum space

$$T_0(q) = \left[\frac{1}{\tilde{V}(q)} - \frac{m}{4\pi\hbar^2} \int \frac{dp}{p^2 - q^2 + i\kappa} \right]^{-1} \, , \tag{1.32}$$

with $\tilde{V}$ being the Fourier transform of the interaction potential, namely $\tilde{V}(\mathbf{q}) = \int d^3\mathbf{q} \exp(i\mathbf{q} \cdot \mathbf{r}) V(r)$. For a zero-range interaction as in Eq. (1.24) the Fourier transform is simply given by $\tilde{V}(q) = g_0$, being independent from momentum. Through standard contour techniques, the integral in Eq. (1.32) can be analytically solved, reading

$$T_0(q) = \left[\frac{1}{g_0} + i \frac{m\, q}{4\pi\hbar^2} \right]^{-1} \, . \tag{1.33}$$

Now, by noticing that a zero-range approximation implies $r_s = 0$, we can easily match Eq. (1.33) and Eq. (1.30) term by terms. This leads to the well known result for $d = 3$ reported in Eq. (1.26). Apart from a different numerical factor, the calculation recipe is similar in $d = 1$, while for $d = 2$ we have to face a complication due to the existence of a scattering bound state [21].

We do not report here the details for the calculation of the transition matrix in the low-energy limit for systems with reduced dimensionality. However, since the zero-range approximation has a great relevance as a starting platform for the study of dilute quantum gases, it is worth to at least mention the final results [21, 22, 23, 8]. In terms of the (small) positive energy scale $\epsilon_q = \hbar^2 q^2/(2m)$, one gets

$$T(\epsilon_q + i\kappa) = \begin{cases} -\frac{2\pi\hbar^2}{m} \dfrac{1}{\log\left(\frac{a_s e^\gamma}{2}\sqrt{\frac{m\epsilon_q}{\hbar^2}}\right) + i\frac{\pi}{2}} & \text{for } d = 2\,, \\ \frac{2\hbar^2}{m} \dfrac{1}{-a_s + i\sqrt{\frac{\hbar^2}{m\epsilon_q}}} & \text{for } d = 1 \end{cases} \tag{1.34}$$

with $\gamma = 0.577$ the Euler-Mascheroni constant.

As we noted above, we remark that the choice of a contact pseudo-potential as in Eq. (1.24) implies that its Fourier transform does not vanish at high momenta. This is the origin of the ultraviolet divergences that one has to face while developing a perturbative theory. In the next chapter we are going to consider the first correction to the zero-range framework, where the pseudopoential depends on the momentum and consequently $r_s \neq 0$.

1.2.2 Thermodynamic properties: mean-field and Gaussian fluctuations

A dilute gas made of bosonic atoms interacting via a contact interaction can be modelled via the langrangian density in Eq. (1.25), which we report here for clarity

$$\mathcal{L}\big[\psi, \psi^*\big] = \psi^*(\mathbf{r}, \tau)\Big[\partial_\tau - \frac{\hbar^2\nabla^2}{2m} - \mu\Big]\psi(\mathbf{r}, \tau) + \frac{1}{2}g_0\big|\psi(\mathbf{r}, \tau)\big|^4\,, \tag{1.35}$$

where the field $\psi = \psi(\mathbf{r}, \tau)$ obeys the usual bosonic periodicity conditions. Also with the simplest choice for $V(\mathbf{r})$, the resulting theory has to be approached from a perturbative point of view, because of the quartic term in Eq. (1.25) encoding the presence of the interaction

potential. Within the functional integration framework, excellent reviews of the perturbation theory in dilute Bose gases can be found in [24, 25, 26]. It is worth mentioning that, in this subsection, we are going to consider the case $g_0 > 0$, corresponding to a repulsive atom-atom interaction. The picture arising from an attractive two-body interaction is surely interesting and it will be briefly mentioned later in the thesis.

As remarked earlier, Eq. (1.25) falls in the ψ^4-theories set, meaning a global $U(1)$ gauge symmetry can be spontaneously broken and a superfluid phase then occurs. In order to take into account this possibility, the bosonic quantum field can be decomposed in two different contributions, namely

$$\psi(\mathbf{r}, \tau) = v + \eta(\mathbf{r}, \tau) \tag{1.36}$$

where the field $\eta(\mathbf{r}, \tau)$ represents the space-time dependent fluctuations around the order parameter v. The physical interpretation of the latter is evident in $d = 3$, where the superfluid transition can be characterized in terms of the condensate density, while it is more subtle for lower dimensions. Indeed, no true long-range order can be achieved for $d \leq 2$ [12, 13] and v then describes, at maximum, the so-called quasi-condensate.

The mean-field picture can be derived by neglecting the fluctuations and assuming that the ordered phase is uniform and stationary, i.e. v is taken as a real constant. By following the saddle-point scheme, we have to look for the maximum contribution governing the partition function integral in Eq. (1.4). In order to identify this configuration, one has to find the stationary points of the Euclidean action, i.e. the ones solving $\delta S[v] = 0$, where $S[v]$ is given by Eq. (1.25) with gradient and time-derivative terms set to zero.

Thus, by replacing the *full* bosonic field $\psi(\mathbf{r}, \tau)$ in Eq. (1.25) with v, representing a uniform and stationary configuration, one gets the saddle-point action

$$S[v] = \beta\hbar\, L^d \Big(-\mu v^2 + \frac{1}{2} g_0\, v^4 \Big) \,. \tag{1.37}$$

Through the relation $\mathcal{Z}_{\rm mf} = e^{-S_{\rm mf}[v]/\hbar} = e^{-\beta\Omega_{\rm mf}}$, it is immediate to derive the mean-field grand potential density

$$\frac{\Omega_{\rm mf}}{L^d}(\mu, v) = -\mu v^2 + \frac{1}{2} g_0 v^4 \,. \tag{1.38}$$

In Fig. 1.1 we report the behaviour of $\Omega_{\rm mf}(v, \mu)$ by remarking the role played by the chemical

potential in the occurring of the superfluid transition.

By deriving in respect to v, one immediately realize how symmetry breaking is controlled by the sign of the chemical potential. Indeed

$$\left(\frac{\delta S[v]}{\delta v}\right)_{\mu,L^d} = 0 \quad \Longrightarrow \quad v^2 = \begin{cases} 0 & \text{for } \mu < 0 \\ \dfrac{\mu}{g_0} & \text{for } \mu > 0 \end{cases} \tag{1.39}$$

By replacing the saddle-point results in Eq. (1.38), the leading contribution to the thermodynamical potential in the broken-symmetry phase is given by

$$\frac{\Omega_{\rm mf}}{L^d}(\mu) = -\frac{\mu^2}{2g_0} \, . \tag{1.40}$$

Obviously, in deriving Eq. (1.40) we have only considered the contribution coming from the

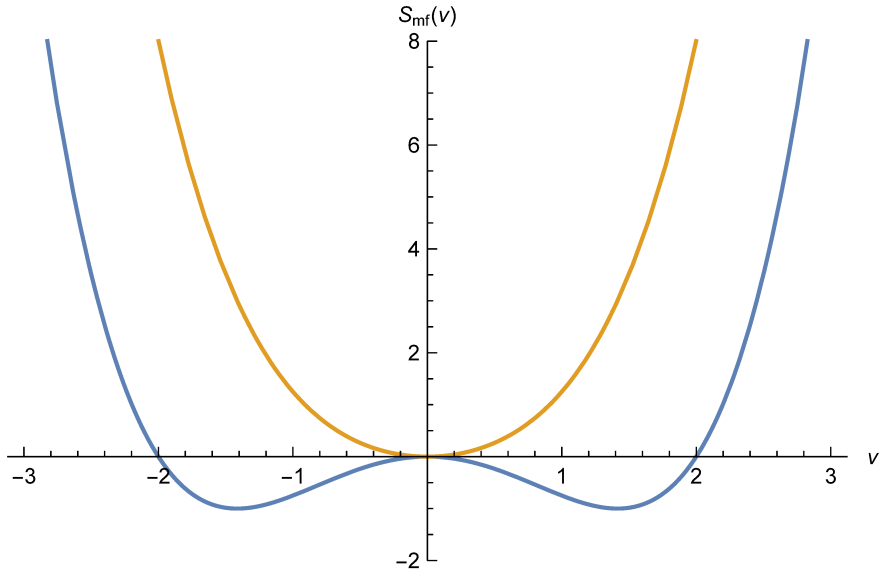

Figure 1.1: Behaviour of the Mean-field grand potential $\Omega_{\rm mf}$ for the broken-symmetry phase (solid blue line) corresponding to the regime $\mu > 0$ and the disordered one characterised by $\mu < 0$. The dependence of $\Omega_{\rm mf}$ on v can be immediately inferred from Eq. (1.37). Therefore, it is evident that the superfluid transition occurs at the critical point $\mu = 0$.

classical value of the bosonic field. Therefore, this result completely lacks any information about quantum (and temperature) fluctuations. In order to encode them in our theory, we let $\eta(\mathbf{r}, \tau) \neq 0$ in Eq. (1.36). By replacing it in Eq. (1.25), the minimal approximation strategy beyond the mean-field picture consists in retaining only the quadratic (Gaussian) terms in

the fluctuation fields. Since we are considering fluctuations above the uniform ground state determined by solving the saddle-point equation, linear terms in $\eta(\mathbf{r},\tau)$ and $\eta^*(\mathbf{r},\tau)$ equate to zero. Moreover, we move to the Fourier space via Eq. (1.2) in order to transform differential operators into algebraic terms. The resulting partition function factorised into the mean-field contribution (see Eq. (1.37)) and the one describing the fluctuations dynamics. The corresponding Gaussian action is given by

$$S_g\big[\eta,\eta^*\big] = \frac{1}{2}\sum_{\mathbf{q},n}\begin{pmatrix}\tilde{\eta}^*(\omega_n,\mathbf{q})\\ \tilde{\eta}(-\omega_n,-\mathbf{q})\end{pmatrix}^T \mathbb{M}(\omega_n,\mathbf{q})\begin{pmatrix}\tilde{\eta}(\omega_n,\mathbf{q})\\ \tilde{\eta}^*(-\omega_n,-\mathbf{q})\end{pmatrix}, \tag{1.41}$$

where the sum is obviously intended over the bosonic Matsubar frequencies $\omega_n = 2\pi n/(\beta\hbar)$ and the 2×2 matrix $\mathbb{M}(\omega_n,\mathbf{q})$ is the inverse fluctuation propagator. While the formal structure of Eq. (1.41) is similar to the non-interacting case in Eq. (1.6), interactions crucially affect the fluctuations propagator. Indeed, while the free propagator $\mathcal{G}_0$ in Eq. (1.7) is diagonal, even within the simplest two-body interaction modelling, the matrix $\mathbb{M}(\omega_n,\mathbf{q})$ reads [1, 8, 26]

$$\mathbb{M}(\omega_n,\mathbf{q}) = \beta\begin{pmatrix}-i\hbar\omega_n + \frac{\hbar^2q^2}{2m} - \mu + 2g_0v^2 & g_0v^2\\ g_0v^2 & i\hbar\omega_n + \frac{\hbar^2q^2}{2m} - \mu + 2g_0v^2\end{pmatrix}. \tag{1.42}$$

The first beyond-mean-field correction can then be computed via $\Omega_g = -\beta^{-1}\log\mathcal{Z}_g$, where the fluctuating partition function is defined by Eq. (1.41) and Eq. (1.42). With the aid of the matrix identity $\mathrm{Tr}\log A = \log\det A$, the Gaussian functional integration leads to

$$\begin{aligned}\Omega_g(\mu,v) &= \frac{1}{2\beta}\sum_{\mathbf{q},n}\log\big[\det\mathbb{M}(\omega_n,\mathbf{q})\big]\\ &= \frac{1}{2\beta}\sum_{\mathbf{q},n}\log\big[\beta^2(\hbar^2\omega_n^2 + E_{\mathbf{q}}^2)\big]\end{aligned} \tag{1.43}$$

where $E_{\mathbf{q}}$ is given by

$$E_{\mathbf{q}}(\mu,v) = \sqrt{\left(\frac{\hbar^2q^2}{2m} - \mu + 2g_0v^2\right)^2 - g_0^2v^4}\,. \tag{1.44}$$

The physical meaning of $E_{\mathbf{q}}$ can be understood by recalling that the (Gaussian) fluctua-

tion propagator is $\mathbb{M}^{-1}(\omega_n, \mathbf{q})$. A crucial information encoded in the propagator concerns the frequencies of collective excitations above the uniform ground state. These frequencies correspond to the poles of the propagator [10], i.e. solution of an equation like $\hbar^2\omega^2 + E_q^2 = 0$.

By referring to Appendix A for the details, the Matsubara sum in Eq. (1.43) can be analytically computed by standard countour technique, reading

$$\frac{1}{2\beta}\sum_n \log\left[\beta^2(\hbar^2\omega_n^2 + E_{\mathbf{q}}^2)\right] = \frac{1}{2}E_{\mathbf{q}} + \frac{1}{\beta}\log\left(1 - e^{-\beta E_{\mathbf{q}}}\right) . \tag{1.45}$$

Within the Gaussian approximation, the grand potential counts three different terms

$$\Omega(\mu, T, v) = \Omega_{\rm mf}(\mu, v) + \Omega_g^{(0)}(\mu, v) + \Omega_g^{(T)}(\mu, T, v) , \tag{1.46}$$

where $\Omega_{\rm mf}$ is given by Eq. (1.38), while $\Omega_g^{(0)}$ and $\Omega_g^{(T)}$ represent the fluctuation contribution. They are respectively given by

$$\Omega_g^{(0)}(\mu, v) = \frac{1}{2}\sum_{\mathbf{q}} E_{\mathbf{q}}(\mu, v) \tag{1.47}$$

$$\Omega_g^{(T)}(\mu, v, T) = \frac{1}{\beta}\sum_{\mathbf{q}} \log\left(1 - e^{-\beta E_{\mathbf{q}}}\right) , \tag{1.48}$$

with $E_{\mathbf{q}}$ as in Eq. (1.44). More precisely, $\Omega_g^{(0)}$ is a purely quantum-mechanical term arising from the imaginary-time axis integration[1], then it contains the information about quantum statistics. In other words, it is the zero-point energy of bosonic excitations above the uniform ground state described by the saddle-point equation. On the other hand, the role of thermal fluctuations is encoded in $\Omega_g^{(T)}$. By following a perturbative approach, we now replace v in the equations above with its saddle-point value specified by Eq. (1.39) in the broken-symmetry phase ($\mu > 0$). It is crucial to observe now that the excitation spectrum in Eq. (1.44) is made gapless by this substitution. This is mandatory, since we are dealing with a system where a continuous symmetry is broken and the Goldstone theorem consequently states that low-momenta excitations with no energy cost have to arise [11]. Indeed, with

[1] By moving to the Fourier space, the integration along the imaginary-time axis becomes the Matsubara sum.

$v^2 = \mu/g_0$ we recover the well-known Bogoliubov spectrum [1]

$$E_{\mathbf{q}} = \sqrt{\frac{\hbar^2 q^2}{2m}\left(\frac{\hbar^2 q^2}{2m} + 2\mu\right)} \,. \tag{1.49}$$

In the continuum limit $\sum_{\mathbf{q}} \longrightarrow L^d \int \frac{d^d\mathbf{q}}{(2\pi)^d}$, one immediately gets from Eq. (1.47)

$$\frac{\Omega_g^{(0)}}{L^d} = \frac{1}{2} K_d \int_0^{+\infty} dq\, q^{d-1} \sqrt{\frac{\hbar^2 q^2}{2m}\left(\frac{\hbar^2 q^2}{2m} + 2\mu\right)} \tag{1.50}$$

where $K_d \equiv S_d/(2\pi)^d$, $S_d = 2\pi^{d/2}/\Gamma(d/2)$ being the d-dimensional solid angle. Here we encounter an important obstacle: the zero-point energy given by Eq. (1.50) has an ultraviolet (UV) divergence for any integer dimension d. Before outlining a strategy to tackle down this unphysical divergence, we remark that our functional integration recipe is closely related to the Bogoliubov approximation within the second-quantization picture [10]. The original Bogoliubov formulation relied on the fact that, given the grand canonical Hamiltonian

$$\hat{K} = \sum_{\mathbf{q}} (\epsilon_{\mathbf{q}} - \mu) \hat{\psi}^\dagger_{\mathbf{q}} \hat{\psi}_{\mathbf{q}} + \frac{g_0}{2L^d} \sum_{\mathbf{q}_1,\mathbf{q}_2,\mathbf{q}_3,\mathbf{q}_4} \hat{\psi}^\dagger_{\mathbf{q}_1} \hat{\psi}^\dagger_{\mathbf{q}_2} \hat{\psi}_{\mathbf{q}_3} \hat{\psi}_{\mathbf{q}_4} \delta_{\mathbf{q}_1+\mathbf{q}_2,\mathbf{q}_3+\mathbf{q}_4} \,, \tag{1.51}$$

in presence of condensation the state $\mathbf{q} = 0$ can be modelled by a simple constant. Indeed, being macroscopically occupied, the operators $\hat{\psi}_0$ and $\hat{\psi}_0^\dagger$ *almost* commute. Concerning the fluctuating part (i.e. $\mathbf{q} \neq 0$ terms), the Bogoliubov approach retains only quadratic corrections. The resulting Hamiltonian can then be safely diagonalized by means of a canonical transformation. In the end, one obtains a quasiparticles spectrum equal to Eq. (1.49).

■ 1.3 Regularization strategies

Starting from the local Lagrangian density in Eq. (1.25), we have derived the Gaussian contribution to the grand potential coming from quantum (i.e. zero temperature) and thermal fluctuations. Unfortunately, the zero-range field theory we are developing unavoidably leads to a UV divergence in the zero-point energy. Indeed, the contact pseudopotential $V(\mathbf{r} - \mathbf{r}') = g_0\ \delta(\mathbf{r} - \mathbf{r}')$ has a constant Fourier transform. This is in contrast with the vanishing at large momenta required from a reasonable two-body interaction potential [26].

1.3.1 Momentum cut-off regularization

At first, one can try to make sense of a divergent theory by simply introducing a UV cutoff Λ. Related to the non-physical choice of the interaction potential, one should notice that a momentum cutoff implies a length one, below which atoms can no longer be considered elementary particles and modelled through the field $\psi(\mathbf{r},\tau)$. In this unknown region, our model completely breaks down because new physics arises: for example, the internal structure of atoms, or molecules, has to be taken into account.

By following this recipe [1, 8], the UV cutoff marks the excluded region whose residual effect can be absorbed by redefining the coupling parameters of our theory. Thus, Eq. (1.50) has to be integrated not on the whole $\mathbb{R}^d$ space, but only on an internal shell described by $|\mathbf{q}| < \Lambda$, i.e.

$$\frac{\Omega_g^{(0)}}{L^d} = \frac{1}{2} K_d \int_0^\Lambda dq\, q^{d-1} \sqrt{\frac{\hbar^2 q^2}{2m}\left(\frac{\hbar^2 q^2}{2m} + 2\mu\right)} \,. \tag{1.52}$$

For a gapless excitation spectrum, Eq. (1.52) can be computed analytically. For the case $d = 3$, a large-Λ expansion retaining all the divergent contributions reads

$$\frac{\Omega_g^{(0)}}{L^3}(\mu,\Lambda) = \frac{8}{15\pi^2}\left(\frac{m}{\hbar^2}\right)^{3/2} \mu^{5/2} - \frac{m\mu^2}{4\pi^2\hbar^2}\Lambda + \frac{\mu}{12\pi^2}\Lambda^3 + \mathcal{C}\Lambda^5 + \mathcal{O}\big(\Lambda^{-1}\big) \tag{1.53}$$

where $\mathcal{C}$ is a constant independent from thermodynamic variables. This implies that we can safely neglect the contribution proportional to Λ^5. Thus, we have two terms in Eq. (1.53) diverging for $\Lambda \to +\infty$. As we already stated, these power divergences are artifacts of the particular choice we have made for the interaction potential. We also observe that the theory preserves its local character since large momentum correspond to infinitesimally small length scale. This is a crucial point because, otherwise, these terms could not be absorbed by redefining the coupling constants of the theory. Indeed, by recalling the saddle-point result $\mu = g_0 v^2$, we can check that the terms proportional to Λ and Λ^3 have the same form of the ones present in Eq. (1.38), i.e.

$$\frac{\Omega_{\mathrm{mf}}^{(\Lambda)}}{L^3}(\mu, v, \Lambda) = -\mu v^2 + \frac{1}{2} g_0 v^4 - \frac{m g_0^2 \Lambda}{4\pi^2\hbar^2} v^4 + \frac{g_0 \Lambda^3}{12\pi^2} v^2 \,. \tag{1.54}$$

It is immediate to notice that, up to this order, the proper definitions of the *dressed* coupling

constants in terms of the bare ones are given by

$$\begin{aligned} \mu_\Lambda &= \mu - \frac{g_0}{12\pi^2}\Lambda^3 \\ g_{0,\Lambda} &= g_0 - \frac{m g_0^2}{2\pi^2\hbar^2}\Lambda \ , \end{aligned} \tag{1.55}$$

which, in turn, lead to the renormalized 3-dimensional zero-temperature Gaussian grand potential

$$\frac{\Omega_{\text{eff}}^{(0)}}{L^3} = -\mu_\Lambda v^2 + \frac{1}{2} g_{0,\Lambda} v^4 + \frac{8}{15\pi^2}\left(\frac{m}{\hbar^2}\right)^{3/2} \mu_\Lambda^{5/2} \ . \tag{1.56}$$

One can perform exactly the same steps for the $d = 1$ case, where Eq. (1.52) reads

$$\frac{\Omega_g^{(0)}}{L} = -\frac{2}{3\pi}\left(\frac{m}{\hbar^2}\right)^{1/2} \mu^{3/2} + \frac{\hbar^2}{12\pi m}\Lambda^3 + \frac{\mu}{2\pi}\Lambda + \mathcal{O}(\Lambda^{-1}) \ . \tag{1.57}$$

As usual, all terms independent from the thermodynamic variables can be neglected (the one $\propto \Lambda^3$ in this case). In a similar way to the $d = 3$ case, a comparison between the power divergences in Eq. (1.57) and the mean-field grand potential in Eq. (1.38) makes clear that only the chemical potential needs to be renormalized. The remaining divergence can be absorbed by defining a dressed chemical potential in terms of the bare one, as in Eq. (1.55), namely

$$\mu_\Lambda = \mu - \frac{g\Lambda}{2\pi} \ . \tag{1.58}$$

This, at $T = 0$, the one-dimensional grand potential is given by

$$\frac{\Omega_{\text{eff}}^{(0)}}{L} = -\frac{\mu_\Lambda^2}{2g_0} - \frac{2}{3\pi}\left(\frac{m}{\hbar^2}\right)^{1/2} \mu_\Lambda^{3/2} \ . \tag{1.59}$$

In other words, by redefining the chemical potential in Eq. (1.58) we include in the mean-field contribution exactly the proper counterterm to erase the UV divergence in Eq. (1.57). We are then left with the $d = 2$ case, which is highly non-trivial, since this is exactly the lower critical dimension for a ψ^4-theory. By approaching the regularization of the zero-point energy in Eq. (1.52) with a cutoff strategy, we find not only power divergences as in the $d = 3$ and $d = 1$ case, but also a logarithmic one. While the former are artifacts of the theory (more precisely, of our zero-range approximation), the latter are physical [26] and need to

be handled carefully.

While a UV-cutoff regularization can be performed also in $d = 2$ case [8], we proceed now to outline a different approach based on dimensional regularization.

1.3.2 Dimensional regularization

As anticipated in the previous sections, Eq. (1.56) and Eq. (1.59) can be derived without imposing a high momentum cutoff by means of the so-called dimensional regularization [1, 8, 26]. This technique was first developed by 't-Hooft and Veltman [9] and relies upon the integral dependence on a complex parameter which has to be analytically continued to real values corresponding to physical cases. Concerning the calculation of the zero-point energy of a d-dimensional Bose gas, the complex parameter to consider in Eq. (1.52) is the spatial dimension d.

From a formal point of view, one has to perform the integral in a complex dimension $\mathfrak{D} = d - 2\epsilon$, where the result can be analytically continued to the proper real value by taking the limit $\epsilon \to 0$. The main advantage of dimensional regularization is the possibility to set power divergences to zero. This crucial feature is enabled by the following conjecture [9] proved in [27]:

$$\mathrm{I}_0 = \int_0^{+\infty} dq\, q^{d-1} q^{2n-2} = 0 \qquad \text{for } n \in \mathbb{N} \text{ and } d \in \mathbb{C}. \tag{1.60}$$

It is immediate to check that this (somewhat) astonishing property readily solves the divergence arising in the free case without the necessity to add a convergence factor (compare Eq. (1.13) and the final result in Eq. (1.18)).

We now move to regularize the UV-divergent zero-point energy in Eq. (1.52) by following this strategy. The momentum integral of the Bogoliubov spectrum $E_{\mathbf{q}}$ can be simplified thanks to the Euler beta function, defined as

$$B(x, y) = \int_0^{+\infty} dv \frac{v^{x-1}}{(1+v)^{x+y}} \tag{1.61}$$

for positive $\mathrm{Re}(x)$ and $\mathrm{Re}(y)$. Indeed, after a little bit of algebra, Eq. (1.52) reads

$$\frac{\Omega_g^{(0)}}{L^d} = \frac{1}{4} K_d \left(\frac{2m}{\hbar^2}\right)^{d/2} (2\mu)^{d/2+1} B\left(\frac{d+1}{2}, -\frac{d+2}{2}\right). \tag{1.62}$$

Since d is complex, the beta function can be expressed in terms of Euler Gamma functions as

$$B(x,y) = \frac{\Gamma(x)\Gamma(y)}{\Gamma(x+y)} \,. \tag{1.63}$$

The function $\Gamma(x)$ is defined only in the right half of the complex plane, i.e. for $\mathrm{Re}(x) > 0$ and it is then necessary to continue it to the left half, for negative real parts. It is possible to check that this continuation is analytic everywhere except for zero negative integers. Thanks to Eq. (1.63), one finally gets the following equation for the zero-point energy:

$$\frac{\Omega_g^{(0)}}{L^d} = \frac{1}{4} K_d \left(\frac{2m}{\hbar^2}\right)^{d/2} (2\mu)^{d/2+1} \frac{\Gamma\left(\frac{d+1}{2}\right)\Gamma\left(-\frac{d+2}{2}\right)}{\Gamma\left(-\frac{1}{2}\right)} \,. \tag{1.64}$$

By replacing in the equation above $d = 3$ or $d = 1$ we immediately recover the results in Eq. (1.56) and Eq. (1.59). This example highlights the relevance of dimensional regularization among all the other procedures employed to remove UV divergences and simplify calculations. Indeed, power divergences do not need to be explicitly renormalized and they are treated for what they are: unphysical relics due to the choice of an over-simplified model.

Obviously, this is not the whole story: there are divergences that dimensional regularization does not manage to suppress by default. As we anticipated in the previous subsection, this is case for $d = 2$, where also the analytical continuation of $\Gamma(x)$ diverges. A simple comparison with the cutoff procedure makes us realize that this surviving divergence appears a a logarithm of the high-momentum threshold Λ. Within this framework, its arising can be understood by considering the following expansion for the Gamma function, which reads, for $d \in \mathbb{N}$,

$$\Gamma(-d+\epsilon) \underset{\epsilon\to 0}{\simeq} \frac{(-1)^d}{n!} \left[\frac{1}{\epsilon} + \psi(d+1)\right] . \tag{1.65}$$

The $\psi(x)$ is the digamma function, defined as

$$\psi(x) \equiv \frac{\mathrm{d}\log\Gamma(x)}{\mathrm{d}x} \,. \tag{1.66}$$

From Eq. (1.65), it is evident [1, 26] that logarithmic divergences, i.e. $\propto \log(\Lambda/\kappa)$ with κ being a proper length scale, arise as poles $1/\epsilon$ within this procedure. The case of the lower critical dimension $d = 2$ hence needs an explicit renormalization. In order to reach a finite

effective contribution to the zero-temperature grand potential $\Omega^{(0)}_{\rm eff}/L^2$, we begin from the formal result in Eq. (1.64). By taking the limit $d \to 2$ and letting the ϵ-dependence explicit, we get

$$\frac{\Omega^{(0)}_g}{L^2} = -\frac{m}{4\pi\hbar^2\kappa^\epsilon}\mu^2\,\Gamma\!\left(-2+\frac{\epsilon}{2}\right) \simeq_{\epsilon\to 0^+} -\frac{m\,\mu^2}{4\pi\hbar^2\,\epsilon\,\kappa^\epsilon}\,, \tag{1.67}$$

where the factor κ^ϵ appears because of dimensional reasons. Now, the equation above has been put in a form which can be easily compared to the mean-field result $\frac{\Omega_{\rm mf}}{L^2} = -\frac{\mu^2}{2\,g_0}$. As noted in [1], there is a certain freedom (or ambiguity) in defining the proper length scale κ^{-1}. This is due to the gapless nature of the excitation specturm in Eq. (1.49). On the contrary, in absence of a Goldstone mode, the spectrum gap would appear in place of κ. The comparison between Eq. (1.67) and Eq. (1.40) leads us to identify the renormalized coupling constant as

$$\frac{1}{g_{\rm e}} = \frac{\kappa^\epsilon}{g_0}\left(1+\frac{m}{2\pi\hbar^2}\,\frac{g_0}{\epsilon\kappa^\epsilon}\right). \tag{1.68}$$

Within the renormalization group theory it is useful to define the flow equation, describing the motion of the *running* coupling constant in the parameter space [2, 11], namely

$$\beta\big(g_{\rm e}\big) \equiv \frac{{\rm d}g_{\rm e}}{{\rm d}\kappa} = \kappa^{-1}\left(-\epsilon\,g_{\rm e}+\frac{m}{2\pi\hbar^2}\,g_{\rm e}^2\right). \tag{1.69}$$

In order to recover the Gaussian critical value of the coupling for $d = 2$ (while there is no required renormalization for μ up to the order $\mathcal{O}(\epsilon)$), one has simply to equate $\beta\big(g_{\rm e}\big)$ in Eq. (1.69) to zero. Moreover, by solving Eq. (1.69) we get

$$\frac{1}{g_{\rm e}(\kappa_0)} - \frac{1}{g_{\rm e}(\kappa)} = -\frac{m}{2\pi\hbar^2}\,\log\left(\frac{\kappa_0}{\kappa}\right). \tag{1.70}$$

The high energy scale can be pointed out by setting $1/g_{\rm e}(\kappa_0) = 0$, resulting in $\hbar^2\kappa_0/(2m) = \varepsilon_{\rm h}$. Then, κ can be interpreted as the actual energy of the system [8, 28], i.e. $\hbar^2\kappa^2/(2m) = \mu$ and, as a consequence, the renormalized coupling constant depends now on the chemical potential and on the high-energy cutoff in the following way:

$$g_{\rm e} = \frac{m}{4\pi\hbar^2}\log\left(\frac{\varepsilon_{\rm h}}{\mu}\right) \tag{1.71}$$

The last step then consists simply in replacing g_e given by Eq. (1.71) in Eq. (1.40), reading

the final non-divergent zero-temperature grand potential, namely

$$\frac{\Omega_{\rm eff}^{(0)}}{L^2} = -\frac{m\,\mu^2}{8\pi\hbar^2}\,\log\left(\frac{\epsilon_{\rm h}}{\mu}\right). \tag{1.72}$$

■ 1.4 Fluctuations, Correlations and the Superfluid Density

In the previous two sections, within the framework of functional integration, we have reported some major achievements of the Bogoliubov theory, whose original formulation [29] dates back to 1947. Despite the following intense theoretical effort [16, 17, 30], its experimental confirmation had to wait until 1995, when Bose-Einstein condensation was achieved for the first time [31, 32]. The Bogoliubov approach has proved to be extremely reliable in modelling weakly interacting Bose gases, together with the mean-field dynamical description provided by the Gross-Pitaevskii equation [33]. Back in time when these theoretical tools were originally formulated, liquid Helium experiments were the only way to probe the non-classical behaviour of fluids at low temperatures. Unfortunately, ^{4}He typical experimental values for densities and interactions are well beyond the range of applicability of the Bogoliubov theory.

Despite this *experimental distance*, cold atoms and liquid Helium are both wonderful platforms to investigate the superfluid properties of matter. Therefore, it appeared rather natural to attempt the theoretical investigation of superfluid Helium by means of the tools provided by the Bogoliubov theory. Obviously, describing ^{4}He as a weakly interacting gas leads, at maximum, to a qualitative picture of its superfluid features.

The microscopic theory of superfluid Helium proves to be a formidable task [34], where the only reliable approach is the numerical one, due to the implementation of powerful Path Integral Monte Carlo algorithms [34]. On the other hand, one can follow the phenomenological approach by Landau [35, 36], which, in its original formulation, does not require an atomic perspective or the onset of Bose-Einstein condensation. The crucial point in Landau theory is that, beyond a certain critical temperature, the system is actually a mixture of a superfluid part and a normal one, i.e. $n_{\rm tot} = n_s + n_n$. The other fundamental assumption is that also the mass current density has to be decomposed as $\mathbf{g} = m\big[n_s\mathbf{v}_s + n_n\mathbf{v}_n\big]$.

Here we are interested in the reverse path: we want to analyze the superfluid features of

weakly interacting Bose gases by applying the core ideas of the two-fluid model. We mainly focus on the calculation of the superfluid density, but a great and complete review about two-fluid model and its relation to a bosonic order parameter can be found in [37].

We begin by considering again the Euclidean action of a d-dimensional Bose gas. As usual, our starting point is the Lagrangian density given in Eq. (1.23), which takes into account a generic (for now) two-body central interaction. Similarly to the Ginzburg-Landau approach, a mean-field theory can be derived by means of the saddle-point method. Here, we have to set the field $\psi(\mathbf{r},\tau)$ at its classical value, i.e. the one solving $\frac{\partial S}{\partial \psi^*}[\psi,\psi^*]=0$. Up to the saddle-point contribution, one immediately derive the Hartree equation

$$\left[\hbar\partial_\tau\psi - \frac{\hbar^2\nabla^2\psi}{2m} + \int d^d\mathbf{r}'|\psi(\mathbf{r}',\tau)|^2 V(|\mathbf{r}-\mathbf{r}'|)\right]\psi(\mathbf{r},\tau) = \mu\psi(\mathbf{r},\tau) \tag{1.73}$$

while for a uniform and static configuration $\psi(\mathbf{r},\tau)=v\in\mathbb{R}$ one gets Eq. (1.38) and Eq. (1.39), i.e. $-\mu v^2+\tilde{V}_0\,v^3=0$ with its correspondent solutions.

For a generic two-body interaction, we replace the constant g_0 with $\tilde{V}_0=\tilde{V}(\mathbf{q}=0)$, $\tilde{V}(\mathbf{q})$ being the Fourier transform of the two-body interaction $\tilde{V}=\int d^d\mathbf{r}\,e^{-i\mathbf{q}\cdot\mathbf{r}}\,V(\mathbf{r})$. As outlined in Sec. 1.2.2, from the equivalent of Eq. (1.39), namely $-\mu v^2+\tilde{V}_0 v^3=0$, it is evident that a phase transition occurs, depending on the sign of μ. Indeed, for $\mu<0$ we have $v^2=0$ while, for positive value of the chemical potential, one gets $\bar{v}^2=\mu/\tilde{V}_0$.

The saddle-point approximation only considers the contribution of the classical trajectory on the system thermodynamics, while classical and quantum fluctuations are completely neglected. Therefore, all particles enter the condensate in the ordered phase $\mu>0$. When classical and quantum fluctuations are taken into account, this causes a depletion of both the condensate and superfluid density: atoms are kicked out from the ground state, entering in the thermal cloud. There, they can contribute to dissipation processes and are involved in collisions with condensed atoms [38, 39, 40, 41].

Moreover, we have also to remind that v^2 plays the role of the order parameter describing the phase transition occuring because of the spontaneous breaking of a $U(1)$ gauge symmetry; on the other hand, the superfluid density n_s is a transport quantity. It is then crucial to discern these two different quantities, since there is no clear one-to-one correspondence between condensation and superfluidity. For example, in a strongly interacting system like

liquid ^{4}He, only the 8% of the atoms populates the ground-state $|\mathbf{q}=0\rangle$ at $T=0$, while all of them partecipate to the superfluid dynamics.

Differently from Sec. 1.2, we now describe the fluctuations by moving to the phase-density formalism, where the bosonic field is represented by

$$\psi(\mathbf{r},\tau)=\sqrt{\bar{v}^2+\delta n(\mathbf{r},\tau)}\;e^{i\varphi(\mathbf{r},\tau)}\;. \tag{1.74}$$

Density fluctuations have to be considered small in the sense that the bosonic field can be expanded as $\psi\simeq\bar{v}(1+\delta n/2\bar{v}^2)e^{i\varphi}$. This implies that $n(\mathbf{r},\tau)=|\psi(\mathbf{r},\tau)|^2=\bar{v}^2+\delta n(\mathbf{r},\tau)$ and, concerning the condensate density, $n_0=\langle|\psi(\mathbf{r},\tau)|\rangle^2$. Note that, in general, $n_0\neq n=\langle|\psi(\mathbf{r},\tau)^2\rangle$ but, within the Gaussian level where $\langle\delta n\rangle\approx 0$, one can approximate $n_0\approx n$. Now, by replacing Eq. (1.74) in Eq. (1.23), the change of coordinates $\{\psi,\psi^*\}\to\{\delta n,\varphi\}$ requires the calculation of the corresponding Jacobian. This can be easily computed by recalling that in the many-body path integral formulation $\mathcal{D}[\psi,\psi^*]$ is intended as $\propto d\mathrm{Re}\psi\; d\mathrm{Im}\psi$ where [3, 4]

$$\begin{aligned}\mathrm{Re}\psi&=\sqrt{\bar{v}^2+\delta n}\;\cos\varphi\;;\\ \mathrm{Im}\psi&=\sqrt{\bar{v}^2+\delta n}\;\sin\varphi\;.\end{aligned} \tag{1.75}$$

It is immediate to check that $\det\mathbb{J}(\delta n,\varphi)=1/2$ and, being independent from thermodynamic variables, can be absorbed into the measure, leading to

$$\mathcal{Z}=\int\mathcal{D}[\psi,\psi^*]e^{-S[\psi,\psi^*]/\hbar}=\int\mathcal{D}[\delta n,\varphi]e^{-S[\delta n,\varphi]/\hbar} \tag{1.76}$$

where the Bose statistics is encoded in the periodic boundary conditions $\delta n(\beta\hbar)=\delta n(0)$ and $\varphi(\beta\hbar)=\varphi(0)$.

By defining $n=\bar{v}^2+\delta n$, we replace $\psi=\sqrt{n}e^{i\varphi}$ in Eq. (1.23), resulting in the following Euclidean action [2]

$$\begin{aligned}S[n,\varphi]=\int_0^{\beta\hbar}d\tau\int_{L^d}d^d\mathbf{r}\Bigg[&i\hbar n\frac{\partial\varphi}{\partial\tau}+\frac{\hbar^2(\nabla n)^2}{8m\,n}+\frac{\hbar^2\,n(\nabla\varphi)^2}{2m}-\mu\,n+\\&+\frac{1}{2}\int d^d\mathbf{r}'V(|\mathbf{r}-\mathbf{r}'|)n(\mathbf{r},\tau)n(\mathbf{r}',\tau)\Bigg]\;,\end{aligned} \tag{1.77}$$

where terms like $\hbar\,\partial_\tau\,n$ can be eliminated via integration by parts.

Concerning Eq. (1.77), it is possible to perform an expansion for small density fluctuation by making the dependence on δn explicit again. Hence, one finally gets a structure like

$$S[\delta n, \varphi] = S_g[\delta n, \varphi] + S_{\rm int}[\delta n, \varphi] \tag{1.78}$$

where $S_g[\delta n, \varphi]$ gathers all terms up to the quadratic (i.e. Gaussian) order in the fluctuations field, while $S_{\rm int}[\delta n, \varphi]$ represents the first beyond-Gaussian correction. Explicitly [2],

$$\begin{aligned} S_g[\delta n, \varphi] = -\frac{1}{2}\beta\hbar L^d\, \tilde{V}_0\, \bar{v}^4 + \int_0^{\beta\hbar} d\tau \int_{L^d} d^d\mathbf{r} \Bigg[i\hbar\delta n \frac{\partial\varphi}{\partial\tau} + \frac{\hbar^2\bar{v}^2(\nabla\varphi)^2}{2m} + \frac{\hbar^2(\nabla\delta n)^2}{8m\bar{v}^2} \\ + \frac{1}{2}\int d^d\mathbf{r}' V(|\mathbf{r}-\mathbf{r}'|)\delta n(\mathbf{r},\tau)\, \delta n(\mathbf{r}',\tau) \Bigg] \end{aligned} \tag{1.79}$$

where we used the saddle-point results $\mu = \tilde{V}_0\bar{v}^2$ and

$$S_{\rm int}[\delta n, \varphi] = \int_0^{\beta\hbar} d\tau \int_{L^d} d^d\mathbf{r} \left[\frac{\hbar^2\delta n(\nabla\varphi)^2}{2m} - \frac{\hbar^2\delta n(\nabla\delta n)^2}{8m\bar{v}^2} \right] . \tag{1.80}$$

In the following, we neglect the contribution of $S_{\rm int}[\delta n, \varphi]$ and focus on the Gaussian theory specified by $S_g[\delta n, \varphi]$. In Fourier space one has

$$S_g[\delta n, \varphi] = -\frac{1}{2}\beta\hbar\, \tilde{V}_0\, \bar{v}^4 + \frac{1}{2\beta\hbar L^d}\sum_{\mathbf{q},\omega_l} \big(\varphi(-\mathbf{q},-\omega_l), \delta n(-\mathbf{q},-\omega_l)\big)\mathbb{M}(\mathbf{q},\omega_l) \begin{pmatrix} \varphi(\mathbf{q},\omega_l) \\ \delta n(\mathbf{q},\omega l) \end{pmatrix} \tag{1.81}$$

where ω_l are the usual bosonic Matsubara frequencies. In Eq. (1.81), the matrix $\mathbb{M}$ is the inverse propagator of Gaussian fluctuations. Again, within a perturbative approach, the propagator dependence on the order parameter can be eliminated by making use of the saddle-point relation between $\bar{v}$ and μ reported in Eq. (1.39). This scheme leads us to

$$\mathbb{M}(\mathbf{q},\omega_l) = \begin{pmatrix} \bar{v}^2\frac{\hbar^2q^2}{m} & -\hbar\omega_l \\ \hbar\omega_l & \frac{\hbar^2q^2}{4m\bar{v}^2} + \tilde{V}(\mathbf{q}) \end{pmatrix} . \tag{1.82}$$

In order to derive the phase and density correlation up to the Gaussian level one simply has

to invert $\mathbb{M}(\mathbf{q},\omega_l)$. This results in [2, 42]

$$\hbar\mathbb{M}^{-1}(\mathbf{q},\omega_l) = \mathcal{G}(\mathbf{q},\omega_l) = \frac{\hbar}{\hbar^2\omega_l^2 + E_{\mathbf{q}}^2}\begin{pmatrix} \frac{m}{\bar{v}^2\hbar^2q^2}E_{\mathbf{q}}^2 & \hbar\omega_l \\ -\hbar\omega_l & \bar{v}^2\frac{\hbar^2q^2}{m}\end{pmatrix} \tag{1.83}$$

with

$$E_{\mathbf{q}} = \sqrt{\frac{\hbar^2q^2}{2m}\Big[\frac{\hbar^2q^2}{2m} + 2\tilde{V}(q)\ \bar{v}^2\Big]}\ . \tag{1.84}$$

Eq. (1.83) implies that the two-field correlations can be immediately computed through

$$\langle m_i(\mathbf{q},\omega_l)m_j(\mathbf{q}',\omega_{l'})\rangle = (2\pi)^d\ \delta(\mathbf{q}+\mathbf{q}')\delta_{m,-m'}(\beta\hbar)\mathcal{G}_{ij}(\mathbf{q},\omega_l) \tag{1.85}$$

where $i,j = 1,2$ with $m_1(\mathbf{q},\omega_l) = \varphi(\mathbf{q},\omega_l)$ and $m_2(\mathbf{q},\omega_l) = \delta n(\mathbf{q},\omega_l)$.

The beyond-Gaussian correction in Eq. (1.80) can be neglected only when $|V(\mathbf{q})|$ is small enough (weakly-interacting systems) or when the pair-potential is strong but it holds $a_s \ll n^{-1/d}$, a_s being the s-wave scattering length. It can be shown [43] that, within the Bogoliubov theory, the expansion parameter is given by $g^2 \propto n^{(d-2)/d}\tilde{V}_0$, with $g = \frac{4\pi\hbar^2}{m}a_s$. This signals that the case $d = 2$ has to be handled very carefully, since the perturbative parameter cancels.

In the gaussian framework, we can then finally consider the current-current correlator

$$\gamma_{ij}(\mathbf{r},\tau;\mathbf{r}',\tau') = \langle g_i(\mathbf{r},\tau)g_j(\mathbf{r}',\tau')\rangle - \langle g_i(\mathbf{r},\tau)\rangle\langle g_j(\mathbf{r}',\tau')\rangle \tag{1.86}$$

with $\mathbf{g} \equiv m\mathbf{j} = mn\mathbf{v}_s$. According to the phase-amplitude representation, one gets

$$\mathbf{g} = \hbar\, n(\mathbf{r},\tau)\nabla\varphi(\mathbf{r},\tau) = \hbar\big[\bar{v}^2 + \delta n(\mathbf{r},\tau)\big]\nabla\varphi(\mathbf{r},\tau)\ . \tag{1.87}$$

Therefore, correlators in Eq. (1.86) read

$$\begin{aligned}\langle g_i(\mathbf{r},\tau)g_j(\mathbf{r}',\tau')\rangle = \hbar^2\bar{v}^4\left\langle\nabla\varphi(\mathbf{r},\tau)_i\nabla\varphi(\mathbf{r}',\tau')_j\right\rangle + \\ + \hbar^2\left\langle\delta n(\mathbf{r},\tau)\delta n(\mathbf{r}',\tau')\nabla\varphi(\mathbf{r},\tau)_i\nabla\varphi(\mathbf{r}',\tau')_j\right\rangle\end{aligned} \tag{1.88}$$

where all odd terms vanish in the Gaussian framework due to parity argument.

The second part of Eq. (1.86) reads

$$\langle g_i(\mathbf{r},\tau)\rangle \langle g_j(\mathbf{r}',\tau')\rangle = \hbar^2 \langle \delta n(\mathbf{r},\tau)\nabla\varphi(\mathbf{r},\tau)_i\rangle \left\langle \delta n(\mathbf{r}',\tau')\nabla\varphi(\mathbf{r}',\tau')_j\right\rangle \tag{1.89}$$

The four-field correlator in Eq. (1.88) can be decomposed by means of the Wick theorem, since we are considering Gaussian distributed variables [3, 10]. The decomposition follows the pattern $\langle ABCD\rangle = \langle AB\rangle\langle CD\rangle + \langle AC\rangle\langle BD\rangle + \langle AD\rangle\langle BC\rangle$. One can easily check that one of these contraction is equal to Eq. (1.89). Thus, Eq. (1.86) becomes

$$\begin{aligned}\gamma_{ij}(\mathbf{r},\tau;\mathbf{r}',\tau') = \hbar^2\bar{v}^4 \left\langle \nabla\varphi(\mathbf{r},\tau)_i\nabla\varphi(\mathbf{r}',\tau')_j\right\rangle + \\ + \hbar^2 \left\langle \delta n(\mathbf{r},\tau)\delta n(\mathbf{r}',\tau')\right\rangle \left\langle \nabla\varphi(\mathbf{r},\tau)_i\nabla\varphi(\mathbf{r}',\tau')_j\right\rangle + \\ + \hbar^2 \left\langle \delta n(\mathbf{r},\tau)\nabla(\mathbf{r}',\tau')_j\right\rangle \left\langle \delta n(\mathbf{r}',\tau')\nabla\varphi(\mathbf{r},\tau)_i\right\rangle \ .\end{aligned} \tag{1.90}$$

In the Fourier space, the equation above corresponds to

$$\begin{aligned}\gamma_{ij}(\mathbf{q},\omega_l;\mathbf{q}',\omega_{l'}) = -\bar{v}^4 q_i q_j \left\langle \varphi(\mathbf{q},\omega_l)\varphi(\mathbf{q}',\omega_{l'})\right\rangle + \\ - \frac{1}{(\beta L^d)^2} \sum_{\substack{\mathbf{k},\omega_m \\ \mathbf{k}',\omega_{m'}}} \Big[\left\langle \delta n(\mathbf{q}-\mathbf{k},\omega_{l-m})\delta n(\mathbf{q}'-\mathbf{k}',\omega_{l'-m'})\right\rangle \left\langle \varphi(\mathbf{k},\omega_m)\varphi(\mathbf{k}',\omega_{m'})\right\rangle + \\ + \left\langle \delta n(\mathbf{k}-\mathbf{q},\omega_{m-l})\varphi(\mathbf{k}',\omega_{m'})\right\rangle \left\langle \delta n(\mathbf{k}'-\mathbf{q}',\omega_{m'-l'})\varphi(\mathbf{k},\omega_m)\right\rangle \Big] \ .\end{aligned} \tag{1.91}$$

The two-field correlation functions are given by the matrix elements of $\hbar\mathcal{G}(\mathbf{q},\omega_l)$ in Eq. (1.83). According to the recipe outlined in [44, 45], we are interested in the transverse component of the current-current correlation function. Within this formalism, it corresponds to

$$\gamma^T(\mathbf{q},\omega_l) = \frac{1}{\hbar(d-1)} \sum_{ij} \mathcal{P}^T_{ij}\, \gamma_{ij}(\mathbf{q},\omega_l) \tag{1.92}$$

where $\mathcal{P}^T_{ij} \equiv \delta_{ij} - q_i q_j/q^2$ is the transverse projector. With the aid of Eq. (1.83), one can compute term by term the transverse component of $\gamma_{ij}(\mathbf{q},\omega_l)$ in Eq. (1.91), reading

$$\gamma^T(\mathbf{q},\omega_l) = \frac{1}{(d-1)\beta L^d} \sum_{\mathbf{k},\omega_m} \frac{q^2k^2 - (\mathbf{qk})^2}{q^2k^2} \frac{\hbar^2(\mathbf{q}-\mathbf{k})^2 E^2_{\mathbf{k}} + \hbar^4 k^2 \omega_{l-m}\omega_m}{(\hbar^2\omega^2_{l-m} + E^2_{\mathbf{q}-\mathbf{k}})(\hbar^2\omega^2_m + E^2_{\mathbf{k}})} \ . \tag{1.93}$$

The normal density can be derived now from Eq. (1.93) via a limit procedure, namely

$$\rho_n = \lim_{q\to 0}\lim_{\omega_l\to 0}\gamma^T(\mathbf{q},\omega_l) = \frac{1}{d\beta L^d}\sum_{\mathbf{k},\omega_m} k^2 \frac{E_{\mathbf{k}}^2 - \hbar^4\omega_m^2}{(\hbar^2\omega_m + E_{\mathbf{k}}^2)^2} \ . \tag{1.94}$$

The limit procedure has carried out a factor $1/d$ due to isotropy assumption and another factor $(d-1)$ because of the longitudinal component removal. The Matsubara sum can be performed analytically (cfr. [10, 42]), resulting in

$$\lim_{\delta\to 0^+}\frac{\hbar}{\beta}\sum_m \frac{(E_{\mathbf{k}}^2 - \hbar^2\omega_m^2)e^{i\omega_m\delta}}{(\hbar^2\omega_m^2 + E_{\mathbf{k}}^2)^2} = \frac{\beta\hbar}{4}\frac{1}{\sinh^2\left(\beta E_{\mathbf{q}}/2\right)} \tag{1.95}$$

such that Eq. (1.94) reads, for a generic two-body interaction $\tilde{V}(\mathbf{q})$:

$$\rho_n = \frac{\beta\hbar^2}{4d}\int \frac{d^d\mathbf{q}}{(2\pi)^d}\ \frac{q^2}{\sinh^2\left(\beta E_{\mathbf{q}}\,/\,2\right)} \ . \tag{1.96}$$

Concerning the long-wavelength limit $q \to 0$, in presence of a U(1)-Goldstone mode, the elementary excitations display a linear dispersion relation

$$E_{\mathbf{q}} \underset{q\sim 0}{\longrightarrow} \hbar c_B q \qquad \text{where} \qquad c_B = \sqrt{\frac{\mu}{m}} \tag{1.97}$$

In this regime, Eq. (1.96) reads the following analytical result in a generic dimension d

$$\rho_n = \frac{\Gamma(d+2)\zeta(d+1)}{2^{d-1}\pi^{d/2}\ d\,\Gamma(d/2)}\frac{(k_BT)^{d+1}}{\hbar^d c_B^{d+2}} \ . \tag{1.98}$$

Focusing on the $d = 3$ and $d = 2$ case we get

$$\rho_n(d=3) = \frac{2\pi^2}{45\hbar^3}\ \frac{(k_BT)^4}{c_B^5} \tag{1.99}$$

$$\rho_n(d=2) = \frac{3\zeta(3)}{2\pi\hbar^2}\frac{(k_BT)^3}{c_B^4} \tag{1.100}$$

which are consistent with what one can derive by following slightly different approaches [45, 46] and with the phenomenological theory by Landau [36]. At the end, we underline a crucial point in our calculation. By recalling Eq. (1.88) and Eq. (1.90), we realize that the current-current correlation (and consequently the normal density) cannot be simply

proportional to the Gaussian phase correlator

$$\left\langle \varphi(\mathbf{q},\omega_l)\varphi(\mathbf{q}',\omega_{m'})\right\rangle = (2\pi)^d \beta\hbar\delta_{m,-m'}\delta(\mathbf{q}-\mathbf{q}')\mathcal{G}_{11}(\mathbf{q},\omega_m) \tag{1.101}$$

with $\mathcal{G}_{11}(\mathbf{q},\omega_m)$ given by the proper matrix element of Eq. (1.83). If one had only considered this phase-phase term, there would be no contribution to the normal density ρ_n, since only a purely longitudinal term $q_i q_j$ would be present. This means that, in order to at least derive the Landau formulation one has to take into account both phase and density fluctuation. For systems falling into the XY universality class [11, 47] the leading term arises from phase fluctuations, so it seems natural to work with a simple only-phase action. However, in Eq. (1.93) is evident that the crucial non-zero contribution to the transverse response function is due to the next-to-leading corrections involving density (amplitude) fluctuations. In the language of the functional integration [42], this means that we have to take into account the correction above the Gaussian framework by including the four-field correlator $\langle \delta n(x)\nabla\varphi(x)\delta n(x')\nabla\varphi(x')\rangle$ in Eq. (1.90).

■ 1.5 Condensate Depletion and Green's Functions

Here we aim to derive the equation for the condensate fraction up to the Gaussian order in the fluctuations. As outlined in [10], a perturbative treatment of an interacting Bose system can be developed around the normal and anomalous Green's function, which are defined as

$$G(\mathbf{r},\tau;\mathbf{r}',\tau') = \langle \psi(\mathbf{r},\tau)\psi^*(\mathbf{r}',\tau')\rangle - n_0 \tag{1.102}$$

$$G_{12}((\mathbf{r},\tau;\mathbf{r}',\tau') = \langle \psi(\mathbf{r},\tau)\psi(\mathbf{r}',\tau')\rangle - n_0 \ , \tag{1.103}$$

where n_0 is the condensate density. According to the Dyson equation [10], the general structure of the Green's functions within the Fourier space is given by

$$G(\mathbf{q},\omega_l) = \frac{1}{\hbar D(\mathbf{q},\omega_l)}\Big[i\hbar\omega_l + \frac{\hbar^2 q^2}{2m} - \mu + \hbar\Sigma_{11}(-\mathbf{q},-\omega_l)\Big] \tag{1.104}$$

$$G_{12}(\mathbf{q},\omega_l) = -\frac{\Sigma_{12}(\mathbf{q},\omega_l)}{D(\mathbf{q},\omega_l)} \tag{1.105}$$

with Σ_{11} and Σ_{12} defining the self-energies. The denominator $D(\mathbf{q},\omega_l)$ reads [10]

$$D(\mathbf{q},\omega_l) = -\Big[i\omega_l + \frac{1}{2}\big(\Sigma_{11}(\mathbf{q},\omega_l) - \Sigma_{11}(-\mathbf{q},-\omega_l)\big)\Big]^2 + \\ + \frac{1}{\hbar}\Big[\frac{\hbar^2 q^2}{2m} - \mu + \frac{1}{2}\big(\Sigma_{11}(\mathbf{q},\omega_l) + \Sigma_{11}(-\mathbf{q},-\omega_l)\big)\Big]^2 - \big|\Sigma_{12}(\mathbf{q},\omega_l)\big|^2 . \tag{1.106}$$

For a system of non-interacting bosons, one simply has $\Sigma_{11} = \Sigma_{12} = 0$ and only the free propagator survives, i.e.

$$G_0(\mathbf{q},\omega_l) = \frac{\hbar}{-i\hbar\omega_l + \frac{\hbar^2 q^2}{2m} - \mu} \tag{1.107}$$

Here, we aim to compute Eq. (1.102) and (1.103) from which it is possible to extract relevant informations about the system, such as the condensate depletion. We start by expanding Eq. (1.74) up to the first order in the fluctuations field where

$$\psi(\mathbf{r},\tau) \simeq \bar{v}\Big(1 + \frac{\delta n}{2\bar{v}^2} + i\varphi\Big) . \tag{1.108}$$

Up to the quadratic order, Eq. (1.102) and Eq. (1.103) become [42]

$$G(\mathbf{q},\omega_l;\mathbf{q}',\omega_{l'}) = \frac{1}{4\bar{v}^2}\langle\delta n(\mathbf{q},\omega_l)\delta n(\mathbf{q}',\omega_{l'})\rangle - \frac{i}{2}\langle\delta n(\mathbf{q},\omega_l)\varphi(\mathbf{q}',\omega_{l'})\rangle \\ + \frac{i}{2}\langle\varphi(\mathbf{q},\omega_l)\delta n(\mathbf{q}',\omega_{l'})\rangle - \bar{v}^2\langle\varphi(\mathbf{q},\omega_l\varphi(\mathbf{q}',\omega_{l'})\rangle \tag{1.109}$$

and

$$G_{12}(\mathbf{q},\omega_l;\mathbf{q}',\omega_{l'}) = \frac{1}{4\bar{v}^2}\langle\delta n(\mathbf{q},\omega_l)\delta n(\mathbf{q}',\omega_{l'})\rangle + \frac{i}{2}\langle\delta n(\mathbf{q},\omega_l)\varphi(\mathbf{q}',\omega_{l'})\rangle \\ + \frac{i}{2}\langle\varphi(\mathbf{q},\omega_l)\delta n(\mathbf{q}',\omega_{l'})\rangle - \bar{v}^2\langle\varphi(\mathbf{q},\omega_l\varphi(\mathbf{q}',\omega_{l'})\rangle \ . \tag{1.110}$$

In the same way of section 1.4, two-field correlation functions are given by matrix elements of the Gaussian fluctuations propagator $\mathcal{G}(\mathbf{q},\omega_l)$ in Eq. (1.83) with the excitation spectrum given by Eq. (1.84). Replacing in Eq. (1.109) and Eq. (1.110) the proper two-field

correlations given by Eq. (1.85), we get

$$G(\mathbf{q},\omega_l) = \frac{\hbar}{\hbar^2\omega_l^2 + E_{\mathbf{q}}^2}\left[i\hbar\omega_n + \frac{\hbar^2 q^2}{2m} + \bar{v}^2\tilde{V}(\mathbf{q})\right] \tag{1.111}$$

$$G_{12}(\mathbf{q},\omega_l) = -\frac{\hbar\,\bar{v}^2\tilde{V}(\mathbf{q})}{\hbar^2\omega_l^2 + E_{\mathbf{q}}^2}\,. \tag{1.112}$$

By making use again of Eq. (1.39), the self-energies read

$$\begin{aligned}
\Sigma_{11}(\mathbf{q},\omega_l) &= \frac{\bar{v}^2}{\hbar}\big[\tilde{V}_0 + \tilde{V}(\mathbf{q})\big] \\
\Sigma_{12} &= \frac{\bar{v}^2\tilde{V}(\mathbf{q})}{\hbar} \\
D(\mathbf{q},\omega_l) &= \frac{1}{\hbar^2}\big(\hbar^2\omega_l^2 + E_{\mathbf{q}}^2\big)\,.
\end{aligned} \tag{1.113}$$

We underline one more time that the results obtained up to the Gaussian order are exactly the same obtained through a Bogoliubov transformation [10]. Thus, in analogy with the second-quantization recipe, we define the auxiliary functions

$$\begin{aligned}
u_{\mathbf{q}}^2 &= \frac{1}{2}\left[\frac{\bar{v}^2\tilde{V}(\mathbf{q}) + \frac{\hbar^2 q^2}{2m}}{E_{\mathbf{q}}} + 1\right] \\
v_{\mathbf{q}}^2 &= \frac{1}{2}\left[\frac{\bar{v}^2\tilde{V}(\mathbf{q}) + \frac{\hbar^2 q^2}{2m}}{E_{\mathbf{q}}} - 1\right]
\end{aligned} \tag{1.114}$$

where $u_{\mathbf{q}}^2 - v_{\mathbf{q}}^2 = 1$ and $u_{\mathbf{q}}v_{\mathbf{q}} = \bar{v}^2\tilde{V}(\mathbf{q})/(2E_{\mathbf{q}})$ hold. At this point we are finally ready to compute the condensate depletion up to quadratic (i.e. Gaussian) order in the fluctuations fields.

The condensate depletion is given by [10]

$$\begin{aligned}
n - n_0 &= \int d^d\mathbf{r}\big[\,\langle\psi(\mathbf{r},\tau-0^+)\psi^*(\mathbf{r},\tau+0^+)\rangle - n_0\big] \\
&= \frac{1}{(\beta\hbar)^2}\int\frac{d^d\mathbf{q}}{(2\pi)^d}\sum_{\omega_l,\omega_{l'}} e^{-i(\omega_l-\omega_{l'})\tau}e^{i(\omega_l+\omega_{l'})0^+}G(\mathbf{q},\omega_l;-\mathbf{q},-\omega_l) \\
&= \frac{1}{\beta\hbar}\int\frac{d^d\mathbf{q}}{(2\pi)^d}\sum_{\omega_l} e^{i\omega_l 0^+}G(\mathbf{q},\omega_l)
\end{aligned} \tag{1.115}$$

where in the last line we assumed translational invariance in time. The factor $e^{i\omega_l 0^+}$ arises naturally within the path-integral formalism [2], encoding the proper time ordering of in-

finitely small time slices and it is crucial to ensure the convergence of Matsubara summation [48]. By expressing Eq. (1.111) in terms of Bogoliubov functions defined in Eq. (1.114), Eq. (1.115) becomes

$$n - n_0 = \int \frac{d^d\mathbf{q}}{(2\pi)^d} \frac{1}{\beta} \sum_{\omega_l} e^{i\omega_l 0^+} \left[\frac{u_{\mathbf{q}}^2}{-i\hbar\omega_l + E_{\mathbf{q}}} + \frac{v_{\mathbf{q}}^2}{i\hbar\omega_l + E_{\mathbf{q}}} \right] . \tag{1.116}$$

Again, Matsubara sums can be solved by means of contour integration, reading the following useful results

$$\begin{aligned} \frac{1}{\beta} \sum_{\omega_l} \frac{e^{i\omega_l 0^+}}{i\hbar\omega_l - E_{\mathbf{q}}} &= -\frac{1}{e^{\beta E_{\mathbf{q}}} - 1} \\ \frac{1}{\beta} \sum_{\omega_l} \frac{e^{i\omega_n 0^+}}{i\hbar\omega_n + E_{\mathbf{q}}} &= \frac{e^{\beta E_{\mathbf{q}}}}{e^{\beta E_{\mathbf{q}}} - 1} . \end{aligned} \tag{1.117}$$

Thus, Eq. (1.115) can be expressed as

$$n - n_0 = \int \frac{d^d\mathbf{q}}{(2\pi)^d} \left[\frac{u_{\mathbf{q}}^2}{e^{\beta E_{\mathbf{q}}} - 1} + \frac{e^{\beta E_{\mathbf{q}}} v_{\mathbf{q}}^2}{e^{\beta E_{\mathbf{q}}} - 1} \right] = \int \frac{d^d\mathbf{q}}{(2\pi)^d} \left[v_{\mathbf{q}}^2 + \frac{u_{\mathbf{q}}^2 + v_{\mathbf{q}}^2}{e^{\beta E_{\mathbf{q}}} - 1} . \right] \tag{1.118}$$

It is clear that we have now separated two different contribution: the first one is $\propto v_{\mathbf{q}}^2$, describing the zero-temperature depletion occurring because of the interaction between particles. On the other hand, the second one models the effect of thermal fluctuations in draining the condensate.

At zero-temperature and within the zero-range approximation detailed in the previous sections, where $\tilde{V}(\mathbf{q}) = \tilde{V}_0$, the integral $\int d^d\mathbf{q}\, v_{\mathbf{q}}^2$ can be computed analytically for a generic dimension d. Hence, one finds

$$\Delta n(T=0) = n(T=0) - n_0 = \frac{2^{d-3}\, \pi^{d/2}\, (d-2)\Gamma\left(\frac{d-1}{2}\right)\Gamma(-\frac{d}{2})}{(2\pi)^d \sqrt{\pi}\, \Gamma(d/2)} (m\, n_0\, \tilde{V}_0)^{1/2} \tag{1.119}$$

where we identified $\bar{v}^2 \approx n_0$ in $E_{\mathbf{q}}$ and Eq. (1.114). In $d = 3$ we have $\tilde{V}_0 = 4\pi\hbar^2 a_s/m$ and consequently

$$\Delta n(T=0, d=3) = \frac{8}{3\sqrt{\pi}} \left(n_0 a_s\right)^{3/2} , \tag{1.120}$$

while in $d = 2$, since $\lim_{d\to 2}(d-2)\Gamma(-d/2) = 2$

$$\Delta n(T=0, d=2) = \frac{m\tilde{V}_0 n_0}{4\pi\hbar^2} . \tag{1.121}$$

The contribution to the depletion from thermal fluctuations can be analytically computed in the long-wavelength limit $q \to 0$ where $E_{\mathbf{q}} \approx \hbar c_B q$. In a generic dimension we get

$$\Delta n(T \neq 0) = \frac{\Gamma(d-1)\zeta(d-1)}{2^{d-1}\pi^{d/2}\Gamma(d/2)} \frac{m(k_B T)^{d-1}}{\hbar^d \, c_B^{d-2}} \tag{1.122}$$

while, for $d = 3$ and $d = 2$ one finds

$$d = 3 \qquad \Longrightarrow \qquad \Delta n(T \neq 0) = \frac{m(k_B T)^2}{12\hbar^3 c_B} \tag{1.123}$$

$$d = 2 \qquad \Longrightarrow \qquad \Delta n(T \neq 0) \to \infty \, . \tag{1.124}$$

The divergence for $d = 2$ at finite temperature should not be surprising since, as stated by the Mermin-Wagner theorem [12, 13], this is lower critical dimension of a ψ^4-theory and a true long-range order is not possible at finite temperature due to the unbalanced growth of fluctuations.

■ 1.6 The case of sound propagation in the 2d Bose gas

Up to this point, we have presented a set of theoretical tools to describe an ultracold and weakly interacting Bose gas. In Sec. 1.4 we have briefly outlined the two-fluid model within a functional formalism. Besides the derivation of the famous Landau formula for the superfluid density in Eq. (1.96), it would be possible to derive a self-consistent hydrodynamic theory based on the two crucial assumptions $n_{\rm tot} = n_s + n_n$ and $\mathbf{g} = m\big[n_s \mathbf{v}_s + n_n \mathbf{v}_n\big]$ [36]. As previously mentioned, the original formulation by Landau did not rely upon an atomic perspective and, actually, did not imply at all the concept of Bose-Einstein condensation [37]. The resulting two-fluid hydrodynamic equations provide a reliable description of superfluid Helium and have been extensively employed also in the field of ultracold quantum gases.

However, this does not imply that the connection between these equations and the Gross-Pitaevskii one, modelling the condensed gas, has always been clear. Since the first experimental realization of Bose-Einstein condensates, it appeared evident that atomic physicists would have to deal with regimes of temperatures and density really far away from the one of superfluid Helium.

First of all, one should find a way to include thermal fluctuations within the Gross-Pitaevskii framework, in order to take into account a non-negligible condensate depletion. A wide range of theoretical strategies has been developed during the years in order to tackle down this non-trivial issue. One of the most relevant is surely the kinetic approach proposed by Zaremba, Nikuni and Griffin (ZNG) [38, 39, 41]. Moving from a pioneering work by Kirkpatrick and Dorfman [49], they model the partially condensed Bose gas at finite temperature through a modified Gross-Pitaevskii coupled to a Boltzmann-like equation. The equation for the condensate part includes a dissipative term, accounting for the losses due to collisions between thermal and condensed atoms. On the other hand, the kinetic equation for the thermal cloud is derived by a BBGKY hierarchy [6] with the zero-range coupling g as expansion parameter. The mean-field term recovers the Hartree interaction term, while the collisional integral can be built upon two different collision processes: the $2 \rightleftharpoons 2$ scattering within the thermal cloud and the $2 \rightleftharpoons 1$ one between a two thermal atoms and a condensed one.

Clearly this is not the only possible approach: for a detailed review of analytical and numerical tools to effectively describe a partially condensed Bose gas at finite temperature we point the reader to [50, 51]. Among the most successful strategies, we surely have to mention the stochastic Gross-Pitaevskii equation [52, 53]. In this framework, the dissipative coupling of the condensed part with the thermal atoms is basically modelled through a stochastic noise term.

In this section, we aim to apply the kinetic strategy to the problem of sound propagation in a two-dimensional Bose gas. We work in the collisionless regime where the ZNG Boltzmann equation reduces to a Landau-Vlasov one. Despite the label, by collisionless we actually mean that we neglect the collisional integral, while the mean-field interaction is still present, supporting also the presence of collective modes [54, 55]. Sound propagation is then possible, as known from previous study on collisionless Fermi gases [56, 57].

On the other hand, we are already aware that the case of two-spatial dimensions is a peculiar situation. Mermin-Wagner theorem prevents the occuring of Bose-Einstein condensation at finite temperature, while superfluidity and quasi-condensates can be observed below the Berezinskii-Kosterlitz-Thouless critical temperature T_c [58, 59]. Very recently, the group of J. Dalibard performed a measurement of the sound velocity in a uniform 2d Bose gas made

of ^{87}Rb atoms [60]. The results were puzzling, since they agree with theoretical predictions [61, 62] based on the Landau-Khalatnikov framework only well below T_c. The authors of [60] correctly noticed that such discrepancy is due to the fact that they are effectively working in a collisionless regime. Indeed, a hydrodynamic approach can be safely adopted when the time between two consecutive collisions $\tau_{\rm col}$ is much smaller than the time scale of small perturbation with frequency ω, i.e. $\tau_{\rm col}\omega \ll 1$. In this regimes collisions are an efficient mechanism to restore the local thermodynamic equilibrium required by hydrodynamics. According to the experimental values, this was not the case in [60], where $\tau_{\rm col}\omega \simeq 1.6 \div 3.4$. Thus, we should not expect that the gas dynamics will follow the two-fluid model predictions. Here, we are going to assume that the dynamics of normal component is collisionless, above and below the critical temperature. Therefore, in our case, we do not need the full complexity of ZNG equations, since condensation does not occur and the collisional integral can be neglected.

Let us then begin by considering a dilute and ultracold three-dimensional (3D) gas made of N identical bosonic atoms of mass m. Atom-atom interactions are modelled through the usual zero-range pseudo-potential with a coupling constant given by $g = 4\pi\hbar^2 a_s/m$. The system is under an external confinement whose shape is given by the sum of a generic potential $\mathcal{U}(\mathbf{r})$ throughtout the xy-plane and a harmonic confinement along the longitudinal axis. Thus, we have

$$U_{\rm ext}(\mathbf{r}, z) = \mathcal{U}(\mathbf{r}) + \frac{1}{2} m\omega_z^2 z^2 \,, \tag{1.125}$$

where $\mathbf{r} = (x, y)$ is the radial position of one atom. If the harmonic confinement is strong enough, one can engineer an effective two-dimensional (2d) configuration. In order to constrain the atoms on the transverse plane, we have to require that the characteristic energy of the longitudinal confinement is much larger than the average kinetic contribution, namely

$$\hbar\omega_z \gg (p_x^2 + p_y^2)/(2m) \,. \tag{1.126}$$

In the actual experiments, this condition can be fulfilled quite easily. When Eq. (1.126) is satisfied, the three-dimensional system is forced to occupy the longitudinal ground state. At the same time, the planar distribution function $f(\mathbf{r}, \mathbf{p})$ in the 4d single-particle phase space

($(\mathbf{r},\mathbf{p})=(x,y,p_x,p_y)$) obeys to the effective 2d Landau-Vlasov equation [63]

$$\left[\frac{\partial}{\partial t}+\frac{\mathbf{p}}{m}\cdot\nabla_{\mathbf{r}}-\nabla_{\mathbf{r}}\Big(\mathcal{U}+\mathcal{U}_{\rm mf}\Big)\cdot\nabla_{\mathbf{p}}\right]f(\mathbf{r},\mathbf{p},t)=0\;, \tag{1.127}$$

where

$$\mathcal{U}_{\rm mf}(\mathbf{r},t)=g_{2D}\int\frac{d^2\mathbf{p}}{(2\pi\hbar)^2}\;f(\mathbf{r},\mathbf{p},t) \tag{1.128}$$

is the self-consistent Hartree mean-field term [41]. The only memory of the original three-dimensional character of the system is encoded within the effective 2d coupling constant

$$g_{2D}=\frac{\sqrt{8\pi}\hbar^2}{m}\left(\frac{a_s}{a_z}\right) \tag{1.129}$$

with $a_z=\sqrt{\hbar/(m\omega_z)}$ the characteristic length of the axial harmonic confinement. In the following of this section, we are going to prove that a dynamical description based on Eq. (1.127) manages to recover the experimental results obtained in a homogeneous configuration [60]. If we assume a box potential, we can set $\mathcal{U}(\mathbf{r})=0$, thus

$$f(\mathbf{r},\mathbf{p},t)=f_0(\mathbf{p})+\delta f(\mathbf{r},\mathbf{p},t) \tag{1.130}$$

where $f_0(\mathbf{p})$ is a stationary and isotropic distribution and $\delta f(\mathbf{r},\mathbf{p},t)$ a very small perturbation around it. We can perform a stability analysis against a small perturbation like δf by considering the linearized Landau-Vlasov equation

$$\left[\frac{\partial}{\partial t}+\frac{\mathbf{p}}{m}\cdot\nabla_{\mathbf{r}}\right]\delta f(\mathbf{r},\mathbf{p},t)=g_{2D}\int\frac{d^2\mathbf{p}'}{(2\pi\hbar)^2}\nabla_{\mathbf{r}}\delta f(\mathbf{r},\mathbf{p}',t)\cdot\nabla_{\mathbf{p}}f_0(\mathbf{p})\;. \tag{1.131}$$

Moving to the Fourier space, according to $\widehat{\delta f}(\mathbf{k},\mathbf{p},\omega)=\int dt\int d^2\mathbf{r}\,\delta f(\mathbf{r},\mathbf{p},t)\exp\left(i(\mathbf{k}\cdot\mathbf{r}-\omega t)\right)$, Eq. (1.131) leads us to an implicit formula for the dispersion relation, i.e.

$$1-g_{2D}\int\frac{d^2\mathbf{p}}{(2\pi\hbar)^2}\;\frac{\mathbf{k}\cdot\nabla_{\mathbf{p}}f_0(\mathbf{p})}{\mathbf{p}\cdot\mathbf{k}/m-\omega}=0\;. \tag{1.132}$$

In the equation above $\mathbf{k}$ is a 2d wavevector and ω an angular frequency. As in [64], Eq. (1.132) can be derived within the random-phase approximation (RPA). In that framework, solutions of Eq. (1.132) identify the poles of the dynamic response function. In [64], this equation

has been solved by setting initially the system at equilibrium in presence of a stationary sinusoidal potential. With the removal of the external potential, density modulations begin to oscillates with a damped amplitude. From this damped oscillatory motion one extracts the sound velocity by means of a fitting procedure.

Here, we address the solution of Eq. (1.132) by a fully analytical point of view. The key point in our strategy is the proper treatment of the singularity on the integration path for $\omega = \mathbf{p}\cdot\mathbf{k}/m$. Hence, the integral is Eq. (1.132) is meaningful only with the *caveat* of interpreting ω as a complex quantity, i.e. $\omega = \omega_R + i\omega_I$. Moreover, we impose $\omega_I > 0$ to avoid an unphysical exponential growth of the perturbation [56].

It is possible to further simplify the solution procedure, without any loss of generality, by taking $\mathbf{k} \parallel \hat{e}_x$, i.e. $\mathbf{k} = (k, 0)$. Thus, one easily finds that

$$1 - g_{2D}\int \frac{dp_x}{(2\pi\hbar)}\frac{\partial \tilde{f}_0(p_x)}{\partial p_x}\frac{1}{\frac{p_x}{m} - c} = 0\ . \tag{1.133}$$

In the equation above we have defined $c = \omega/k$ and $\tilde{f}_0(p_x) = \int f_0(p_x, p_y)dp_y/(2\pi\hbar)$. We are now ready to extract the sound velocity from Eq. (1.133). Because of our hypothesis about $\omega \in \mathbb{C}$, it descends that c will be a complex number, too. We then introduce its real and imaginary part, respectively given by $c_R = \omega_R/k$ and $c_I = \omega_I/k$.

Elegant coupled equations for c_R and c_I can be obtained within the limit of weak damping [63]. Concerning the real part of the sound velocity, from Eq. (1.133) we have

$$1 - g_{2D}\mathcal{P}\int \frac{dp_x}{(2\pi\hbar)}\left[\frac{\partial \tilde{f}_0(p_x)/\partial p_x}{p_x/m - c_R}\right] - \pi c_I \frac{\partial \phi(c)}{\partial c}\bigg|_{c_R} = 0\ , \tag{1.134}$$

where $\phi(c) = \frac{mg_{2D}}{(2\pi\hbar)}\frac{\partial \tilde{f}_0}{\partial p_x}\Big|_{p_x = mc}$ and $\mathcal{P}$ denotes the Cauchy principal value. On the other hand, the equation for the imaginary part c_I reads

$$c_I = \frac{\pi \frac{\partial \tilde{f}_0(p_x)}{\partial p_x}\Big|_{p_x = mc_R}}{\frac{\partial}{\partial c_R}\left\{\mathcal{P}\int \frac{dp_x}{(2\pi\hbar)}\left[\frac{\partial \tilde{f}_0(p_x)/\partial p_x}{p_x/m - c_R}\right]\right\}}\ . \tag{1.135}$$

In order to investigate the dynamical behaviour of a quasi-uniform Bose gas in two spatial

dimension, we choose the Bose-Einstein distibution as initial condition, namely

$$f_0(\mathbf{p}) = \frac{1}{L^2}\frac{1}{e^{\beta(\frac{p^2}{2m}+g_{2D}n-\mu)}-1}\,, \tag{1.136}$$

where L^2 is the area enclosing the system. The function $f_0(\mathbf{p})$ given in the equation above describes the thermal equilibrium distribution for gaseous system made of weakly-interacting bosons with uniform density n. The Hartree interaction term $g_{2D}n$ can be absorbed by a simple shifting of the chemical potential $\tilde{\mu} = \mu - g_{2D}n$. The equation of state establishes the connection between the modified chemical potential $\tilde{\mu}$ and the number density n. It can be derived immediately from the normalization $N = \int \frac{d^2\mathbf{r}d^2\mathbf{p}}{(2\pi\hbar)^2} f_0(\mathbf{p})$, reading

$$\tilde{\mu} = k_B T\ \ln\left(1 - e^{-T_B/T}\right) \tag{1.137}$$

where $k_B T_B = 2\pi\hbar^2 n/m$ is the temperature of Bose degeneracy. From Eq. (1.137) it is also clear that $\tilde{\mu} < 0$. Analytical results can be obtained within the regime of temperatures $T \ll T_B$ with $c_R^2 \ll k_B T/m$ holding at the same time. In this window of parameters, we can safely approximate $f_0(\mathbf{p})L^2 \simeq k_B T/(p^2/(2m) - \tilde{\mu})$ from which $L^2\tilde{f}_0(p_x) = k_B T/(\hbar\sqrt{(p_x^2/m) - 2\tilde{\mu}})$. Hence, Eq. (1.134) and Eq. (1.135) respectively read

$$1 + \frac{\tilde{g}_{2D}k_B T}{2\pi}\left[\frac{2}{mc_R^2 - 2\tilde{\mu}} + \frac{\sqrt{mc_R^2}}{(mc_R^2 - 2\tilde{\mu})^{3/2}}\ln\left(\frac{\sqrt{mc_R^2 - 2\tilde{\mu}} - \sqrt{mc_R^2}}{\sqrt{mc_R^2 - 2\tilde{\mu}} + \sqrt{mc_R^2}}\right)\right] + \\ + \tilde{g}_{2D}k_B T c_I \frac{mc_R^2 + \tilde{\mu}}{\sqrt{m}(mc_R^2 - 2\tilde{\mu})^{5/2}} = 0 \tag{1.138}$$

and

$$c_I = -\left[\frac{c_R}{\sqrt{m}(mc_R^2 - 2\tilde{\mu})^{3/2}}\right]\cdot\left[\frac{6\,c_R}{(mc_R^2 - 2\tilde{\mu})^2} + \frac{2(mc_R^2 + \tilde{\mu})}{\sqrt{m}(mc_R^2 - 2\tilde{\mu})^{5/2}}\log\left(\frac{\sqrt{mc_R^2 - 2\tilde{\mu}} - \sqrt{mc_R^2}}{\sqrt{mc_R^2 - 2\tilde{\mu}} + \sqrt{mc_R^2}}\right)\right]^{-1}\,, \tag{1.139}$$

where $\tilde{g}_{2D} = mg_{2D}/\hbar^2$ is the adimensional interaction strength. By inserting Eq. (1.139) in Eq. (1.138) we get an equation for c_R. At this point, Eq. (1.138) can be solved numerically and, by taking into account Eq. (1.137) we can express the zero-sound velocity as a function of T at fixed values of $\tilde{g}_{2D}$. The results of our calculations are reported in Fig. 1.2, where they

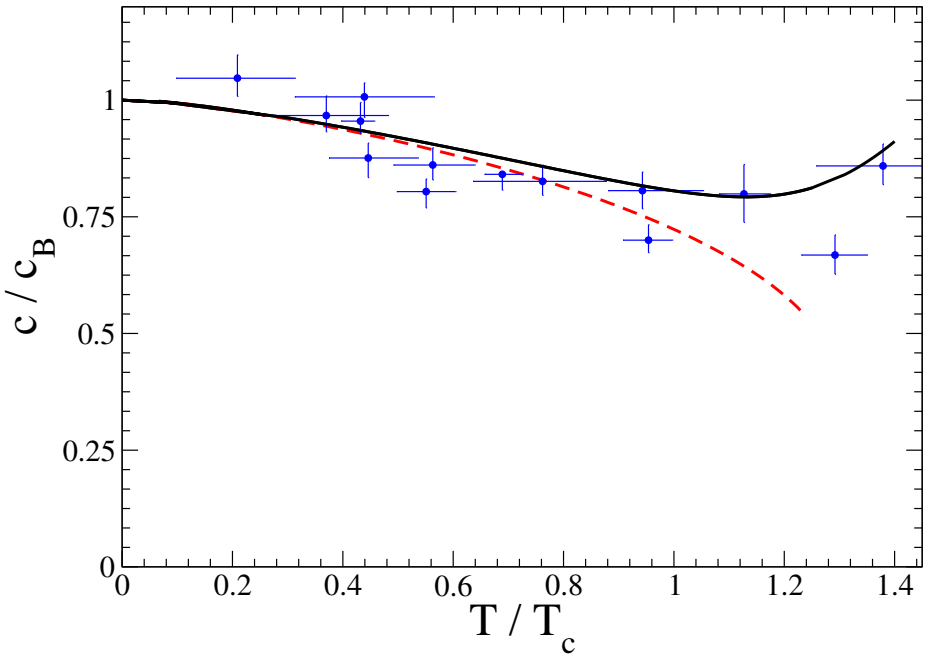

Figure 1.2: Sound velocity c_R in units of $c_B = \sqrt{g_{2D} n/m}$ as a function of the scaled temperature T/T_c for $\tilde{g}_{2D} \simeq 0.16$. The solid black line represents our prediction based on Eqs. (1.138) and (1.139) while the blue dots are the experimental data of Ref. [60]. The red dashed line is obtained by using Eq. (1.138) with $c_I = 0$. On the basis of universal relations [47], for $\tilde{g}_{2D}$ the Berezinskii-Kosterlitz-Thouless critical temperature is $T_c = 0.13\, T_B$.

are compared to experimental data obtained in [60]. We remark the very good agreement between our semi-analytic results and the data points, both in the low-temperature limit and close to the critical temperature. Differently from the prediction based on the two-fluid model [61, 36, 62], our c_R does not exhibit any discontinuity at the Berezinskii-Kosterlitz-Thouless temperature. This fact highlights how the collisionless sound velocity in Eq. (1.138) is not related to any superfluid features of the system.

The red dashed line in Fig. 1.2 has been obtained by neglecting the $\propto c_I$ correction in Eq. (1.138). It is then evident that the perturbation damping (i.e. $c_I \neq 0$) is crucial in determining the exact sound velocity across a wide range of temperatures. In Fig. 1.3 we report the absolute value of c_I as predicted by Eq. (1.139), with c_R given by solution of Eq. (1.138). We remark that Eq. (1.134) and (1.135) are derived by assuming a weakly-damped

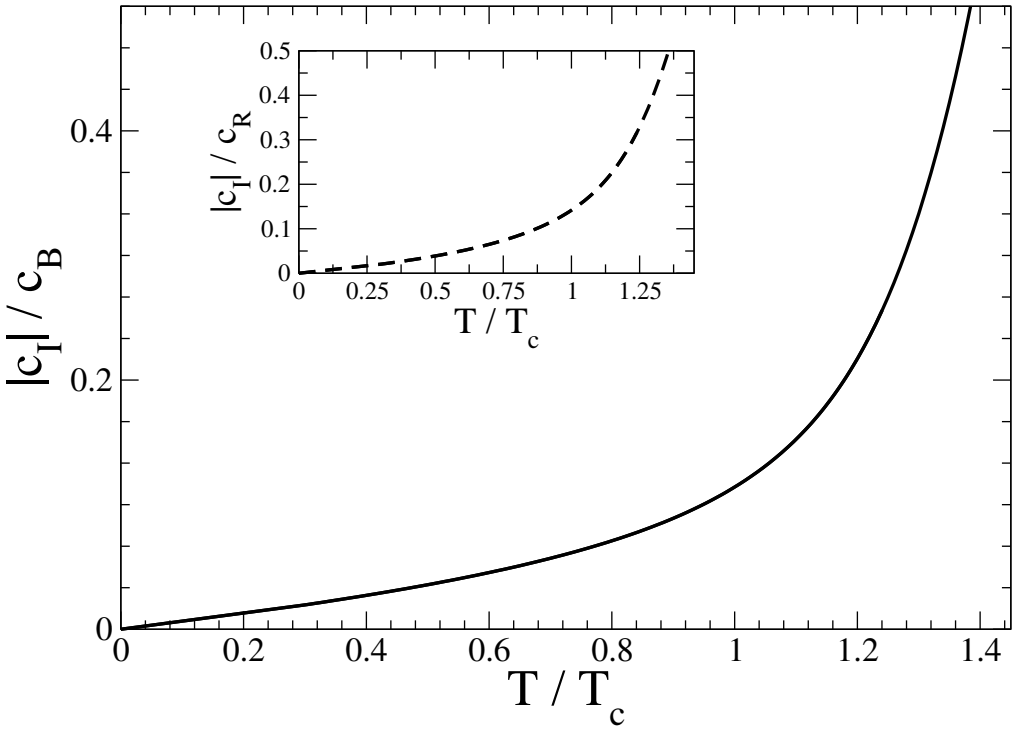

Figure 1.3: *Main panel*: Imaginary part c_I of the sound velocity in units of $c_B = \sqrt{g_{2D}n/m}$ as a function of the scaled temperature T/T_c for $\tilde{g}_{2D} \simeq 0.16$. The solid black line is obtained from Eq. (1.139) where c_R has derived by solving Eq. (1.138). *Inset*: Ratio between the imaginary and the real part of c as a function of the temperature.

perturbation, i.e. $c_I \ll c_R$. From Fig. 1.3 it is evident that our approximation is reliable in the low-temperatures regime, where Landau damping plays a negligible role, but also in the proximity of the transition temperature T_c. The rapid growth of c_I/c_R with the temperature T above T_c is in agreement with the large damping of sound oscillations found in Ref. [60]. A large value of c_I/c_R also signals the breaking of our theoretical scheme.

2

FINITE-RANGE THERMODYNAMICS OF ULTRACOLD BOSONIC GASES

In this chapter we begin to move beyond the zero-range approximation for the atom-atom interaction potential. So far, we have considered a Dirac δ-like pseudopotential and explored some consequences related to this choice, such as the beyond-mean-field equation of state in a generic dimension, the condensate depletion and the superfluid density computed within the Landau two-fluid model. Now, we aim to study a dilute and ultracold Bose gas by considering an effective field theory taking into account a finite-range pseudopotential. Within the formalism of functional integration, we derive beyond-mean-field analytical results depending on the scattering length and the effective range of the interaction. In particular, we calculate the equation of state of the bosonic system as a function of these interaction parameters both at zero and finite temperature including one-loop Gaussian fluctuations. As in the first chapter of this thesis, we do not only focus on the case of $d = 3$ spatial dimensions, but we also analyze the role played by finite-range effects in lower dimensionalities.

■ 2.1 Finite-range thermodynamics for $d = 3$

2.1.1 Zero-range approximation: the thermodynamical instability

Throughout the whole previous chapter, we have reported a detailed description of how one can derive the first beyond-mean-field correction to the equation of state (EoS) of an ultracold and weakly-interacting Bose gas. However, all these results have to be placed inside the context of the zero-range approximation for the atom-atom interaction potential. A first improvement can be made by following the pseudopotential approach. As for the Fermi pseudopotential, we replace the *true* inter-atomic potential with a pseudo one which at least reproduces the low energy scattering properties of the system.

Within the zero-range approximation, in Sec. 1.2 the two-body interaction in Eq. (1.23) is replaced by the δ-like pseudopotential $V_{p,0}(r) = g_0\delta^{(3)}(r)$. In order to highlight the physical meaning of the coupling constant g_0 and to clearly set a characteristic length (or energy) scale, the key-point consists in relating it to scattering parameters that can be measured in cold-atoms experiments with great precision. As mentioned before, one can then follow the procedure detailed in [25, 65], resulting in Eq. (1.26), i.e. $g_0 = \big(4\pi\hbar^2/m\big)a_s$, a_s being the s-wave scattering length. This recipe can be quite naturally extended to systems with lower dimensionalities [8, 66], leading to Eq. (1.34).

The choice of a contact pseudopotential brings us to a local lagrangian as the one in Eq. (1.25), namely

$$\mathcal{L} = \psi^*(\mathbf{r},\tau)\left[\hbar\frac{\partial}{\partial\tau} - \frac{\hbar^2\nabla^2}{2m} - \mu\right]\psi(\mathbf{r},\tau) + \frac{1}{2}g_0|\psi(\mathbf{r},\tau)|^4 \,,$$

where all terms have the same physical meaning of Chap. 1. Below the critical temperature, the starting point to describe the thermodynamics consists in splitting the field $\psi(\mathbf{r},\tau) = v + \eta(\mathbf{r},\tau)$, as in Eq. (1.36). Hence, the mean-field (saddle-point) plus Gaussian (one-loop) approximation is derived by inserting it in Eq. (1.25) and expanding above the saddle-point classical field v up to the quadratic terms in the fluctuations fields η and η^*. This procedure leads us to identify three different contribution to the mean-field grand potential, as detailed in Eq. (1.46). Quantum fluctuations are encoded in the zero-point energy, the integral of the Bogoliubov excitation spectrum over the whole momentum space (cfr. Eq. (1.50)). Through

one of the regularization recipes outlined in Sec. 1.3, a finite contribution can be extracted, reading the beyond-mean-field correction first computed by Lee, Huang and Yang [16]:

$$\frac{\Omega_g^{(0)}}{L^3} = \frac{8}{15\,\pi^2}\left(\frac{m}{\hbar^2}\right)^{3/2}\mu^{3/2}\,. \tag{2.1}$$

It can be worth to interpret this result within a slightly different frame, by remembering that the pressure is nothing else than the opposite of the grand potential density, i.e.

$$P(\mu, T) = -\frac{\Omega(\mu, T)}{L^3}\,. \tag{2.2}$$

At zero-temperature, by taking into account the quantum (Gaussian) fluctuations, we have

$$P^{(0)}(\mu) = \frac{\mu^2}{2\,g_0} - \frac{8}{15\,\pi^2}\left(\frac{m}{\hbar^2}\right)^{3/2}\mu^{3/2}\,. \tag{2.3}$$

In the previous chapter, we have begun to point out unphysical consequences of the zero-range approximantion in modelling the atom-atom interacting. In particular, we mentioned the occuring of UV-divergences in the zero-point energy, related to the fact that Fourier transform $\tilde{V}_{p,0}(\mathbf{q}) = \mathcal{F}\big[V_{p,0}(\mathbf{r})\big] = g_0$ does not vanish at high momenta.

Here, we have to remember another crucial point, namely that we are following a perturbative scheme which, by definition, is reliable only within a precise window of the parameters space. In this case, the breakdown point can be identified exactly by searching for values of μ making the pressure in Eq. (2.3) negative. Actually, the uniform configuration is thermodynamically stable if and only if [67]

$$\frac{\partial^2 P(\mu)}{\partial \mu^2} > 0\,. \tag{2.4}$$

Eq. (2.3) implies thermodynamical instability for $\mu > \mu_c = \pi(\hbar^2/(2m))^{3/4}/\sqrt{2g_0}$. The zero-temperature number density $n^{(0)}$ can be related to μ thanks to the following equation

$$n^{(0)}(\mu) = -\frac{\partial \Omega^{(0)}(\mu)}{\partial \mu} = \frac{\mu}{g_0} - \frac{4}{3\pi^2}\left(\frac{m}{\hbar^2}\right)^{3/2}\mu^{3/2}\,. \tag{2.5}$$

Therefore, we can numerically determine the chemical potential corresponding to given val-

ues of the gas parameter na_s^3. This frame is summarized in Fig. 2.1 where we plot the chemical potential vs. the gas parameter as specified by Eq. (2.5). In absence of finite-range

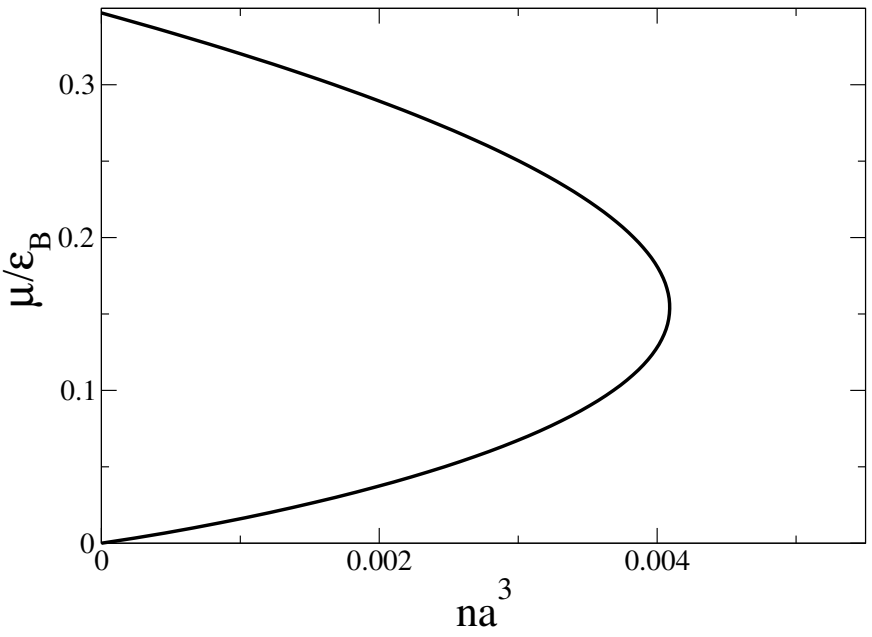

Figure 2.1: Chemical potential as a function of the gas parameter $n\,a_s^3$ within the zero-range approximation by taking into account quantum fluctuations up to the Gaussian level, according to our Eq. (2.5). Energies are expressed in units of $\epsilon_B = \hbar^2/(ma_s^2)$ and a_s is the s-wave scattering length. It is evident that the systems undergoes a thermodynamical instability signalling the breakdown of the zero-temperature perturbative theory.

corrections, it appears clear from Fig. 2.1 that, besides the prediction of two branches for the chemical potential, close to $na_s^3 \simeq 0.004$ a thermodynamic instability occurs since Eq. (2.5) has no more solutions above this critical value. Therefore, the uniform configuration does not exist anymore for $na_s^3 > 0.004$.

A grand canonical formulation clarifies the range of applicability of one simple analytical result that appears naturally in second-quantization many-body theory [10, 67]. Indeed, from Eq. (2.5) by using a perturbative expansion where $g_0 n \ll \mu$, one gets

$$\mu(n) = g_0 n + \frac{4g_0}{3\pi^2}\left(\frac{m}{\hbar^2}\right)^{3/2}(g_0 n)^{3/2}\,. \tag{2.6}$$

The first term of this chemical potential was derived by Bogoliubov [29] while the second term is the one first computed by Lee, Huang and Yang [16, 17]. Keeping in mind the discussion about Eq. (2.5) and Fig. 2.1, it is extremely important to remind that Eq. (2.5) is obtained assuming a very small gas parameter na_s^3. Thus, it cannot give back reliable predictions when the system is thermodynamically unstable. Close to the instability, the contribution of Gaussian fluctuations in Eq. (2.1) becomes of the same order of the mean-field term; this signals that quantum fluctuations are strong enough to destabilize the uniform configuration. Consequently the critical value $(na_s^3)_c \simeq 0.004$ specifies the upper threshold of applicability of the zero-range Gaussian theory and, consequently, of Eq. (2.5).

2.1.2 The finite-range effective potential and thermodynamic results

An improvement of the contact (zero-range) approximation can be achieved by replacing the interaction potential $\tilde{V}(\mathbf{q})$ with the finite-range pseudo-potential

$$\tilde{V}_{p,2}(q) = g_0 + g_2\, q^2 \,. \tag{2.7}$$

The relation with the true inter-atomic potential appearing in Eq. (1.23) is given by the following equations

$$g_0 = \tilde{V}(0) = \int d^3\mathbf{r}\; V(r) \tag{2.8}$$

$$g_2 = \frac{1}{2}\tilde{V}''(0) = -\frac{1}{6}\int d^3\mathbf{r}\; r^2\; V(r) \tag{2.9}$$

where, as usual, we define the Fourier transform of the atom-atom potential as $\tilde{V}(\mathbf{q}) = \int d^3\mathbf{r} \exp(i\mathbf{q}\cdot\mathbf{r})V(r)$. It has been shown [18, 68] that, in real space, the pseudo-potential in Eq. (2.7) is given by

$$V_p(r) = g_0\,\delta(r) - \frac{g_2}{2}\left[\overleftarrow{\nabla}^2\,\delta(r) + \delta(r)\,\overrightarrow{\nabla}^2\right] . \tag{2.10}$$

Within the framework of the effective-field theory (EFT), the connection with experimental quantities such as the s-wave scattering length a_s and the s-wave effective range r_s can be established by requiring that the expansion parameters of Eq. (2.7) matches the ones

obtained with a pseudo-potential $V_p(q)$ depending on the s-wave phase shift. In sec. 1.2.1 we detailed the application of this principle to the zero-range approximation by means of the T-matrix.

As is [18, 19, 65] we adopt

$$\tilde{V}_p(q) = \frac{4\pi\hbar^2}{m}\frac{\tan\left(\delta_0(q)\right)}{q} \ . \tag{2.11}$$

The phase shift $\delta_0(q)$ is related to the s-wave scattering parameters by the equation

$$\delta_0(q) = \arctan\left(\frac{1}{-\frac{1}{a_s} + \frac{1}{2}r_s q^2 + O(q^4)}\right) , \tag{2.12}$$

where r_s is the s-wave effective range of the interaction. One can thus expand $\tilde{V}_p(q)$ and $\delta_0(q)$, respectively Eq. (2.11) and Eq. (2.12), up to the second order for small q. In this way, one finds that the coupling constants g_0 and g_2 are related to the physical parameters a_s and r_s according to following equations

$$g_0 = \frac{4\pi\hbar^2}{m}a_s \ , \tag{2.13}$$

$$g_2 = \frac{2\pi\hbar^2}{m}a_s^2 r_s \ . \tag{2.14}$$

At this point, we can keep track of the finite-range character of interaction by simply performing the steps we have detailed for the zero-range approximation. We then begin by replacing the modified potential given by Eq. (2.7) in the general non-local langrangian reported in Eq. (1.23). One then easily gets

$$\mathcal{L} = \psi^*(\mathbf{r},\tau)\left[\hbar\frac{\partial}{\partial\tau} - \frac{\hbar^2\nabla^2}{2m} - \mu\right]\psi(\mathbf{r},\tau) + \frac{g_0}{2}|\psi(\mathbf{r},\tau)|^4 - \frac{g_2}{2}|\psi(\mathbf{r},\tau)|^2\nabla^2|\psi(\mathbf{r},\tau)|^2 \ . \tag{2.15}$$

The relation between the coupling of the above lagrangian density and the measurable scattering parameters is the key result of an EFT-based approach. The remaining part of this section is then based on this simple generalization of the usual local lagrangian density in Eq. (1.25). A Gaussian (one-loop) analysis relying upon Eq. (2.15) has been performed in Refs. [65, 26], but limited to the perturbative regime at zero temperature. Here we explicitly prove that the inclusion of the effective-range term can remove the *artificial* instability

occuring in the zero-range theory. Therefore, it is possible to extend the applicability range of a Bogoliubov-like theory beyond the critical value pointed out in sec. 2.1.1. Moreover, we compare our EFT calculatons with Monte Carlo data and analyze finite-temperature effects.

As a first and immediate application of the lagrangian density in Eq. (2.15), we can derive a generalized Gross-Pitaevskii equation for the stationary but space-dependent field $\psi_0(\mathbf{r})$. Indeed, we can apply the saddle-point approximation to the action $S[\psi,\psi^*] = \int d\tau \int d^3\mathbf{r}\,\mathcal{L}$, with $\mathcal{L}[\psi,\psi^*]$ given by Eq. (2.15), i.e. $\delta S\big[\psi_0^*(\mathbf{r}),\psi_0(\mathbf{r})\big] = 0$ Stationary configurations are described by the following equation

$$\Big[-\frac{\hbar^2\nabla^2}{2m} + g_0\big|\psi_0(\mathbf{r})\big| - g_2\nabla^2\big|\psi_0(\mathbf{r})\big|^2\Big]\psi_0(\mathbf{r}) = \mu\psi_0(\mathbf{r})\;, \tag{2.16}$$

which was derived for the first time in [68] for a Bose gas trapped under an external confinement. In this case, numerical results based on Eq.(2.16) lead to a better agreement with Quantum Monte Carlo simulations concerning, for instance, the ground state energy. Moreover, by using Eq.(2.16) it is possible to study how space-dependent topological solutions, such as vortex and solitons, are affected by the effective-range expansion [69].

As usual thoroughout this thesis, we split the field as $\psi(\mathbf{r},\tau) = v + \eta(\mathbf{r},\tau)$ and then expand the action $S[\psi,\psi^*]$ around a uniform and stationary v up to quadratic (Gaussian) order in $\eta(\mathbf{r},\tau)$ and $\eta^*(\mathbf{r},\tau)$. The mean-field (saddle-point) can be derived from Eq. (2.16) and Eq. (2.15) by considering a real uniform scalar field, i.e $\psi_0(\mathbf{r}) \to v$. Indeed, from Eq. (2.16) we get the crucial relation between the chemical potential potential and the order parameter. Even by taking into account the finite-range interaction potential in $\mathcal{L}$, up to the saddle-point level it is easy to check that $\mu = g_0 v^2$ as in Eq. (1.39). Similarly, the mean-field grand potential exactly corresponds to Eq. (1.38), i.e. $\Omega_{\rm mf}(\mu,v) = L^3\big(-\mu v^2 + \frac{1}{2}g_0\,v^4\big)$. So, finite-range corrections due to $g_2 \neq 0$ do not affect the uniform mean-field configuration.

We then move to analyze the Gaussian action describing the dynamics of fluctuations. From a formal point of view, moving to the Fourier space we get the analogous of Eq. (1.41)

$$S_g\big[\eta,\eta^*\big] = \frac{1}{2}\sum_Q \begin{pmatrix}\tilde\eta^*(Q) & \tilde\eta(-Q)\end{pmatrix}\,\mathbb{M}(Q)\,\begin{pmatrix}\tilde\eta(Q)\\ \tilde\eta^*(-Q)\end{pmatrix}\;, \tag{2.17}$$

where, for the sake of clarity, we have defined here the 4-vector $Q \equiv (\mathbf{q}, i\omega_n)$. The bosonic

frequencies ω_n are given, as usual, by Eq. (1.3). The crucial difference between the finite-range case and the zero-range approximation is encoded in the inverse fluctuation propagator $\mathbb{M}$ appearing in Eq. (2.17). Indeed, one has

$$\mathbb{M}(\omega_n, \mathbf{q}) = \beta \begin{pmatrix} -i\hbar\omega_n + \frac{\hbar^2 q^2}{2m} - \mu + \left[g_0 + \tilde{V}_p(q)\right] v^2 & v^2\, \tilde{V}_p(q) \\ v^2\, \tilde{V}_p(q) & i\hbar\omega_n + \frac{\hbar^2 q^2}{2m} - \mu + \left[g_0 + \tilde{V}_p(q)\right] v^2 \end{pmatrix} . \tag{2.18}$$

The dispersion relation of excitations above the uniform ground state can be derived by computing the poles of the propagator or, in equivalent terms, the zeros of $\det \mathbb{M}(\mathbf{q}, i\omega_n)$. It results in the following equation

$$E_{\mathbf{q}}(\mu, \psi_0) = \sqrt{\left[\frac{\hbar^2 q^2}{2m} - \mu + v^2(g_0 + \tilde{V}_p(q))\right]^2 + v^4 \tilde{V}_p^2(q)} \, , \tag{2.19}$$

where the dependence on the effective-range r_s is contained in the Fourier transform of the pseudopotential. By using Eq. (1.39) to remove the dependence on v in $E_{\mathbf{q}}$, our theory is consistent with the Goldstone theorem also in presence of a finite-range interaction. Indeed, from Eq. (2.19) we obtain a gapless spectrum

$$E_q(\mu) = \sqrt{\frac{\hbar^2 q^2}{2m}\left[\frac{\hbar^2 q^2}{2m} + \frac{2\mu \tilde{V}_p(q)}{g_0}\right]} = \sqrt{\frac{\hbar^2 q^2}{2m}\left[(1 + \chi\mu)\frac{\hbar^2 q^2}{2m} + 2\mu\right]} \, , \tag{2.20}$$

where the relevance of finite-range effects is controlled by the parameter χ,

$$\chi \equiv \frac{4m}{\hbar^2}\frac{g_2}{g_0} \, . \tag{2.21}$$

By referring to sec. 1.3.1, up to the Gaussian level we have three different contributions to the thermodynamics potential $\Omega(\mu)$: first, the mean-field one $\Omega_{\rm mf}/L^3$ given by Eq. (1.40), which is not modified by the inclusion of the effective range in $\tilde{V}_p(q)$. Then, we have to consider the contribution coming from quantum and thermal fluctuations, respectively $\Omega_g^{(0)}$ and $\Omega_g^{(T)}$ in Eqs. (1.47) and (1.48).

The zero-temperature Gaussian grand potential is still UV-divergent also for finite values of χ. This divergence can be healed by making use of dimensional regularization as in Sec. 1.3.2. In this way, it is easy to check that the zero-temperature Gaussian grand potential is

given by

$$\frac{\Omega_g^{(0)}}{L^3} = \frac{8}{15\pi^2}\left(\frac{m}{\hbar^2}\right)^{3/2}\frac{\mu^{5/2}}{(1+\chi\mu)^2}\,. \tag{2.22}$$

At this point, it is worth to point out an immediate (and maybe trivial) consistency check for our theory: by setting $\chi = 0$ we manage to recover all the results obtained with a contact pseudopotential, namely Eqs. (1.49) and (2.3).

The zero-temperature number density n is obtained by using the number equation $n(\mu) = -\frac{\partial\Omega}{\partial\mu}$ with $\Omega(\mu) = \Omega_{\rm mf}(\mu) + \Omega_g^{(0)}(\mu) + \Omega_g^{(T)}(\mu, T)$. At zero temperature we get

$$n^{(0)}(\mu) = \frac{\mu}{g_0} - \frac{4}{3\pi^2}\left(\frac{m}{\hbar^2}\right)^{3/2}\frac{\mu^{3/2}}{(1+\chi\mu)^2} + \frac{64}{15\pi^2}\left(\frac{m}{\hbar^2}\right)^{5/2}\frac{g_2}{g_0}\frac{\mu^{5/2}}{(1+\chi\mu)^3}\,. \tag{2.23}$$

From Eq. (2.23) we are able determine μ as a function of na_s^3 for different values of χ at fixed density n, in a similar way to what we did for Eq. (2.5). The results are shown in Fig. 2.2, where α is proportional to the ratio g_2/g_0 in adimensional units, namely

$$\alpha = \frac{\hbar^2}{ma_s^2}\chi = 4\frac{g_2}{g_0 a_s^2} = 2\frac{r_s}{a_s}\,. \tag{2.24}$$

As previously discussed, Fig. (2.1) clearly shows that in absence of finite-range corrections ($\alpha = 0$) the chemical potential μ versus n has no solutions above the critical value for the gas parameter $(na_s^3)_c \simeq 0.004$. This problem is indeed solved by using a positive value of α larger than about 0.25, while for $\alpha < 0$ the problem gets worse. The different behaviour of numerical solutions of Eq. (2.23) for $\alpha \neq 0$ compared to Eq. (2.5) can be understood thanks to the modified dependence on μ of Eq. (2.22): for $\alpha \gtrsim 0.25$ the finite-range Gaussian correction never becomes of the same order, or bigger, than the mean field term. Differently from the zero-range case, the finite-range correction manages to control the growth of fluctuations and it stabilizes the system, as highlighted by the dashed and dashed-dotted lines in Fig. (2.2): for these values of α there is no critical value of the gas parameter.

It is then interesting to compare our theory with Quantum Monte Carlo (QMC) simulations performed for a system made of hard-spheres bosons [70] based on the path-integral ground state algorithm. The case of hard spheres is particularly interesting because the s-wave scattering length a_s and effective range r_s are related in a very simple way by $r_s/a_s = 2/3$ [68, 65, 71]. As a consequence, the adimensional parameter α in Eq. (2.24)

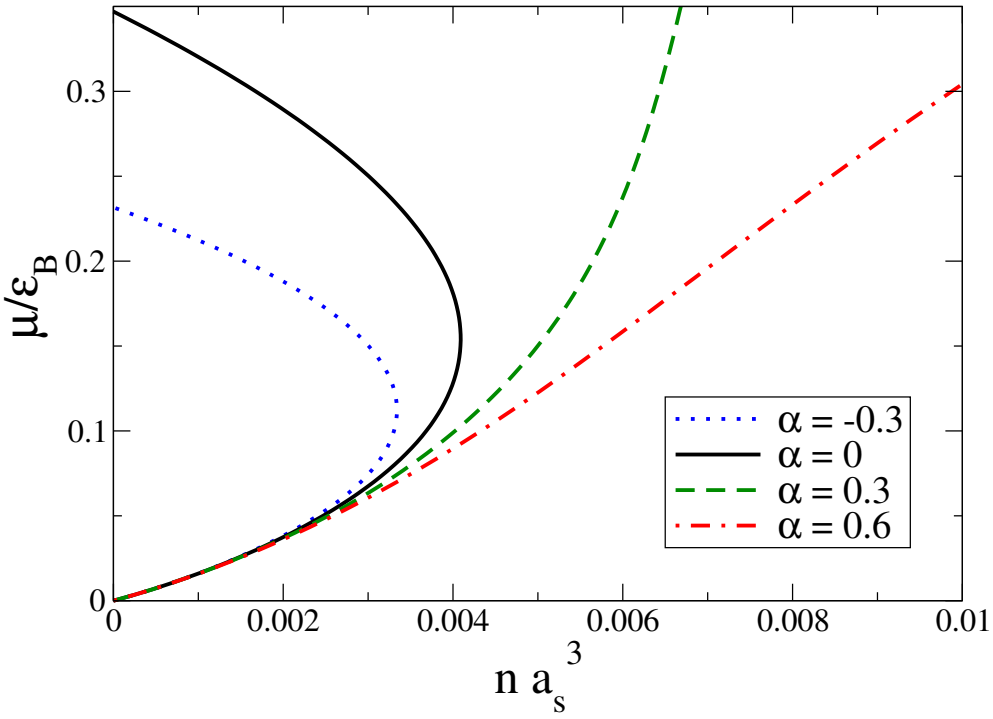

Figure 2.2: Chemical potential μ in units of $\epsilon_B = \hbar^2/(ma_s^2)$ as a function of the gas parameter na_s^3 (cfr Fig.2.1) obtained from Eq. (2.23) for different values of $\alpha = 2r_s/a_s$, where a_s is the s-wave scattering length and r_s the corresponding effective range. The solid black line for $\alpha = 0$ represents the zero-range equation of state as in Eq. (2.5) and Fig. 2.1.

must be set to $\alpha = 4/3$. Fig. 2.3 highlights that the Monte Carlo data (filled circles) are reproduced reasonably well by our EFT results with $\alpha = 4/3$ (solid line) also for values of the gas parameter na_s^3 larger than 0.004. So, we do not only recover the zero-range curve, reliable up to $na_s^3 \simeq 0.004$, but also QMC points for a more dense system. QMC simulations are performed with a hard-core potential while our Gaussian theory introduces an effective range r_s which is related to a_s by $r_s = (2/3)a_s$. In the case of the hard-core potential, at fixed scattering length a_s (and consequently at fixed effective range r_s), by increasing the gas parameter na_s^3, the number density n increases while the average distance $\delta \simeq n^{-1/3}$ between atoms reduces. In this way, by tuning the number density n, it is possible to reduce δ such that it becomes comparable to the effective range r_s. Therefore, deviations from the zero-range framework become sizable and can be revealed while measuring thermodynamic quantities as, for instance, the pressure.

We have to mentioned the relevant fact [72] that beyond the Gaussian level, the thermodynamic potential displays a correction arising from two-loops diagrams proportional to

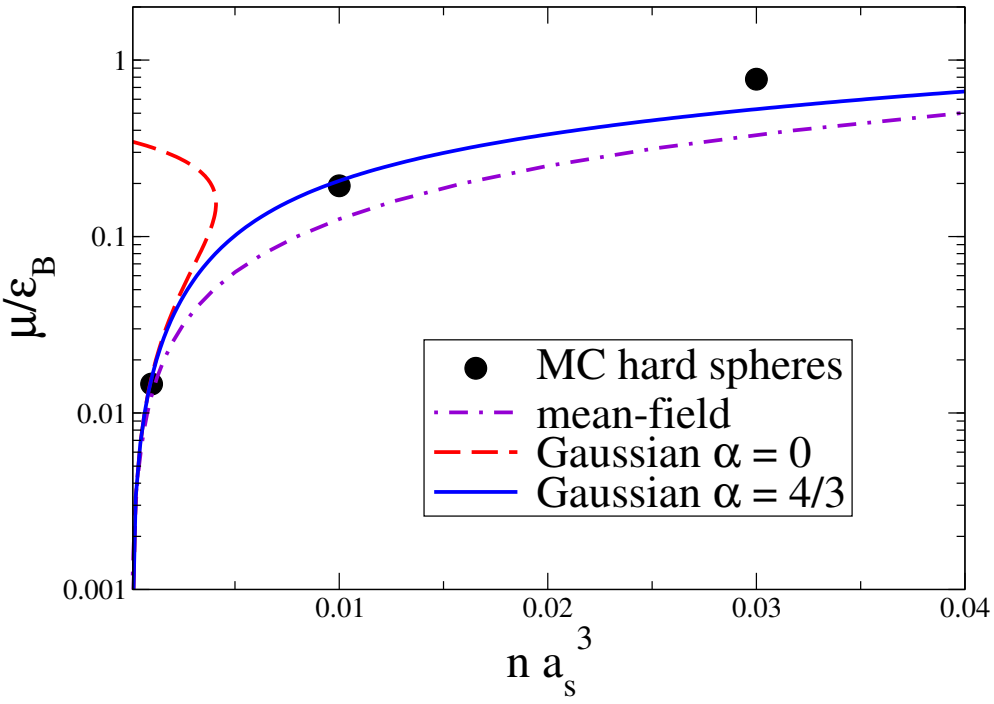

Figure 2.3: Monte Carlo (MC) data (filled circles) of the chemical potential μ vs gas parameter na_s^3 for a Bose gas of hard spheres [70]. Dot-dashed line is the mean-field theory, $\mu = 4\pi\hbar^2 a_s n/m$. Solid and dashed lines are the results of our zero-temperature Gaussian EFT, Eq. (2.23), for two different values of the effective-range adimensional parameter $\alpha = 2r_s/a_s$. The case $\alpha = 0$ corresponds to usual scheme with a zero-range interaction while $\alpha = 4/3$ correspond to the case of a hard-core interaction potential. Also here $\epsilon_B = \hbar^2/(ma_s^2)$ is the characteristic energy of the interacting Bose gas, a_s is the s-wave scattering length, r_s is the effective range, and n is the number density.

na_s^3 whose coefficient is unknown within the zero-range approximation. Braaten and Nieto [72, 25] showed that, in general, a meaningful expression for this coefficient requires at least the knowledge of the three-body interaction strength, i.e. the coupling constant of a term $\propto |\psi|^6$ in the Lagrangian density. Anyway, if one restricts to the case of alkali atoms, the second-order quantum corrections are proportional to the logarithm of an additional length scale fixed by the van der Waals interaction.

In order to complete our analysis concerning the finite-range corrections to the beyond-mean-field equation of state, we have to briefly consider the $T \neq 0$ case. The finite-temperature Gaussian contribution to the equation of state is given by $\Omega_g^{(T)}(\mu)$ in Eq. (1.48).

Through an integration by parts, we can express it in the alternative form

$$\frac{\Omega_g^{(T)}(\mu)}{L^3} = -\frac{1}{6\pi}\int_0^\infty dq\, q^3\, \frac{dE_q}{dq}\frac{1}{e^{\beta E_q(\mu)}-1}\ . \tag{2.25}$$

It is useful to introduce now the variable $x = \beta E_q(\mu)$ which leads us to the following equation

$$\frac{\Omega_g^{(T)}(\mu)}{L^3} = -\frac{1}{6\pi^2\beta}\int_0^\infty dx\, q(x,\mu)^3\frac{1}{e^x-1}\ , \tag{2.26}$$

where $q(x,\mu)$ is given by

$$q(x,\mu) = \sqrt{\frac{2m\mu}{\hbar^2(1+\chi\mu)}}\sqrt{-1+\sqrt{1+\frac{(1+\chi\mu)x^2}{\mu^2\beta^2}}}\ . \tag{2.27}$$

By means of a low temperatures expansion, the integral in the equation above can be computed analytically up to the order $(k_BT)^6$, reading

$$\frac{\Omega_g^{(T)}(\mu)}{L^3} = -\frac{\pi^2}{90}\left(\frac{m}{\hbar^2}\right)^{3/2}\frac{(k_BT)^4}{\mu^{3/2}}\left[1-\frac{5\pi^2}{7}(k_BT)^2\frac{1+\chi\mu}{\mu^2}\right]\ . \tag{2.28}$$

Thus, thanks to a simple derivative, the finite-temperature contribution $n_g^{(g)}$ to the total number density n consists in

$$n_g^{(T)}(\mu) = -\frac{\pi^2}{60}(\frac{m}{\hbar^2})^{3/2}\frac{(k_BT)^4}{\mu^{5/2}}\left(1-\frac{5\pi^2}{21}(k_BT)^2\frac{7+5\chi\mu}{\mu^2}\right)\ . \tag{2.29}$$

Within the perturbative expansion approach ($|\mu - g_0 n| \ll 1$) previously discussed, we can extract the behavior of the chemical potential in terms of the number density

$$\mu(n) = \mu_0(n) + \mu_g^{(0)}(n) + \mu_g^{(T)}(n)\ , \tag{2.30}$$

where $\mu_0(n) + \mu_g^{(0)}(n)$ can be derived by inverting Eq. (2.23). The finite-temperature contribution behaves as

$$\mu_g^{(T)}(n) = -\frac{\pi^2}{60}\left(\frac{m}{\hbar^2}\right)^{3/2}\frac{g_0\,(k_BT)^4}{(g_0n)^{5/2}}\left[1-\left(\frac{5\pi^2}{21}\right)\frac{7+5\chi(g_0n)}{(g_0n)^2}(k_BT)^2\right]\ . \tag{2.31}$$

Our results, namely Eqs. (2.23) and (2.29) generalize the old familiar one obtained in 1958 by Lee and Yang [16, 17].

2.2 Finite-range thermodynamics for $d = 1$

2.2.1 The one-dimensional Bose gas: not a simple toy-model

For almost eighty years one-dimensional (1d) quantum systems have been subject of an intense fascination, albeit mostly theoretical. Indeed, from the seminal work of Bethe in 1931 concerning the Heisenberg model [73], 1d physics was then explored in great detail, providing exact and approximate solutions to a wide variety of systems [74]. These 1d physical systems were considered toy models, until recent advances in experimental setups, like Josephson nano-junctions [75, 76] and magneto-optical trapping of cold atoms [77, 78, 79, 80], have achieved the realization of 1d quantum fluids.

Cold atoms experiments proves to be extremely fruitful because of the possibility to realize these systems in an extremely well-monitored environment [81, 82] where the most relevant parameters can be tuned with a precision never seen before. Together with these recent groundbreaking experimental advances, theoretical studies over the years have shown that 1d quantum fluids display a significantly rich phenomenology. At the same time, the analytical effort to adequately model and describe them is not too burdensome, thanks to the presence of only one spatial dimension. A similar point can be obviously made about numerical simulations. Keeping in mind all these peculiar features, 1d quantum fluids are extraordinary candidates to answer a lot of textbook questions about, for instance, non-equiibrium statistical mechanics and quantum transport [83, 84, 85].

The basic theoretical tools for 1d bosonic systems consists in the Lieb-Lininger equations (LL), providing an exact description of $T = 0$ K thermodynamic quantities [86, 87], while approximated analytical expressions and numerical results at finite temperature can be extracted from the Yang-Yang theory [88, 89], which obviously recovers the LL one at zero temperature. As for 3d weakly interacting Bose gases, the first step in modelling the interaction potential passes through a Fermi δ-like potential. Therefore, it is not surprising that the resulting thermodynamics is universal, since the only dependence from the inter-

atomic potential is via a properly defined scattering length. However, as mentioned in sec. 2.1.2, deviations from universality due to the finite-range potential have been shown to be quite relevant for a better understanding of static and dynamical properties of 3d Bose gases [90, 65, 18, 68, 91, 26, 19, 92, 93, 94, 69, 67]. Finite-range effects naturally arise by modelling the two-body interactions beyond the unphysical zero-range approximation. In systems with lower dimensionalities, their role can be become much more interesting, since they naturally affect the beyond-mean-field terms in the equation of state. Within a perturbative field-theory framework, they enter in the loops corrections to the saddle-point classical solution.

The most interesting situation is surely the $d = 2$ case, briefly described in the next section. As recently shown in [28], since finite-range corrections affect the behavior of quantum and thermal fluctuations, they have to be taken into account also in lower dimensional system, where fluctuations are naturally strongly enhanced (Mermin-Wagner-Hohenberg theorem [12, 13]).

A detailed analysis, both analytical and numerical, about the role of fluctuations is mandatory, since improvements in cold-atoms experiments are providing a precision benchmark which makes possible to explore in great details beyond-mean-field effects [77, 78, 95, 96]. Concerning the relevance of fluctuations in ultracold quantum fluids, the most immediate consequence consists in deviations from mean-field predictions for thermodynamic quantities like, for instance, pressure [67], chemical potential or the condensate fraction. Since we work actually in a perturbative scheme, it seems also natural to guess that these deviations are present but not so crucial. Fortunately, this is not the whole story; indeed, it was recently shown, both theoretically and experimentally, that quantum fluctuations provides a stabilization mechanism against collapse, as predicted by the mean-field theory, both in dipolar condensate and binary Bose mixture [97, 98, 99, 100, 101].

Moreover, we have to add the possibility offered by Feshbach resonances: in actual experiments one can reach and explore regimes where the effective range of interaction is comparable the scattering length. In these situations, a universal GPE-based description is no more reliable, and one has to consider finite-range corrections. These peculiar situations, which aroused a lot of interest in the last ten years, will be deeply analyzed in the proceeding of the thesis, with particular focus on the dipole-dipole interaction (for a preliminar review about this issue we refer to [102]).

In this section, mainly based on our work in [103], we investigate the role of non-universal corrections to the thermodynamics of the 1d Bose gas, both at zero and finite temperature. By following the effective-field-theory scheme [65, 18, 67, 28, 25], we derive a novel equation of state, taking into account the finite-range character of the atom-atom interaction potential.

Similarly to sec.2.1.1, these corrections are computed at Gaussian (one-loop) level, where non-physical divergences are removed by using dimensional regularization. However, differently from the $d = 3$ case, one-dimensional quantum systems are endowed with the exact theory developed by Lieb and Lininger, providing a strong benchmark to evaluate our results.

Our Gaussian theory reproduces extremely well the LL equation of state from weak up to intermediate couplings [103]. Finite-range effects are then analyzed by considering measurable quantities such as the grand potential, the pressure and the sound velocity.

2.2.2 Effective field theory for the one-dimensional Bose gases

The Euclidean Lagrangian density of identical bosonic particles of mass m and chemical potential μ in a 1D configuration is our starting point. Similarly to the $d = 3$ case, it is given by [1, 2, 3]

$$\mathcal{L} = \psi^*(x,\tau)\left[\hbar\partial_\tau - \frac{\hbar^2}{2m}\frac{\partial^2}{\partial x^2} - \mu\right]\psi(x,\tau) + \frac{1}{2}\int dx'|\psi(x',\tau)|^2 V(|x-x'|)|\psi(x,\tau)|^2 \ , \quad (2.32)$$

where the complex field $\psi(x,\tau)$ describes the bosons, whose two-body interaction potential is represented by $V(|x-x'|)$.

In Chap. 1, within a functional formalism, we have derived the Bogoliubov theory for an ultracold and dilute Bose gas by approximating the atom-atom interaction with a zero-range pseudopotential as in Eq. (1.24). In the first part of this chapter we have extended our analysis by including finite-range corrections solving the emergences of a spurious thermodynamic instability. So, we aim to proceed in a similar way for the $d = 1$ case. In order to analyze the role played by the finite-range corrections, let us begin by considering a low-momentum expansion for interaction potential, namely

$$\tilde{V}_p(q) = g_0 + g_2 q^2 + \mathcal{O}(q^4) \ , \quad (2.33)$$

where $\tilde{V}_p(q)$ has the obvious meaning of the Fourier transform of the interaction potential. As in Eq. (2.7), we aim to generalize the constant behaviour (in the Fourier space) of the Fermi pseudopotential [26]. Following the spirit of the effective-field-theory, the crucial point in this analysis consists in connecting the coupling constants g_0 and g_2 to physical and measurable parameters like the 1d scattering length and the corresponding effective range.

In this section we use a slightly different technique respect to sec. 2.1.2, by explicitly making use of the t-matrix technique [2] instead of relying upon a proper pseudopotential (cfr. Eq. (2.11)). In order to fulfill these premises, we begin by recalling some notions from the scattering theory [104]. In particular, for $d = 1$ we do not have to deal with additional complications due to the expansion in partial waves, but we simply consider the scattering amplitude for the even scattered wavefunction. This amplitude can be expressed in terms of a phase shift

$$f_0(q) = q e^{i\delta_0(q)} \sin \delta_0(q) \; . \tag{2.34}$$

Similarly to the three-dimensional case, it holds a relation between the phase shift, the scattering length and the effective range, namely [104]

$$q \tan \delta_0(q) = \frac{1}{a_s} + \frac{1}{2} r_e q^2 + \mathcal{O}(q^4) \; . \tag{2.35}$$

We have to underline that the equation above has not to be confused with its 3d corresponding in Eq. (2.12). By assuming that the most relevant scattering processes in the systems are the ones described by $f_0(q)$ as in Eq. (2.34), the t-matrix defined in Eq. (1.27) is then approximated by

$$T_0(q) \simeq -\frac{2\hbar^2}{m} f_0(q) \; . \tag{2.36}$$

At the same time, the Lippmann-Schwinger equation for t-matrix reads the formal solution in terms of operators

$$\hat{T} = \left[\frac{1}{\hat{V}} - \frac{1}{E - \hat{H}_0} \right]^{-1} \; , \tag{2.37}$$

where $\hat{V}$ is the interaction operator and $\hat{H}_0$ the free Hamiltonian. Moving to a basis in which

$\hat{H}_0$ is diagonal, in the limit of low momenta, Eq. (2.37) reads [2, 65, 103]

$$T_0(q) = \left[\frac{1}{\tilde{V}(q)} - \frac{m}{2\pi\hbar^2}\int \frac{dp}{p^2 - q^2 + i\kappa}\right]^{-1} . \tag{2.38}$$

In the equation above κ has to be intended as a limit procedure $\kappa \to 0^+$ which has to be taken after the calculation of the integral. It is easy to check that its inclusion is crucial to remove the singularities along the integration path, consenting the application of the residue theorem. More precisely, we have to compute an integral of the following kind

$$\mathcal{I} = \int_{-\infty}^{+\infty} \frac{dp}{p^2 - q^2 + i\kappa} \tag{2.39}$$

whose poles are given by $p^2 = q^2 - i\kappa \equiv z$. In order to apply the residue theorem, we are required to identify the position of the isolated poles in the complex plane. The square root of the complex number z is provided by the De Moivre formula, such that in polar coordinates we get $\sqrt{z} = |z|^{1/2}\exp(i\theta/2)$. The modulus of z is easy to compute, i.e. $|z| = q^2\sqrt{1 + \kappa^2/q^4} \simeq q^2 + \kappa^2/(2q^2)$. On the other hand, the phase can be expressed as $\theta = -\arctan(\kappa/q^2) \simeq -\kappa/q^2$. Thus, the poles of $\mathcal{I}$ are found to be

$$p_{1,2} \simeq \pm\sqrt{q^2 + \frac{\kappa^2}{2q^2}}\left[\cos\left(\theta/2\right) + i\sin\left(\theta/2\right)\right] \simeq \pm q\left(1 - i\frac{i\delta}{2q^2}\right) , \tag{2.40}$$

one in the upper half-plane, the other in the lower one. Since the integrand function falls off as $1/|p|^2$, the contour can be closed indifferently upper or down. The residue theorem is then applied, leading to the final result

$$\frac{m}{2\pi\hbar^2}\int_{-\infty}^{+\infty} \frac{dp}{p^2 - q^2 + i\kappa} = -\frac{im}{2\hbar^2 q} . \tag{2.41}$$

By replacing Eq. (2.41) in Eq. (2.38) and taking $\tilde{V}(q)$ as in Eq. (2.33), we get

$$T_0(q) = \left[\frac{1}{g_0} - \frac{g_2 q^2}{g_0^2} + \mathcal{O}(q^3) + \frac{im}{2\hbar^2 q}\right]^{-1} . \tag{2.42}$$

On the other hand, we have an explicit equation for $T_0(q)$ involving the phase shift and consequently, thanks to Eq. (2.35) and the identity $e^{i\delta}\sin\delta = 1/(\cot\delta - i)$, Eq. (2.36) leads

us to the following alternative expression

$$T_0(q) = -\frac{2\hbar^2}{m}\left[a_s - \frac{1}{2}r_e a_s^2 q^2 + \mathcal{O}(q^3) - \frac{i}{q}\right]^{-1} . \tag{2.43}$$

By matching Eq. (2.42) and Eq. (2.43), it is then possible to derive an equation for the coupling constants in the 1d Lagrangian density, i.e.

$$\begin{aligned} g_0 &= -\frac{2\hbar^2}{m a_s} , \\ g_2 &= -\frac{\hbar^2}{m} r_e . \end{aligned} \tag{2.44}$$

We remark that our EFT procedure recovers the familiar result for the 1D coupling constant g_0 [105, 106] and a remarkably simple formula relating g_2 to r_e. A similar procedure to get a relationship between g_2 and r_e has been used for the 3D Bose gas [67, 65], while in 2D the connection between g_2 and r_e is much more complicated due to a logarithmic dependence on momentum in the t-matrix.

2.2.3 Thermodynamic properties

After having clarified the relation between the EFT coupling constants and the scattering parameters, the derivation of the finite-range thermodynamics can proceed as in the previous parts of the thesis. We aim to compute, as usual, the thermodynamic potential as the logarithm of the partition function, $\Omega = \beta^{-1} \log \mathcal{Z}$, with $\mathcal{Z}$ defined as the functional integral over the whole set of possible configuration for the bosonic field $\psi(x, \tau)$. The perturbative framework is developed around the splitting $\psi(x, \tau) = v + \eta(x, \tau)$, where one has to expand the action around the saddle-point trajectory up to the Gaussian order in η and η^*.

Since we have already detailed all the technical steps involved in the calculation, we now simply report the final result. For $d = 1$ the Gaussian grand potential is still given by Eq. (1.46), namely

$$\Omega(\mu, v) = \Omega_{\mathrm{mf}}(\mu, v) + \Omega_g^{(0)}(\mu, v) + \Omega_g^{(T)}(\mu, v, T) .$$

The saddle-point equation relating μ and v^2 remains $\mu = g v^2$ as stated by Eq. (1.39) so we still get, at the mean-field level, $\Omega_{\mathrm{mf}} = -\mu^2/(2g_0)$. Since $\Omega(\mu)$ is defined as the opposite of

the pressure, we then have the basic result

$$P_{\rm mf} = \frac{\mu^2}{2g_0} \,, \tag{2.45}$$

which is not affected by any finite-range corrections, as we already know from the previous section. This extremely simple results perfectly reproduces the LL outcome for weak coupling. The double contribution to $\Omega(\mu)$ arising from Gaussian fluctuations counts zero-point energy in Eq. (1.47) and its finite temperature counterpart in Eq. (1.48). They both contain the spectrum of excitations above the uniform mean-field configuration which is, in general, given by Eq. (2.20), made gapless by inserting Eq. (1.39) in it.

As usual, by means of the dimensional regularization, we can heal the UV divergence in the zero-point energy. This leads us to the zero-temperature Gaussian contribution for the pressure $P(\mu)$, i.e.

$$P_g^{(0)}(\mu) = \frac{2}{3\pi}\sqrt{\frac{m}{\hbar^2}}\,\frac{\mu^{3/2}}{1+\chi\mu} \,, \tag{2.46}$$

with the definition $\chi = (4m/\hbar^2)g_2/g_0$ like in Eq. (2.21). It is interesting to note that the contribution of quantum fluctuations has an opposite sign compared to its 3-d counterpart in Eq. (2.22). This is not a secondary fact, since it has been recently shown that it changes significantly the scenario of droplet formation at the mean-field stability threshold for binary Bose mixture [98]. This beyond-mean-field Gaussian contribution depends explicitly on the parameter χ in Eq. (2.21), then finite-range effects are acting up to this level of approximation.

The zero-temperature number density n of the system is immediately derived from

$$n = \frac{\partial}{\partial\mu}\left[P_0(\mu) + P_g^{(0)}(\mu)\right] \tag{2.47}$$

and the corresponding speed of sound reads

$$c_s = \sqrt{\frac{n}{m}\frac{\partial\mu}{\partial n}} \,. \tag{2.48}$$

Again, the consistency of our theory can be effectively checked by comparing it to the exact picture derived from the LL formalism [86, 87]. The latter is universal since no other length

scale plays a role in the thermodynamic pictures besides the scattering length. In order to match the original zero-range assumption for the interaction, in the upper panel of Fig. 2.4 we report the sound velocity as predicted by our Gaussian theory (solid black line) by setting $\chi = 0$ in Eq. (2.46) and comparing it to the solution of LL equations (dashed red line). The zero-range interaction strength can be characterized by the parameter $\gamma \equiv (mg_0)/(\hbar^2 n)$ [106, 107]. As evident from Fig. 2.4, our Gaussian theory considerably refines the mean-field result derived from Eq. (2.46), namely $c_s^{(mf)}(\gamma) = \hbar n\sqrt{\gamma}/m$, which is reliable only in the weak-coupling limit (dotted line in the upper panel). Quite remarkably, the range of applicability of our Gaussian theory is up to $\gamma \simeq 10$. Only the very strong coupling (Tonks-Girardeau) regime of impenetrable bosons is not captured by the Gaussian theory, despite an interesting (but merely qualitative) trend agreement.

In the lower panel of Fig. 2.4 we plot the behavior of our Gaussian sound velocity for different values of the finite-range adimensional parameter $\alpha = (\hbar^2\chi)/(ma_s^2) = 4r_e/a_s$. The figure clearly shows that the inclusion of finite range effects deeply affects the zero-temperature sound velocity: at fixed zero-range strength the sound velocity becomes larger with a positive effective range, while the opposite happens for a negative effective range.

As previously stated, enhanced quantum fluctuations play a crucial role in low-dimensional atomic quantum gases [12, 13], since they cannot be effectively controlled by lowering the temperature. Thus, the usual mean-field scheme is particularly inadequate for systems with low dimensionalities: it is mandatory to include at least Gaussian fluctuations in the thermodynamic and dynamical description provided, respectively, by the grand potential $\Omega(\mu)$ and the Gross-Pitaevskii equation (GPE).

It has been shown that these corrections deeply affects the stability of 2D and 1D Bose-Bose mixtures, enabling a transition from the homogeneous ground state to liquid-like self-bound states [97, 98]. Despite the fact that in the proceeding of the thesis we are going to deeply focus only on three-dimensional binary Bose mixtures, it is worth to underline that Gaussian fluctuations are not only responsible for deviations from the mean-field scheme, but they can drive the nucleation of new quantum phases. The recent observation of a new peculiar quantum phase at the mean-field collapse threshold is the most striking evidence of the existence of these, in a certain sense *mystical*, fluctuations. We are going to deepen this point in the next chapters.

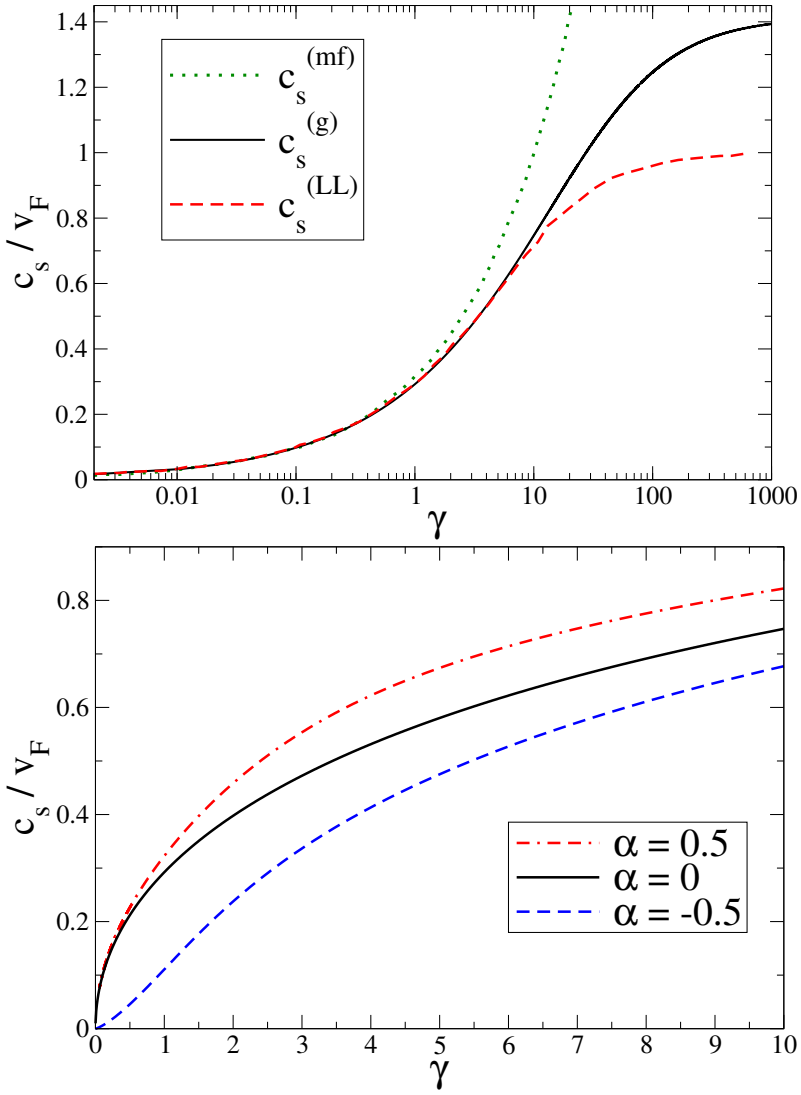

Figure 2.4: Upper panel: Zero-temperature sound velocity in units of the Fermi velocity $v_F = \hbar\pi n/m$ as a function of the adimensional zero-range interaction parameter $\gamma = (mg_0)/(\hbar^2 n)$ [108, 107]. We compare our Gaussian sound velocity $c_s^{(g)}$ (solid line), with the exact solution of LL equation [107] (dashed line), and the mean-field result $c_s^{(mf)}$ (dotted line). Lower panel: Gaussian sound velocity for different values of the adimensional parameter $\alpha = \hbar^2\chi/(ma_s^2) = 4r_e/a_s$, which encodes the role played by the finite range of the inter-atomic potential.

Moreover, Fano-Feshbach resonances now enable a precise fine tuning of the interaction parameters, the effective range r_e being among them. Finite-range effects can then be greatly enhanced and this pushes experiments towards regime where a universal picture is not sufficient [91, 19, 94]. Indeed, dynamical analysis based upon a GPE-like framework are reliable only under a precise separation among the length scales characterizing the system,

namely $r_e \ll a_s \ll \delta$, with δ being the average distance between atoms.

In regimes where $r_s \approx a_s$, deviations from universality are relevant, and every dynamical picture of the system has to take into account Gaussian finite-range corrections modelled according to our Eq. (1.47). In present experiments one can tune the scattering length a_s and in turn the adimensional parameter $\alpha = 4r_e/a_s$. Meanwhile, the effective range r_e remains practically fixed at $\sim 10^{-10}$ m, generally smaller than a_s. Then, there is nothing that prevents us from the experimental observation of the nontrivial behavior of the sound velocity c_s given by Eq. (2.48), reported in the lower panel of Fig. 2.4. Indeed, by fixing a value of the magnetic field for the Feshbach resonances, and consequently a_s and r_e, one can use the number density as a knob to tune the adimensional interaction parameter γ.

It is likewise possible to regard our thermodynamic description of 1d bosonic quantum gases as complementary to the one in [109]. There, collective excitations of a one-dimensional Bose gas were analyzed by following a hydrodynamic framework based on a GP-like equation. However, their theory is not a pure mean-field scheme, since the chemical potential was phenomenologically modelled around the LL exact solution.

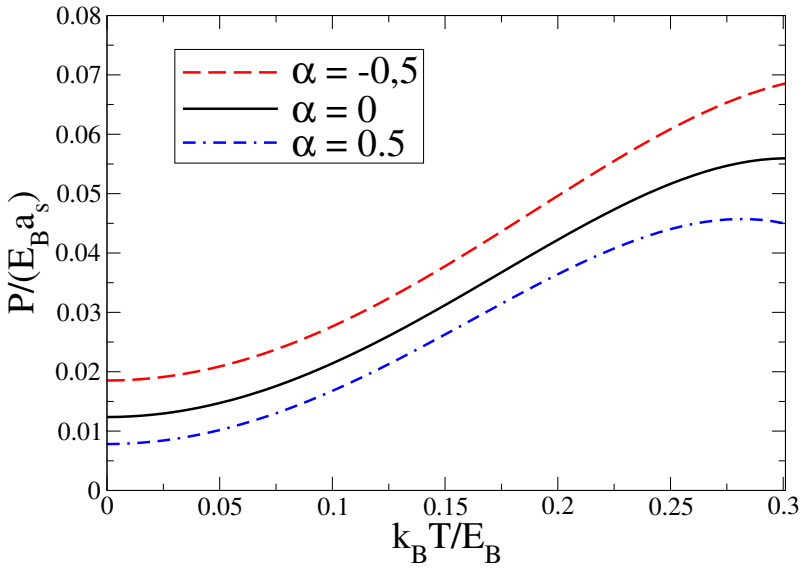

Figure 2.5: We plot the pressure $P(\mu, T)$ in Eq. (2.53), with $k_B T$ in units, and μ in units of $E_B = \hbar^2/(m a_s^2)$, at the fixed value $\mu/E_B = 0.3$. We consider three different values of the adimensional parameter $\alpha = 4r_e/a_s$. The case $\alpha = 0$ corresponds to the zero-range approximation of the inter-atomic potential.

Similarly to sec. 2.1.2, we conclude by deriving the thermal fluctuations contribution.

In the continuum limit, by taking the opposite of Eq. (1.48) for $d = 1$, the correction to the pressure is given by

$$P_g^{(T)}(\mu, T) = \frac{1}{\pi} \int_0^{+\infty} dq\, q \frac{\mathrm{d}E_q}{\mathrm{d}q} \left(\frac{1}{e^{\beta E_q} - 1} \right) . \tag{2.49}$$

Thanks to usual change of integration variable, i.e. $x = \beta E_q(\mu)$, one gets

$$P_g^{(T)}(\mu, T) = \frac{1}{\pi\beta} \int_0^{+\infty} dx\, q(x) \frac{1}{e^x - 1} \tag{2.50}$$

where

$$q(x) = \sqrt{\frac{2m\mu}{\hbar^2(1+\chi\mu)}} \sqrt{-1 + \sqrt{1 + \frac{(1+\chi\mu)x^2}{\mu^2}(k_B T)^2}} . \tag{2.51}$$

By inserting Eq. (2.51) in Eq. (2.50), a low-temperatures expansion leads us to the following final result

$$P_g^{(T)}(\mu, T) = \frac{\pi}{6} \sqrt{\frac{m}{\hbar^2\mu}} (k_B T)^2 \left[1 - \frac{\pi^2}{20} \frac{1+\chi\mu}{\mu^2} (k_B T)^2 \right] . \tag{2.52}$$

So, by recalling Eq. (2.45) and Eq. (2.46), the grand canonical ensemble pressure is given by

$$P(\mu, T) = P_0(\mu) + P_g^{(0)}(\mu) + P_g^{(T)}(\mu, T) . \tag{2.53}$$

In Fig. 2.5 we report the pressure P as a function of temperature T at fixed chemical potential μ for three values of the finite-range adimensional parameter $\alpha = 4r_e/a_s$, obtained from Eq. (2.52). At finite temperature non-universal effects slightly increase as ratio $(k_B T/\mu)^4$ grows. This is explained by recalling that the details of the inter-atomic potential become more relevant when atoms scatter at higher energy.

■ 2.3 Finite-range thermodynamics for $d = 2$

In this concluding section, we are left with the two-dimensional case. We have already pointed out that, from a technical point of view, this is the most difficult situation: the usual ψ^4-model foresees exactly $d = 2$ as its critical dimension, where fluctuations growth undergoes an outbreak. This obviously prevents the formation of an ordered phase and consequently the *true* long-range order characterising the Bose-Einstein condensation [6, 37].

This peculiar situation affects the possibility to describe the two-dimensional Bose gases within a perturbative framework. As highlighted by Fisher and Hohenberg [43], the usual perturbative parameter for dilute gases is given by $n^{(d-2)/d}a_s$ which is identically null for $d = 2$. In [110] Schick derived for the first time a reliable equation of state, which displays a peculiar non-polynomial behaviour. These preliminar results were significantly improved by Popov, who was the first to propose a generalized diagrammatic theory, tackling down the divergences occuring in the Bogoliubov approach. While these relevant technical topics are not discussed in this thesis, one has to keep in mind that a field-theory description of two dimensional superfluid is still an ongoing research topic, also in the weakly interacting regime [111, 112, 113, 28]. In particular, finite-range effects on the equation of state of a 2d Bose gases has been investigated for the first time in [28] within a functional formalism. Let us then consider a Lagrangian density $\mathcal{L}$ with a generic two-body interaction $V(r)$, whose Fourier transform is defined as $\tilde{V}(q)$. At low momenta, it is possible to consider the expansion in Eq. (2.7), namely $\tilde{V}(q) \simeq g_0 + g_2 q^2$. The resulting theory is defined by

$$\mathcal{L} = \psi^*(\mathbf{r},\tau)\left(\hbar\partial_\tau - \frac{\hbar^2\nabla^2}{2m} - \mu\right)\psi(\mathbf{r},\tau) + \frac{g_0}{2}|\psi(\mathbf{r},\tau)|^4 - \frac{g_2}{2}|\psi(\mathbf{r},\tau)|^2\nabla^2|\psi(\mathbf{r},\tau)|^2 \,. \quad (2.54)$$

It is immediate to check that the coupling constant of $\mathcal{L}(\psi,\psi^*)$ are defined, in terms of the the original potential $V(r)$ as

$$g_0 = \tilde{V}(0) = \int d^2\mathbf{r}\, V(r) \quad (2.55)$$

and

$$g_2 = \frac{1}{2}\tilde{V}''(0) = -\frac{1}{4}\int d^2\mathbf{r}\, r^2\, V(r) \,. \quad (2.56)$$

At this point, one should try to give an expression of the constants defined above in terms of the scattering parameters. This is certainly one of the possible way to proceed, but in $d = 2$ these relations are highly non-linear, with a non-polynomial dependence on the momentum q [21, 114]. In order to provide a more limpid analysis and a length scale for the interaction range, we follow an alternative path, by defining the characteristic range as in [28]:

$$R^2 = 4\left|\frac{g_2}{g_0}\right| = \left|\frac{\int d^2\mathbf{r}\, r^2 V(r)}{\int d^2\mathbf{r}\, V(r)}\right| \,. \quad (2.57)$$

Depeding on the potential we choose, we get a certain dependence of R on the length scale entering in $V(r)$. For instance, by assuming $V(r) = V_0 e^{-r^2/\sigma^2}$, the characteristic range in Eq. (2.57) reads $R = \sigma$, which depends only on the gaussian width and not on the strength V_0. In [28] Eq. (2.57) is computed also the for the square-well potential and the Yukawa one, finding that the independence from the strength V_0 holds for all these three choices.

Defining the finite range of the interaction potential as in Eq. (2.57) marks a relevant difference between this section and the previous two. After having clarified this issue, we are then ready to start the usual machinery. By expanding Eq. (2.54) above the saddle-point configuration $\mu = g_0 v^2$, up to the Gaussian order in the fluctuations fields, we can derive the well-known equations for the grand potential. For the sake of clarity, we report them in the following,

$$\begin{aligned}
\frac{\Omega_{\rm mf}}{L^2} &= -\frac{\mu^2}{2g_0} \\
\frac{\Omega_g^{(0)}}{L^2} &= \frac{1}{2}\int \frac{d^2\mathbf{q}}{(2\pi)^2} E_q \\
\frac{\Omega_g^{(T)}}{L^2} &= -\frac{1}{4\pi}\int_0^{+\infty} dq\, q^2 \frac{\mathrm{d}E_q}{\mathrm{d}q}\left(\frac{1}{e^{\beta E_q}-1}\right)
\end{aligned}$$

where the gapless Bogoliubov spectrum is given by Eq. (2.20)

$$E_q(\mu) = \sqrt{\frac{\hbar^2 q^2}{2m}\left[(1+\chi\mu)\frac{\hbar^2 q^2}{2m} + 2\mu\right]}\,.$$

Differently from the previous section let us now mention first the finite-temperature Gaussian grand potential. The reason is that the calculation proceeds exactly in the same way of the $d = 3$ and $d = 1$ case. By changing variable to $x = \beta E_q$, one has to solve the following integral

$$\frac{\Omega_g^{(T)}}{L^2} = \frac{1}{4\pi\beta}\int_0^{+\infty} dx\, q(x)^2 \frac{1}{e^x - 1}\,, \tag{2.58}$$

with $q(x)$ given by Eq. (2.27). At low temperatures, we get the analytical expression

$$\frac{\Omega_g^{(T)}}{L^2} = -\frac{m}{4\pi\hbar^2}(k_B T)^3\left[\Gamma(3)\zeta(3) - \Gamma(5)\zeta(5)\frac{1+\chi\mu}{4\mu^2}(k_B T)^2\right], \tag{2.59}$$

where $\zeta(x)$ is the Riemann zeta function.

On the contrary, the zero-temperature contribution $\Omega_g^{(0)}$ has to be treated with much

more attention than in the previous section. As in sec. 1.3.2, we can note that dimensional regularization does not succeed in healing the UV divergence in the zero-point energy since the outcome is proportional to $\Gamma(-2) \to +\infty$. Therefore, in order to properly extend the integral to a generic complex dimension, we consider a sort of ϵ-expansion: we take $d \to \mathrm{D} = 2 - \epsilon$, with the displacement from the desired dimensionality ϵ has to be intended as a limit procedure to take at the end of the computation, i.e. $\epsilon \to 0^+$. Thus, this dimensional generalization leads us to the following, still divergent, contribution

$$\frac{\Omega_g^{(0)}}{L^{\mathrm{D}}} = -\frac{m}{4\pi\hbar^2(1+\chi\mu)^{3/2}\,\kappa^\epsilon}\Gamma\bigg(-2+\frac{\epsilon}{2}\bigg)\,. \tag{2.60}$$

In the equation above, κ is an arbitrary inverse length scale appearing for dimensional reasons. We notice that if the spectrum E_q had been gapped, the gap would have appeared in place of κ [1]. The parameter χ defined in Eq. (2.21) depends only on the ratio g_2/g_0, then its dimension is not affected by the shifting to $\mathrm{D} = 2 - \epsilon$ [28]. Up to the leading order $1/\epsilon$, $\Gamma(-2+\epsilon/2) = 1/\epsilon + \mathcal{O}(1)$, so

$$\frac{\Omega_g^{(0)}}{L^{\mathrm{D}}} = -\frac{m\,\mu^2}{4\pi\hbar^2\,(1+\chi\mu)^{3/2}\,\epsilon\kappa^\epsilon}\ . \tag{2.61}$$

We then have isolated the divergence as a single pole in ϵ. Notice now that, in $\mathrm{D} = 2 - \epsilon$, the whole zero-temperature grand potential can be expressed as

$$\frac{\Omega^{(0)}}{L^{\mathrm{D}}} = \frac{\Omega_{\mathrm{mf}}}{L^{\mathrm{D}}} + \frac{\Omega_g^{(0)}}{L^{\mathrm{D}}} = -\frac{\mu^2}{2\xi_r(\mu,\kappa,\epsilon)}\,, \tag{2.62}$$

where the running coupling constant is given by

$$\frac{1}{\xi_r(\mu,\kappa,\epsilon)} = \frac{1}{g_0\kappa^\epsilon} + \frac{m}{2\pi\hbar^2(1+\chi\mu)^{3/2}\,\epsilon\kappa^\epsilon}\,. \tag{2.63}$$

By following the renormalization recipe, the flow equation for the running constant reads

$$\frac{1}{\xi_r^2(\mu,\kappa,\epsilon)}\frac{\mathrm{d}\xi_r(\mu,\kappa,\epsilon)}{\mathrm{d}\kappa} = \frac{\epsilon}{g_0\kappa^{\epsilon+1}} + \frac{m}{2\pi\hbar^2(1+\chi\mu)^{3/2}\,\kappa^{\epsilon+1}} \tag{2.64}$$

which becomes, in the limit $\epsilon \to 0^+$,

$$\frac{1}{\xi_r^2(\mu,\kappa,0)}\frac{\mathrm{d}\xi_r(\mu,\kappa,0)}{d\kappa} = \frac{m}{2\pi\hbar^2(1+\chi\mu)^{3/2}\,\kappa}\,. \tag{2.65}$$

The equation above is immediate to solve, leading us to

$$\frac{1}{\xi_r(\mu,\Lambda,0)} - \frac{1}{\xi_r(\mu,\kappa,0)} = -\frac{m}{2\pi\hbar^2(1+\chi\mu)^{3/2}}\log\left(\frac{\Lambda}{\kappa}\right). \tag{2.66}$$

The parameter Λ can be regarded as a high-energy cutoff, namely $\hbar^2\Lambda^2/(2m) = \varepsilon_\Lambda$, so $1/\xi_r(\mu,\Lambda,0) = 0$. This choice implies the crucial fact that now the regulator κ corresponds to the actual energy of the system, in the sense that $\hbar^2\kappa^2/(2m) = \mu$. Thus, by collecting all the pieces, for D $\to 2$ (i.e. $\epsilon \to 0^+$) the zero-temperature grand potential has the following structure

$$\frac{\Omega^{(0)}}{L^2} = -\frac{m\,\mu^2}{8\pi\hbar^2(1+\chi\mu)^{3/2}}\,\log\left(\frac{\varepsilon_\Lambda}{\mu}\right). \tag{2.67}$$

The high-energy cutoff was computed for the first time in [115], so we set it at the value

$$\varepsilon_\Lambda = \frac{4\hbar^2}{m a_s^2\, e^{2\gamma+1/2}} \tag{2.68}$$

with $\gamma \simeq 0.5772$ being the Euler-Mascheroni constant. In [28], it has been also underlined that, given a two-body interaction potential, the s-wave scattering length can be extracted from the corresponding phase shift $\delta_0(q)$, which in two dimensions obeys to

$$\cot[\delta_0(q)] \simeq \frac{2}{\pi}\log\left(\frac{q}{2}a_s e^{\gamma}\right) \tag{2.69}$$

up to $\mathcal{O}(q^2)$ contributions. As a consistency check, we underline that by switching off finite-range corrections, i.e. $\chi = 0$ in (2.67), one recovers the Popov result [116, 117].

As evident from its definition in Eq. (2.21), the parameter χ weights the deviations from universality due to the finite-range character of the interaction potential. It is interesting then to give at least a rough estimation of the finite-range relevance, by comparing Eq. (2.67) to its zero-range counterpart. By recalling the definition of R in Eq. (2.57), one has

$$\left|\frac{\Omega^{(0)}(\mu,\chi) - \Omega^{(0)}(\mu,\chi=0)}{\Omega^{(0)}(\mu,\chi=0)}\right| \simeq \left|\frac{1}{(1+\chi\mu)^{3/2}} - 1\right| \simeq \frac{12\pi^2\, nR^2}{|\log(na_s^2)|}\,. \tag{2.70}$$

Besides Eq. (2.57), in the equation above we have considered the leading contribution to the chemical potential μ, namely

$$\mu = -\frac{8\pi\hbar^2\, n}{m|\log(na_s^2)|} \tag{2.71}$$

arising from the inversion of the number equation $n(\mu) = -L^{-2}\partial_\mu \Omega^{(0)}(\mu)$. When R is comparable to the scattering length, finite-range effects become sizable. Indeed [28], for ^{87}Rb atoms one has $R \simeq 10^{-8}$ m, while a_s can be be widely tuned via Feshbach resonances [118] to, for instance, $a_s = 1,4 \cdot 10^{-10}$ m. As a consequence, $nR^2 \simeq 5 \cdot 10^{-2}$ against the two-dimensional gas parameter $na_s^2 \simeq 10^{-5}$. In this regime, Eq. (2.70) gives back a correction to the pressure of $\sim 20\%$.

3

GROUND-STATE PROPERTIES AND QUANTUM DROPLETS IN BOSE MIXTURES

In this third chapter, we are going to present the effects of quantum fluctuations in the equation of state of ultracold and dilute mixtures made by two different bosonic species. In particular, we are going to focus on Bose gases where atoms of the same species are in two different hyperfine states. This also offers the possibility to turn on a Rabi coupling between them, driving the flipping of atoms from one state to the other. We analyze both the cases and underline the eventual differences. Moreover, in the case of attractive inter-species interaction, a striking novel phenomenon can occur. Indeed, it has been recently observed that quantum fluctuations can drive the stabilization of a collapsing mixture into a self-bound state with finite equilibrium density also in free space. Through an effective variational formalism, we will be able to characterize the droplet in terms of its static and dynamical properties.

3.1 A first approach to multicomponent quantum fluids

Throughout the preceding two chapters, we have dealt with bosonic superfluids made of only one atomic species. However, immediately after the groundbreaking results with alkali atoms [31, 32], an intense experimental effort was devoted in reaching the quantum degeneracy limit also with multicomponent bosonic gases [119, 120, 121]. A bosonic mixtures can be made of different atomic species or atoms of the same element in different hyperfine states.

The great interest in multicomponent quantum fluids steams from their rich phenomenology which is basically due to the spinorial nature of the order parameter. The first theoretical analysis [122] was developed between the boundaries of Landau hydrodynamic picture [35, 123, 124, 125]. Among the following theoretical development for coupled superfluids, it is surely worth to mention the result by Andreev and Bashkin [126]: by correcting a mistake in the Khalatnikov equations [122], they predicted that a mutual drag force has to act between the two superfluid species. Unfortunately, until the advent of ultracold and dilute atomic gases, the research on multicomponent superfluid systems were confined mostly on the theoretical side. The reason lies on the diluteness criterion of ^{3}He, which does not allow the revealing of fermionic superfluidity [36].

Mixtures made of atomic gases provide much more flexibility for the same reasons listed on the previous chapter. We have exquisite control on the experimental parameters, screening on noise coming from the external environment and temperatures down to the nanokelvin scale. Within the quantum degeneracy regime, multicomponent condensates can be used to explore the dynamics of quantum spinors and the related physical effects. All around the world, a wide range of spinorial quantum fluids can now be engineered to probe an interesting and exotic phenomenology. Indeed, besides the above mentioned Andreev-Bashkin effect, one can explore the arising of persistent supercurrents, internal Josephson dynamics [127, 128, 129] and itinerant ferromagnetism in fermionic mixtures [130, 131]. Moreover, ultracold atomic mixtures have been proved to be an effective platform for quantum simulations of cosmological topics, from analog of the Hawking radiation [132, 133, 134] to the inflaton tunneling from a false vacuum [135, 136, 137].

As clear from the vast literature we have mentioned, the intense scientific interest in

multicomponent atomic fluids is in part due to the possibility of working with the same atomic species, but in different hyperfine states. In these setups, one can turn on a coherent coupling between the internal states. Moreover, at least for alkali atoms, experimentalists have been able to classify the properties of scattering processes between different internal states. Thus, for binary mixtures, it is possible to tune the strength of three different interactions: two intra-components processes and the inter-component one. In this way, one can explore a more complex picture than the one displayed by single-component systems. Indeed, in the latter we have a black-or-white situation, since, according to the sign of the scattering length, the effective interaction is repulsive or attractive. A condensed cloud has stable configurations for a repulsive two-body potential (i.e. $a_s > 0$). On the contrary an atom-atom effective attraction ($a_s < 0$) produces an instability moving the system towards states with increasingly higher density [33], until three-body recombinations kick all atoms out the confining potential.

On the contrary, the interplay between interactions in binary mixtures requires much more attention in drawing the stability threshold for the mean-field ground states. In order to understand this important point we begin by considering a simple theoretical analysis.

3.1.1 The miscibility criterion for binary mixtures

Since we are still dealing with weakly interacting and dilute systems, it is natural to move from a simple generalization of the Gross-Pitaevskii description. For now, we consider a fixed number N of atoms and no internal coupling between the condensates. We then start by writing down the following zero-temperature energy functional [36]

$$E\big[\psi_1,\psi_2\big] = \int d^3\mathbf{r} \sum_{i=1,2} \left[\psi_i^* \Big(-\frac{\hbar^2\nabla^2}{2m_i} + V_{i,\mathrm{ext}} + \frac{1}{2} g_{ii} \big|\psi_1\big|^2 \Big) \psi_i + g_{i,3-i} \big|\psi_i\big|^2 \big|\psi_{3-i}\big|^2 \right] . \quad (3.1)$$

In the equation above, ψ_1 and ψ_2 are the order parameters of the two condensates composing the mixture, m_1 and m_2 specify the atomic masses and we acknoledge the fact that, generally, the confining potentials $V_{1,\mathrm{ext}}$ and $V_{2,\mathrm{ext}}$ can differ from each other. Concerning the atom-atom interaction, for the intra-component coupling we have the usual $g_{ii} = 4\pi\hbar^2 a_{ii}/m_i$ for $i = 1, 2$, while the inter-component one is defined as $g_{12} = 2\pi\hbar^2 a_{12}/m_{\mathrm{re}}$, with $m_{\mathrm{re}} = m_1 m_2/(m_1 + m_2)$ being the reduced mass. In order to ensure the intra-component stability,

thoughtout the chapter we assume a repulsive interaction between atoms of the same species [138, 139]. Based on detailed analysis on Feshbach resonances, this proves to be a reliable and practical assumption, since we can use a_{12} as a single knob to change the character of the effective global interaction.

In Eq. (3.1) we made another simplifying assumption by neglecting the coupling between the velocity fields defined as $\mathbf{v}_i = \hbar\nabla\theta_i/m$ in sec. 1.4. This hypothesis prevents us from describing phenomena based on the relative motion between the components, such as the Andreev-Bashkin effect. For those interested in the understanding of this elusive phenomenon in dilute atomic gases, we refer to the recent analysis in [140].

It is easy to derive the set of coupled Gross-Pitaevskii equations by minimizing the functional $E[\psi_1, \psi_2]$ in Eq. (3.1). From

$$i\hbar\dot{\psi}_j = \frac{\delta E[\psi_j, \psi_{3-j}]}{\delta\psi_j} \quad \text{for } \; j = 1, 2 \; , \tag{3.2}$$

one can easily arrive to

$$i\hbar\dot{\psi}_j = \left[-\frac{\hbar^2\nabla^2}{2m_j} + V_{j,\text{ext}}(\mathbf{r}) + g_{jj}\left|\psi_j\right|^2 + g_{j,3-j}\left|\psi_{3-j}\right|^2 \right]\psi_j \; . \tag{3.3}$$

Obviously, within a quantum field theory perspective, the equation above can be derived from an Euclidean action as defined in Eq. (1.23), where the order parameter has a spinorial nature instead of being a scalar quantity. Then, by applying the saddle-point recipe, we can recover Eq. (3.3) as the equation describing the dynamics of the classical trajectory contributing to the partition function $\mathcal{Z} = \int \mathcal{D}[\Psi, \bar{\Psi}] \exp(-S[\Psi, \bar{\Psi}]/\hbar)$. We will soon deepen the path integral approach in the proceeding of the chapter, but for now we focus on Eq. (3.1). In order to further simplify this functional, one can assume the fields as constant and homogenous or, equivalently, that the confining potentials are simply a box. Despite appearing as a textbook approximation, box potentials are now experimentally available to probe uniform configuration properties [127].

From simple energetic considerations, one can inferred that two uniform condensates can arrange themselves in two different ground states. We can have a miscible configuration,

where the energy density is given by

$$\frac{E_{\rm mix}}{L^3} = \frac{1}{2L^6}\sum_{i=1,2}\left[g_{ii}N_i^2 + g_{i,3-i}N_iN_{3-i}\right] \tag{3.4}$$

and L is the side of the box enclosing the system. On the other hand, a ground-state where the two components are separated in space is likewise possible. In this case, the energy density reads

$$\frac{E_{\rm sep}}{L^3} = \frac{1}{2L^3}\sum_{i=1,2} g_{ii}\frac{N_i^2}{V_i^3} \tag{3.5}$$

with V_i the volume occupied by the i-component, so $L^3 = V_1 + V_2$. Mechanical stability requires that $\partial E_{\rm sep}/\partial V_1 = \partial E_{\rm sep}/\partial V_2$, resulting in [36]

$$g_{11}\left(\frac{N_1}{V_1}\right)^2 = g_{22}\left(\frac{N_2}{V_2}\right)^2 . \tag{3.6}$$

Thanks to the equation above, Eq. (3.5) can then be expressed in terms of L^3, namely

$$\frac{E_{\rm sep}}{L^3} = \frac{1}{2L^6}\sum_{i=1,2}\left[g_{ii}N_i^2 + \sqrt{g_{ii}g_{i,3-i}}\,N_iN_{3-i}\right] . \tag{3.7}$$

Miscibility occurs where $E_{\rm mix} < E_{\rm sep}$, therefore a comparison between Eq. (3.4) and Eq. (3.7) leads us to the criterion $g_{12} < \sqrt{g_{11}g_{22}}$. However, this is not enough, since we have to also impose that the system is robust against density fluctuations. Technically, this corresponds to require that the Hessian matrix $\partial^2 E_{\rm mix}/\partial N_1\partial N_2$ is defined positive. Being a 2×2 matrix, it is sufficient to check that its determinant is positive. At the end, the criterion for a stable miscible configuration is given by

$$|g_{12}| < \sqrt{g_{11}g_{22}} . \tag{3.8}$$

When $g_{12} > \sqrt{g_{11}g_{22}}$ the mixture is unstable towards a phase separated configuration. On the other hand, for a strong enough inter-component attraction, i.e. $g_{12} < -\sqrt{g_{11}g_{22}}$ the intra-component repulsion does not manage to counterbalance it and the mixtures is unstable towards higher density configuration. We then recover the condensate collapse for single-component systems.

It is evident that the physics of multicomponent atomic quantum gases is inherently richer also under the most simplifying hypothesis. Thanks to a similar approach, we can also derive the ground states configurations in presence of an internal coupling.

3.1.2 Ground states for coherently-coupled mixtures: a functional approach

In this section, we consider a Bose gas with two relevant hyperfine states in a volume L^3 with chemical potential μ. In addition to the usual intra- and inter-component contact interactions, transitions between the two states are induced by an an external coherent Rabi coupling of frequency ω_R. As in the previous section, we aim to identify the possible ground-state configurations and to point out their stability criterion. Despite being mainly interested in zero-temperature properties we choose to adopt the path integral formalism in imaginary time which provides, in principle, both zero and finite-temperature informations.

Each bosonic component is described by a complex field ψ_i $(i = 1, 2)$. Given the spinor $\mathbf{\Psi} = (\psi_1, \psi_2)^T$ [1, 2, 141], the partition function of the system reads:

$$\mathcal{Z} = \int \mathcal{D}[\mathbf{\Psi}, \bar{\mathbf{\Psi}}] \exp\left\{ -\frac{1}{\hbar} S[\mathbf{\Psi}, \bar{\mathbf{\Psi}}] \right\}. \tag{3.9}$$

The Euclidean action $S[\mathbf{\Psi}, \bar{\mathbf{\Psi}}]$, in terms of spinor components, is given by

$$S\big[\Psi, \bar{\Psi}\big] = \int_0^{\beta\hbar} d\tau \int_{L^3} d^3\mathbf{r} \sum_{i=1,2} \Bigg[\psi_i^* \left(\hbar\partial_\tau - \frac{\hbar^2\nabla^2}{2m} - \mu + \frac{1}{2}\, g_{ii}|\psi_i|^2 + \frac{1}{2}\, g_{i,3-i}|\psi_{3-i}|^2 \right) \psi_i - \hbar\omega_R\, \psi_i^* \psi_{3-j} \Bigg] \tag{3.10}$$

with $\beta \equiv 1/(k_B T)$ and $g_{ij} = 4\pi\hbar^2 a_{ij}/m$ being a_{ij} the scattering length for collisions between the component i and the j one (specifically a_{11}, a_{22}, and a_{12}). We remark that here we are considering a mixtures of two hyperfine states of the same atomic species, so $m_1 = m_2$.

All relevant thermodynamical quantities can be derived from the grand potential $\Omega = -\frac{1}{\beta}\ln\big(\mathcal{Z}\big)$. We work in the superfluid phase, where a U(1) gauge symmetry is spontaneously broken. The presence of the Rabi coupling in the Euclidean action in equation (3.10) implies that both components do not have a fixed particle number. By generalizing the usual splitting

of the field in Eq. (1.36), we define

$$\mathbf{\Psi}_i(\mathbf{r},\tau) = \mathbf{v} + \mathfrak{H}(\mathbf{r},\tau)\ , \tag{3.11}$$

where $\mathbf{v} = (v_1, v_2)^T$ is the uniform order parameters spinor, whose entries control the onset of Bose-Einstein condensation within each component. On the other hand, the spinor $\mathfrak{H}(\mathbf{r},\tau) = (\eta_1(\mathbf{r},\tau), \eta_2(\mathbf{r},\tau))^T$ gathers the fluctuations fields above $\mathbf{v}$.

The mean-field plus Gaussian approximation is obtained by expanding equation (3.10) up to the second order in $\eta_i(\mathbf{r},\tau)$ and $\eta_i^*(\mathbf{r},\tau)$. In this way, one recovers the following structure

$$S \simeq S_{\rm mf}[\mu, \mathbf{v}] + S_g[\mu, \mathbf{v}, \mathfrak{H}] + S_{\rm int}[\mu, T, \mathbf{v}, \mathfrak{H}] \tag{3.12}$$

where S_g groups the Gaussian (i.e. quadratic) terms in the fluctuations, while S_{int} the linear ones. In our searching for the ground states we are now interested in $S_{\rm mf}$, the contribution independent from fluctuations.

If we aim to describe the excitations above the ground state configuration in a perturbative framework, the mean-field equation of state can be derived through the well-known saddle-point approximation. Indeed, the major contribution to thermodynamic quantities comes from the solution of the classical equation of motion $\delta S_{mf}/\delta \mathbf{v} = 0$. Let us recall that, in principle, the order parameter of the superfluid transition is a complex number. As a consequence, it admits a density-phase representation (cfr. sec. 1.4)

$$v_i = \sqrt{n_i}\ e^{i\varphi_i} \quad \text{for } i = 1, 2, \tag{3.13}$$

with n_i being the density. By replacing Eq. (3.13) in $S_{\rm mf}$ appearing in Eq. (3.12), the mean-field thermodynamic potential is given by [142]

$$\frac{\Omega_{\rm mf}[\mu, v_1, v_2]}{L^3} = \sum_{i=1,2}\left[\frac{1}{2}\Big(g_{ii}v_i^4 + g_{i,3-i}\ v_i^2\, v_{3-i}^2\Big) - \hbar\omega_R\cos(\Phi)\sqrt{v_i^2\, v_{3-i}^2} - \mu v_i^2\right] \tag{3.14}$$

where we made use of $\Omega_{\rm mf} = L^3(\hbar\beta)^{-1}S_{\rm mf}[\mu, v_1, v_2]$ and $\Phi \equiv \varphi_1 - \varphi_2 + \varphi_{\omega_R}$. We assume that $\omega_R \in \mathbb{R}^+$, so $\varphi_{\omega_R} = 0$. From Eq. (3.14) it is immediate to check that the minimum energy configuration corresponds to $\cos\Phi = +1$, where $\varphi_1 - \varphi_2 = 0$. The configuration

corresponding to $\cos\Phi = -1$ is still a stationary point of the action, but it obviously cannot be a global minimum. Remarkably, coherently-coupled mixtures are a good platform for quantum simulations of the early universe [135, 136, 137] precisely because of this energy landscape. Indeed, the coexistence of a global minimum with other stationary points can be used to simulate the inflaton tunneling from a false vacuum, as described by the renowned Coleman equation [143, 144].

In the global minimum characterized by $\cos\Phi = +1$, it is possible to simplify Eq. (3.14) to

$$\frac{\Omega_{\rm mf}}{L^3} = \left[\sum_{i=1,2}\left(-\mu v_i^2 + \frac{1}{2}g_{ii}v_i^4\right) + g_{12}v_1^2v_2^2 - 2\hbar\omega_R v_1 v_2\right] . \tag{3.15}$$

The saddle-point equation of state can now be easily computed, leading us to the following set of coupled algebraic equations for $i = 1, 2$:

$$(g_{ii}v_i^2 + g_{i,3-i}v_{3-i}^2)v_i - \hbar\omega_R v_{3-i} = \mu v_i \, . \tag{3.16}$$

The character of the possible ground states of a Rabi-coupled binary mixture can be better understood in terms of the canonical energy density. Up to the mean-field level, $v_1^2 = n_1$ and $v_2^2 = n_2$ with $n = n_1 + n_2$ the total density. For the sake of simplicity we also assume that $g_{11} = g_{22}$. Through a Legendre transform $E/L^3 = \Omega_{\rm mf}/L^3 + \mu n$, we get then

$$\frac{E_{\rm mf}}{L^3} = \frac{1}{2}g(n_a^2 + n_b^2) + g_{ab}n_a n_b - 2\hbar\omega_R\sqrt{n_a n_b} \, . \tag{3.17}$$

The equilibrium configuration is a stationary point of $E_{\rm mf}/L^3$, corresponding to the solution of the equation

$$\left[g - g_{ab} + \frac{\hbar\omega_R}{\sqrt{n_a n_b}}\right](n_a - n_b) = 0 \, . \tag{3.18}$$

By means of the population imbalance between the species $\Delta = n_a - n_b$, it is possible to characterize the equilibrium configurations in a very transparent way. In terms of Δ, the solutions of equation (3.18) are given by [142]

$$\begin{aligned} &\text{Symmetric Ground State :} && \Delta = 0 \\ &\text{Polarized Ground State :} && \Delta = \pm n\sqrt{1 - \left[\frac{2\hbar\omega_R}{n(g - g_{ab})}\right]^2} \, . \end{aligned} \tag{3.19}$$

As in the previous section, a crucial-point concerns the stability of the stationary points in Eq. (3.19). This can be clarified by computing the determinant of the energy density Hessian matrix (we assume an intra-species repulsion). Over the symmetric ground state,

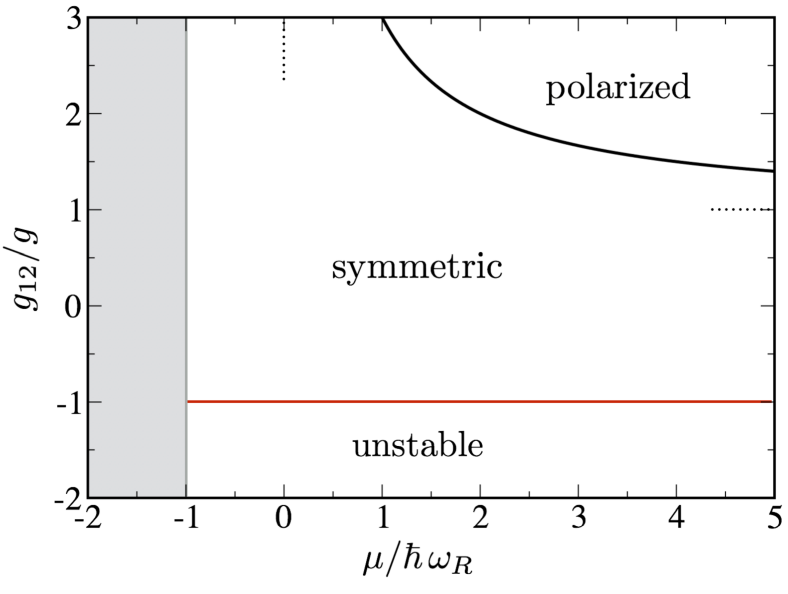

Figure 3.1: Mean field phase diagram based on the grand potential $\Omega_{\rm mf}(\mu, v_1, v_2)$ of Eq. (3.15) under the assumption $g_{11} = g_{22}$. In the symmetric ground state the two components appear with the same particle density $|v_1|^2 = |v_2|^2$, whereas in the polarized phase densities are unequal. Dotted lines represent the asymptotic phase boundaries of the polarized region for large g_{12}/g and $\mu/\hbar\omega_R$ ratios respectively. For $g_{12}/g < -1$ the symmetric solution is unstable in the *thermodynamic limit*. The grey region for $\mu < \hbar\omega_R$ corresponds to the trivial solution $|v_1|^2 = |v_2|^2 = 0$.

one finds

$$\det\left[\frac{1}{L^3}\frac{\partial^2 E_{\rm mf}}{\partial n_a \partial n_b}\right] = \big(g + g_{ab}\big)\left(g - g_{ab} + \frac{2\hbar\omega_R}{n}\right) . \tag{3.20}$$

By imposing it to be positive, the following stability condition arises [142]

$$g_{ab} < g + 2\frac{\hbar\omega_R}{n} . \tag{3.21}$$

In the symmetric ground-state, the density in terms of μ reads

$$n/2 = \big(\mu + \hbar\omega_R\big)/\big(g + g_{ab}\big) . \tag{3.22}$$

On the other side, for the polarized ground-state, since $n = \mu/g$, the normalized imbalance

equals

$$\frac{\Delta}{n} = \pm\sqrt{1 - \left[\frac{2g\omega_R}{\mu\big(g - g_{ab}\big)}\right]^2}\,, \tag{3.23}$$

leading to the stability condition

$$g_{ab} > \frac{2\hbar\omega_R}{\mu} g\,. \tag{3.24}$$

The results of stability analysis of the stationary points of mean-field free energy are reported in Fig. 3.1. In order to summarize our results, the mean-field picture of coherently-coupled binary Bose-mixtures provides us two stable ground-state configuration, distinguished by the population imbalance Δ. In the symmetric ground state we have $\Delta = 0$, while a finite imbalance characterized the polarized one. We remark that [142] the switching on of a Rabi coupling prevents the system from displaying a separated phase, replaced by a finite polarization. By assuming equal intra-component repulsion $g_{11} = g_{22} = g > 0$ as for Fig. 3.1, for $g_{12} < -g$ the attractive component of the interaction processes dominates, driving the system towards a collapse instability.

■ 3.2 Quantum fluctuations and droplets

In this section, we derive the zero-temperature beyond-mean-field equation of state for a binary Bose mixture. We take into account quantum fluctuations above the ground state up to the Gaussian (i.e. quadratic) order. The lowest-energy configurations have been identified in the previous section.

3.2.1 Quantum fluctuations and droplets: the case $\omega_R = 0$

We consider here a binary mixtures made of bosonic atoms in two different hyperfine states, in absence of internal coupling ($\omega_R = 0$). We also assume that the miscibility condition in Eq. (3.8) holds. The Euclidean action describing the mixtures is then given by

$$S\big[\mathbf{\Psi}, \bar{\mathbf{\Psi}}\big] = \int_0^{\beta\hbar} d\tau \int_{L^3} d^3\mathbf{r} \sum_{i=1,2} \psi_i^* \left(\hbar\partial_\tau - \frac{\hbar^2\nabla^2}{2m} - \mu_i + \frac{1}{2}\, g_{ii}|\psi_i|^2 + \frac{1}{2}\, g_{i,3-i}|\psi_{3-i}|^2\right)\psi_i \tag{3.25}$$

where $\mathbf{\Psi} = (\psi_1, \psi_2)^T$. We underline that the equation above is similar to Eq. (3.10) with $\omega_R = 0$ and another relevant difference. Indeed, since no states flipping is allowed, it is

possible to define a chemical potential μ for each component. The mean-field plus Gaussian approximation is obtained by replacing the spinor $\mathbf{\Psi}$ with Eq. (3.11), resulting in a structure like the one in Eq. (3.12). In absence of internal coupling, the mean-field contribution, independent from the fluctuations fields, is given by

$$S_{\rm mf} = \hbar\beta L^3 \sum_{i=1,2} \Big[-\mu_i v_i^2 + \frac{1}{2}\, g_{ii} v_i^2 + \frac{1}{2}\, g_{i,3-i}\, v_i^2\, v_{3-i}^2 \,. \Big] \tag{3.26}$$

The corresponding thermodynamic contribution is derived by noticing that, at this level, $\Omega_{\rm mf}/L^3 = (\hbar\beta)^{-1} S_{\rm mf}$. Therefore, by assuming that $v_i^2 \simeq n_i$, Eq. (3.26) leads to Eq. (3.4), which was derived in sec. 3.1.1 by generalizing the Gross-Pitaevskii energy functional [36]. Let us also notice that in Eq. (3.26) we assume uniform condensates. The corresponding equation of state can be found by solving $\delta S_{\rm mf}/\delta v_i = 0$, resulting in

$$\mu_i = g_{ii} v_i^2 + g_{i,3-i} v_{3-i}^2 \,. \tag{3.27}$$

We then proceed by consider the role played by fluctuations above the ground-state specified by the saddle-point result in Eq. (3.27). By definition, this erases terms linear in η_i and η^*, i.e. $S_{int} = 0$ in Eq. (3.12). Moving to Gaussian terms, in real space we find

$$\begin{aligned} S_g = \int_0^{\beta\hbar} d\tau \int d^3\mathbf{r} \sum_{i=1,2} \Bigg[\eta_i^* \Big(\hbar\frac{\partial}{\partial\tau} - \frac{\hbar^2\nabla^2}{2m} + 2g_{ii} v_i^2 + g_{i,3-i} v_{3-i}^2 - \mu_i \Big) \eta_i + \\ + \frac{g_{ii} v_i^2}{2} \big(\eta_i^* \eta_i^* + \eta_i \eta_i \big) \Bigg] + \int_0^{\beta\hbar} d\tau \int d^3\mathbf{r} \Big[g_{12} v_1 v_2 \big(\eta_1\eta_2 + \eta_1^*\eta_2 + \eta_1\eta_2^* + \eta_1^*\eta_2^* \big) \Big] \,. \end{aligned} \tag{3.28}$$

In the Fourier space, we can cast the quadratic action in Eq. (3.28) as

$$S_g\big[\Psi(\mathbf{q},\omega_n), \overline{\Psi}(\mathbf{q},\omega_n) \big] = -\frac{\hbar}{2} \sum_{\mathbf{q},\omega_n} \Psi \mathbb{M}(\mathbf{q},\omega_n) \overline{\Psi} \tag{3.29}$$

where Ψ and $\overline{\Psi}$ are the spinors, $\{\omega_n\}_n$ is the set of bosonic Matsubara frequencies and the 4×4 matrix $\mathbb{M}$ is the inverse of the propagator [2]. We can rename 2×2 blocks composing

this matrix as [141]:

$$-\hbar\mathbb{M}(\mathbf{q},\omega_n) = \begin{pmatrix} -\hbar\mathcal{G}_1^{-1}(\mathbf{q},\omega_n) & \hbar\Sigma_{12} \\ \hbar\Sigma_{12} & -\hbar\mathcal{G}_2^{-1}(\mathbf{q},\omega_n) \end{pmatrix} . \tag{3.30}$$

The diagonal blocks corresponds to the (inverse) propagator for a species taken singularly, whose structure [1, 2] has been analyzed in Chap. 1. Then, it is immediate to write down

$$-\hbar\mathcal{G}_i^{-1} = \begin{pmatrix} -i\hbar\omega_n + h_i & g_i v_i \\ g_i v_i & +i\hbar\omega_n + h_i \end{pmatrix} , \tag{3.31}$$

where

$$h_i = \frac{\hbar^2 q^2}{2m} + 2g_{ii}v_i^2 + g_{i,3-i}v_{3-i}^2 - \mu_i . \tag{3.32}$$

On the other hand, the off-diagonal blocks of Eq. (3.30), coupling two different hyperfine states, are given by

$$\hbar\Sigma_{12} = g_{12}\, v_1\, v_2 \begin{pmatrix} 1 & 1 \\ 1 & 1 \end{pmatrix} . \tag{3.33}$$

In order to compute the zero-point energy, we can define the matrix $\mathbb{E}(\mathbf{q}) = -\hbar\mathbb{M}(\mathbf{q},0)$ whose eigenvalues give us back the collective excitation spectra [145, 146]. As underlined in [2, 10, 141] the matrix $\mathbb{E}(\mathbf{q})$ has to be diagonalized by keeping in mind the bosonic nature of excitations, which means that the eigenvectors entries have to satisfy a bosonic commutation relation; this can be achieved by diagonalizing not $\mathbb{E}(\mathbf{q})$, but instead $\mathbb{I}\cdot\mathbb{E}(\mathbf{q})$, where

$$\mathbb{I} = \begin{pmatrix} \sigma_z & \mathbb{O}_2 \\ \mathbb{O}_2 & \sigma_z \end{pmatrix}$$

with σ_z being the third Pauli matrices and $\mathbb{O}$ the 2×2 null matrix. The resulting algebraic system is

$$\big[\mathbb{I}\cdot\mathbb{E}(\mathbf{q})\big]v_\pm(\mathbf{q}) = E_\pm(\mathbf{q})v_\pm(\mathbf{q}) . \tag{3.34}$$

The matrices product in the equation above can be write down by recalling Eq. (3.32) and the saddle-point result in Eq. (3.27). In presence of internal coupling between the component, i.e. $\omega_R \neq 0$ in Eq. (3.10), we are going to obtain a similar structure for the

propagator. It is then worthwhile to write down the matrix of the eigensystem in Eq. (3.34), namely

$$\mathbb{I}\cdot\mathbb{E}(\mathbf{q}) = \begin{pmatrix} h_1 & g_{11}\,v_1^2 & g_{12}\,v_1v_2 & g_{12}\,v_1v_2 \\ -g_{11}\,v_1^2 & -h_1 & -g_{12}\,v_1v_2 & -g_{12}\,v_1v_2 \\ g_{12}\,v_1v_2 & g_{12}\,v_1v_2 & h_2 & g_{22}v_2^2 \\ -g_{12}\,v_1v_2 & -g_{12}\,v_1v_2 & -g_{22}v_2^2 & -h_2 \end{pmatrix} . \tag{3.35}$$

Instead of solving Eq. (3.34), the eigenenergies of $\mathbb{I}\cdot\mathbb{E}(\mathbf{q})$ can be derived in a less demanding way from the corresponding secular equation $\det\left[\mathbb{I}\cdot\mathbb{E}(\mathbf{q})-\lambda 1_2\right]=0$. Within the Bogoliubov regime, where the condensate depletion is small, one can approximate $v_i^2\simeq n_i$. Thus, the resulting excitation spectrum has two branches, namely

$$E_{\pm}(q) = \sqrt{\frac{1}{2}\big(E_{sc,1}^2+E_{sc,2}^2\big) \pm \sqrt{\frac{1}{4}\big(E_{sc,1}^2-E_{sc,2}^2\big)^2+\frac{g_{12}n_1n_2}{m^2}\,\hbar^4q^4}} . \tag{3.36}$$

In the equation above, $E_{sc,i}$ is the Bogoliubov spectrum for the i^{th}-component

$$E_{sc,i} = \sqrt{\frac{\hbar^2q^2}{2m}\left(\frac{\hbar^2q^2}{2m}+2g_{ii}n_i\right)} . \tag{3.37}$$

Despite the fact that Eq. (3.36) was derived for the first time in 1963 by Larsen [147], we underline our alternative approach based on functional integration. In addition, both branches of the Bogoliubov spectrum are gapless, since the original Hamiltonian (or the Euclidean action in Eq. (3.25)) has a $U(1)\times U(1)$ symmetry. This means that two Goldstone modes arise within the broken-symmetry phase. On the contrary, when the internal coupling is turned on, a $U(1)$ gauge symmetry holds, so we will expect only one gapless branch.

Our scheme aims include quantum fluctuations within the thermodynamic description of the system. Up to the Gaussian level, the zero-temperature grand potential corresponds to the zero-point energy of collective excitations. By extending Eq. (1.47) to our two-branches spectrum in Eq. (3.36), one finds that

$$\frac{E_g^{(0)}}{L^3} = \frac{1}{2}\int\frac{d^3\mathbf{q}}{(2\pi)^3}\big[E_+(q)+E_-(q)\big] . \tag{3.38}$$

As expected, the zero-point energy is UV-divergent. Anyway, since the branches of the

Bogoliubov spectrum are both gapless, nothing prevents us from applying the dimensional regularization scheme to Eq. (3.38). The calculation proceed exactly in the same fashion as in sec. 1.3.2, leading us to

$$\frac{E_g^{(0)}}{L^3} = \frac{8}{15\pi^2}\left(\frac{m}{\hbar^2}\right)^{3/2}\frac{(g_{11}n_1)^{5/2}}{4\sqrt{2}}\sum_{\pm}\left[1+\frac{g_{22}n_2}{g_{11}n_1}\pm\sqrt{\left(1-\frac{g_{22}n_2}{g_{11}n_1}\right)^2+\frac{4g_{12}^2n_2}{g_{11}^2n_1}}\,\right]^{5/2}. \quad (3.39)$$

The equation above is the binary-mixtures generalization of the Lee-Huang-Yang correction in single-component condensed Bose gases [16, 17]. The same result can be derived within a second-quantization framework by making use of the Bogoliubov canonical transformation.

We also remark that dimensional regularization is not the only strategy to heal the divergent behavior of the integral in Eq. (3.38). By following [2], regularizing counterterms can appear for two reasons. First, as explained in 1.2.1, it is possible to add a convergence factor $e^{i\omega_n 0^+}$ to the Gaussian action in the Fourier space (cfr. Eq. (3.29) and the following ones). The remaining divergent terms are removed by renormalizing the scattering length [8]. Indeed, from second-quantized scattering theory [10], one easily derived that

$$g_{ii} \simeq g_{ii,0} + \frac{m g_{ii,0}}{\hbar^2}\int\frac{d^3\mathbf{q}}{(2\pi)^3}\frac{1}{q^2} \quad (3.40)$$

with $g_{ii,0} = 4\pi\hbar^2 a_s/m$. Following this path, Eq. (3.38) is modified into [97]

$$\frac{E_g^{(0)}}{L^3} = \frac{1}{2}\int\frac{d^3\mathbf{q}}{(2\pi)^3}\left[E_+(q)+E_-(q)-\sum_{i=1,2}\Big(\frac{\hbar^2q^2}{2m}+g_{ii}n_i-\frac{mg_{ii}^2n_i^2+mg_{i,3-i}n_i\,n_{3-i}}{\hbar^2q^2}\Big)\right], \quad (3.41)$$

which correctly gives back Eq. (3.39) obtained with dimensional regularization.

Differently from the single-component case, we are going to detail in the following that the quantum fluctuations contribution in Eq. (3.39) is not confined to perturbative deviations of thermodynamic quantities from the mean-field picture. On the contrary, in a recent and ground-breaking paper [97], Petrov argued they can crucially influence the system stability against the collapse.

By following his argument, we have to remember the mean-field stability criterion for a miscible mixture in Eq. (3.8), namely $g_{12}^2 < g_{11}g_{22}$ with $g_{11} > 0$ and $g_{22} > 0$. The Gaussian correction $E_g^{(0)}/L^3$ is computed in the miscible uniform ground state where Eq. (3.8) holds.

We now consider our system to be on the mean-field instability threshold ($g_{12}^2 = g_{11}g_{22}$) or slightly beyond it. We characterize its position in the space of coupling constants by defining

$$\Delta g = g_{12} + \sqrt{g_{11}g_{22}}\ , \tag{3.42}$$

a definition basically involving the scattering lengths. In the following we consider slightly unstable configuration, in the sense that Δg is negative but small compared to g_{11} and g_{22}. This instability can be easily understood by diagonalizing Eq. (3.4) expressed in terms of density. It results that

$$\frac{E_{\rm mix}}{L^3} = \begin{pmatrix} n_1 & n_2 \end{pmatrix} \begin{pmatrix} g_{11} & g_{12} \\ g_{12} & g_{22} \end{pmatrix} \begin{pmatrix} n_1 \\ n_2 \end{pmatrix} = \sum_{\alpha=\uparrow,\downarrow} \varepsilon_\alpha n_\alpha^2 \tag{3.43}$$

where

$$\begin{aligned} \varepsilon_\uparrow &\simeq \frac{1}{2}\big(g_{11}+g_{22}\big) \quad \text{and} \quad n_\uparrow = \frac{n_1\sqrt{g_{11}} - n_2\sqrt{g_{22}}}{\sqrt{g_{11}+g_{22}}} \\ \varepsilon_\downarrow &\simeq \frac{\Delta g\sqrt{g_{11}g_{22}}}{g_{11}+g_{22}} \quad \text{and} \quad n_\downarrow = \frac{n_1\sqrt{g_{11}} + n_2\sqrt{g_{22}}}{\sqrt{g_{11}+g_{22}}}\ . \end{aligned} \tag{3.44}$$

The eigensystem highlights that, from an energetic point of view, $n_\downarrow$ has to be increased while, on the contrary, one must lower $n_\uparrow$. Remarkably, up to the mean-field level, the ratio between the components densities remains constant, namely $n_2/n_1 = \sqrt{g_{11}/g_{22}}$. Thus, when $\Delta g < 0$ the system evolves towards the collapse. Within the Bogoliubov scheme, this instability is signalled by the branch $E_-(q)$ in Eq. (3.36) becoming imaginary for small momenta (or long wavelength in the real space). However, Petrov noticed [97] that the major contribution to the Gaussian correction $E_g^{(0)}$ comes from high momenta (i.e. short wavelengths) where the dependence on Δg is weak. The resulting density growth $\propto n^{5/2}$ dominates the collapsing mean-field contribution $\propto n^2$: the mean-field instability at long wavelengths is consequently inhibited by quantum fluctuations at shorter wavelength.

Petrov showed that, in order to model the system slighty beyond the mean-field stability threshold $\Delta g = 0$, an effective action can be derived by considering only $E_+(q)$ in computing $E_g^{(0)}$. This means that one has first to integrate out the high-momentum modes. As second step, the collapsing branch $E_-(q)$ can be computed at $g_{12}^2 = g_{11}g_{22}$ by considering (imaginary) corrections $\propto \Delta g$ as negligible. Under this assumption, Eq. (3.39) is simplified

to [148]

$$\frac{E^{(0)}_{g,\mathrm{eff}}}{L^3} = \frac{8}{15\pi^2}\left(\frac{m}{\hbar^2}\right)^{3/2}\left(g_{11}n_1 + g_{22}n_2\right)^{5/2} . \tag{3.45}$$

Let us note that the quantum fluctuations correction is positive, counterbalancing the attraction of the negative mean-field term. Because of this interplay, it is possible for the mixture to survive at finite density also in absence of an external trapping. If $E^{(0)}_{\mathrm{eff}}/L^3 = [E_{\mathrm{mix}}+E^{(0)}_g]/L^3$, the lowest-energy configuration reads

$$n_i^{(0)} = \frac{25\pi}{1024}\frac{(a_{12}+\sqrt{a_{11}a_{22}})^2}{a_{11}a_{22}a_{ii}(\sqrt{a_{11}}+\sqrt{a_{22}})^5} . \tag{3.46}$$

Omitting the numerical prefactors, the structure of the energy functional at zero temperature also reads an interesting asymptotic behaviour for the equilibrium density $n^{(0)}$. Indeed, it can be checked that $n^{(0)}$ in Eq. (3.46) is $\propto a^{-3}(\Delta g/g)^2$. This is interesting because, provided $(\Delta g/g)^2 \ll$, it implies that the stabilized configuration is still diluted, i.e. $na^3 \ll 1$. Obviously, this analysis holds at the thermodynamic limit. For a finite number of atoms, the finite-density configuration of Eq. (3.46) is replaced by the so-called droplet state [97, 98, 101, 148]. In analogy with the Gross-Pitaevskii energy functional (cfr. Eq. (3.1)), each component can be represented by a complex field Ψ_i whose dynamics results from the following real-time low-energy effective action

$$S = \int dt\, d^3\mathbf{r}\Big[\sum_{j=1,2}\frac{i\hbar}{2}\left(\Psi_j^*\partial_t\psi_j - \Psi_j\partial_t\Psi_j^*\right) - \mathcal{E}_{\mathrm{tot}}\left(\Psi_1,\Psi_2\right)\Big] , \tag{3.47}$$

under the normalization $n_j = |\Psi_j|^2$. The total energy density $\mathcal{E}_{\mathrm{tot}}$ reads

$$\begin{aligned}\mathcal{E}_{\mathrm{tot}} = \sum_{j=1,2}\left[\frac{\hbar^2}{2m}|\nabla\Psi_j|^2 + V_{\mathrm{ext}}(\mathbf{r})|\Psi_j|^2 + \frac{1}{2}g_{jj}|\Psi_j|^4\right] \\ + g_{12}|\Psi_1|^2|\Psi_2|^2 + \mathcal{E}_{\mathrm{g}}(\Psi_1,\Psi_2) ,\end{aligned} \tag{3.48}$$

where we have included also the possibility to turn on an external potential $V_{\mathrm{ext}}(\mathbf{r})$. The beyond-mean-field term $\mathcal{E}_{\mathrm{g}}$ arises from the zero-point energy of Bogoliubov collective exci-

tations [147, 97]. It is then modelled around Eq. (3.39), reading

$$\mathcal{E}_{\rm g} = \frac{8}{15\pi^2}\left(\frac{m}{\hbar^2}\right)^{3/2}(g_{11}n_1)^{5/2} f\left(\frac{g_{12}^2}{g_{11}g_{22}}, \frac{g_{22}n_2}{g_{11}n_1}\right) \tag{3.49}$$

with $f(x,y) = \sum_{\pm}[1+y\pm\sqrt{(1-y)^2+4xy}]^{5/2}/(4\sqrt{2})$. By applying the saddle-point method to Eq. (3.47), it is immediate to derive the set of generalized Gross-Pitaevskii equation

$$i\hbar\frac{\partial\Psi_j}{\partial t} = \left[-\frac{\hbar^2\nabla^2}{2m} + V_{\rm ext} + \mu_j(\Psi_1,\Psi_2)\right]\psi_i \tag{3.50}$$

with

$$\mu_j = g_{jj}\Psi_1 + g_{12}\Psi_2 + \frac{\delta\mathcal{E}_g}{\partial n_j}\,. \tag{3.51}$$

Under Petrov assumption, by computing the beyond-mean-field term at $g_{12}^2 = g_{11}g_{22}$, the correction to Eq. (3.50) can be considered in the following simplified form

$$\frac{\delta\mathcal{E}_g}{\partial n_j} = \frac{32}{3\sqrt{\pi}}g_{jj}\left(a_{11}|\Psi_1|^2 + a_{22}|\Psi_2|^2\right)^{3/2}\,. \tag{3.52}$$

The set of Eq. (3.50) with the correction Eq. (3.52) was first solved in [148], both in real and imaginary times. Remarkably, the real-time dynamics confirmed that the condensate collapse can be prevented by including the $\delta\mathcal{E}_g/\delta n_j$ given by Eq. (3.52). Moreover, simulations based on Eq. (3.50) are in good agreement with experimental observation [101, 148] for mixtures of ^{39}K atoms in the hyperfine states $|1\rangle = |F=1, m_F=-1\rangle$ and $|2\rangle = |F=1, m_F=0\rangle$. While in [101, 148] we have the first direct confirmation of Petrov's theoretical proposal for collapsing binary mixtures, the stabilizing role of quantum fluctuations has been investigated also in dipolar condensates. In [149, 150, 151] it was shown that self-bound structures can appear by including the Gaussian contribution of quantum fluctuations in the Gross-Pitaevskii equation.

3.2.2 Self-bound states classification for $\omega_R = 0$: The case of the soliton-droplet crossover

In this section, we aim to achieve a deeper insight in the peculiar features of this novel droplet state predicted in [97, 98]. From a theoretical point of view, the appearance of this

unexpected phase has an intrisically quantum nature, since quantum fluctuations control its formation. Their inclusion in the thermodynamic picture provides a sort of quantum pressure preventing the instability towards the collapse. Within a mean-field frame, the collapse occurs when inter-component attraction is dominant, i.e. $\Delta g < 0$. Experiments confirming Petrov's guess [101, 148] are, actually, the most effective way to probe the existence and the properties of quantum fluctuations. It is then clear why this proposal has resonated so much within the atomic physics community.

At the same time, another self-bound state, the bright soliton, has been observed and studied in Bose-Einstein condensates for a much longer time. A soliton, or groups of solitons, can appear because of sudden quenches in the interaction strength or, more generally, as excitations in confined geometries with reduced dimensionalities. In principle, only pure one-dimensional systems can sustain stable solitons. When the atom-atom interaction is repulsive (self-defocusing non-linearity) one recovers localized dark solitons, while attractive condensates (self-focusing non-linearity) can display bright solitons. For an exhaustive and detailed review, we point the reader to [152]. We only mention that solitons can be studied also in three-dimensional setups by means of optical waveguides or cigar-shaped trapping potential which are able to stabilize them.

Here, inspired by the recent Tarruell's group experiment [153] in Barcelona, we proceed to characterize the droplet state by comparing it to the solitonic one. In [153], the formation of dilute self-bound states in a two-component BEC was studied in a tight optical waveguide. Interestingly, above a critical value of the magnetic field a smooth crossover interpolating between droplets and bright soliton states was observed. Below such critical magnetic field and for small particle numbers a bistable region is detected, corresponding to different minima of the energy functional. As underlined above, droplets and solitons appear because of different mechanisms: for the droplets, an interplay between mean-field attraction and fluctuations repulsion, while solitons are genuine system excitations.

In the following we are going to analyze the structural properties and the collective modes of droplets and soliton confined in an optical waveguide. In order to properly distinguish these two types of self-bound states, we have to recall that collective modes acts as a tool to characterize the behavior of an ultracold atomic gas. In presence of non-local interactions, such as soft-core [154, 155, 156] or dipolar potentials [149, 151], collective modes are cru-

cial in detecting quantum phase transitions from uniform ground states to more structured configurations.

Binary systems naturally support modes where the two components move in phase, such as monopole and quadrupole oscillations. They are expected to be the lowest energy excitations and their analysis can be greatly simplified by assuming that, over the oscillation period, the components occupy the same spatial mode. More interestingly, the spinorial nature of the order parameter allows nontrivial collective modes where the internal components move out of phase around the equilibrium configuration. The simplest case is represented by the so-called spin-dipole excitation. For a repulsive two-component Bose gas the spin-dipole oscillation frequency depends crucially on the presence of an external confining potential as well as on the reciprocal interaction strength. They were recently characterized in an experiment in Trento [157]. On the contrary, for attractive binary mixtures, we observe [158] that spin-dipole oscillations may take place even in the absence of an external potential. In this case, the inter-component attraction plays the role of the restoring force, without the need to superimpose an external trapping.

For a binary Bose mixtures made of atoms in two different hyperfine states in a volume L^3, the starting point of our analysis is the real-time low-energy effetive action in Eq. (3.47). For the sake of clarity, we report it below

$$S = \int dt\, d^3\mathbf{r} \Big[\sum_{j=1,2} \frac{i\hbar}{2} \big(\Psi_j^* \partial_t \Psi_j - \Psi_j \partial_t \Psi_j^* \big) - \mathcal{E}_{\rm tot}\big(\Psi_1, \Psi_2\big) \Big] \,,$$

where $\mathcal{E}_{\rm tot}$ is given by Eq. (3.48). We recall that $V_{\rm ext}(\mathbf{r})$ is the confining potential, while $g_{jk} = 4\pi\hbar^2 a_{jk}/m$. The fields are normalized to the species density, i.e. $|\Psi_j|^2 = n_j$. The total energy density $\mathcal{E}_{\rm tot}$ includes the Gaussian contribution of quantum fluctuations $\mathcal{E}_g$, given by Eq. (3.49). As anticipated, an analysis of in-phase collective excitations can be greatly simplified by assuming that the fields share the same spatial configuration. This means that we can redefine

$$\Psi_j = \sqrt{n_j}\, \phi(\mathbf{r}, t) \qquad \text{for } j = 1, 2. \tag{3.53}$$

This assumption neglects the inter-component dynamics, resulting inadequate to probe, for example, spin-dipole oscillations. The minima of mean-field energy density Eq. (3.4) fix the

ratio between the components of the population at which the spatial overlap is maximized, i.e. $N_1/N_2 = \sqrt{a_{22}/a_{11}}$ [97, 153], which we assume from now on. Moreover, we slightly modify our notation by defining

$$\Delta a = a_{12} + \sqrt{a_{11}a_{22}}\,, \tag{3.54}$$

instead of Δg in Eq. (3.42). By replacing Eq. (3.53) in Eq. (3.48), in terms of the scattering lengths we get

$$\begin{aligned}\mathcal{E}_{\rm tot} = \frac{\hbar^2 n_{\rm tot}}{2m}\big|\nabla\phi\big|^2 + n_{\rm tot}V_{\rm ext}(\mathbf{r})\big|\phi\big|^2 + \frac{4\pi\hbar^2}{m}\frac{\Delta a\sqrt{a_{22}/a_{11}}}{\Big(1+\sqrt{a_{22}/a_{11}}\Big)^2}n_{\rm tot}\big|\phi\big|^4 \\ + \frac{256\sqrt{\pi}\hbar^2}{15m}\left(\frac{n_{\rm tot}\sqrt{a_{11}a_{22}}}{1+\sqrt{a_{22}/a_{11}}}\right)^{5/2} f\left(\frac{a_{12}^2}{a_{11}a_{22}}, \sqrt{\frac{a_{22}}{a_{11}}}\right)\big|\phi\big|^5\,,\end{aligned} \tag{3.55}$$

with $n_{\rm tot} = n_1 + n_2$ the total density. In order to properly model the experiment performed in [153] we assume a harmonic confinement on the transverse plane, namely $V_{\rm ext} = \frac{1}{2}m\omega_\perp^2(x^2 + y^2)$. In the following, all lengths are in units of $a_\perp$ and energies in units of $\hbar\omega_\perp$. Scattering lengths will be rescaled in units of the Bohr radius a_0 for convenience. The beyond-mean-field phase diagram and the static properties of the ground-state configurations have been studied in [101, 148].

The variational framework provides a possibility to analytically explore the properties of the system. Here, we take a Gaussian ansatz

$$\phi(\mathbf{r}) = \sqrt{\frac{L^3}{\pi^{3/2}\sigma_x\sigma_y\sigma_z}}\exp\left(-\sum_{r_i=x,y,z}\frac{r_i^2}{2\sigma_{r_i}^2}\right) \tag{3.56}$$

whose variational parameters are σ_x, σ_y and σ_z. The original condition $||\psi||^2 = N$ is preserved by the prefactors in Eq. (3.56). By replacing it in Eq. (3.55) and taking the infinite volume limit, the variational energy per particle is given by [153]

$$\begin{aligned}\frac{E}{N\hbar\omega_\perp} = \frac{1}{4}\Big(\frac{1}{\tilde\sigma_x^2}+\frac{1}{\tilde\sigma_y^2}+\frac{1}{\tilde\sigma_z^2}\Big) + \frac{\tilde\sigma_x^2+\tilde\sigma_y^2}{4} + \frac{2N\Delta\tilde a}{\sqrt{2\pi}\tilde\sigma_x\tilde\sigma_y\tilde\sigma_z}\frac{\sqrt{\tilde a_{22}/\tilde a_{11}}}{\Big(1+\sqrt{\tilde a_{22}/\tilde a_{11}}\Big)^2} \\ + \frac{512\sqrt{2}}{75\sqrt{5}\pi^{7/4}}\frac{N^{3/2}}{(\tilde\sigma_x\tilde\sigma_x\tilde\sigma_z)^{3/2}}\left(\frac{\sqrt{\tilde a_{11}\tilde a_{22}}}{1+\sqrt{\tilde a_{22}/\tilde a_{11}}}\right)^{5/2} f\left(\frac{\tilde a_{12}^2}{\tilde a_{11}\tilde a_{22}}, \sqrt{\frac{\tilde a_{22}}{\tilde a_{11}}}\right)\,.\end{aligned} \tag{3.57}$$

In the equation above the tilde signals a length in units of $a_\perp$. By considering ^{39}K atoms [138], the condition $\Delta a < 0$ can be achieved via Feshbach resonances by tuning only one of the three scattering lengths while leaving the others fixed. At the end of this section, we will provide a little more details on the experimental numbers. Both droplets and solitons can be observed because of the simultaneous presence of quantum fluctuations and external confinement.

For low particles number or, equivalently small values of $|\Delta a|$, the system is in the so-called solitonic state, whose shape crucially depends on the trapping profile. Indeed, $\sigma_x = \sigma_y \sim a_\perp$, while σ_z is much greater. Beyond-mean-field corrections are not necessary for the stability of this state. This is confirmed by the good agreement between mean-field simulations [159] and quantities like energy and density profiles.

The situation changes by increasing the particle number or lowering Δa. Within these regimes, the ground state is isotropic, i.e. ($\sigma_x = \sigma_y = \sigma_z < a_\perp$) and, more importantly, it is not affected by the aspect ratios of the external confinement. This self-bound state can be predicted only by taking into account the contribution of Gaussian quantum fluctuations in the variational energy, see Eq. (3.49).

The results of our variational analysis based on Eq. (3.56) are reported in Fig.3.2 where we plot the width as a function of N at fixed values of Δa (panels Fig. 3.2(a)-(c)) and, in turn, as a function of Δa for fixed values of N (panels Fig. 3.2(d)-(f)). At fixed Δa, the system approaches the droplet state by increasing the particle number. In order to reach a pure isotropic state, the effective mean-field attraction, i.e. Δa, has to be strong enough. For example, at $\Delta a = -5.1\, a_0$, σ_z remains two times larger than the radial width even at $N = 10000$, while for $\Delta a = -10.6\, a_0$ the system approaches a spherical configuration already at $N \simeq 5000$ particles. For weak attractive interactions (small negative Δa) the shift from one bound state to the other occurs via a smooth crossover (see Fig. 3.2 for $\Delta a = -8.7\, a_0$). At stronger interactions (large negative Δa) the system undergoes a bistability where competing minima are present in the energy functional leading to a sharp structural change of the condensate as in Fig. 3.2 at $\Delta a = -10.6\, a_0$ [153]. A similar picture emerges by considering a fixed particles number and tuning the effective mean-field attraction as in the panels (d)-(f) of Fig. 3.2.

Beyond the structural properties of the ground state summarized in Fig. (3.2), a deeper

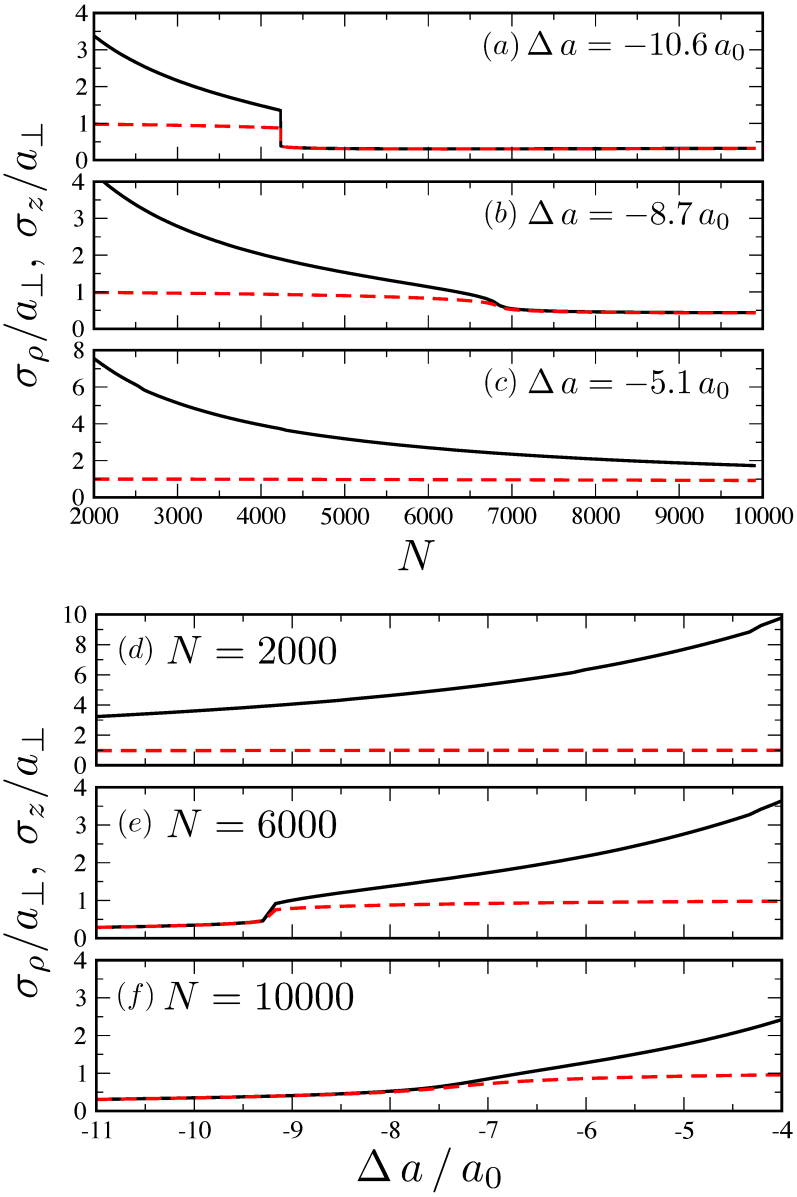

Figure 3.2: Widths of the ground-state energy predicted by the variational Gaussian energy in Eq. (3.57). Widths σ_i with $i = x, y, z$ are expressed in units of the oscillator length $a_\perp = \sqrt{\hbar/(m\omega_\perp)}$ for several values of $\Delta a(a_0)$ (units of the Bohr's radius). In the plots σ_z (solid black line), the gaussian width along the longitudinal direction, and σ_ρ (red dashed line) along the transverse plane. Due to cylindrical symmetry of the confiment, $\sigma_x = \sigma_y$. Panels (a)-(c): Variational widths as a function of the particles number N for three different values of (a) $\Delta a = -10.6$, (b) -8.7, (c) -5.1. In (a) a sharp change of σ_r and σ_z is observed for $N \approx 4200$ signaling a bistability. Panels (d)-(f): Variational widths as a function of Δa for three different values of (d) $N = 2000$, (e) 6000, (f) 10000.

insight into the differences between solitons and droplets is provided by the collective excitations frequencies. These modes are computed around the minima of $E/(N\hbar\omega_\perp)$ of Eq.

(3.57) with the Gaussian ansatz given by Eq. (3.56). Concerning the excitation frequencies, the Gaussian approach provides a effective and semi-analytical tool to extract reliable results throughout a wide range of quantum fluids. For instance, concerning purely one-dimensional Bose mixtures, a recent and detailed study has been carried out in [160]. There, numerical solutions of a Gross-Pitaevskii equation were compared to variational Gaussian outcomes. Moreover, this theoretical recipe was applied to model droplet-like structures and surface effects in trapped Fermi gases. In [161], density functional simulations well reproduced variational results.

Three different oscillation modes (ω_I, ω_{II}, ω_{III}) are expected by solving the eigenvalue problem for the Hessian matrix $\mathrm{Hess}(E) = \frac{\partial^2 E}{\partial\sigma_i \partial\sigma_j}$ computed at the energy minimum. The outcomes of our variational calculation are then reported in Fig. 3.3 and 3.4.

The frequency ω_I (black solid line in Fig. 3.3) can be easily excited along the solitonic side of the crossover. This feature reflects the absence of confinement along one direction. The other two modes ω_{II} and ω_{III} (red and green solid line) are degenerate and converge to $\simeq 2$ (in units of $\hbar\omega_\perp$) as in a weakly interacting BEC [159]. The degeneracy is an obvious consequence of the cylindrical symmetry of the radial confinement. This structure is clearly represented in panel (d) of Fig. 3.3, where mode frequencies are depicted for the $N = 2000$ case: $\omega_{II} = \omega_{III} \simeq 2$, two order of magnitude higher than ω_I. This property survives in the solitonic side of the crossover also for higher particle numbers or lower values of Δa (cfr. Fig. 3.3, panels (b), (c), (e) and (f)).

In the droplet side of the crossover, Fig. 3.3 also shows the particle-emission-threshold $-\mu$. The chemical potential μ is obtained by differentiating the total energy in Eq. (3.55) with respect to N within the Gaussian ansatz in Eq. (3.56). Throughout the droplet regime, in place of small amplitude oscillations around the ground state configuration, the system damps the energy excess by simply expelling particles from the droplet. This peculiar self-evaporation process has been predicted by Petrov [97] and seems confirmed by the first experimental check on his proposal [148]. We want to remark the peculiarity of this situation: for instance, also in the BCS-BEC crossover we are in presence of a negative chemical potential, but collective modes can be anyway detected. The reason is that Fermi gases are trapped, while droplets do not effectively sense the presence of the waveguide.

In the solitonic state, $\mu > 0$ for every value of Δa, thus ω_I can be excited and experimen-

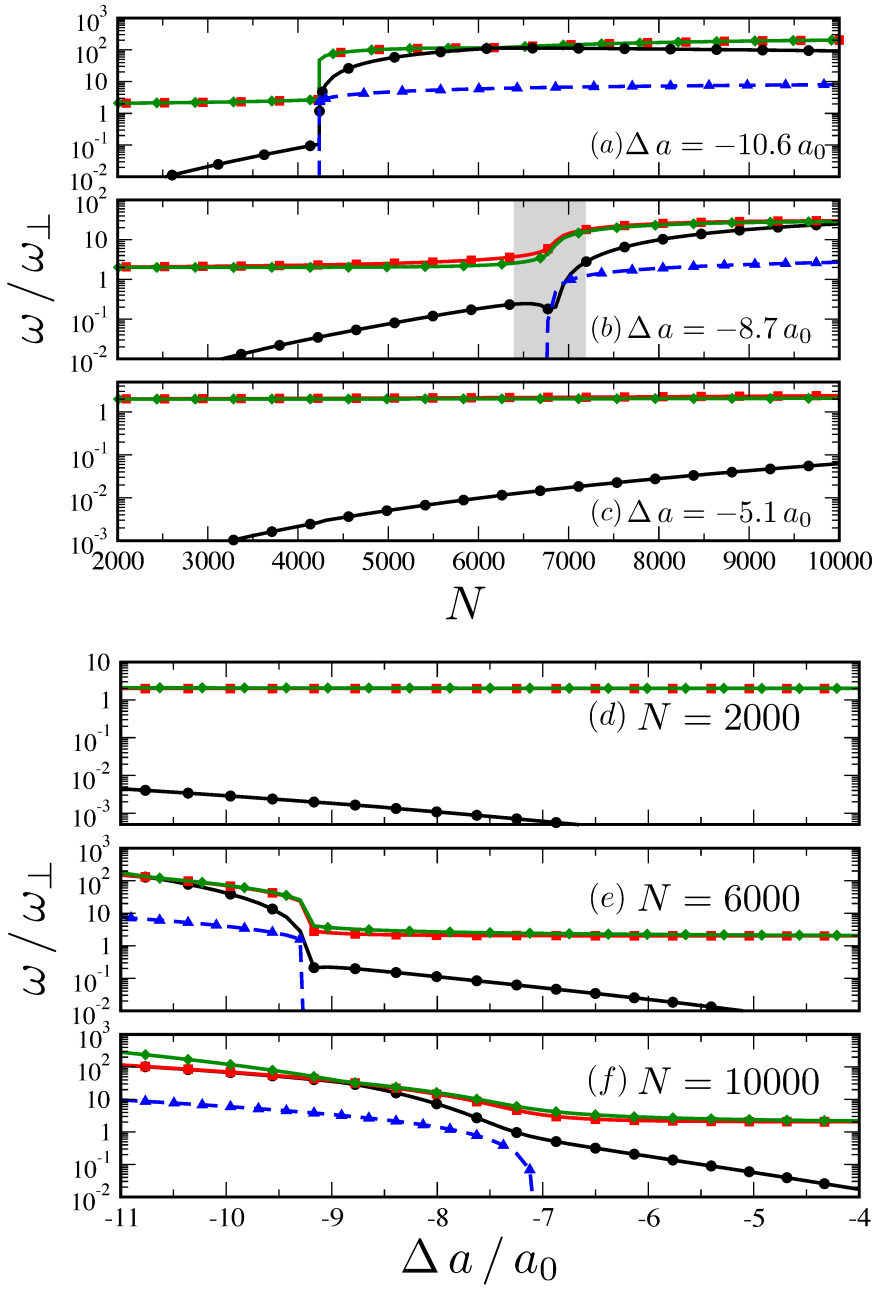

Figure 3.3: Excitation frequencies $\omega_I, \omega_{II}, \omega_{III}$ and the particle-emission threshold $-\mu$, in units of $\hbar\omega_\perp$ as functions of Δa in units of Bohr's radius a_0. The emission threshold (blue triangles) is shown only in the droplet side of the crossover. The excitation frequencies correspond to the eigenvalues of the Hessian matrix of Eq. (3.57) Panels (a)-(c): Frequencies as functions of the particle number N for three different values of the parameter (a) $\Delta a = -10.6$, (b) -8.7, (c) -5.1. In (b) the grey region denotes the interval of particle numbers where the monopole mode is lower than the particle emission spectrum in the droplet phase. See also Fig.3.4 for a magnification of this area. Panels (d)-(f): Frequencies as functions of Δa for three different values of N: (d) $N = 2000$, (e) 6000, (f) 10000.

tally revealed. Its corresponding eigenvector displays the monopole character of ω_I, since $\mathbf{v}_I = \pm\alpha(1,1,1)^T$.

Moving to the droplet-side of the crossover, frequencies lie above the emission threshold in agreement with the prediction of [97, 148]. This implies that excitations of the system are damped by expelling particles from the droplet in a peculiar self-evaporation process. We also verified that, for $\Delta a = -5.1\, a_0$ (cfr. Fig. 3.3(c)), upon increasing the particle number to larger values one enters into the self-evaporation regime ($5.2\cdot 10^4 < N < 1.4\cdot 10^5$). Increasing even more the system size, self-evaporation ceases and the excitations are, at least in principle, observable. It is also interesting to observe that droplet radial size increases almost linearly with the particle number already for $N \geq 4\cdot 10^4$.

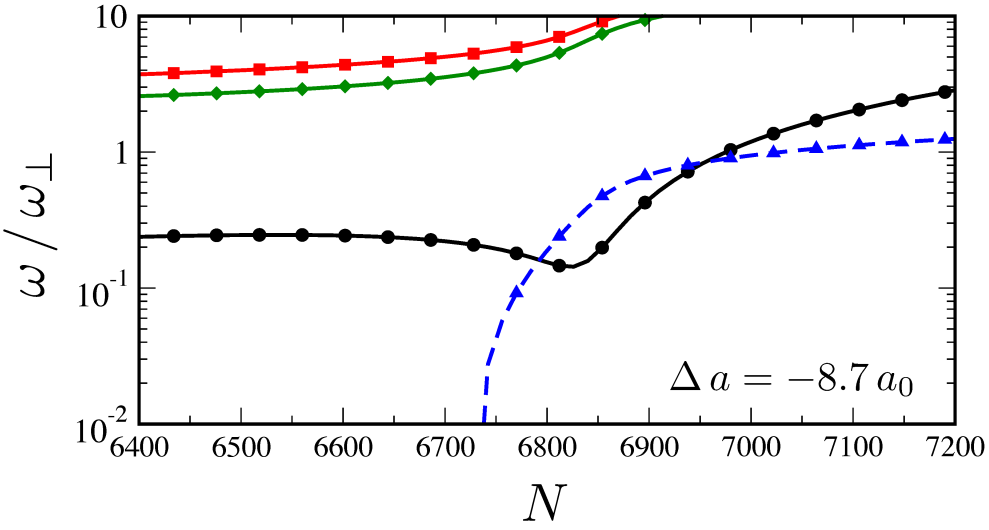

Figure 3.4: Magnification of the grey region of Fig.3.3(b) with $N = 6400 - 7200$. In the range $6780 \lesssim N \lesssim 6950$ monopole oscillations (black line-dots) are higher than the particle emission spectrum (dashed blue line - triangles).

We have described monopole and quadrupole modes as in-phase excitations, meaning that Eq. (3.53) holds. Obviously, in binary mixtures, this cannot be the whole story. A single-field approximation neglects by definition the relative dynamics between the components. The simplest out-of-phase excitation is the so-called spin-dipole oscillation, arising when the two-components are displaced from the center of the harmonic trap. With the purpose of a more physically transparent analysis, we add in the following a weak confinement along the longitudinal axis with an aspect ratio $\lambda_z = \omega_z/\omega_\perp$. We must then modify the Gaussian ansatz in Eq. (3.56) to account the displacement of the components. For simplicity, we

assume it occurs along the z-axis, resulting in the following generalized ansatz

$$\Psi_j = \sqrt{\frac{N_j}{\pi^{3/2}\sigma_r^2\sigma_z}} e^{-\frac{x^2+y^2}{2\sigma_r^2}} \exp\Big[-\frac{(z-z_j)^2}{2\sigma_z^2} + i\alpha_j z\Big] , \tag{3.58}$$

where the fields Ψ_1 and Ψ_2 obey the normalization condition $\int d^3\mathbf{r}|\Psi_j|^2 = N_j$. In the equation above we have assumed cylindrical symmetry $\sigma_x = \sigma_y = \sigma_r$, while $\{\alpha_i\}_{i=1,2}$ describe the corresponding slopes of $\{z_i\}_{i=1,2}$. The set of variational parameters [162, 163] is then given by $\{z_1, z_2, \alpha_1, \alpha_2\}$. Replacing (3.58) into the action in Eq. (3.47), we derive the Lagrangian

$$\begin{aligned} L = \sum_j \Big\{ &- \hbar N_j z_j \dot{\alpha_j} - \frac{\hbar^2 N_j}{2m}\alpha_j^2 - \frac{\hbar^2 N_j}{2m}\Big(\frac{1}{\sigma_r^2} + \frac{1}{2\sigma_z^2}\Big) - \frac{N_j}{4} m\omega_0^2\big(2\sigma_r^2 + \lambda_z^2\sigma_z^2 + 2\lambda_z^2 z_j^2\big) \\ &- \frac{1}{2}\frac{g_{jj}N_j^2}{2\sqrt{2}\pi^{3/2}\sigma_r^2\sigma_z}\Big\} - \frac{g_{12}N_1N_2\exp\Big[-\frac{(z_j-z_k)^2}{2\sigma_z^2}\Big]}{2\sqrt{2}\pi^{3/2}\sigma_r^2\sigma_z} + \mathcal{E}_g \, . \end{aligned} \tag{3.59}$$

The quantum fluctuations contribution in Eq. (3.49) is simplified by assuming $g_{12}^2 = g_{11}g_{22}$ [148]. This implies the system is close to the mean-field instability threshold [36]. The Gaussian correction $\mathcal{E}_g$ to energy density then reads

$$\mathcal{E}_g = \Big(\frac{m}{\hbar^2}\Big)^{3/2} \int d^3\mathbf{r}\big(g_{11}|\Psi_1|^2 + g_{22}|\Psi_2|^2\big)^{5/2} \, . \tag{3.60}$$

Analytical results can be derived by considering a symmetric mixture, where $g_{11} = g_{22}$ and consequently $N_1 = N_2$. The Euler-Lagrange equation are computed from Eq. (3.59) via $\frac{\mathrm{d}}{\mathrm{d}t}\frac{\partial L}{\partial \dot{\mathbf{q}}_i} - \frac{\partial L}{\partial \mathbf{q}_i} = 0$, with $\mathbf{q}$ being the vector of variational parameters. Accordingly, the equation for the slope $\alpha_i = m\dot{z}_i/\hbar$ is elementary, so its dynamics it is completely determined by the one of z_i. The resulting (linearized) system of differential equations is then given by

$$\begin{aligned} \ddot{z}_1 + \omega_0^2\lambda_z^2 z_1 = &\sqrt{\frac{2}{\pi}}\Big(\frac{a_{12}\hbar^2 N_1}{m^2\sigma_r^2\sigma_z^3}\Big)(z_1 - z_2) - \frac{1024}{25\pi^{1/4}}\Big(\frac{a_{11}^{5/2}\hbar^2 N_1^{3/2}}{m^2\sigma_r^3\sigma_z^{7/2}}\Big)(z_1 - z_2) \\ &(z_1 \rightleftharpoons z_2) \, . \end{aligned} \tag{3.61}$$

The equation for z_2 is exactly equal to the one for z_1 except for a global minus sign on the right hand side. From Eqs. (3.61), we can immediately infer the equations of motion for the center of mass and the relative coordinate $\tilde{z} = z_1 - z_2$. The former corresponds to the sum

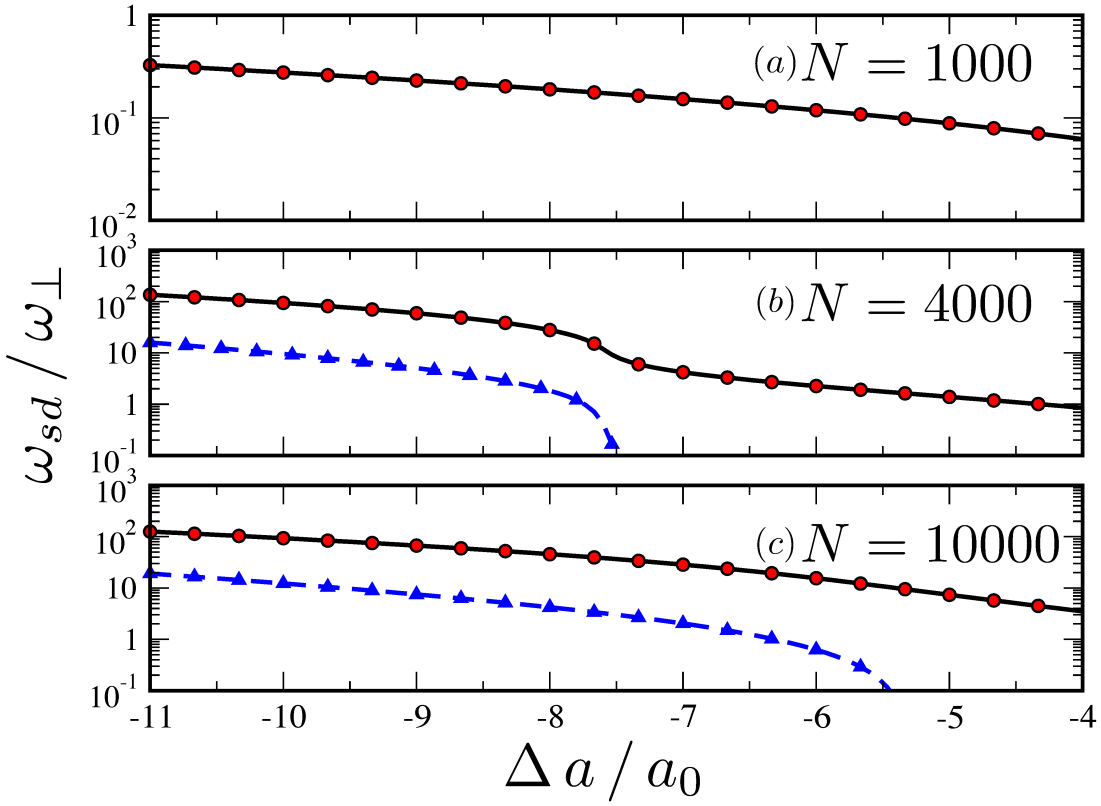

Figure 3.5: (Red dots) Spin dipole oscillations frequency and (Blue triangles) single-particle emission threshold $-\mu$ for $N = 1000, 4000, 10000$ particles. For $N = 1000$ the chemical potential is positive in the range shown in the figure (soliton regime). In all cases the spin-dipole frequency is higher than $-\mu$ by more than one order of magnitude. The plots shown are done with equal intra-species interaction $g_{11} = g_{22}$.

of the equations for z_1 and z_2, resulting in a simple oscillatory motion determined by $\omega_0\lambda_z$ (as stated by the Kohn's theorem). On the other hand, we get that

$$\ddot{\tilde{z}} + \omega_{\rm rel}^2 \tilde{z} = 0 \,. \tag{3.62}$$

In the equation above, $\omega_{\rm rel}$ is the so-called spin-dipole oscillation frequency. In units of $\omega_\perp$, it reads

$$\frac{\omega_{rel}^2}{\omega_\perp^2} = \lambda_z^2 - \sqrt{\frac{8}{\pi}}\,\frac{N_1\big(a_{12}/a_\perp\big)}{\sigma_r^2\sigma_z^3} + \frac{2048}{25\pi^{1/4}}\,\frac{(a_{11}/a_\perp)^{5/2}N_1^{3/2}}{\sigma_r^2\sigma_z^{7/2}} \,. \tag{3.63}$$

By turning off the longitudinal confinement (i.e. $\lambda_z = 0$) and in presence of an effective mean-field attraction ($\Delta a \lesssim 0$), the spin-dipole $\omega_{\rm rel}$ is always a positive defined quantity. The results of our numerical analysis are summarized in Fig. 3.5 for a wide range of interaction

strengths and three different particle numbers.

Similarly to our study of in-phase excitations, in the droplet side of the crossover we have to compare the spin-dipole excitation energy to the particle-emission threshold. We observe that only in the soliton regime spin oscillations become observable ($N = 1000$). In the droplet phase self-evaporation is the dominant mechanism.

In Eq. (3.63), we can identify two different contribution to spin-dipole oscillation. First, we have the mean-field attraction between the components, which is $\propto a_{12}$. Then, we have the Gaussian quantum fluctuations contribution encoded in $\mathcal{E}_g$ given by Eq. (3.60). From its structure, it is evident that it cannot be split into two terms, one for each component.

Self-bound states in binary Bose mixtures are peculiar also for another reason highlighted by Eq. (3.63): spin-dipole oscillations are not inhibited by turning off the longitudinal confining. Indeed, a restoring force driving the oscillatory motion is established by the interplay between mean-field attraction and quantum fluctuations repulsion. This then an extension from the scenario depicted in [157].

Let us now conclude this section by pointing out the relevant experimental parameters in the self-bound states classification. Following the original proposal in [97], experiments to probe quantum droplets in binary Bose mixtures are performed by now with ^{39}K atoms in two different internal states, $|1\rangle = |F = 1, m_F = -1\rangle$ and $|2\rangle = |F = 1, m_F = 0\rangle$. By tuning the magnetic field between $B = 54 \div 57.5$ G, where $a_{11} = 33.5\, a_0$ and $a_{12} = -53.6\, a_0$, the corresponding Feshbach resonance [138] for a_{22} provides a wide range of values for Δa, from $-15\, a_0$ to $+10\, a_0$. In-phase collective excitations (such as monopole and quadrupole modes) can be studied in a setup similar to the one develop by the group of L. Tarruell in Barcelona [153]. Within a variational framework, our results confirm the dominant role played by self-evaporation along the droplet side of the crossover. Indeed, monopole and quadrupole are observable, in principle only in a restricted window in the parameters space, as reported in Fig. (3.4). Moreover, we developed zero-temperature analysis, leaving unanswered every question about what happens for small, but finite temperatures.

A tighter range of experimental values is required to probe our analytical prediction about out-of-phase excitations. This is due to the symmetry requirement $g_{11} = g_{22}$. As in [67], we consider the symmetric mean-field ground state given by the condition $a_{11} \simeq a_{22} \simeq 33.5\, a_0$ at $B = 54.5\, G$, where $a_{12} = -54\, a_0$. The experimental protocol is then similar to the one

proposed in [157], where a supplementary effort has to be devoted to the fine tuning of the magnetic fields and scattering lengths. The displacement from a state with complete spatial overlap can be achieved through a magnetic field gradient δB along the longitudinal axis, generated by two coils in anti-Helmoltz configuration. A longitudinal trapping is not mandatory to experimentally probe spin-dipole oscillations, because of the peculiar structure of Gaussian fluctuations contribution to the energy density. From an experimental perspective, our study may provide a complementary insight to that of [157]. Finally, we mention that the effect of three-body losses could be included into a full description of the excitation dynamics. This can done with the inclusion of a term $-i\hbar\frac{L_3}{2}|\psi|^4$ in the right side of the Gross-Pitaevskii equation [164].

3.2.3 Quantum fluctuations and droplets: the case $\omega_R \neq 0$

In this section we consider again the case of Rabi-coupled binary Bose mixture as in sec. 3.1.2. The coherent-coupling between the two hyperfine states enables the flipping of atoms from one component to the other, as specified by the ω_R-term in Eq. (3.10). Our analysis of the possible ground-states of the system leads us to the mean-field phase diagram in Fig. 3.1. There are two stable lowest-energy configuration according to the minima of Eq. (3.15): a symmetric ground state, with no population imbalance, and a polarized one, where $n_1 - n_2 \neq 0$.

In the proceeding of the section, we focus on the symmetric ground state (SGS) existing in presence of Rabi coupling, where $v_1 = v_2 \equiv v/\sqrt{2}$ and equal intra-component interaction. Over this configuration, Eq. (3.15) becomes

$$\frac{\Omega_0(\mu, v)}{L^3} = -\mu v^2 + \frac{1}{4}(g + g_{12})v^4 - \hbar\omega_R v^2 \,. \tag{3.64}$$

The important relation between the chemical potential μ and the order parameter can now be derived from Eq. (3.16). Above the (SGS) we have a single equation, reading $v^2 = 2(\mu + \hbar\omega_R)/(g + g_{12})$. In this case, Eq. (3.64) reduces to

$$\frac{\Omega_0(\mu)}{L^3} = -\frac{(\mu + \hbar\omega_R)^2}{g + g_{12}}. \tag{3.65}$$

We have to remark that we are considering the coherently-coupled mixture within a regime where polarization due to ω_R does not occur. The absence of polarization holds also when Gaussian fluctuations are taken into account. However, this does not mean that the Rabi coupling is not relevant. Indeed, we are going to show that it still affects the stability of the balanced configuration on the mean-field threshold separating the SGS from the collapsing phase.

The zero-temperature Gaussian contribution $\Omega_g^{(0)}$ can be computed by means of the usual machinery outlined in Chap. 1. Because of Rabi-coupling, the Gaussian action S_g in Eq. (3.28) has an additional term, namely $\int d\tau \int d^3\mathbf{r}\, \hbar\omega_R \sum \eta_i^* \eta_{3-1}$. Moving to the Fourier space, this implies a slight modification in the 2×2 off-diagonal blocks of $\mathbb{M}(\mathbf{q}, \omega_n)$ given by Eq. (3.30). Specifically, we find

$$\hbar\Sigma_{12} = \begin{pmatrix} g_{12}v^2/2 - \hbar\omega_R & g_{12}v^2/2 \\ g_{12}v^2/2 & g_{12}v^2/2 - \hbar\omega_R \end{pmatrix} . \tag{3.66}$$

Keeping in mind the modified $\hbar\Sigma_{12}$ in the equation above, the spectrum of elementary excitations above the SGS can be obtained by diagonalizing the matrix $-\hbar\mathbb{I} \cdot \mathbb{M}(\mathbf{q}, 0)$, as in Eqs. (3.34) and (3.35). The dependence on the order parameter can be removed by making use of the saddle-point equation of state. The resulting Bogoliubov spectrum has two branches:

$$E_{(+)}(\mathbf{q}) = \sqrt{\frac{\hbar^2 q^2}{2m}\left[\frac{\hbar^2 q^2}{2m} + 2\big(\mu + \hbar\omega_R\big)\right]} \tag{3.67}$$

$$E_{(-)}(\mathbf{q}) = \sqrt{\frac{\hbar^2 q^2}{2m}\left[\frac{\hbar^2 q^2}{2m} + 2\,A(\mu, \omega_R)\right] + B(\mu, \omega_R)} \, . \tag{3.68}$$

By defining

$$\epsilon = \frac{a_{12}}{a} \tag{3.69}$$

as the ratio between the inter-component scattering length and the intra-component one,

the functions $A(\mu,\omega_R)$ and $B(\mu,\omega_R)$ are given by

$$A(\mu,\omega_R)=\frac{1-\epsilon}{1+\epsilon}(\mu+\hbar\omega_R)+2\hbar\omega_R \tag{3.70}$$

$$B(\mu,\omega_R)=4\hbar\Omega_R\left[\frac{1-\epsilon}{1+\epsilon}(\mu+\hbar\omega_R)+\hbar\omega_R\right]. \tag{3.71}$$

At $T=0$ K, the Gaussian grand potential corresponds to the zero-point energy of bosonic excitations, given by

$$\Omega_g(\mu,v)=\frac{1}{2}\sum_{\mathbf{q}}\left[E^{(+)}_{\mathbf{q}}(\mu,v)+E^{(-)}_{\mathbf{q}}(\mu,v)\right]. \tag{3.72}$$

By taking the continuum limit, we stumble upon the usual UV divergence. In order to remove it and exctract a finite contribution, in this case we do not make use of dimensional regularization. Instead, we prefer to add a convergence factor in the Matsubara summation, i.e. in Eq. (3.29), which generates the proper counterterms balancing the polynomial divergences [2, 48, 165]. These counterterms can also be computed by expanding the branches at high momenta. The zero-temperature beyond-mean-field grand potential is then given by equation (3.65) plus the regularized zero-point energy, namely

$$\frac{\Omega^{(0)}(\mu)}{L^3}=-\frac{(\mu+\hbar\omega_R)^2}{g+g_{12}}+\frac{8}{15\pi^2}\left(\frac{m}{\hbar^2}\right)^{3/2}\big(\mu+\hbar\omega_R\big)^{5/2}+\frac{A^{5/2}}{2\sqrt{2}\pi^2}\left(\frac{m}{\hbar^2}\right)^{3/2}I(\mu,\omega_R,\epsilon)\,, \tag{3.73}$$

where

$$I\big(\mu,\omega_R,\epsilon\big)=\int_0^{+\infty}dy\left[\sqrt{y}\sqrt{y^2+2y+\frac{B}{A^2}}-y^{3/2}-\sqrt{y}-\frac{\big(\frac{B}{A^2}-1\big)}{2\sqrt{y}}\right]. \tag{3.74}$$

The energy density $\mathcal{E}=E^{(0)}/L^3$ is given by $\mathcal{E}=\Omega^{(0)}/L^3+\mu n$ with $\Omega^{(0)}$ as in Eq. (3.73), while $n=-\frac{1}{L^3}\frac{\partial\Omega}{\partial\mu}$. In the experimentally relevant limit of small coupling frequencies [134], the energy density $\mathcal{E}$ has an analytical expression. By rescaling energies in units $E_B=\hbar^2/ma^2$ (then $\hbar\omega_R=\bar{\omega}_R E_B$), we get

$$\frac{\mathcal{E}}{E_B/a^3}=\pi\big(1+\epsilon\big)\bar{n}^2-\bar{\omega}_R\bar{n}+\frac{8}{15\pi^2}\big[2\pi\bar{n}(1+\epsilon)\big]^{5/2}+\frac{8}{15\pi^2}\big[2\pi\bar{n}(1-\epsilon)\big]^{5/2}+\frac{14}{3\pi^2}\bar{\omega}_R\big[2\pi\bar{n}(1-\epsilon)\big]^{3/2}\,, \tag{3.75}$$

where $\bar{n}=na^3$ is the gas parameter. As a consistency check, notice that for $\bar{\omega}_R=0$ one

recover the Larsen's zero-temperature equation of state [147]. Concerning the stability of this symmetric configuration, it is immediate to realize that for $|\epsilon| > 1$ the uniform, balanced, ground state is not stable. For a strong inter-component repulsion, i.e. $\epsilon > 1$, we expect a polarizing instability. On the contrary, for $\epsilon < -1$ the term proportional to $[(1+\epsilon)\bar{n}]^{5/2}$ becomes imaginary. This imaginary term acts as a dissipative mechanism [97, 150]. However, as for other sources of losses (for instance three-body losses), in order to study the short-time dynamics, this dissipative term can be neglected if $\bar{n}$ is not too large. In [97], it was shown, for instance, that the dissipation induced by the imaginary branch acts on much larger time scale than three-body losses. The latter remains, in any case, the main source of instability for condensed mixtures. As in sec. 3.2.1, the energy density in Eq. (3.75) displays the Lee-Huang-Yang $n^{5/2}$ dependence, competing with mean-field attraction proportional to n^2. This is exactly the scenario depicted by Petrov in [97, 98] for the case $\omega_R = 0$ and recently applied also in dipolar systems [149, 150, 151]. Therefore, for $\epsilon < -1$, the system sustains a finite equilibrium density also in free space, as opposed to the mean-field collapsing scenario. By minimizing Eq. (3.75) with respect to $\bar{n}$ and neglecting the small imaginary term, we arrive at the following result

$$\bar{n}_{\pm} = \left(\frac{5\sqrt{\pi}|1+\epsilon|}{32\sqrt{2}(1+|\epsilon|)^{5/2}} \left[1 \pm \sqrt{1 - \frac{1792\,\bar{\omega}_R}{15\pi^2} \frac{(1+|\epsilon|)^4}{|1+\epsilon|^2}} \right] \right)^2 . \tag{3.76}$$

The solution $\bar{n}_-$ is a local maximum. The equilibrium value is given by the minimum $\bar{n}_+$. Rabi frequency is limited by $\bar{\omega}_R < \frac{15\pi^2}{1792} \frac{|1+\epsilon|^2}{(1+|\epsilon|)^4}$ in order to make $\bar{n} \in \mathbb{R}$. For larger $\bar{\omega}_R$ there is only the absolute minimum with zero energy at $\bar{n} = 0$, corresponding to an evaporating mixture, since there is no confining potential.

In sec. 3.2.2 we propose a theoretical approach to model the self-bound droplet state with a finite number of particles. By assuming that the components share the same spatial modes, as in Eq. (3.53) we define a space-time dependent complex field $\phi(\mathbf{r}, t)$ such that $n(\mathbf{r}, t) = \left|\phi(\mathbf{r}, t)\right|^2$ is the space-time dependent local number density and $N = \int d^3\mathbf{r}\; n(\mathbf{r}, t)$. The dynamics of $\phi(\mathbf{r}, t)$ is controlled by the real-time effective action

$$S_{\text{eff}}[\phi^*, \phi] = \int dt\, d^3\mathbf{r} \left[\frac{i\hbar}{2} \big(\phi^* \partial_t \phi - \phi \partial_t \phi^* \big) - \mathcal{E}_{\text{tot}}\big(|\phi|^2\big) \right], \tag{3.77}$$

where $\mathcal{E}_{\rm tot} = \frac{\hbar^2|\phi|^2}{2m} + \mathcal{E}^{(0)}(|\phi|^2)$. The term $\mathcal{E}^{(0)}(|\phi|^2)$ is modelled around the real part of the energy density in Eq. (3.75). In the upper panel of Fig. 3.6 we plot the droplet density profile obtained by solving the Gross-Pitaevskii equation associated to Eq. (3.77). The numerical evolution is performed in imaginary time by varying the number of particles at $\omega_R/2\pi = 1$ kHz. The solution indeed corresponds to a self-bound spherical droplet whose radial width increases with the number of atoms. For large atoms numbers, the density profile displays a plateau approaching the corresponding value in the thermodynamic limit, specified by equation (3.76). On the contrary, the droplet does not exist for $N \lesssim 977$, and the mixture evaporates. Further insight into the droplet features is provided by a variational analysis. Therefore, we impose an Gaussian ansatz for the in-phase field ϕ, similar to Eq. (3.56), namely

$$\tilde{\phi}(\tilde{\mathbf{r}}, \tilde{t}) = \frac{\sqrt{\tilde{N}}}{\pi^{3/4}\sqrt{\tilde{\sigma}_1\tilde{\sigma}_2\tilde{\sigma}_3}} \prod_{i=1}^{3} \exp\left[-\frac{\tilde{x}_i^2}{2\tilde{\sigma}_i^2} + i\tilde{\beta}_i\tilde{x}_i^2 \right] . \tag{3.78}$$

The Gaussian width $\tilde{\sigma}_i(t)$ and the curvature $\tilde{\beta}_i(t)$ are in units of the intra-component scattering length a. Here, by setting $\mathbf{r} = a\,\tilde{\mathbf{r}}$ and $|\phi| = \sqrt{n}|\tilde{\phi}|$, the normalization condition is modified in $\int d^3\tilde{\mathbf{r}}|\tilde{\phi}|^2 = \tilde{N}$. The real particle number is recovered by $N = \tilde{N}\bar{n}$. By inserting equation (3.78) in Eq. (3.77), the Euler-Lagrange equations for the variational parameters $\{\tilde{\sigma}_i, \tilde{\beta}_i\}_i$ are [162, 163]:

$$\tilde{\beta}_i = \frac{\dot{\tilde{\sigma}}_i}{2\tilde{\sigma}_i} \qquad \text{and} \qquad \ddot{\tilde{\sigma}}_i = -\partial\bar{U}\big(\tilde{\sigma}_1, \tilde{\sigma}_2, \tilde{\sigma}_3\big)/\partial\tilde{\sigma}_i \, . \tag{3.79}$$

The functional $\bar{U}\big(\tilde{\sigma}_1, \tilde{\sigma}_2, \tilde{\sigma}_3\big)$ is given by

$$\bar{U}\big(\tilde{\sigma}\big) = \frac{1}{2}\sum_{i=1}^{3}\frac{1}{2\tilde{\sigma}_i^2} - \frac{\big|1+\epsilon\big|\,N}{2\sqrt{2\pi}\big(\tilde{\sigma}_1\tilde{\sigma}_2\tilde{\sigma}_3\big)} + \alpha\frac{(1+|\epsilon|)^{5/2}\,N^{3/2}}{\big(\tilde{\sigma}_1\tilde{\sigma}_2\tilde{\sigma}_3\big)^{3/2}} + \gamma\frac{(1+|\epsilon|)^{3/2}\,\bar{\omega}_R\,N^{1/2}}{\big(\tilde{\sigma}_1\tilde{\sigma}_2\tilde{\sigma}_3\big)^{1/2}} \tag{3.80}$$

where $\alpha = \frac{128}{75\sqrt{5}\pi^{7/4}}$ and $\gamma = \frac{112}{9\sqrt{3}\pi^{5/4}}$. The energy per particle of the ground state is simply $\bar{E}_{\rm gs}/N = \bar{U}(\tilde{\sigma}_m)$ where $\tilde{\sigma}_m$ is the minimum of the effective potential energy. In absence of an external trapping, the system preserves its spherical symmetry, i.e. stationary points of the effective potential in equation (3.80) are reached for $\tilde{\sigma}_{m1} = \tilde{\sigma}_{m2} = \tilde{\sigma}_{m3}$. In the lower panel of Fig. 3.6 we report the stability diagram of the droplet phase. Upon increasing the number of atoms droplets appear to be more stable. On the other side, for small N,

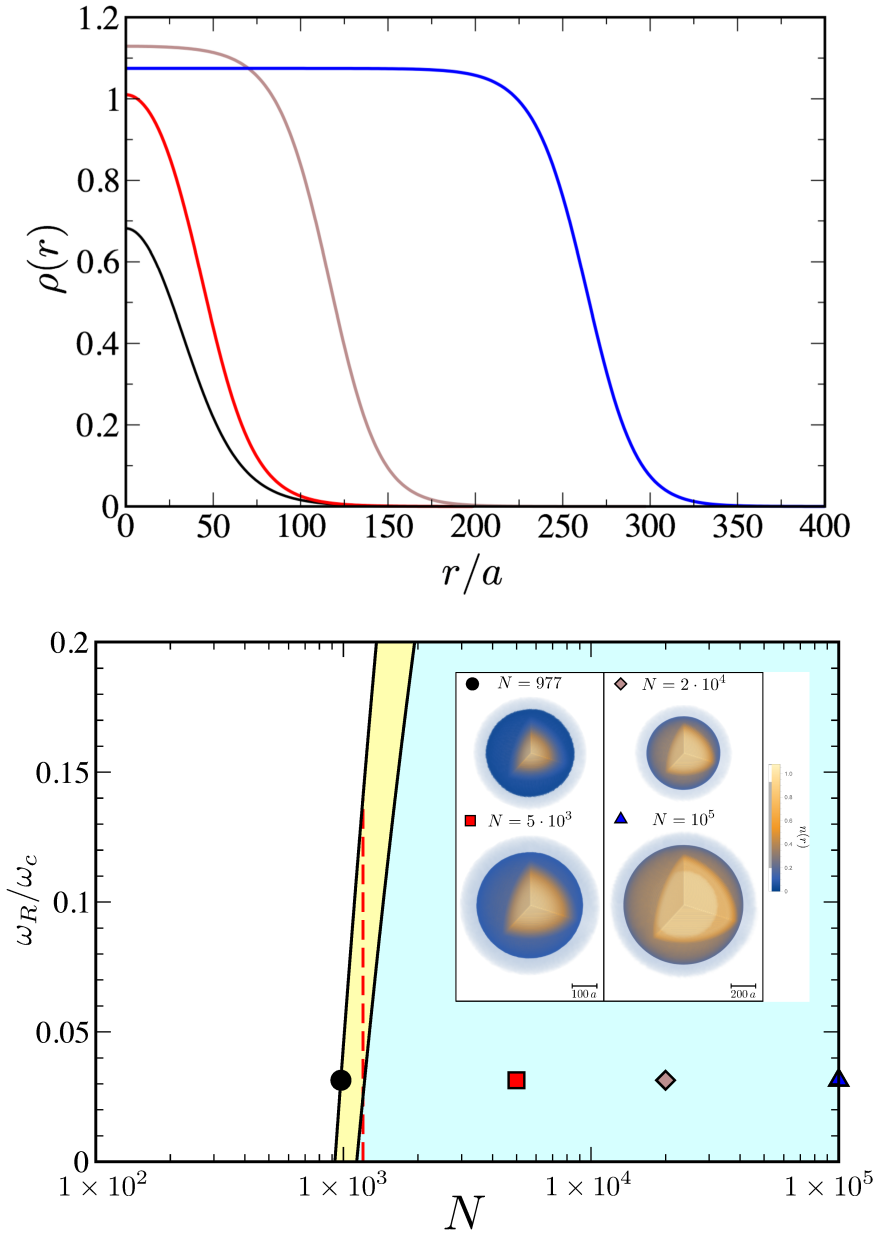

Figure 3.6: We identify the phases of a Rabi-coupled Bose mixture with equal number of particles upon the minimization of the energy functional $\bar{U}(\tilde{\sigma}_1, \tilde{\sigma}_2, \tilde{\sigma}_3)$ of equation (3.80). We observe three phases: a stable droplet-phase region (light green) of spherical self-bound droplets, a metastable droplet phase (yellow) where the energy of the droplet is positive and larger than a uniform background with vanishing density, and an unstable (white region) for small particle number N or high Rabi coupling ω where droplet evaporate. Here we consider $|1+\epsilon| = 0.5$ which corresponds to $\omega_c \simeq 31.8\,\text{kHz}$. In the inset we plot the three dimensional density profile $n(r)$ of droplets from the numerical solution of the Gross-Pitaevskii equation for different particle numbers at $\omega_R/2\pi = 1\text{kHz}$, from the metastable region $N = 977$ and gaussian density limit $N = 5 \cdot 10^3$ to the Thomas-Fermi regime $N = 2 \cdot 10^4$ and $N = 10^5$ where system density is roughly constant up to a critical droplet radius. Moving along the vertical axis, increasing the Rabi coupling, droplets become metastable and finally unstable. Red dashed line refers to a system of $N = 1200$ particles.

a metastable region occurs: $\bar{U}(\tilde{\sigma}_1, \tilde{\sigma}_2, \tilde{\sigma}_3)$ has a local minimum with positive energy. The lowest-energy configuration corresponds instead to a dispersed gas with vanishing density. It is interesting to observe that Rabi coupling acts as additional knob tuning the droplet stability. As underlined by the red dashed line $N \simeq 1200$ atoms in the lower panel of Fig. 3.6, by increasing ω_R one can cross the boundary between the droplet and the unstable phase.

Fig. 3.7 shows the energy per particle of the self-bound droplet: the numerical approach relying on imaginary-time evolution is in reasonable agreement with the variational one based on Eq. (3.78). Remarkably, above a critical Rabi frequency the internal energy of the droplet becomes positive, signaling that the droplet enters in a metastable configuration. At a a slightly larger critical Rabi frequency the droplet evaporates. The low-energy collective

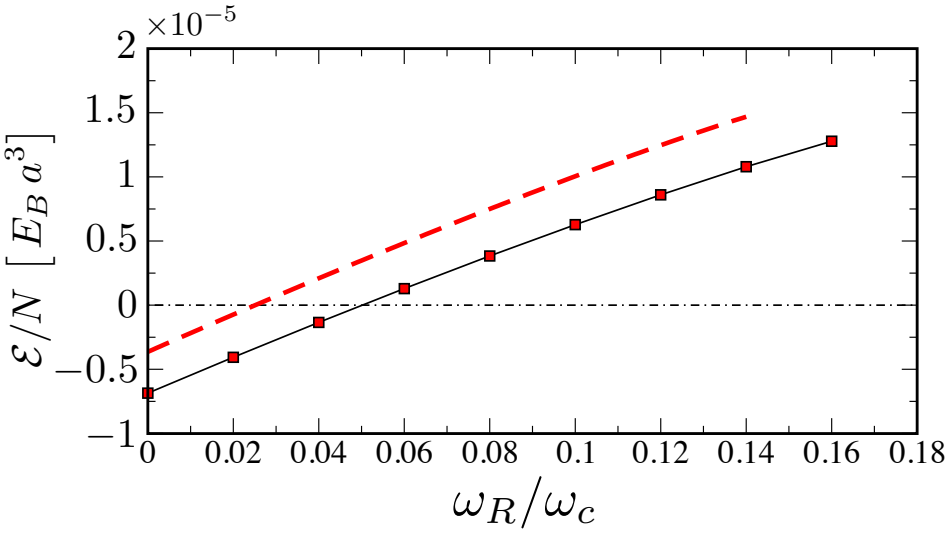

Figure 3.7: Energy per particle of a system of $N = 1200$ particles as a function of the Rabi coupling along the vertical line of Fig. 3.6. Red dashed line: Variational energy from equation (3.80). Squared dots: Energy per particle from the numerical solution of the Gross-Pitaevskii equation. Increasing the Rabi coupling to values larger than $\omega \simeq 0.16\,\omega_c$ the *metastable* droplet evaporates.

excitations of the self-bound droplet are investigated by solving the eigenvalues problem for the Hessian matrix of effective potential energy in equation (3.80). Our Gaussian ansatz in Eq. (3.78) naturally enables two different excitation modes, a monopole (breathing) and a quadrupole with frequencies given by ω_M and ω_Q, respectively.

In Fig. 3.8 monopole and quadrupole frequencies are reported as a function of the

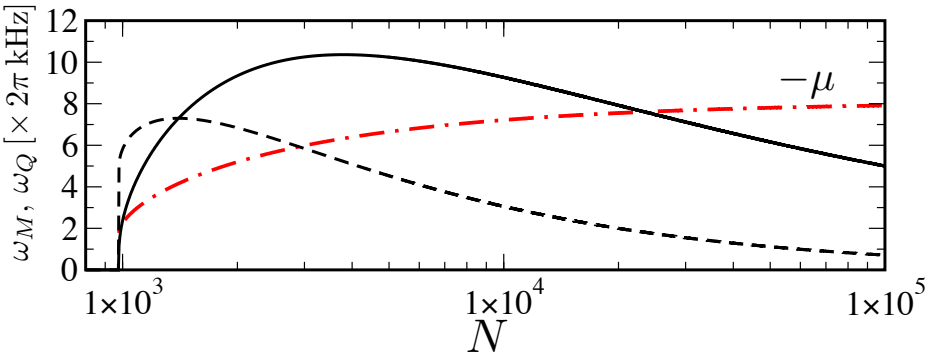

Figure 3.8: Monopole (breathing) mode frequency ω_M (solid) and quadrupole mode frequency ω_Q (dashed) with $\left|1+\epsilon\right| = 0.5$. Upper panel: frequencies as a function of particle number and $\omega_R/2\pi = 1\,\mathrm{kHz}$. Below $N \simeq 977$ the droplet becomes unstable. These modes have to be compared with the particle-emission threshold $-\mu$ (dashed-dotted red line).

number N of atoms in the droplet, at fixed coupling frequency and scattering lengths. Since the droplet is in free space, one has to compare these excitation frequencies with the single-particle emission threshold (dashed-dotted red line). We immediately notice that, differently from the soliton-droplet crossover in Fig. 3.3, collective modes can in principle be detected for rather well extended range of atoms numbers.

The experimental observation of a droplet phase with Rabi coupled internal states is within experimental reach. A promising candidate is a gas of ^{39}K atoms loaded in hyperfine states $|F=1, m_F=0\rangle$ and $|F=1, m_F=-1\rangle$. The narrow Feshbach resonance at $B \simeq 54.5$ G for collisions between atoms in $|1,0\rangle$, allows to tune intra-component scattering length to $a_1 = a_2 \simeq 33.5\ a_0$, where a_0 is the Bohr radius [138, 139]. The corresponding inter-component scattering length is $a_{12} \simeq -54.5\, a_0$, which gives $\epsilon \simeq -1.6$. For Rabi coupling frequencies of the order of $\omega_R/2\pi = 1$ kHz [166] and $N = 10^5$ particles, we predict a droplet with a FWHM $\simeq 1.45\ \mu$m.

4

QUANTUM FLUCTUATIONS IN SUPERFLUID DIPOLAR BOSONS

In this chapter we investigate the structural and superfluid properties of a single-component Bose-Einstein condensate made of dipolar atoms. Atomic species such as Chromium, Dysprosium and Erbium have a strong magnetic dipole moment and, consequently, the two-body interaction is anisotropic and long-ranged. These peculiar features crucially affect the thermodynamic picture and the ground state configurations, leading to a richer phenomenology than the one displayed by alkali atoms.

We are especially interested in the superfluid character of dipolar condensates, in relation to the occurring of structured ground states driven by the interplay of quantum fluctuations and complex interactions.

Besides our analytical approach based on functional integration, we will present the outcomes of numerical simulations based on the Path-Integral Monte Carlo algorithm.

4.1 Introduction: magnetic atoms in play

4.1.1 Atoms and molecules: new playgrounds for physicists

The first experimental realization of Bose-Einstein condensation [31, 32] was achieved in atomic clouds made of alkali atoms. In these extremely diluted setups, the Bogoliubov theory has provided a reliable, and relatively simple, theoretical frame to interpret the experiments and suggest new research directions. The Bogoliubov theory is often formulated in relation to the zero-range approximation for the atom-atom interaction. This results in a universal theory, meaning that all thermodynamic quantities are independent from the potential shape. The presence of the two-body interaction survives only through the dependence on the s-wave scattering length.

In Chap. 2 we have shown that it is sufficient to increase the density to enter in regimes where the zero-range approximation is not reliable. We provided a possible solution, underlining how finite-range corrections can heal certain spurious instabilities due to the unphysical assumption of a zero-range contact pseudopotential. At the same time, Chap. 3 pointed out that the relevance of quantum fluctuations is not limited to deviations of thermodynamic functions from the mean-field picture, universal or not. Strikingly, by taking them into account, we opened the door to the observation of a new quantum phase in collapsing mixtures. As a matter of fact, the stability of self-bound droplets is driven exclusively by quantum fluctuations. We have to remark here that binary mixtures are an excellent platform to test this idea: there, the mean-field attraction leading to the collapsing instability is counterbalanced by the quantum pressure arising from Gaussian corrections. As already mentioned, from a *historical* point of view, it is interesting to notice that Petrov theoretical proposal [97, 98] did not find its first experimental confirmation in binary mixtures, but instead in dipolar condensates [99, 100].

Moving from this observation, a quick look on the related literature [102, 167, 168] should make us immediately aware of the uniquely rich phenomenology arising thanks dipole-dipole interaction in atomic clouds. It has to be acknowledged that the atomic physics community realized the oustanding opportunities provided by dipolar quantum gases soon after the alkali condensation. In order to engineer this kind of quantum fluids, the most promising

platforms rely upon polar molecules and strongly magnetic atoms. Polar molecules as KRb, ND_3 and HCN are the most natural candidates because of their extremely strong electric dipole moment. As a matter of fact, electric dipolar coupling is much higher than the magnetic one. These feature can be understood by considering the interaction potential of two particles with dipole moments orientend along $\hat{\mathbf{d}}_1$ and $\hat{\mathbf{d}}_2$, with $\|\hat{\mathbf{d}}_i\|= 1$ for $i = 1, 2$. At a distance r, one has that

$$V_{\rm ddi}(\mathbf{r}) = \frac{C_{\rm dd}}{4\pi} \frac{r^2(\hat{\mathbf{d}}_1 \cdot \hat{\mathbf{d}}_2) - 3(\hat{\mathbf{d}}_1 \cdot \mathbf{r})(\hat{\mathbf{d}}_2 \cdot \mathbf{r})}{r^5} \tag{4.1}$$

where the coupling constant is given by

$$C_{\rm dd} = \begin{cases} = \mu_0^2 d_m^2 & \text{for magnetic dipoles} \\ = d_e^2/\epsilon_0 & \text{for electric dipoles} \end{cases} . \tag{4.2}$$

In the equation above μ_0 is vacuum magnetic permeability, d_m the magnetic moment, d_e the electric one and ϵ_0 the vacuum electric permeability. Typical values of parameters in the equations above provide a first evaluation of the relative strength between electric and magnetic coupling. Concerning electric dipoles, we have that $d \sim e a_0$, e being the electron charge and a_0 the Bohr radius. The characteristic scale of magnetic dipoles is instead given by the Bohr magneton $\mu_B = e\hbar/(2m_e)$, where m_e is the electron mass. Thus, one has [102]

$$\frac{\mu_0 d_m^2}{d_e^2/\epsilon_0} \sim \alpha^2 \sim 10^{-4} \tag{4.3}$$

with $\alpha \simeq 1/137$ the fine-structure constant. In order to quantify the *strength* of dipole-dipole interaction between atoms or molecules, it is useful to define a characteristic length, namely

$$a_{\rm dd} \equiv \frac{m\, C_{\rm dd}}{12\pi\hbar^2} . \tag{4.4}$$

It is common to evaluate the relevance of dipolar interaction in an ultracold quantum gas by considering the ratio [102]

$$\epsilon_{\rm dd} \equiv \frac{a_{\rm dd}}{a_s} . \tag{4.5}$$

For alkali atoms, magnetic dipole moment is $\simeq 1.0\mu_B$, leading to $a_{\rm dd} \simeq 0.7\, a_0$. For typical

values of the scattering length, one gets $\epsilon \sim 10^{-3}$. For chromium atoms, condensed in 2005 by Pfau's group in Stuttgart [169], we have $d_m \simeq 6\mu_B$, meaning that $a_{\rm dd} \simeq 16\, a_0$ and $\epsilon \sim 10^{-1}$. Nowadays, the current research on dipolar atomic gases is focused on Erbium [170] and Dysprosium [171]. By means of Feshbach resonances, one can engineer systems with $\epsilon \gtrsim 1$, a regime where beyond-mean-field effects and strong correlations arise [99, 172].

Despite the achievements in the atomic setups, the final goal in this research line is focused on realizing degenerate gases of polar molecules. This is actually due to their strong electric dipole moment leading to $a_{\rm dd} \sim 10^3\, a_0$ and $\epsilon_{\rm dd} \sim 10^2$. Degenerate gases of ultracold molecules have remained for years only a dream within the community, until the groundbreaking results of Yun Je's group at JILA [173]. They report the first experimental realization of a Fermi degenerate gas of KRb molecules, paving the way for a bright future research.

4.1.2 Peculiar features of the dipole-dipole interaction

By following [102], in this section we briefly outline the peculiar features of the dipole-dipole interaction. This is the most immediate way to highlight that Bose-Einstein condensates made of magnetic atoms require a theoretical analysis beyond the usual zero-range Bogoliubov framework.

We begin by considering again Eq. (4.1), where the dipole-dipole interaction (DDI) is defined in the most general way. In order to simplify the analysis, it is possible to consider a set of polarized dipoles. For instance, atoms like Dysprosium and Erbium are oriented along the z-axis by turning on a field $\mathbf{B}(\mathbf{r}) = (0, 0, B_z)$. Eq. (4.1) is then modified in

$$V_{\rm ddi}(\mathbf{r}) = \frac{C_{\rm dd}}{4\pi} \frac{1 - 3\cos^2\theta}{r^3} \tag{4.6}$$

where θ is the angle between the polarization axis and the relative position of atoms. From Eq. (4.6), it is also evident another relevant property of DDI. In the zero-range approximation the energy of the system is in fact an extensive quantity in the thermodynamic limit. On the other hand, when the interaction is truly long-range, also the total number of particles affects the energy density. So, a necessary condition for the interaction to be short-range is that the integral $\int_{r_0}^{+\infty} d^d\mathbf{r} V_{\rm int}(\mathbf{r})$ converges, with r_0 being a cutoff. Looking at $V_{\rm ddi}(\mathbf{r})$ in Eq.

(4.6) we immediately realize that the DDI has a long-range character in $d = 3$. We remember that the distinction between intensive and extensive quantities holds in the thermodynamic limit, so this definition does not apply to finite-size systems.

The angular dependence in Eq. (4.6) highlights the anisotropic nature of the DDI. The factor $1 - 3\cos^2\theta$ varies within the interval $[-2, 1]$ for angles $\theta \in [0, \pi/2]$. This is a crucial point, because it implies that the DDI is purely attractive for dipoles in a *head-to-tail* configuration, while repulsion occurs when they are confined side by side. While this is basically the whole picture for a static polarizing field, time-dependent magnetic field provides a tool to tune the strength and the character (attractive or repulsive) of the DDI. In [174] dipoles are aligned according to the following field

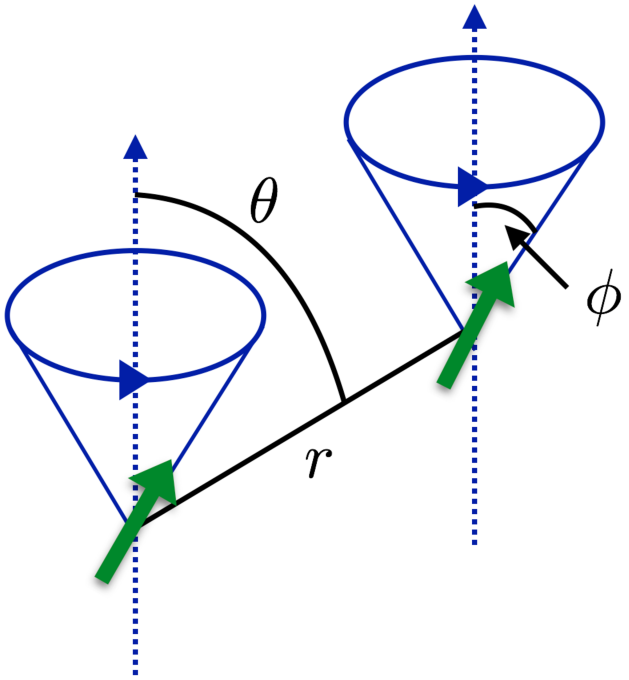

Figure 4.1: Dipole-dipole interaction can be tuned by enabling the dipole precession around the polarization axis. This can be achieved by means of a magnetic field as in Eq. (4.7)

$$\mathbf{B}(t) = B\,\hat{\mathbf{e}}_B(t) = B \begin{pmatrix} \cos(\Omega t)\sin\phi \\ \sin(\Omega t)\sin\phi \\ \cos\phi \end{pmatrix} . \tag{4.7}$$

In addition to the static field along the z-axis, the rotating field in the transverse plane

causes the rotation of dipoles with frequency Ω around the longitudinal axis. Since dipoles follow the trajectory given by $\hat{\mathbf{e}}_B(t)$, Eq. (4.6) acquires an explicit time dependence, namely

$$V_{\rm ddi}(\mathbf{r},t) = \frac{C_{\rm dd}}{4\pi}\frac{1-3\big[\hat{\mathbf{e}}_B(t)\cdot\hat{\mathbf{e}}_r\big]^2}{r^3} \tag{4.8}$$

with $\hat{\mathbf{e}}_r = \mathbf{r}/r$. This experimental protocol is schematically reported in Fig. 4.1.

The precession frequency has to be much smaller than the Larmor one $\mu_{\rm Lar} = d_{\rm m}B/\hbar$ and, at the same time, we need to tune it such that atoms do not significantly move over a period. For a confined system, this implies that Ω is much greater than the trapping frequencies. If these conditions are matched, the effective interaction is obtained from the time average of Eq. (4.8) over a period $2\pi/\Omega$. This average procedure results in [174]

$$V_{\rm ddi}^{(\rm eff)}(r,\theta,\phi) = \frac{C_{\rm dd}}{4\pi}\frac{1-3\cos^2\theta}{r^3}\left(\frac{3\cos^2\phi-1}{2}\right). \tag{4.9}$$

The equation above is equal to Eq. (4.6) except for an additional factor depending on the tilt angle ϕ. By varying it from 0 to $\pi/2$ we can change the sign of the DDI, moving from repulsion to an effective attraction, or viceversa.

In order to describe dipolar condensates within a second-quantization or a functional framework, it is convenient to develop our analysis in the Fourier space. Therefore, we have to consider the Fourier transform of the dipole-dipole interaction which is defined, as usual, by the integral

$$\tilde{V}_{\rm ddi}(\mathbf{q}) = \int d^3\mathbf{r} e^{-i\mathbf{q}\cdot\mathbf{r}}\, V_{\rm ddi}(\mathbf{r})\,, \tag{4.10}$$

with $V_{\rm ddi}(\mathbf{r})$ given by Eq. (4.6). The Fourier transform can be computed by moving to spherical coordinates $(x,y,z)\mapsto(r,\theta,\varphi)$. In order to simplify the notation without losing generality, one can choose the polar axis parallel to the wavevector $\mathbf{q}$, with the dipole moment lying on the xz-plane. Thus, with $\theta_{\mathbf{q}}$ representing the angle between the dipole moment and $\mathbf{q}$, one finds that

$$\tilde{V}_{\rm ddi}^{(r_0)}(\mathbf{q}) = \frac{C_{\rm dd}}{4\pi}\int_{r_0}^{+\infty} dr \int_0^{\pi} d\theta \int_0^{2\pi} d\varphi\, \sin\theta \frac{1-3\big(\sin\theta_{\mathbf{q}}\sin\theta+\cos\theta_{\mathbf{q}}\cos\theta\big)^2}{r}\,. \tag{4.11}$$

The integration over the radial variable requires a cutoff r_0 to ensure convergence. The

integration over φ is immediate and together with the change of variable $x = \cos\theta$ reads

$$\begin{aligned}\tilde{V}_{\rm ddi}^{(r_0)}(\mathbf{q}) &= C_{\rm dd}(1-3\cos^2\theta_{\mathbf{q}})\int_{qr_0}^{+\infty} d(qr)\left[\frac{\sin(qr)}{(qr)^2}+\frac{3\cos(qr)}{(qr)^3}-\frac{3\sin(qr)}{(qr)^4}\right] \\ &= C_{\rm dd}(1-3\cos^2\theta_{\mathbf{q}})\left[\frac{qr_0\cos(qr_0)-\sin(qr_0)}{(qr_0)^3}\right].\end{aligned} \tag{4.12}$$

The limit $r_0 \to 0$ provides the final result

$$\tilde{V}_{\rm ddi}(\mathbf{q}) = C_{\rm dd}\left(\cos^2\theta_{\mathbf{q}} - \frac{1}{3}\right), \tag{4.13}$$

which has the peculiar feature of being independent from the modulus of $\mathbf{q}$.

■ 4.2 The Bogoliubov theory for dipolar condensates

4.2.1 Mean-field theory and excitations

In order to theoretically investigate the thermodynamic properties of dipolar condensates, we follow the procedure outlined in Chap. 1, by reproducing the Bogoliubov theory within a functional framework [1, 2]. We then begin by considering the non-local Euclidean Langrangian density as in Eq. (1.23), namely

$$\mathcal{L}[\psi,\psi^*] = \psi^*(\mathbf{r},\tau)\left(\hbar\frac{\partial}{\partial\tau}-\frac{\hbar^2\nabla^2}{2m}-\mu\right)\psi(\mathbf{r},\tau)+\frac{1}{2}\int d^3\mathbf{r}'\left|\psi(\mathbf{r}',\tau)\right|^2 V(\mathbf{r}-\mathbf{r}')\left|\psi(\mathbf{r},\tau)\right|^2. \tag{4.14}$$

Differently from the usual zero-range approximation, we have to take into account the dipole-dipole interaction between the atoms. Following [175, 176], we choose to effectively described the interaction processes between atoms by means of

$$V_{\rm eff}(\mathbf{r}) = \frac{4\pi\hbar^2 a_s(a_{\rm dd})}{m}\delta(\mathbf{r}) + \frac{C_{dd}}{4\pi}\frac{1-3\cos^2\theta}{r^3}. \tag{4.15}$$

We have two different contributions to the atom-atom interaction. The first one represents the zero-range binary collision between atoms. On the other hand, the second term accounts for the DDI, as discussed in Eqs. (4.6) and (4.13).

Remarkably, the two interaction processes are not independent. An intense effort, both theoretical and numerical, was devoted to build a proper pseudopotential. In two pioneering

papers [175, 176], Yi and Yu showed that this task can be rigorously fulfilled, at least in a perturbative way. Their calculation exactly results in an interaction potential like the one in Eq. (4.15). As we said, these analytical results have to be intended as perturbative, since they are derived within the first Born approximation [20]. The functional relation between a_s and $a_{\rm dd}$ can be quantitatively understood through a numerical approach. In [177, 178] Monte Carlo simulations have been used to test the reliability of mean-field calculations. The latter are essentially numerical solution of a modified Gross-Pitaevskii equation derived by minimizing the following energy functional [102]

$$E[\Psi] = \int d^3\mathbf{r} \left[\frac{\hbar^2 |\nabla\Psi|^2}{2m} + V_{\rm ext}(\mathbf{r})|\Psi|^2 + \frac{1}{2}\int d^3\mathbf{r}' \, |\Psi(\mathbf{r})|^2 V_{\rm eff}(\mathbf{r}-\mathbf{r}')|\Psi(\mathbf{r}')|^2 \right] \tag{4.16}$$

where $V_{\rm eff}(\mathbf{r})$ is given by Eq. (4.15). A good agreement was found between Monte Carlo outcomes and the solutions of the modified Gross-Pitaevskii equation. The crucial point consists in modelling the functional relation $a_s = a_s(a_{\rm dd})$ in a proper way. This can be achieved by comparing the low-energy scattering amplitude in the Born approximation [175, 176] and the full one obtained by solving the Schroedinger's equation for the scattered wavefunction. The final result is reported in Fig. 4.2. We underline that, within this

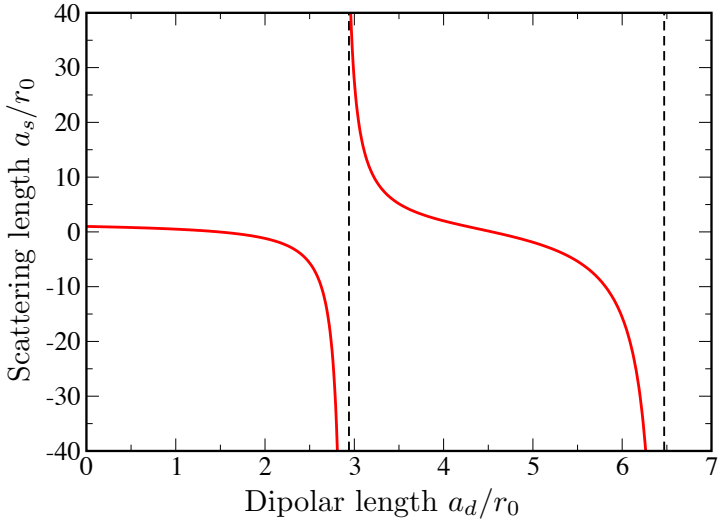

Figure 4.2: Relation between the s-wave scattering length a_s and the dipolar one $a_{\rm dd}$ derived in [177, 178] by comparing the analytical, but perturbative result obtained with Eq. (4.15) and the full numerical solution of the scattering equations. Lengths are both in units of the short-range cutoff r_0.

picture [175, 176, 177, 178], the only relevant parameters are a_s and $a_{\rm dd}$, while r_0 plays no physical role. The resulting theory is then universal, in the sense that it is independent from the short-range details of the interaction process. In the following, the zero-range coupling constant $g_0 = 4\pi\hbar^2 m/a_s$ has to be intended as implicitly dependent on $a_{\rm dd}$.

It is worth mentioning that it is certainly possible to consider more realistic potentials (by including a sort of Van der Waals short-range contribution) in order to describe binary collisions of strongly magnetic atoms [179]. These potentials eventually lead to the same effective potential. In Eq. (4.15), with $a_{\rm dd}$ depending on the short range scattering length.

Coming back to the thermodynamic description of dipolar condensates, we begin, as usual, by deriving the mean-field picture. Within the broken symmetry phase, the field $\psi(\mathbf{r},\tau)$ is taken as in Eq. (1.36): the condensate is described by a stationary field $v(\mathbf{r})$, while $\eta(\mathbf{r},\tau)$ and $\eta^*(\mathbf{r},\tau)$ are the fluctuation fields. By neglecting, for now, quantum and thermal fluctuations, the saddle-point method leads us to identify the contribution due to the classical field trajectory. Keeping in mind Eq. (1.4), the mean-field thermodynamic potential is then given by (1.5), namely

$$\Omega_{\rm mf}(\mu, v) = -\frac{1}{\beta}\log \mathcal{Z}_{\rm mf}(\mu, v)\ , \tag{4.17}$$

where $\mathcal{Z}_{\rm mf} = \exp\big(-S_{\rm mf}[v]/\hbar\big)$. In absence of a confining potential, the order parameter v can be assumed as a real constant. Its value is fixed by the solutions of $\delta S_{\rm mf}[v] = 0$. The chemical potential and the order parameter are related by the following familiar equation (cfr. Eq. (1.39)), i.e.

$$\mu = \tilde{V}_{\rm eff}(0)\ v^2 \tag{4.18}$$

where $\tilde{V}_{\rm eff}(0)$ is the limit for $\mathbf{q} \to 0$ of the Fourier transform of the effective potential in Eq. (4.15). The dipole-dipole contribution to $\tilde{V}_{\rm eff}(0)$ is reported in Eq. (4.13). By simply applying the definition of Fourier transform, it is easy to realize that, in real space, one finds

$$\tilde{V}_{\rm eff}(0) = \int_{\mathcal{V}} d^3\mathbf{r}\, V_{\rm eff}(\mathbf{r})\ . \tag{4.19}$$

In the equation above, we denote by $\mathcal{V}$ the large, but finite spherical domain enclosing the system. Due to this assumption, up to the mean-field level, the dipole-dipole interaction does

not explictly contribute to $\Omega_{\rm mf}/\mathcal{V}$. Indeed, by looking at Eq. (4.13), the whole dependence on the wavevector is encoded in $\cos^2\theta_{\mathbf{q}}$. Since the dipole moment is along the z-axis, in terms of wavevector q components we have

$$\cos\theta_{\mathbf{q}} = \frac{q_z}{\sqrt{q_x^2+q_y^2+q_z^2}} \,. \tag{4.20}$$

At the same time, a spherical domain with finite radius $R = \left[3\mathcal{V}/(4\pi)\right]^{1/3}$ implies the existence of a minimal wavenumber $\left|q_{\rm min}\right| = 2\pi/R$. By letting $\mathcal{V}$ going to infinity, clearly $\left|q_{\rm min}\right|$ approaches zero in the same way along all the direction. At this point, Eq. (4.13) can be arranged in terms of $\epsilon_{\rm dd}$. With the addition of the zero-range contribution, we get

$$\tilde{V}_{\rm eff}(\mathbf{q}) = g_0\left[1-\epsilon_{\rm dd}+3\epsilon_{\rm dd}\cos^2\theta_{\mathbf{q}}\right] . \tag{4.21}$$

At the limit $\mathbf{q}\to 0$, we then obtain

$$\tilde{V}_{\rm eff}(0) = g_0 \,. \tag{4.22}$$

This is a crucial point: thermodynamic quantities computed above the unform configuration have to be scalars [180]. Indeed, the mean-field grand potential is given by $\Omega_{\rm mf}(\mu,v)/\mathcal{V} = (\beta\hbar)^{-1}S_{\rm mf}[v]$. In terms of the order parameter and the chemical potential, it reads the usual bottleneck shape $\Omega_{\rm mf}(\mu,v)/\mathcal{V} = \mu v^2 + \frac{1}{2}\tilde{V}_{\rm eff}(0)v^4$. Through Eqs. (4.18) and (4.22), we arrive again to the well-known result

$$\frac{\Omega_{\rm mf}(\mu)}{\mathcal{V}} = -\frac{\mu^2}{2g_0} \,. \tag{4.23}$$

The equation above is equal to Eq. (1.40), reported for the first time in Chap. 1, within the pure zero-range approximation.

In order to compute the first beyond-mean-field correction we need to take into account the fluctuations field up to the quadratic (i.e. Gaussian) order. In the Fourier space the Gaussian action describing the fluctuations is formally equal to Eq. (1.41). The presence of dipole-dipole interaction in encoded in the inverse of the propagator $\mathbb{M}(\mathbf{q},\omega_n)$, appearing in

Eq. (1.41), i.e.

$$\mathbb{M}(\mathbf{q},\omega_n) = \beta \begin{pmatrix} -i\hbar\omega_n + \frac{\hbar^2 q^2}{2m} + \mu\frac{\tilde{V}_{\text{eff}(\mathbf{q})}}{\tilde{V}_{\text{eff}}(0)} & \mu\frac{\tilde{V}_{\text{eff}(\mathbf{q})}}{\tilde{V}_{\text{eff}}(0)} \\ \mu\frac{\tilde{V}_{\text{eff}(\mathbf{q})}}{\tilde{V}_{\text{eff}}(0)} & i\hbar\omega_n + \frac{\hbar^2 q^2}{2m} + \mu\frac{\tilde{V}_{\text{eff}(\mathbf{q})}}{\tilde{V}_{\text{eff}}(0)} \end{pmatrix} , \tag{4.24}$$

with $\tilde{V}_{\text{eff}}(\mathbf{q})$ as in Eq. (4.21). As stated by Eq. (1.43), the Gaussian correction to $\Omega_{\text{mf}}(\mu)/\mathcal{V}$ requires the determinant of $\mathbb{M}(\mathbf{q},\omega_n)$, also describing the excitations spectrum. By means of the saddle-point relation in Eq. (4.18), we get to the Bogoliubov spectrum for dipolar condensates

$$E_{\mathbf{q}} = \sqrt{\frac{\hbar^2 q^2}{2m}\left[\frac{\hbar^2 q^2}{2m} + 2\mu\big(1 - \epsilon_{\text{dd}} + 3\epsilon_{\text{dd}}\cos^2\theta_{\mathbf{q}}\big)\right]} . \tag{4.25}$$

For $\epsilon_{\text{dd}} > 1$, the system displays unstable low-energy modes as phonons ($q \to 0$) frequencies acquire an imaginary part. This threshold signals a collapsing instability, where the condensed atomic cloud evolves towards states with increasingly higher density until three-body recombinations expel all particles out of the condensates [181]. The collapse of the uniform configuration is due to the partially attractive nature of DDI which dominates over the short-range repulsion. It is interesting to note that the most unstable situation corresponds to a perturbation with wavevector orthogonal to the dipole orientation (i.e. $\theta_{\mathbf{q}} = \pi/2$). Indeed, for a sample polarized along the z-axis, phonons with $\mathbf{q} \perp \hat{\mathbf{e}}_z$ create planes with higher densities of dipoles in a head-to-tail configuration. Thus, the attractive character of DDI prevails and the collapse occurs easier.

Thanks to Eq. (4.25), the Gaussian correction counts two contributions, one at zero temperature, i.e.

$$\frac{\Omega_g^{(0)}}{\mathcal{V}} = \frac{1}{2}\sum_{\mathbf{q}} E_{\mathbf{q}} \tag{4.26}$$

and the second taking into account thermal fluctuations, namely

$$\frac{\Omega_g^{(T)}}{\mathcal{V}} = \frac{1}{\beta}\sum_{\mathbf{q}} \log\left(1 - e^{-\beta E_{\mathbf{q}}}\right) . \tag{4.27}$$

Focusing on zero-temperature fluctuations, in the continuum limit we have

$$\frac{\Omega_g^{(0)}}{\mathcal{V}} = \frac{1}{4\pi^2}\int_0^1 d\chi \int_0^{+\infty} dq\, q^2 E_{\mathbf{q}} \tag{4.28}$$

with $q = |\mathbf{q}|$ and $\chi = \cos\theta_{\mathbf{q}}$. The zero-point energy in Eq. (4.28) is ultraviolet divergent. Since the Bogoliubov spectrum is gapless, dimensional regularization can be applied in a similar way to sec. 1.3.2. In a generic dimension d we then have

$$\frac{\Omega_g^{(0)}}{\mathcal{V}} = \frac{S_{d-1}}{(2\pi)^d}\int_0^1 d\chi \int_0^{+\infty} dq\, q^{d-1}\sqrt{\frac{\hbar^2 q^2}{2m}\left[\frac{\hbar^2 q^2}{2m} + 2\mu(1-\epsilon_{dd}+3\epsilon_{dd}\chi^2)\right]}\,. \tag{4.29}$$

By assuming $d \in \mathbb{C}$, the integral on momentum can be carried out as

$$\frac{\Omega_g^{(0)}}{\mathcal{V}} = \frac{S_{d-1}}{2(2\pi)^d}\left(\frac{2m}{\hbar^2}\right)^{\frac{d}{2}} B\left(\frac{d+1}{2}, -\frac{d+2}{2}\right)\mu^{\frac{d+2}{2}}\int_0^1 d\chi \left[2(1-\epsilon_{dd}+3\epsilon_{dd}\chi^2)\right]^{\frac{d+2}{2}} \tag{4.30}$$

where the Euler's Beta function is then analytically continued to $B(x,y) = \Gamma(x)\Gamma(y)/\Gamma(x+y)$. By taking the limit $d \to 3$, we get the final equation for $\Omega_g^{(0)}$,

$$\frac{\Omega_g^{(0)}}{\mathcal{V}} = \frac{8}{15\pi^2}\left(\frac{m}{\hbar^2}\right)^{3/2}\mathcal{Q}_{5/2}(\epsilon_{\rm dd})\,\mu^{5/2}\,. \tag{4.31}$$

The function $\mathcal{Q}_{5/2}(\epsilon_{\rm dd})$ is the only factor arising due to the presence of dipole-dipole interaction. It is defined as

$$\mathcal{Q}_n(x) \equiv \int_0^1 dt(1-x+3xt^2)^n\,. \tag{4.32}$$

In Fig. 4.3 we report the shape of $\mathcal{Q}_n(x)$ as defined in the equation above for $n = 3/2$ and $n = 5/2$. It is crucial to note that these functions are real for $\epsilon_{\rm dd} \leq 1$ while, beyond this threshold, they acquire a small imaginary part. This is not surprising because Eq. (4.31) is the zero-temperature Gaussian correction above the uniform ground-state, which is unstable exactly for $\epsilon_{\rm dd} > 1$. Proceeding with the derivation of thermodynamic quantities for dipolar condensates, from Eq. (4.31) it is natural to compute number density by means of a simple differentiation. It is easy to check that

$$n = -\frac{1}{\mathcal{V}}\frac{\partial}{\partial\mu}\left[\Omega_{\rm mf} + \Omega_g^{(0)}\right] = \frac{\mu}{g_0} - \frac{4}{3\pi^2}\left(\frac{m}{\hbar^2}\right)^{\frac{3}{2}}\mathcal{Q}_{5/2}(\epsilon_{dd})\,\mu^{3/2}\,. \tag{4.33}$$

Moreover, within a perturbative approach, where $g_0 n \ll \mu$, from Eq. (4.33) one can extract

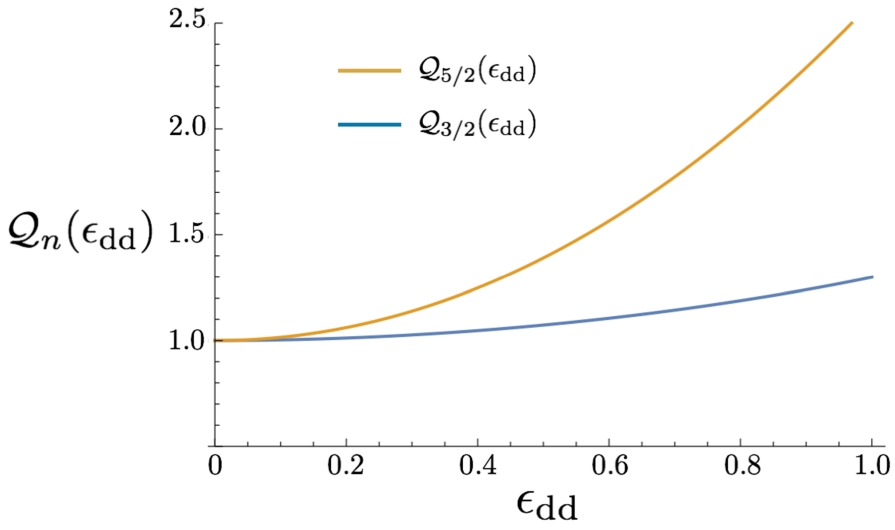

Figure 4.3: Function $\mathcal{Q}_n(\epsilon_{\rm dd})$ as in Eq. (4.32) for $n = 3/2$ (blue lower line) and $n = 5/2$ (orange upper line).

the chemical potential as a function of the number density, namely

$$\mu = g_0\, n + \frac{32}{3\sqrt{\pi}}\mathcal{Q}_{5/2}(\epsilon_{dd})\, g_0 n\sqrt{n a_s^3}\,. \tag{4.34}$$

Via a Legendre transform, Eq. (4.31) and Eq. (4.33) provide the internal energy density

$$\frac{E}{\mathcal{V}} = \frac{1}{2} g_0\, n^2 + \frac{128}{15\sqrt{\pi}}\frac{2\pi\hbar^2}{m}\mathcal{Q}_{5/2}(\epsilon_{dd}) n^2 a_s\sqrt{n a_s^3}\,. \tag{4.35}$$

Our Gaussian correction to the thermodynamic functions agrees with the first derivation by Lima and Pelster in [182]. They carried on their calculation within a second-quantization framework: their corrections to the mean-field picture were derived by diagonalizing the quadratic Hamiltonian through the canonical Bogoliubov transformation [10]. Thus, although Eq. (4.35) has not been derived here for the first, we underline the alternative approach followed in this section. Thanks to an equation similar to our Eq. (1.118), Lima and Pelster also managed to calculate the condensate depletion:

$$\frac{n_0}{n} = 1 - \frac{8}{3\sqrt{\pi}}\sqrt{n a_s^3}\mathcal{Q}_{3/2}(\epsilon_{dd})\,, \tag{4.36}$$

with the function $\mathcal{Q}_{3/2}(\epsilon_{\rm dd})$ plotted in Fig. 4.3. Moreover, they noticed the interesting fact that, since $\mathcal{Q}_{5/2}(1) \simeq 2.6$, quantum fluctuations are strongly enhanced compared to the pure zero-range approximation (where $\epsilon_{\rm dd} = 0$). Thanks to recent possibility of engineering a box trap, this fact can pave the way to a direct measurement of the first beyond-mean-correction in the equation of state.

■ 4.3 Fluctuations and filaments in dipolar condensates

4.3.1 Dipolar droplets and the modified Gross-Pitaevskii equation

In the last section, we have just observed that the partial attractive character of the dipole-dipole interaction may lead to a collapsing instability. The eventual occuring of collapse is clear when one considers the spectrum of excitations above the uniform configuration in Eq. (4.25). There, we observed that imaginary frequencies appears when $\epsilon_{\rm dd} > 1$. In other words, unstable phononic modes occur when dipole-dipole interaction prevails on the short-range repulsion.

Therefore, the usual picture is that uniform condensates collapse for $\epsilon_{\rm dd} > 1$, similarly to attractive condensates when $a_s < 0$. The main difference consists in an anisotropic post-collapse dynamics [181].

The recent results obtained by the group of T. Pfau in Stuttgart radically challenged this understanding [99, 172, 183, 184]. Indeed, in their Dysprosium setup they observed that, by quenching the s-wave scattering length to very low values and then driving the system into the unstable regime, collapse does not occur. On the contrary Dysprosium atoms prefer to form dense bosonic droplets both in trapped configuration [172, 183, 184] and in free space [99]. The formation of dipolar droplets has been confirmed in experiments with Erbium atoms by the F. Ferlaino's group in Innsbruck [100].

These experimental results cannot be interpreted within a mean-field framework. At first, conservative three-body forces were indicted for the droplets nucleation. However, as noticed by many authors [149, 150, 185], their strength should be orders of magnitude larger than three-body losses and there is no convincing way to justify this fact. Moreover, it is not clear if these forces should be related (or not) to the presence of a dipole-dipole interaction.

The other possible candidates are the quantum fluctuations whose thermodynamic weigth we have just analyzed in the previous section. This idea relies upon Petrov's seminal proposal for collapsing Bose mixture [97, 98]: the structures observed by Pfau's group have been indeed the first experimental confirmation of the stabilizing action driven by fluctuations. Saito was the first to suggest that quantum fluctuations can halt the collapsing process in dipolar condensates, providing convincing Monte Carlo simulations [186] in support of his guess. The stabilizing mechanism driven by fluctuations has been explained in Chap. 3: in the collapsing region, the increasing of the local density ruled by the dipole-dipole partially attractive nature can be halted by the repulsion due to fluctuations. Indeed, the collapsing mean-field scales as n^2 in the energy density, while the Gaussian correction as $n^{5/2}$, producing a similar scenario to the one depicted by Petrov.

Almost at the same time, large scale simulations based on a modified Gross-Pitaevskii equations [149, 187, 150, 151] have shown a good agreeement with the density profile and excitation spectra observed in laboratory. The use of a Gross-Pitaevskii equation is strengthened by the experimental study of droplets coherence properties. In [183], it was shown that a single droplet is coherent and thus superfluid, leaving yet unanswered the question of a global phase coherence of the system [188]. In order to model the dipolar droplets arising in collapsing configurations, it is useful to introduce a generalized Gross-Pitaevskii energy functional. By following [149, 150], we add to the mean-field functional in Eq. (4.16) the zero-temperature Gaussian correction in Eq. (4.35). We then have

$$E[\Psi,\Psi^*] = \int d^3\mathbf{r}\,\Psi^*\bigg[-\frac{\hbar^2\nabla^2}{2m} + V_{\rm ext}(\mathbf{r}) + \frac{1}{2}\int d^3\mathbf{r}' V_{\rm eff}(\mathbf{r}-\mathbf{r}')\big|\Psi(\mathbf{r}')\big|^2 + \gamma_g^{(0)}\big|\Psi\big|^3\bigg]\Psi \quad (4.37)$$

where $V_{\rm eff}(\mathbf{r})$ is taken as in Eq. (4.15) and

$$\gamma_g^{(0)} = \frac{128}{15\sqrt{\pi}}\frac{2\pi\hbar^2}{m}\mathcal{Q}_{5/2}(\epsilon_{\rm dd})a_s^{5/2}\,. \quad (4.38)$$

is the coupling constant of the fluctuation term $\propto \big|\Psi\big|^5$. Beyond the mean-field stability threshold (i.e $\epsilon_{\rm dd} > 1$), the function $\mathcal{Q}_{5/2}(\epsilon_{\rm dd})$ becomes complex. Anyway, its imaginary part is typically 10^2 or 10^3 smaller than the real one, provided we are not deeply within the collapsing region ($1 < \epsilon_{\rm dd} < 2$). Thus, the corresponding dissipation process acts on time

scale much longer than the three body losses, as confirmed by the dynamical analysis in [185, 187]. Then we can safely approximate $\mathcal{Q}_{5/2}(\epsilon_{\rm dd})$ as

$$\mathcal{Q}_{5/2}(\epsilon_{\rm dd}) = 1 + \frac{3}{2}\epsilon_{\rm dd} + \mathcal{O}(\epsilon_{\rm dd}^4) \, . \tag{4.39}$$

The equation of motion corresponding to the functional in Eq. (4.37) can be obtained by stationarizing the following action

$$S = \int dt \, d^3\mathbf{r} \left[\frac{i\hbar}{2}\left(\Psi^* \partial_t \Psi - \Psi \partial_t \Psi^*\right) - E_{\rm tot} \right]$$

As in [149, 150], the equation for $\Psi(\mathbf{r}, t)$ is given by

$$i\hbar \frac{\partial \Psi}{\partial t} = \left[-\frac{\hbar^2 \nabla^2}{2m} + V_{\rm ext}(\mathbf{r}) + \int d^3\mathbf{r}' V_{\rm eff}(\mathbf{r}-\mathbf{r}') \left|\Psi(\mathbf{r}')\right|^2 + \frac{5}{2}\gamma_g^{(0)} \left|\Psi\right|^3 \right] \Psi \, . \tag{4.40}$$

The dynamics of dipolar droplets is then investigated by solving Eq. (4.40) or, otherwise, an analytical insight can be gained by approaching the energy functional in Eq. (4.37) within a variational framework. In the theoretical papers by the groups of L. Santos [149, 187] and B. Blakie [150, 185, 151] both way are exploited, resulting in a very detailed picture of droplet formation and stability. We refer the reader to the above-mentioned papers since the remaining part of this chapter will be devoted to study the (eventual) superfluid nature of dipolar droplets. However, we aim to give here a brief justification of the stabilizing mechanism driven by fluctuations in dipolar condensates. More precisely, we are going to show, in a variational framework, that the energy of a single dipolar filament has a minimum also in free space, signalling its stability.

We begin by considering a single Gaussian filament oriented along the z-axis. In order to model this configuration, the following ansatz can be applied

$$\Psi(\mathbf{r}) = A\phi_i(\mathbf{r}_\perp) = A \exp\left\{ -\frac{x^2+y^2}{2\sigma^2} \right\} . \tag{4.41}$$

We underline that, for simplicity, the filament has a constant profile along the z-axis. A similar, but more realistic, choice for $\Psi(\mathbf{r})$ can be found in [149, 150, 185]. The normalization

condition $N = \int d^3\mathbf{r}|\Psi|^2$ leads to the following definition of A, namely

$$A = \frac{\rho_z}{\pi\sigma^2} \tag{4.42}$$

with $\rho_z = N/L_z$ the linear density along the $\hat{\mathbf{e}}_z$ direction and L_z the large, but finite, spatial extension along this axis. At the end of the calculation, we will consider the thermodynamic limit by taking $L_z \to +\infty$. By applying the rules of Gaussian integration, the kinetic and the contact contribution to the total energy read $E_{\rm kin} = \hbar^2/(m\sigma^2)$ and $E_{\rm con} = (\hbar^2/m)a_s\rho_z/\sigma^2$. On the other hand, the dipolar self-interaction contribution is much more complicated. With the dipole-dipole interaction defined as in Eq. (4.6), one has to solve the following integral

$$E_{\rm ddi} = \frac{1}{2}\int d^3\mathbf{r}d^3\mathbf{r}'\phi^2(\mathbf{r})V_{\rm ddi}(\mathbf{r}-\mathbf{r}')\phi^2(\mathbf{r}') \; . \tag{4.43}$$

In order to simplify the calculation, we can move now into the Fourier space, where the convolution theorem transforms the integral over double spatial coordinates in

$$E_{\rm ddi} = \frac{1}{2(2\pi)^3}\int d^3\mathbf{q}\,\tilde{n}(-\mathbf{q})\tilde{V}_{\rm ddi}(\mathbf{q})\tilde{n}(\mathbf{q}) \; . \tag{4.44}$$

In the equation above $\tilde{n}(\mathbf{q})$ is the Fourier transform of $n(\mathbf{r}) = A^2\phi^2(\mathbf{r})$. The product $\tilde{n}(\mathbf{q})\tilde{n}(-\mathbf{q})$ can be computed analytically, reading

$$\tilde{n}(-\mathbf{q})\tilde{n}(\mathbf{q}) = \frac{4A^4}{q_z^2}\sin^2\left(\frac{q_zL_z}{2}\right)\pi^2\sigma^4 e^{-\sigma^2(q_x^2+q_y^2)/2} \; . \tag{4.45}$$

The Fourier transform of dipole-dipole interaction is reported in Eq. (4.13) so Eq. (4.44) becomes, in cylindrical coordinates,

$$E_{ddi} = -\frac{A^4\sigma^4}{4\pi}\,g_0\epsilon_{\rm dd}\int_0^{+\infty}dq_\perp\int_{-\infty}^{+\infty}dq_z\left(1-\frac{3q_z^2}{q_\perp^2+q_z^2}\right)\frac{q_\perp}{q_z^2}\sin^2\left(\frac{q_zL_z}{2}\right)e^{-\sigma^2q_\perp^2/2} \; . \tag{4.46}$$

By performing the last two integral, we finally get that

$$\frac{E_{\rm ddi}}{N} = -\left(\frac{\hbar^2}{m\sigma^2}\right)\frac{a_{\rm dd}\rho_z}{2}f_{\rm se}(\sigma, L_z) \tag{4.47}$$

where the auxiliary function $f_{\rm se}(\sigma, L_z)$ reads

$$f_{\rm se}(\sigma, L_z) = 2 + 3\sqrt{2\pi}\left(\frac{\sigma}{L_z}\right)\left[e^{\frac{L_z^2}{2\sigma^2}}\,\mathrm{Erfc}\left(\frac{L_z}{\sqrt{2}\sigma}\right) - 1\right] . \tag{4.48}$$

At this point, let us notice that $f_{\rm se}(\sigma) = 2$ for $L_z \to +\infty$. The beyond-mean-field contribution to Eq. (4.37) is given by

$$E_g^{(0)} = \gamma_g^{(0)} \int d^3\mathbf{r}|\Psi|^5 , \tag{4.49}$$

resulting in

$$\frac{E_{\rm g}^{(0)}}{N} = \frac{512}{75\pi}\left(\frac{\hbar^2}{m\sigma^2}\right)\left(1 + \frac{3}{2}\epsilon_{dd}^2\right)a_s^{5/2}\frac{\rho_z^{3/2}}{\sigma} . \tag{4.50}$$

Putting all the pieces together, the variational energy of a single dipolar filament is represented by the equation

$$\frac{E}{N} = \frac{\hbar^2}{m\sigma^2}\left[1 + a_s\rho_z - a_{dd}\rho_z + \frac{512}{75\pi}\left(1 + \frac{3}{2}\epsilon_{dd}^2\right)a_s^{5/2}\frac{\rho^{3/2}}{\sigma}\right] . \tag{4.51}$$

The crucial point of this simple, and somewhat sketchy, calculation is the role of the fluctuations correction in Eq. (4.51). Indeed, it can be easily check that for $\epsilon_{\rm dd} > 1$, E/N displays a single minimum at negative energies. This signals that the filament is stable, also compared to an evaporating configuration with vanishing density. On the contrary, by turning off the gaussian term, the system rolls down towards increasingly thinner filaments, since there is no minimum. At a certain point, densities are so high that a complete collapse destroys the filament.

4.3.2 Superfluid dipolar filaments: a numerical approach

During the last year, several valiant papers approached the issue of the structural and dynamical properties of dipolar droplets, both analytically and numerically.

Concerning the numerical analysis, we have shown that a generalized Gross-Pitaevski equation can be derived by taking into account both dipole-dipole interaction and quantum fluctuations. Actually, because of its relative simplicity, the first rigorous quantitative results were produced by solving Eq. (4.40). These large scale simulations provide a confirmation of variational results about the structural and stability properties of droplets. Variational

results are based on Eq. (4.37) where a Gaussian ansatz is assumed for the field Ψ [149, 150]. At the same time, in [151] a rigorous linear stability analysis has been carried on by numerically solving the Bogoliubov-de Gennes equations corresponding to Eq. (4.40). Moreover, in [150], the droplet metastable dynamics has been studied by including a three-body dissipative term in Eq. (4.40). However, the Gross-Pitaevskii equation is essentially only the first step beyond the mean-field scenario. It surely provides a first interpretation to the ground-breaking experimental findings, but it is not the only viable strategy.

Moving from the work of Saito [186], more recent investigations rely upon Quantum Monte Carlo methods. Monte Carlo approaches are more burdensome from a computional point of view than Gross-Pitaevskii simulations. However, their strength consists in the fact that they do not require a set of preliminary hypothesis restraining the regime of applicability. They are *ab initio* methods and, by definition, no perturbative framework is assumed. Concerning dipolar atoms, path-integral Monte Carlo (PIMC) techniques have proved the existence of a window in the parameter space leading to the formation of stable self-bound structures both in free space [186, 188] and in trapped configuration [189, 190]. In presence of an external confinement, it was recover the regular arrangement observed in [172]. However, the above-mentioned works focus on the search for a non-uniform ground state, leaving unanswered a series of question about the superfluid nature of these configurations. This relevant topic was first addressed in [188], on which part of this chapter is based. There, the issue of superfluidity was analyzed for a wide range of dipolar interaction strength. In addition, we probed the superfluidity persistence against thermal fluctuations. In [188], PIMC simulations have been carried on by means of the so-called worm algorithm [191, 192]. This method provides a reliable technique to extract the superfluid density, since it enables the access to the off-diagonal sector of the Green's functions.

The starting point of our numerical simulations is the Hamiltonian for a set of N dipolar bosonic atoms, namely

$$\hat{H} = -\sum_{i=1}^{N} \frac{\hbar^2}{2m}\nabla_i^2 + \sum_{i<j}^{N} V(\mathbf{r}_i - \mathbf{r}_j) \,. \tag{4.52}$$

The binary interaction between atoms $V(\mathbf{r})$ is modelled by imposing a short-range cutoff r_0,

ensuring the stability of the system, and an anisotropic dipolar tail. We then have

$$V(\mathbf{r}) = \begin{cases} \frac{C_{\rm dd}}{4\pi} \frac{1-3\cos^2\theta}{r^3} & \text{for } r \geq r_0 \\ \infty & \text{for } r < r_0 \ , \end{cases} \tag{4.53}$$

where the dipolar coupling $C_{dd}/4\pi$ is given in Eq. (4.2), θ is angle between the vector $\mathbf{r}$ and the z-axis. The hard-core well is required to remove the unphysical r^{-3} attraction at small distances for dipoles in a head-to-tail configuration. By taking r_0 and $\hbar^2/(mr_0^2)$ as units of length and energy, the zero-temperature physics can be completely characterized by the (dimensionless) density nr_0^3 and interaction strength $U = mC_{\rm dd}/(4\pi\hbar^2 r_0)$. For a vanishing dipole-dipole interaction, i.e. $C_{\rm dd} \to 0$, nr_0^3 reduces to the usual definition of the gas parameter na_s^3 [177, 178]. This obviously implies that the short-range cutoff also corresponds to the s-wave scattering length a_s when we turn the interaction off.

As stated by Eq. (4.15), the presence of a dipole-dipole interaction also affects the s-wave scattering length. In Fig. 4.2 we report the precise dependence of a_s on the dipolar length $a_{\rm dd}$. By considering N atoms in a cubic box of volume L^3, a wide range of scaled densities and interaction strengths has been explored with the assumption of periodic boundary conditions. The strongy decay of the dipole-dipole potential prevents the occuring of relevant self-interaction effects, so one has to take into account only the eventual contribution from neighbor images. Typically, at fixed density $n = N/L^3$, N varies between 100 and 400 and it has been checked that the resulting phase diagram does not change according to size variations. So, despite having a finite-size character, it is reasonable to assume that in the thermodynamics limit the picture does not radically change. The phases of the system are probed in the zero-temperature limit, obtained by lowering the temperature until observables do not change anymore. This numerical analysis is summarized in the phase diagram of Fig. 4.4.

For small U we find that the system is in the superfluid phase (SF) (the blue region of Fig. 4.4), characterized by a unitary superfluid fraction. For densities lower than $nr_0^3 \lesssim 10^{-3}$, the SF extends up to $U \simeq 2.1$. This threshold corresponds to $\epsilon_{\rm dd} = 1$, in agreement with the Bogoliubov theory developed in sec. 4.2. For increasing interaction strength, we encounter a cluster phase (CP) (yellow region in the diagram of Fig. 4.4) where superfluidity vanishes and

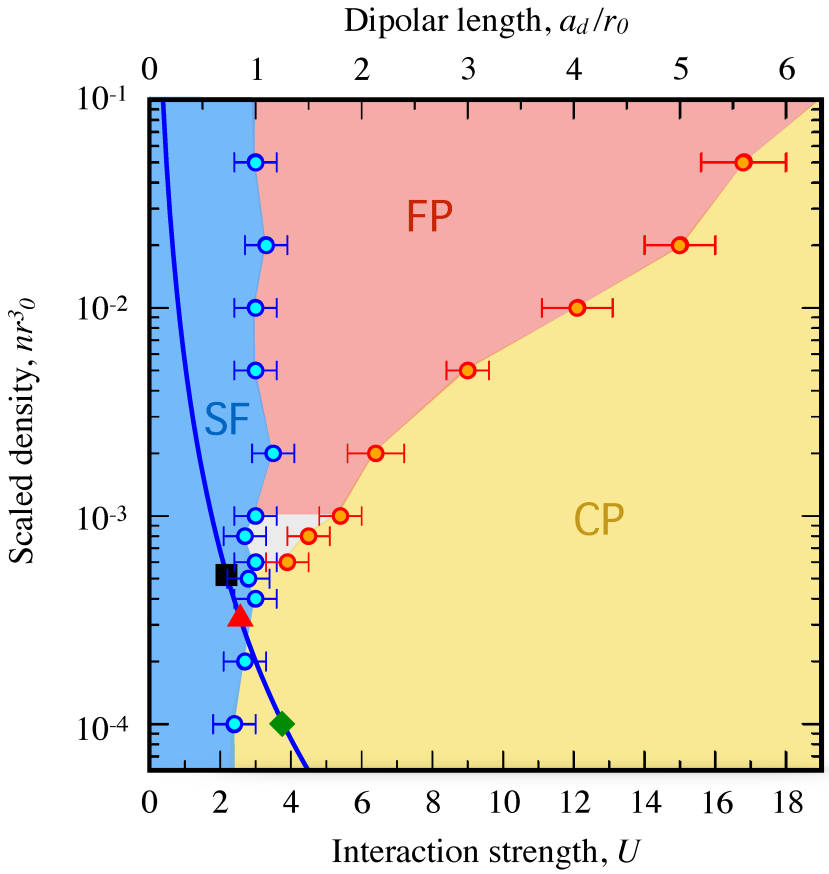

Figure 4.4: Zero-temperature phases of dipolar bosons in three dimensions in free space: Superfluid (SF), superfluid filaments (FP) and cluster phases (CP) for varying dimensionless interaction strength U (or equivalently dipolar length a_d/r_0) and scaled density nr_0^3. For $a_d/r_0 \lesssim 0.9$ the blue SF region corresponds to a uniform superfluid, which agrees with mean-field prediction that predicts stability for $a_d/a_s < 1$. FP is encountered for high densities $nr_0^3 \gtrsim 5 \cdot 10^{-4}$ and for $a_d/r_0 \gtrsim 1$. For small densities $nr_0^3 \lesssim 5 \cdot 10^{-4}$ the system breaks up into tiny clusters. Phase boundaries in the grey region are not resolved. Blue line corresponds to $n = 5 \cdot 10^{20}\,\mathrm{m}^{-3}$ and $a_d = 130\,a_0$. Black/Red dots are experimentally measured background scattering lengths $a_s = 122\,a_0$ (^{162}Dy) / $a_s = 92\,a_0$ (^{164}Dy). Green point at $a_s = 29\,a_0$.

atoms arrange themselves into a series of small droplet structures. Beyond $nr_0^3 \gtrsim 6 \cdot 10^{-4}$, by crossing the SF phase boundary we enter in a peculiar phase (FP) characterized by elongated filaments with anisotropic superfluidity. The filament phase extends from the region corresponding to $\epsilon_{\mathrm{dd}} \gtrsim 1$ to the strongly interacting regime with large (dipolar) interactions and densities. In Fig. 4.4 it also exists a small region at intermediate densities, i.e. $6 \cdot 10^{-4} \lesssim n\,r_0^3 \lesssim 1 \cdot 10^{-3}$, where phase boundaries are not resolved.

On the basis of our phase diagram, we can now move to compare our Monte Carlo outcomes to the experiments involving ^{162}Dy and ^{164}Dy [99, 172, 172, 184]. The dipolar

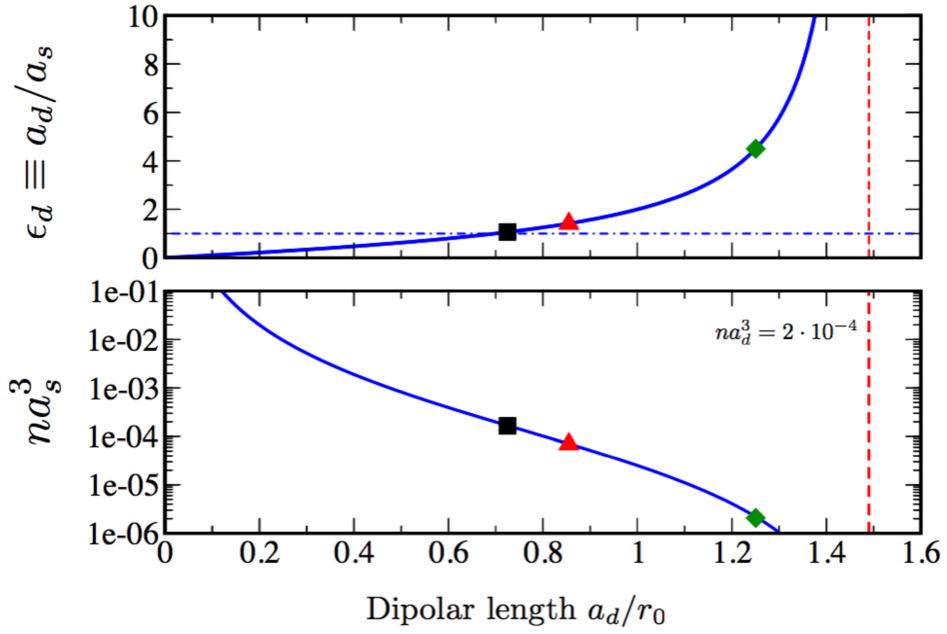

Figure 4.5: (Top). Ratio ϵ_d between the dipolar length a_d and the scattering length a_s computed from Fig.4.2. (Bottom) The gas parameter $n\,a_s^3$ along the blue line in the phase diagram. Both the quantities have bene computed along the blue line in Fig. 4.4, corresponding to the situation $na_{\rm dd}^3 \simeq 2 \cdot 10^{-4}$. The dipolar length are taken equal to $130\,a_0$ for both isotopes, since the deviation is not significant. The red dashed line represents the line for which the scattering length as vanishes. Black square and red triangle correspond to experimental parameters for Dy with their background scattering length ($122\,a_0$ and $92\,a_0$ respectively). Green diamond is the point for Dy with $a_s = 29\,a_0$ for which $n\,r_0^3 = 10^{-4}$ in the CP.

lengths of the two isotopes have been measured to be, respectively, $a_{\rm dd} = 129.2\,a_0$ and $a_{\rm dd} = 130.8\,a_0$, with a_0 being the Bohr's radius. We analyze the situation for an average density $n = 5 \cdot 10^{20} m^{-3}$, which is represented by the solid blue line in Fig. 4.4. Using the functional relation between a_s and $a_{\rm dd}$ in Fig. 4.2, it is possible to identify the points in the phase diagram corresponding to each Dysprosium isotopes. Indeed, with our choice of parameters, we have $na_{\rm dd}^3 \simeq 2 \cdot 10^{-4}$ and

$$nr_0^3 = \frac{na_{\rm dd}^3}{(a_{\rm dd}/r_0)^3}\,. \tag{4.54}$$

In addition, the background scattering lengths for the isotopes have been measured in [193, 194, 195], resulting to be $122\,a_0$ for ^{162}Dy and $92\,a_0$ for ^{164}Dy. Thanks to these previous measures and the parametrization in Fig. 4.2, the black square in Fig. 4.4 corresponds to

the ^{162}Dy case, while the red triangle represents the ^{164}Dy one. In Fig. 4.5, we report the gas parameter na_s^3 and ratio $\epsilon_{\rm dd} = a_{\rm dd}/a_s$ along the blue line in the phase diagram corresponding to $na_{\rm dd}^3 = 2 \cdot 10^{-4}$.

In order to propose an effective characterization of the three phases identified in of Fig. 4.4, we report in Fig. 4.6 typical configurations of the density distribution in each case for $N = 100$ atoms. Below every density distribution panel, we also consider the radial distribution function along the polarization axis $g_{\parallel}(r)$ and on the transverse plane $g_{\perp}(r)$ [196]. The final curves in Fig. 4.6 are an average over 100 different configurations of the same phase. In the panel (a) of Fig. 4.6, we can observe a typical situation within the SF phase.

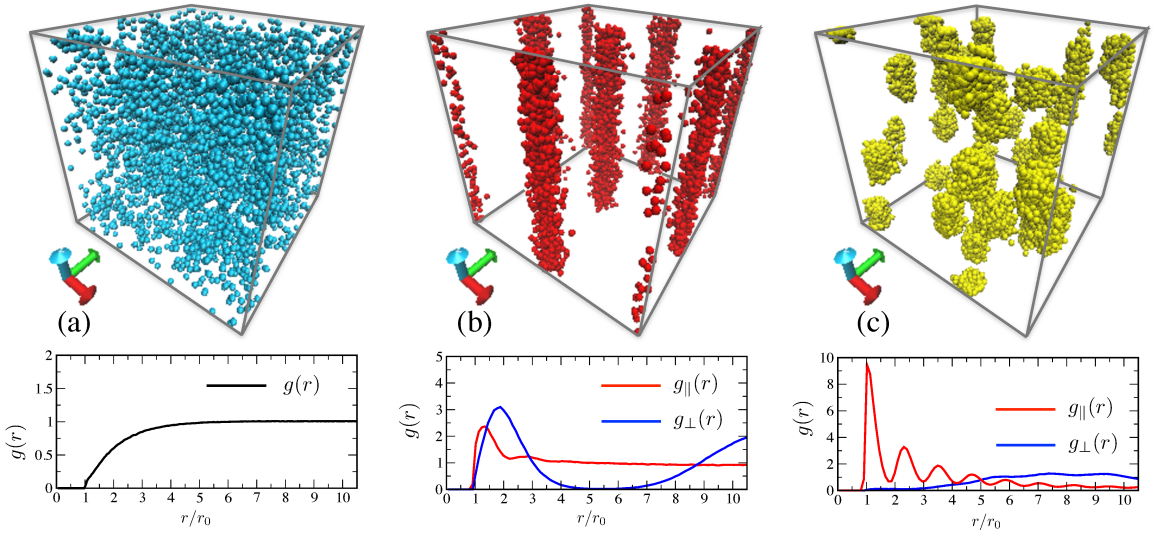

Figure 4.6: Characterization of the phases at $nr_0^3 = 10^{-2}$. Upper panels. PIMC density distribution at different strengths of dipolar interaction: (a) SF at $a_d = 0.6r_0$, (b) superfluid FP at $a_d = 2.6r_0$ and (c) CP at $a_d = 6.0r_0$. Lower panels. (a) radial correlation functions $g(r)$ in the SF. (b) and (c) radial correlation functions $g_{\parallel}(r)$ along the vertical direction (red) and $g_{\perp}(r)$ along the orthogonal plane (blue). $g_{\parallel}(r)$ has a fluid-like profile in the FP. In the CP $g_{\parallel}(r)$ a high peak due to strong attractive interactions appears at distances $r \gtrsim r_0$. $g_{\perp}(r)$ in the FP shows a strong suppression in between two filaments whereas in the CP it flattens at intermediate distances. Simulations are done with 100 particles. Correlation functions are averaged over 100 configurations.

Particles are delocalized into a uniform density configuration. The flat profile of the radial distribution function is peculiar of a fluid phase where atom-atom interaction is basically a hard-core potential. In the middle panel, we see the elongated filaments characterizing the FP, while the small clusters of CP are displayed in the panel (c). These cluster are still slightly elongated along the z-axis, hinting that filaments undergo a fragmentation process

for high values of U. The distinction between the two radial distribution functions, $g_{\parallel}(r)$ and $g_{\perp}(r)$, further specifies the different nature of the inhomogeneous phases. Starting from $g_{\parallel}(r)$ (the red line in the lower panel of Fig. 4.6), we observe a liquid-like behavior in the FP. The peak at $r \simeq r_0$ is a consequence of the partial attractive character of dipole-dipole interaction. On the contrary, within the CP, $g_{\parallel}(r)$ has an oscillatory behavior before vanishing for large distances as a consequence of the finite size of the sample. Moving to $g_{\perp}(r)$ (blue line in Fig. 4.6), we observe a strong suppression in the region between the filaments of the FP. Concerning CP, $g_{\perp}(r)$ reaches a plateau at intermediate distances. This signals the irregular arrangement of cluster along the plane orthogonal to dipoles orientation. A full description of the three phases has to include an estimation of the superfluid fraction $f_s^{(i)}$ as a function of the interaction strength and the temperature. The spatial directions are labelled by $i = x.y, z$. Following [34], an estimator for the superfluidity is provided by the winding number w_i, via the equation

$$f_s^{(i)} = \left(\frac{m}{\beta \hbar^2 \, n} \right) \langle w_i^2 \rangle \ , \tag{4.55}$$

where $\langle \ldots \rangle$ has to be intended as a thermal average. In Fig. 4.7 the superfluid fraction along the three principal directions is analyzed as a function of the dipolar length $a_{\rm dd}$ for $nr_0^3 = 10^{-2}$. As mentioned above, $f_s^{(i)}$ is uniform and unitary within the SF, while a strong anisotropy occurs by crossing the SF-FP boundary. In FP, the superfluid fraction is still unitary along the vertical direction, while it vanishes on the transverse plane. This result seems to suggest that the single filament is phase coherent [183], but the whole system is not. Within the CP, $f_s^{(i)} = 0$ everywhere, providing a further confirmation of filaments fragmentation process. In the end, we aim to investigate the stability of superluid dipolar filaments against thermal fluctuations. The results of PIMC simulations at finite temperatures can be found in Fig. 4.8, for a system with $N = 100$ particles and $nr_0^{-2} = 10^{-2}$. The temperature is in units of the critical temperature of an ideal Bose gas, i.e. $T_0 = \left[2\pi/\zeta(3/2)^{2/3}\right](nr_0^3)^{2/3}$. In the FP, we compare the numerical outcomes with analytical results derived within the Landau-Khalatnikov two-fluid model outlined in Sec. 1.4. In order to take into account the

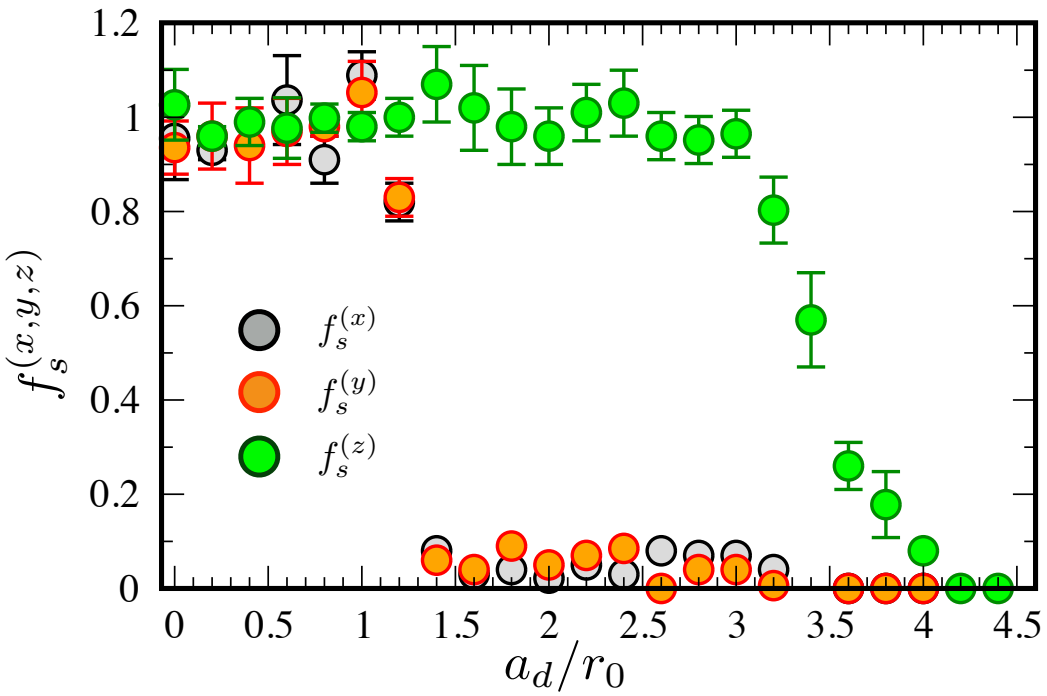

Figure 4.7: Superfluid fraction f_s as a function of the dipolar length, across the transition from superfluid to filament transition at high densities for $nr_0^3 = 10^{-2}$. Dipoles and filaments are aligned along the z-axis. In the SF the superfluid fraction converges to $f_s = 1$ isotropically. Within FP we observe $f_s = 1$ along the vertical axis and vanishing on the orthogonal plane. Error bars are statistical uncertainties.

anisotropic character of DDI, Eq. (1.96) has to be modified as in [197], namely

$$f_s^{(z)} = 1 - \frac{\beta\hbar^2}{4\pi^2 m}\int_0^\infty dq \int_0^\pi d\theta_q q^4 \frac{\sin\theta_q \cos^2\theta_q e^{\beta E_q}}{(e^{\beta E_q}-1)^2} \,. \tag{4.56}$$

In the equation above $E_{\mathbf{q}}$ is given by Eq. (4.25), with the chemical potential as in Eq. (4.34), taking into account at least the contribution from quantum fluctuations. In Fig. 4.8 the superfluid fraction along the z-axis is considered in the pure zero-range caso $a_{\rm dd} = 0$ (solid black line) and at $a_{\rm dd} = 0.6\, r_0$ (red dashed line). In the low-temperatures regime, where our framework effectively holds, it is reasonable to linearize the Bogoliubov spectrum $E_{\mathbf{q}}$ in order to determine a fully analytical equation for $f_s^{(i)}$. We get

$$\tilde{f}_s^{(z)} = 1 - \frac{2\pi^2}{45}\frac{1}{(1-\epsilon_{\rm dd})(1+2\epsilon_{\rm dd})^{3/2}}\left(\frac{m}{\hbar^2}\right)^{3/2}\frac{(k_B T)^4}{n\,\mu^{5/2}} \tag{4.57}$$

appearing to work quite well for $T \lesssim 0.3\, T_0$. In the inset of Fig. 4.8 we report the difference

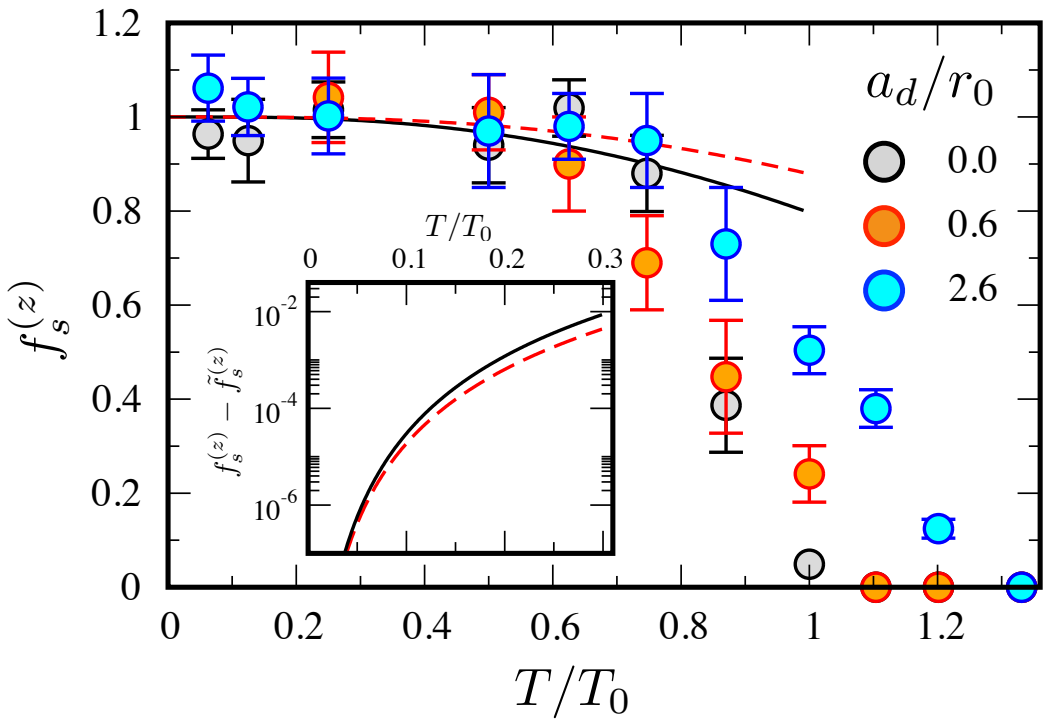

Figure 4.8: Superfluid fraction $f_s^{(z)}$ as a function of the scaled temperature T/T_0 at $nr_0^3 = 10^{-2}$ for three values of the dipolar lengths: a) SF with $a_d = 0$ (hard-core bosons), b) SF with $a_d = 0.6r_0$, c) FP with $a_d = 2.6\,r_0$. Lines refer to the analytical prediction of the temperature dependence of the superfluid fraction at $nr_0^3 = 10^{-2}$ from Eq.(4.56) at $a_d = 0$ (black solid line) and $a_d = 0.6\,r_0$ (red dashed line). Inset. Low temperature limit of $f_s^{(z)}$ from Eq. (4.56) and Eq.(4.57) in the SF at $a_d = 0$ and $a_d = 0.6\,r_0$. Temperatures are in units of T_0, the critical value for a non-interacting Bose gas.

between Eq. (4.56) and Eq. (4.57) for the same value of $a_{\rm dd}$ in the main plot. For $a_{\rm dd} = 2.6$ within the FP, we observe that superfluidity persists along the dipole orientation for a wide range of temperatures. Then, we can surely conclude that filaments exist non only at zero temperature but that their anisotropic superfluidity is finite up to $0.8\,T_0$. At the same time, the orthogonal contribution remains extremely small within the same window in the parameters space.

5

CONCLUSIONS AND FUTURE PERSPECTIVES

Throughtout all the previous chapters, we aim to convince the reader of the relevant role played by quantum fluctuations in dilute and ultracold systems made of bosonic atoms. First, we take into account corrections due to the finite-range character of a reasonable atom-atom interaction potential. Thereafter, we move to consider the case of binary Bose-mixture and dipolar condensates.

Concerning finite-range corrections, we highlight deviations of thermodynamic quantities from the zero-range predictions. We consider the contribution of quantum and thermal fluctuations; the former requires a regularization procedure to produce finite and meaningful contribution. We have also explored how this picture changes in systems with lower dimensionalities. As explained in the text, due to the Mermin-Wagner-Hohenberg theorem, fluctuations play a crucial role in systems with reduced dimensions.

One- and two-dimensional Bose gases are still the focus of an intense experimental research, requiring analytical and numerical tools beyond our perturbative approach. For instance, important experimental group in Zurich and Wien, led respectively by T. Esslinger and J. Schmiedmayer, have adopted one-dimensional gases as an effective platform to probe thermodynamics at the quantum scale. Thanks the outstanding isolation from the external environment, it is possible to understand how a quantum system relaxes (or not) to equilibrium [82, 84]. Recent results appear in [85], where phase-coherence properties of coupled condensates have been investigated in a one-dimensional Josephson junction. The authors report that they have observed a phase locking which escapes a convincing theoretical explanation, despite several attempts with increasingly refined tools. Moreover, textbook situations can be reproduced with cold atoms setups as in [198], where two vessels are connected by an effectively one-dimensional wire. Within the experimental regime of temperatures and

densities, a violation of the Weidemann-Franz relation for heat transport has been observed. This important results make us understand the importance of ultracold quantum gases is not confined in the atomic physics community. On the contrary, ultracold atoms can spark a new technological advancement, by providing useful hints for a future development of quantum devices [199].

Despite many advanced theoretical analysis [111, 112, 113, 28], actual experiments with two-dimensional gases continue to shine lights on new puzzling effects [60]. We have to mention the occuring of Berezinskii-Kosterlitz-Thouless (BKT) transition [58, 59], which has been observed in thin liquid Helium films three decades ago [200]. At the same time, physicists have realized this topological transition still escapes an exhausting comprehension in ultracold Bose gases. In [60], the authors originally aimed to excite a sound mode depending on the superfluid density, but no discontinuity has been revealed at the transition. For now, we have extremely refined Monte Carlo simulations [47] and some experimental results on the proliferation of vortices [201]. A further analytical insight on this topic was provided in [202]. By means of functional renormalization group, the authors have investigated the BKT transition proposing a more rigorous amplitude-phase parametrization. The resulting modified perturbative theory seems to better agree with Monte Carlo simulation.

A clear understanding of the most recent theoretical and experimental advances helps to understand the boundaries of this thesis and the future outlooks in a clearer way. Finite-temperature low-dimensional systems require more refined theoretical approaches: we made this point clear in Fig. 2.4, where Gaussian corrections proved to be not enough to recover the exact Lieb-Lininger solutions. The estimation of the superfluid fraction for dipolar condensates in Fig. 4.8 leads us to a similar point for our finite-temperature results. If we are not too close to the critical temperature, they are certainly reliable, but we do not manage to reproduce the proper scaling at the transition.

A first step in this direction has been made in Sec. 1.6, where we abandoned the functional integration for a moment, in order to show the effectiveness of possible alternative approaches. In that case, we have derived informations about non-equibrium dynamics and sound propagation by following a kinetic approach leading to Eq. (1.127). Obviously, the problem is not functional integration itself but rather the choice of the most suitable framework according to experimental regimes.

Moving to Chap. 3 and Chap. 4, we have investigasted the stabilizing role played by fluctuations in collapsing system. While the first theoretical proposal was formulated in binary mixtures [97, 98], it has been shown to apply as well to dipolar condensates [149, 187, 150, 185]. Concerning multicomponent quantum gases, we have managed to point out a practical characterization of the self-bound droplets besides their peculiar nucleation mechanism. Moreover, by studying Rabi-coupled mixtures, we have identified in the coupling frequency an additional knob to tune the droplet stability. Despite our analysis and the recent experimental developments [101, 153, 148], many questions remain unanswered. The first one concerns the role of thermal fluctuations, since our analytical results only apply at zero-temperature. At first, the occurring of self-evaporation seems to suggest that self-bound quantum droplets immediately dissolve at finite temperature. However, this picture is not reproduced in dipolar condensates, where our Monte Carlo simulations [188] proved the stability of self-bound filaments against temperature fluctuations. It is then natural to ask if finite-temperature corrections would destabilize (or not) the droplet.

In Chap. 3 we also devoted our attention to collective excitations occuring in self-bound states. According to our prediction, self-evaporation prevents the observation of monopole and quadrupole oscillations in two-component droplets. However, recent proposals have paved the way to the engineering of more exotic situation like droplets with non-zero vorticity. Such non-trivial excitations have been studied in binary mixtures [203] but also in dipolar condensates [204]. Another interesting path surely concerns the investigation of Bose-Fermi mixtures for three and lower dimensions [205, 206].

Indeed, the role of dimensionality is fundamental also for droplet nucleation. In our 3d analysis the attraction leading to collapse instability comes from the mean-field contribution to the equation of state. On the contrary, the *quantum pressure* halting the process is due to quantum fluctuations. For one-dimensional systems the situation is exactly the opposite [98]. Another peculiarity of the 1d quantum droplets is that the modified Gross-Pitaevskii equation arising from the analog of our Eq. (3.48) can be solved analytically [160]. In [98] Petrov and Astrakharchik also underline that the most interesting case remains the one provided by two-spatial dimensions, where the occurring of self-bound configurations only requires an inter-component attraction, no matter how small. In [207] and [208] two-dimensional droplets are investigate at finite temperature by means of the time-dependent

Hartree-Fock-Bogoliubov theory. Both in binary mixtures and dipolar atoms, droplets are predicted to be stable, at least below a certain critical temperature.

In order to achieve a further understanding on the mechanism leading to the droplet formation, a possible outlook of this thesis concerns the investigation of eventual modulational instabilities. In analogy to the solitons trains formation in single-component condensed Bose gases [209, 210, 211], a quench of the inter-component scattering length could lead to the droplet fragmentation. It would be then interesting to probe the survival of Bose-Einstein condensation and superfluidity in this situation. The possibility to engineer and control multiple droplets could also open the way to the investigation of droplets dynamics and collisions. Some preliminary steps in this direction have already been made by reviewing the non-dissipative drag (i.e. the Andreev-Bashkin effect) occuring in multicomponent atomic superfluids [140].

Approaching the actual conclusion of this thesis, it is important to remark that, in general, the sparkling interest in dipolar condensates and binary mixtures is not, and it should not be, confined within the boundaries of the atomic and molecular physics community. Dipolar systems are probably the most reliable platform to effectively perform analog quantum simulations of condensed matter models without losing too much complexity. This is even more pressing these days, when degenerate regimes have been achieved for the first time with gases made of polar molecules [173].

On the other hand, the research on multicomponent quantum fluids surely received a great incentive thanks to quantum droplets and their possible applications as cooling components in quantum circuits or in interference apparatuses. The interest in these systems touches also fundamental applications in statistical physics [212] and quantum simulations of exotic symmetry appearing in particle physics [213], models of the early universe and inflationary expansion [135, 136].

In the end, this will continue to be a long and enternaing travel, waiting for passionate scientists to reveal novel features and ground-breaking applications.

A

APPENDIX: BOSONIC MATSUBARA FREQUENCIES SUMS

Here we aim to prove the following useful formula, appearing throughtout this whole thesis:

$$\sum_n \log\left[\beta^2(\hbar^2\omega_n^2 + E_{\mathbf{q}}^2)\right] = \beta E_{\mathbf{q}} + 2\big(1 - e^{-\beta E_{\mathbf{q}}}\big) + (\mathcal{C}) \tag{A.1}$$

where $\mathcal{C}$ is here a infinite constant which can be safely discarded because of its independence from all the thermodynamic variables. Throughtout the derivation we refer to the *classical* thermal field theory monography by J. Kapusta and the equally excellent lectures notes by A. Schmitt [214, 215].

The first step consists in tackling down the logarithm which otherwise forces us to deal with an uneasy-to-handle branch cut. Thus, let us begin by splitting the sum into two contributions with the change of variable $E_{\mathbf{q}} \equiv \frac{x}{\beta}$, namely

$$\sum_n \log\left[\beta^2(\hbar^2\omega_n^2 + E_{\mathbf{q}}^2)\right] = \int_1^{(\beta E_{\mathbf{q}})} d(x^2) \sum_n \frac{1}{(2\pi n)^2 + x^2} + \sum_n \log[1 + (2\pi n)^2]\,. \tag{A.2}$$

The second term in the right-hand-side (RHS) of the equation above is clearly divergent, but independent from any thermodynamic variable so it can be considered harmless. The crucial point is the summation contained in the first term of Eq. (A.2). As underlined in [215], the proper way to solve it relies on contour integration technique. By making use of the residue theorem, it can be expressed as

$$\frac{1}{\beta}\sum_n \frac{1}{\hbar^2\omega_n^2 + E_{\mathbf{q}}^2} = \frac{i}{2\pi\hbar}\oint_\Gamma dz\, \frac{1}{2(z^2 + E_{\mathbf{q}}^2)} \coth\left(\beta\frac{z}{2}\right) \tag{A.3}$$

where the contour Γ has to chosen to enclose only the poles of the $\coth(z)$ function. As

noted in [215], this contour can be deformed in order to reach the *simpler* integral

$$\begin{aligned}\frac{1}{\beta}\sum_n \frac{1}{\hbar^2\omega_n^2 + E_{\mathbf{q}}^2} &= \frac{i}{2\pi\hbar}\left[\int_{-i\infty+\delta}^{+i\infty+\delta} dz \frac{1}{2(z^2 - E_{\mathbf{q}}^2)} \coth\left(\beta\frac{z}{2}\right) + \int_{i\infty-\delta}^{-i\infty-\delta} dz \frac{1}{2(z^2 - E_{\mathbf{q}}^2)} \coth\left(\beta\frac{z}{2}\right)\right] \\ &= \frac{i}{2\pi\hbar}\int_{-i\infty+\delta}^{+i\infty+\delta} \frac{1}{2(z^2 - E_{\mathbf{q}}^2)} \coth\left(\beta\frac{z}{2}\right).\end{aligned} \tag{A.4}$$

Now, the residue theorem can be applied again, this time closing the contour on the half-plane $\mathrm{Re}\, z > 0$ (or $\mathrm{Re}\, z < 0$), leading to

$$\frac{1}{\beta}\sum_n \frac{1}{\hbar^2\omega_n^2 + E_{\mathbf{q}}^2} = \frac{1}{2E_{\mathbf{q}}} \coth\left(\beta\frac{E_{\mathbf{q}}}{2}\right) = \frac{1}{2E_{\mathbf{q}}}\left(1 + \frac{2}{e^{\beta E_{\mathbf{q}}} - 1}\right). \tag{A.5}$$

Finally, we can replace the result above in Eq. (A.2), finding that

$$\begin{aligned}\sum_n \log\left[\beta^2(\hbar^2\omega_n^2 + E_{\mathbf{q}}^2)\right] &= \int_1^{(\beta E_{\mathbf{q}})^2} dx^2 \, \frac{1}{2x}\left(1 + \frac{2}{e^x - 1}\right) + \mathcal{C} \\ &= \beta E_{\mathbf{q}} + 2\log\left(1 - e^{-\beta E_{\mathbf{q}}}\right) + \mathcal{C}\end{aligned} \tag{A.6}$$

BIBLIOGRAPHY

[1] A. Schakel, *Boulevard of Broken Symmetries: Effective Field Theories of Condensed Matter* (World Scientific 2008).

[2] H. Stoof, D. Dickerscheid, and K. Gubbels, *Ultracold Quantum Fields* (Springer 2008).

[3] A. Altland and B. Simons, *Condensed Matter Field Theory* (Cambridge University Press 2010).

[4] J. Negele and H. Orland, *Quantum many-particle systems* (Addison-Wesley Pub. Co. 1988).

[5] N. Nagaosa, *Quantum Field Theory in Condensed Matter Physics* (Springer Berlin Heidelberg 2013).

[6] K. Huang, *Statistical mechanics* (Wiley 1987).

[7] A. Griffin, D. Snoke, and S. Stringari, *Bose-Einstein Condensation* (Cambridge University Press 1996).

[8] L. Salasnich and F. Toigo, Zero-point energy of ultracold atoms, Physics Reports **640**, 1 (2016).

[9] G. 't Hooft and M. J. G. Veltman, Regularization and Renormalization of Gauge Fields, Nucl. Phys. **B44**, 189 (1972).

[10] A. Fetter and J. Walecka, *Quantum Theory of Many-Particle Systems*, Dover Books on Physics (Dover Publications 2012).

[11] M. Kardar, *Statistical Physics of Fields* (Cambridge University Press 2007).

[12] N. D. Mermin and H. Wagner, Absence of Ferromagnetism or antiferromagnetism in one- or two- dimensional isotropic heisenberg models, Physical Review Letters **17**, 1133 (1966).

[13] Hohenberg, P.C., Existence of Long-Range Order in One and Two Dimensions, Physical Review **158**, 383 (1967).

[14] Y. Castin, Bose-einstein condensates in atomic gases: Simple theoretical results, in *Coherent atomic matter waves* (Springer Berlin Heidelberg, Berlin 2001), pp. 1–136.

[15] A. J. Daley, Theoretical aspects of analogue quantum simulation with cold atoms, in *Quantum Simulators* (IOS Press, Amsterdam 2018), pp. 55–110.

[16] T. D. Lee, K. Huang, and C. N. Yang, Eigenvalues and eigenfunctions of a bose system of hard spheres and its low-temperature properties, Phys. Rev. **106**, 1135 (1957).

[17] T. D. Lee and C. N. Yang, Low-temperature behavior of a dilute bose system of hard spheres. i. equilibrium properties, Phys. Rev. **112**, 1419 (1958).

[18] R. Roth and H. Feldmeier, Effective s- and p-wave contact interactions in trapped degenerate fermi gases, Phys. Rev. A **64**, 043603 (2001).

[19] A. Collin, P. Massignan, and C. J. Pethick, Energy-dependent effective interactions for dilute many-body systems, Phys. Rev. A **75**, 013615 (2007).

[20] B. Bransden, C. Joachain, and T. Plivier, *Physics of Atoms and Molecules*, Pearson Education (Prentice Hall 2003).

[21] S. K. Adhikari, Quantum scattering in two dimensions, American Journal of Physics **54**, 362 (1986).

[22] C. Mora and Y. Castin, Extension of bogoliubov theory to quasicondensates, Phys. Rev. A **67**, 053615 (2003).

[23] M. O. M. D. Girardeau, H. Nguyen, Effective interactions, fermi-bose duality, and ground states of ultracold atomic vapors in tight de broglie waveguides, Optics Communications **243**, 3 (2004).

[24] T. Haugset, H. Haugerud, and F. Ravndal, Thermodynamics of a weakly interacting bose–einstein gas, Annals of Physics **266**, 27 (1998).

[25] Braaten, E. and Nieto, A., Quantum corrections to the energy density of a homogeneous bose gas, Eur. Phys. J. B **11**, 143 (1999).

[26] J. O. Andersen, Theory of the weakly interacting Bose gas, Reviews of Modern Physics **76**, 599 (2004).

[27] G. Leibbrandt, Introduction to the technique of dimensional regularization, Rev. Mod. Phys. **47**, 849 (1975).

[28] L. Salasnich, Nonuniversal equation of state of the two-dimensional bose gas, Phys. Rev. Lett. **118**, 130402 (2017).

[29] N. N. Bogolyubov, On the theory of superfluidity, J. Phys.(USSR) **11**, 23 (1947), [Izv. Akad. Nauk Ser. Fiz.11,77(1947)].

[30] T. D. Lee and C. N. Yang, Low-temperature behavior of a dilute bose system of hard spheres. ii. nonequilibrium properties, Phys. Rev. **113**, 1406 (1959).

[31] M. H. Anderson, J. R. Ensher, M. R. Matthews, C. E. Wieman, and E. A. Cornell, Observation of bose-einstein condensation in a dilute atomic vapor, Science **269**, 198 (1995).

[32] K. B. Davis, M. O. Mewes, M. R. Andrews, N. J. van Druten, D. S. Durfee, D. M. Kurn, and W. Ketterle, Bose-einstein condensation in a gas of sodium atoms, Phys. Rev. Lett. **75**, 3969 (1995).

[33] F. Dalfovo, S. Giorgini, L. P. Pitaevskii, and S. Stringari, Theory of bose-einstein condensation in trapped gases, Rev. Mod. Phys. **71**, 463 (1999).

[34] D. M. Ceperley, Path integrals in the theory of condensed helium, Rev. Mod. Phys. **67**, 279 (1995).

[35] L. D. Landau, Theory of superfluidity of Helium-II, Zhurnal Eksperimentalnoi i Teoreticheskoi Fiziki **11**, 592 (1941).

[36] L. Pitaevskii and S. Stringari, *Bose-Einstein Condensation and Superfluidity*, International series of monographs on physics (Oxford University Press 2016).

[37] A. Leggett, *Quantum Liquids: Bose Condensation and Cooper Pairing in Condensed-matter Systems*, Oxford graduate texts in mathematics (OUP Oxford 2006).

[38] E. Zaremba, A. Griffin, and T. Nikuni, Two-fluid hydrodynamics for a trapped weakly interacting bose gas, Phys. Rev. A **57**, 4695 (1998).

[39] T. Nikuni, E. Zaremba, and A. Griffin, Two-fluid dynamics for a bose-einstein condensate out of local equilibrium with the noncondensate, Phys. Rev. Lett. **83**, 10 (1999).

[40] E. Zaremba, T. Nikuni, and A. Griffin, Dynamics of trapped bose gases at finite temperatures, Journal of Low Temperature Physics **116**, 277 (1999).

[41] A. Griffin, T. Nikuni, and E. Zaremba, *Bose-Condensed Gases at Finite Temperatures* (Cambridge University Press 2009).

[42] U. C. Tauber and D. R. Nelson, Superfluid bosons and flux liquids: disorder, thermal fluctuations, and finite-size effects, Physics Reports **296**, 337 (1998).

[43] D. S. Fisher and P. C. Hohenberg, Dilute bose gas in two dimensions, Phys. Rev. B **37**, 4936 (1988).

[44] R. Baym, G in Clark and G. Derrick, *Mathematical Methods in Solid State and Superfluid Theory: Scottish Universities Summer School*, Scottish Universities‘ Summer School (Springer US 1968).

[45] M. Ueda, *Fundamentals and New Frontiers of Bose-Einstein Condensation* (World Scientific 2010).

[46] E. Taylor, A. Griffin, N. Fukushima, and Y. Ohashi, Pairing fluctuations and the superfluid density through the bcs-bec crossover, Phys. Rev. A **74**, 063626 (2006).

[47] B. Svistunov, E. Babaev, and N. Prokof'ev, *Superfluid States of Matter* (Taylor & Francis 2015).

[48] R. B. Diener, R. Sensarma, and M. Randeria, Quantum fluctuations in the superfluid state of the bcs-bec crossover, Phys. Rev. A **77**, 023626 (2008).

[49] T. R. Kirkpatrick and J. R. Dorfman, Transport theory for a weakly interacting condensed bose gas, Phys. Rev. A **28**, 2576 (1983).

[50] N. Proukakis and B. Jackson, Finite-temperature models of bose-??einstein condensation, Journal of Physics B: Atomic, Molecular and Optical Physics **41**, 203002 (2008).

[51] A. Sinatra, C. Lobo, and Y. Castin, The truncated wigner method for bose-condensed gases: limits of validity and applications, Journal of Physics B: Atomic, Molecular and Optical Physics **35**, 3599 (2002).

[52] H. T. C. Stoof and M. J. Bijlsma, Dynamics of fluctuating bose–einstein condensates, Journal of Low Temperature Physics **124**, 431 (2001).

[53] P. B. Blakie, A. S. Bradley, M. J. Davis, R. J. Ballagh, and C. W. Gardiner, Dynamics and statistical mechanics of ultra-cold bose gases using c-field techniques, Advances in Physics **57**, 363 (2008).

[54] A. A. Vlasov, On the kinetic theory of an assembly of particles with collective interaction, J. Phys. USSR **9**.

[55] L. D. Landau, On the vibrations of the electronic plasma, J. Phys.(USSR) **10**, 25 (1946), [Zh. Eksp. Teor. Fiz.16,574(1946)].

[56] E. Lifshitz, L. Pitaevskii, J. Sykes, and R. Franklin, *Physical Kinetics*, Course of theoretical physics (Elsevier Science 1995).

[57] L. Kadanoff and G. Baym, *Quantum statistical mechanics: Green's function methods in equilibrium and nonequilibrium problems*, Frontiers in physics (W.A. Benjamin 1962).

[58] V. L. Berezinskiĭ, Destruction of Long-range Order in One-dimensional and Two-dimensional Systems Possessing a Continuous Symmetry Group. II. Quantum Systems, Soviet Journal of Experimental and Theoretical Physics **34**, 610 (1972).

[59] J. M. Kosterlitz and D. J. Thouless, Ordering, metastability and phase transitions in two-dimensional systems, Journal of Physics C: Solid State Physics **6**, 1181 (1973).

[60] J. L. Ville, R. Saint-Jalm, É. Le Cerf, M. Aidelsburger, S. Nascimbène, J. Dalibard, and J. Beugnon, Sound propagation in a uniform superfluid two-dimensional Bose gas, ArXiv:1804.04037 (2018).

[61] T. Ozawa and S. Stringari, Discontinuities in the first and second sound velocities at the berezinskii-kosterlitz-thouless transition, Phys. Rev. Lett. **112**, 025302 (2014).

[62] M. Ota and S. Stringari, Second sound in a two-dimensional bose gas: From the weakly to the strongly interacting regime, Phys. Rev. A **97**, 033604 (2018).

[63] F. Baldovin, A. Cappellaro, E. Orlandini, and L. Salasnich, Nonequilibrium statistical mechanics in one-dimensional bose gases, Journal of Statistical Mechanics: Theory and Experiment **2016**, 063303 (2016).

[64] M. Ota, F. Larcher, F. Dalfovo, L. Pitaevskii, N. P. Proukakis, and S. Stringari, Collisionless sound in a uniform two-dimensional Bose gas, ArXiv:1804.04032 (2018).

[65] E. Braaten, H.-W. Hammer, and S. Hermans, Nonuniversal effects in the homogeneous bose gas, Phys. Rev. A **63**, 063609 (2001).

[66] J. O. Andersen, Ground state pressure and energy density of an interacting homogeneous Bose gas in two dimensions, European Physical Journal B **28**, 389 (2002).

[67] A. Cappellaro and L. Salasnich, Thermal field theory of bosonic gases with finite-range effective interaction, Phys. Rev. A **95**, 033627 (2017).

[68] H. Fu, Y. Wang, and B. Gao, Beyond the fermi pseudopotential: A modified gross-pitaevskii equation, Phys. Rev. A **67**, 053612 (2003).

[69] F. Sgarlata, G. Mazzarella, and L. Salasnich, Effective-range signatures in quasi-1d matter waves: sound velocity and solitons, Journal of Physics B: Atomic, Molecular and Optical Physics **48**, 115301 (2015).

[70] M. Rossi and L. Salasnich, Path-integral ground state and superfluid hydrodynamics of a bosonic gas of hard spheres, Phys. Rev. A **88**, 053617 (2013).

[71] S. Giorgini, J. Boronat, and J. Casulleras, Ground state of a homogeneous bose gas: A diffusion monte carlo calculation, Phys. Rev. A **60**, 5129 (1999).

[72] E. Braaten and A. Nieto, Renormalization effects in a dilute bose gas, Phys. Rev. B **55**, 8090 (1997).

[73] H. Bethe, Zur theorie der metalle, Zeitschrift für Physik **71**, 205 (1931).

[74] T. Giamarchi, *Quantum Physics in One Dimension*, International Series of Monographs on Physics (Clarendon Press 2003).

[75] E. Chow, P. Delsing, and D. B. Haviland, Length-scale dependence of the superconductor-to-insulator quantum phase transition in one dimension, Phys. Rev. Lett. **81**, 204 (1998).

[76] D. B. Haviland, K. Andersson, and P. Ågren, Superconducting and insulating behavior in one-dimensional josephson junction arrays, Journal of Low Temperature Physics **118**, 733 (2000).

[77] B. Paredes, A. Widera, V. Murg, O. Mandel, S. Fölling, I. Cirac, G. V. Shlyapnikov, T. W. Hänsch, and I. Bloch, Tonks-girardeau gas of ultracold atoms in an optical lattice., Nature **429**, 277 (2004).

[78] T. Kinoshita, T. Wenger, and D. S. Weiss, Observation of a one-dimensional tonks-girardeau gas, Science **305**, 1125 (2004).

[79] E. Haller, M. Gustavsson, M. J. Mark, J. G. Danzl, R. Hart, G. Pupillo, and H.-C. Nägerl, Realization of an excited, strongly correlated quantum gas phase, Science **325**, 1224 (2009).

[80] E. Haller, R. Hart, M. J. Mark, J. G. Danzl, L. Reichsöllner, M. Gustavsson, M. Dalmonte, G. Pupillo, and H.-C. Nägerl, Pinning quantum phase transition for a luttinger liquid of strongly interacting bosons, Nature **466**, 597 (2010).

[81] R. Folman and P. Kr Microscopic atom optics: From wires to an atom chip (Academic Press 2002), *Advances In Atomic, Molecular, and Optical Physics*, volume 48, pp. 263 – 356.

[82] B. Rauer, P. Grišins, I. E. Mazets, T. Schweigler, W. Rohringer, R. Geiger, T. Langen, and J. Schmiedmayer, Cooling of a one-dimensional bose gas, Phys. Rev. Lett. **116**, 030402 (2016).

[83] T. Langen, R. Geiger, and J. Schmiedmayer, Ultracold atoms out of equilibrium, Annual Review of Condensed Matter Physics **6**, 201 (2015).

[84] J. Schmiedmayer, One-dimensional atomic superfluids as a model system for quantum thermodynamics, ArXiv:1805.11539 (2018).

[85] M. Pigneur, T. Berrada, M. Bonneau, T. Schumm, E. Demler, and J. Schmiedmayer, Relaxation to a phase-locked equilibrium state in a one-dimensional bosonic josephson junction, Phys. Rev. Lett. **120**, 173601 (2018).

[86] E. H. Lieb and W. Liniger, Exact analysis of an interacting bose gas. i. the general solution and the ground state, Phys. Rev. **130**, 1605 (1963).

[87] E. H. Lieb, Exact analysis of an interacting bose gas. ii. the excitation spectrum, Phys. Rev. **130**, 1616 (1963).

[88] C. N. Yang and C. P. Yang, Thermodynamics of a one-dimensional system of bosons with repulsive delta-function interaction, Journal of Mathematical Physics **10**, 1115 (1969).

[89] C. P. Yang, One-dimensional system of bosons with repulsive δ-function interactions at a finite temperature, Phys. Rev. A **2**, 154 (1970).

[90] A. Parola, L. Salasnich, and L. Reatto, Structure and stability of bosonic clouds: Alkali-metal atoms with negative scattering length, Phys. Rev. A **57**, R3180 (1998).

[91] J. J. Garcia-Ripoll, V. V. Konotop, B. Malomed, and V. M. Perez-Garcia, A quasi-local gross-pitaevskii equation for attractive bose-einstein condensates .

[92] N. T. Zinner and M. Thøgersen, Stability of a bose-einstein condensate with higher-order interactions near a feshbach resonance, Phys. Rev. A **80**, 023607 (2009).

[93] M. Thøgersen, N. T. Zinner, and A. S. Jensen, Thomas-fermi approximation for a condensate with higher-order interactions, Phys. Rev. A **80**, 043625 (2009).

[94] H. Veksler, S. Fishman, and W. Ketterle, Simple model for interactions and corrections to the gross-pitaevskii equation, Phys. Rev. A **90**, 023620 (2014).

[95] P. A. Murthy, I. Boettcher, L. Bayha, M. Holzmann, D. Kedar, M. Neidig, M. G. Ries, A. N. Wenz, G. Zürn, and S. Jochim, Observation of the berezinskii-kosterlitz-thouless phase transition in an ultracold fermi gas, Phys. Rev. Lett. **115**, 010401 (2015).

[96] S. Murmann, F. Deuretzbacher, G. Zürn, J. Bjerlin, S. M. Reimann, L. Santos, T. Lompe, and S. Jochim, Antiferromagnetic heisenberg spin chain of a few cold atoms in a one-dimensional trap, Phys. Rev. Lett. **115**, 215301 (2015).

[97] D. S. Petrov, Quantum mechanical stabilization of a collapsing bose-bose mixture, Phys. Rev. Lett. **115**, 155302 (2015).

[98] D. S. Petrov and G. E. Astrakharchik, Ultradilute low-dimensional liquids, Phys. Rev. Lett. **117**, 100401 (2016).

[99] M. Schmitt, M. Wenzel, F. Böttcher, I. Ferrier-Barbut, and T. Pfau, Self-bound droplets of a dilute magnetic quantum liquid, Nature **539**, 259 (2016).

[100] L. Chomaz, S. Baier, D. Petter, M. J. Mark, F. Wächtler, L. Santos, and F. Ferlaino, Quantum-fluctuation-driven crossover from a dilute bose-einstein condensate to a macrodroplet in a dipolar quantum fluid, Phys. Rev. X **6**, 041039 (2016).

[101] C. R. Cabrera, L. Tanzi, J. Sanz, B. Naylor, P. Thomas, P. Cheiney, and L. Tarruell, Quantum liquid droplets in a mixture of Bose-Einstein condensates, Science **359**, 301 (2018).

[102] T. Lahaye, C. Menotti, L. Santos, M. Lewenstein, and T. Pfau, The physics of dipolar bosonic quantum gases, Reports on Progress in Physics **72**, 126401 (2009).

[103] A. Cappellaro and L. Salasnich, Finite-range corrections to the thermodynamics of the one-dimensional bose gas, Phys. Rev. A **96**, 063610 (2017).

[104] V. E. Barlette, M. M. Leite, and S. K. Adhikari, Quantum scattering in one dimension, European Journal of Physics **21**, 435 (2000).

[105] M. Olshanii, Atomic scattering in the presence of an external confinement and a gas of impenetrable bosons, Phys. Rev. Lett. **81**, 938 (1998).

[106] M. A. Cazalilla, R. Citro, T. Giamarchi, E. Orignac, and M. Rigol, One dimensional bosons: From condensed matter systems to ultracold gases, Rev. Mod. Phys. **83**, 1405 (2011).

[107] G. De Rosi, G. E. Astrakharchik, and S. Stringari, Thermodynamic behavior of a one-dimensional bose gas at low temperature, Phys. Rev. A **96**, 013613 (2017).

[108] T. Kaminaka and M. Wadati, Higher order solutions of lieb-liniger integral equation, Physics Letters A **375**, 2460 .

[109] S. Choi, V. Dunjko, Z. D. Zhang, and M. Olshanii, Monopole excitations of a harmonically trapped one-dimensional bose gas from the ideal gas to the tonks-girardeau regime, Phys. Rev. Lett. **115**, 115302 (2015).

[110] M. Schick, Two-dimensional system of hard-core bosons, Phys. Rev. A **3**, 1067 (1971).

[111] S. Floerchinger and C. Wetterich, Superfluid bose gas in two dimensions, Phys. Rev. A **79**, 013601 (2009).

[112] N. Dupuis, Unified picture of superfluidity: From bogoliubov's approximation to popov's hydrodynamic theory, Phys. Rev. Lett. **102**, 190401 (2009).

[113] A. Rançon and N. Dupuis, Universal thermodynamics of a two-dimensional bose gas, Phys. Rev. A **85**, 063607 (2012).

[114] N. N. Khuri, A. Martin, J.-M. Richard, and T. T. Wu, Low-energy potential scattering in two and three dimensions, Journal of Mathematical Physics **50**, 072105 (2009).

[115] F. Werner and Y. Castin, General relations for quantum gases in two and three dimensions: Two-component fermions, Phys. Rev. A **86**, 013626 (2012).

[116] J. Niederle, V. Popov, and L. Hlavatỳ, *Functional Integrals in Quantum Field Theory and Statistical Physics*, Mathematical Physics and Applied Mathematics (Springer Netherlands 1983).

[117] V. Popov, V. Popov, C. U. Press, P. Landshoff, D. Nelson, D. Sciama, and S. Weinberg, *Functional Integrals and Collective Excitations*, Cambridge Monographs on Mathematical Physics (Cambridge University Press 1987).

[118] Z. Hadzibabic and J. Dalibard, Two-dimensional Bose fluids: An atomic physics perspective, ArXiv:0912.1490 (2009).

[119] M. R. Matthews, D. S. Hall, D. S. Jin, J. R. Ensher, C. E. Wieman, E. A. Cornell, F. Dalfovo, C. Minniti, and S. Stringari, Dynamical response of a bose-einstein condensate to a discontinuous change in internal state, Phys. Rev. Lett. **81**, 243 (1998).

[120] D. S. Hall, M. R. Matthews, J. R. Ensher, C. E. Wieman, and E. A. Cornell, Dynamics of component separation in a binary mixture of bose-einstein condensates, Phys. Rev. Lett. **81**, 1539 (1998).

[121] D. S. Hall, M. R. Matthews, C. E. Wieman, and E. A. Cornell, Measurements of relative phase in two-component bose-einstein condensates, Phys. Rev. Lett. **81**, 1543 (1998).

[122] I. M. Khalatnikov, Hydrodynamics of solutions of two superfluid liquids, JETP **5** (1956).

[123] L. D. Landau, On the hydrodynamics of helium ii, J. Phys. USSR **8** (1944).

[124] L. D. Landau and I. M. Khalatnikov, The theory of the viscosity of helium ii. i. collisions of elementary excitations in helium ii, Zh. Eksp. Teor. Fiz. **19** (1948).

[125] L. D. Landau and I. M. Khalatnikov, The theory of the viscosity of helium ii. ii. calculation of the viscosity coefficient, Zh. Eksp. Teor. Fiz. **19** (1948).

[126] A. Andreev and E. Bashkin, Three-velocity hydrodynamics of superfluid solutions, JETP **42** (1975).

[127] S. Beattie, S. Moulder, R. J. Fletcher, and Z. Hadzibabic, Persistent currents in spinor condensates, Phys. Rev. Lett. **110**, 025301 (2013).

[128] M.-S. Chang, Q. Qin, W. Zhang, L. You, and M. S. Chapman, Coherent spinor dynamics in a spin-1 bose condensate, Nature Physics **1**, 111 (2005).

[129] T. Zibold, E. Nicklas, C. Gross, and M. K. Oberthaler, Classical bifurcation at the transition from rabi to josephson dynamics, Phys. Rev. Lett. **105**, 204101 (2010).

[130] G. J. Conduit, A. G. Green, and B. D. Simons, Inhomogeneous phase formation on the border of itinerant ferromagnetism, Phys. Rev. Lett. **103**, 207201 (2009).

[131] V. Penna and L. Salasnich, Itinerant ferromagnetism of two-dimensional repulsive fermions with rabi coupling, New Journal of Physics **19**, 043018 (2017).

[132] M. W. Stefano Liberati and S. Weinfurtner, Analogue quantum gravity phenomenology from a two-component bose-einstein condensates, Classical and Quantum Gravity **23**, 3129 (2006).

[133] P.-E. Larré, A. Recati, I. Carusotto, and N. Pavloff, Quantum fluctuations around black hole horizons in bose-einstein condensates, Phys. Rev. A **85**, 013621 (2012).

[134] S. Butera, P. Öhberg, and I. Carusotto, Black-hole lasing in coherently coupled two-component atomic condensates, Phys. Rev. A **96**, 013611 (2017).

[135] B. Opanchuk, R. Polkinghorne, O. Fialko, J. Brand, and P. D. Drummond, Quantum simulations of the early universe, Annalen der Physik **525**, 866 (2013).

[136] O. Fialko, B. Opanchuk, A. I. Sidorov, P. D. Drummond, and J. Brand, The universe on a table top: engineering quantum decay of a relativistic scalar field from a metastable vacuum, Journal of Physics B: Atomic, Molecular and Optical Physics **50**, 024003 (2017).

[137] J. Braden, M. C. Johnson, H. V. Peiris, and S. Weinfurtner, Towards the cold atom analog false vacuum, Journal of High Energy Physics **2018**, 14 (2018).

[138] C. D'Errico, M. Zaccanti, M. Fattori, G. Roati, M. Inguscio, G. Modugno, and A. Simoni, Feshbach resonances in ultracold ^{39}k, New Journal of Physics **9**, 223 (2007).

[139] M. Lysebo and L. Veseth, Feshbach resonances and transition rates for cold homonuclear collisions between ^{39}K and ^{41}K atoms, Phys. Rev. A **81**, 032702 (2010).

[140] J. Nespolo, G. E. Astrakharchik, and A. Recati, Andreev-bashkin effect in superfluid cold gases mixtures, New Journal of Physics **19**, 125005 (2017).

[141] J. Armaitis, H. T. C. Stoof, and R. A. Duine, Hydrodynamic modes of partially condensed bose mixtures, Phys. Rev. A **91**, 043641 (2015).

[142] Abad, Marta and Recati, Alessio, A study of coherently coupled two-component bose-einstein condensates, Eur. Phys. J. D **67**, 148 (2013).

[143] S. Coleman, Fate of the false vacuum: Semiclassical theory, Phys. Rev. D **15**, 2929 (1977).

[144] C. G. Callan and S. Coleman, Fate of the false vacuum. ii. first quantum corrections, Phys. Rev. D **16**, 1762 (1977).

[145] C. P. Search, A. G. Rojo, and P. R. Berman, Ground state and quasiparticle spectrum of a two-component bose-einstein condensate, Phys. Rev. A **64**, 013615 (2001).

[146] P. Tommasini, E. J. V. de Passos, A. F. R. de Toledo Piza, M. S. Hussein, and E. Timmermans, Bogoliubov theory for mutually coherent condensates, Phys. Rev. A **67**, 023606 (2003).

[147] D. M. Larsen, Binary mixtures of dilute bose gases with repulsive interactions at low temperature, Annals of Physics **24**, 89 (1963).

[148] G. Semeghini, G. Ferioli, L. Masi, C. Mazzinghi, L. Wolswijk, F. Minardi, M. Modugno, G. Modugno, M. Inguscio, and M. Fattori, Self-bound quantum droplets of atomic mixtures in free space, Phys. Rev. Lett. **120**, 235301 (2018).

[149] F. Wächtler and L. Santos, Quantum filaments in dipolar bose-einstein condensates, Phys. Rev. A **93**, 061603 (2016).

[150] D. Baillie, R. M. Wilson, R. N. Bisset, and P. B. Blakie, Self-bound dipolar droplet: A localized matter wave in free space, Phys. Rev. A **94**, 021602 (2016).

[151] D. Baillie, R. M. Wilson, and P. B. Blakie, Collective excitations of self-bound droplets of a dipolar quantum fluid, Phys. Rev. Lett. **119**, 255302 (2017).

[152] P. Kevrekidis, D. Frantzeskakis, and R. Carretero-González, *Emergent Nonlinear Phenomena in Bose-Einstein Condensates: Theory and Experiment*, Springer Series on Atomic, Optical, and Plasma Physics (Springer Berlin Heidelberg 2007).

[153] P. Cheiney, C. R. Cabrera, J. Sanz, B. Naylor, L. Tanzi, and L. Tarruell, Bright soliton to quantum droplet transition in a mixture of bose-einstein condensates, Phys. Rev. Lett. **120**, 135301 (2018).

[154] N. Henkel, R. Nath, and T. Pohl, Three-dimensional roton excitations and supersolid formation in rydberg-excited bose-einstein condensates, Phys. Rev. Lett. **104**, 195302 (2010).

[155] T. Macrì, F. Maucher, F. Cinti, and T. Pohl, Elementary excitations of ultracold soft-core bosons across the superfluid-supersolid phase transition, Phys. Rev. A **87**, 061602 (2013).

[156] F. Cinti, T. Macrì, W. Lechner, G. Pupillo, and T. Pohl, Defect-induced supersolidity with soft-core bosons, Nature Communications **5**, 3235 (2014).

[157] T. Bienaimé, E. Fava, G. Colzi, C. Mordini, S. Serafini, C. Qu, S. Stringari, G. Lamporesi, and G. Ferrari, Spin-dipole oscillation and polarizability of a binary bose-einstein condensate near the miscible-immiscible phase transition, Phys. Rev. A **94**, 063652 (2016).

[158] A. Cappellaro, T. Macrì, and L. Salasnich, Collective modes across the soliton-droplet crossover in binary bose mixtures, Phys. Rev. A **97**, 053623 (2018).

[159] L. Salasnich, A. Parola, and L. Reatto, Condensate bright solitons under transverse confinement, Phys. Rev. A **66**, 043603 (2002).

[160] G. E. Astrakharchik and B. A. Malomed, Dynamics of one-dimensional quantum droplets, Phys. Rev. A **98**, 013631 (2018).

[161] F. Ancilotto, L. Salasnich, and F. Toigo, Dispersive effects in the unitary fermi gas, Journal of Low Temperature Physics **171**, 329 (2013).

[162] V. M. Pérez-García, H. Michinel, J. I. Cirac, M. Lewenstein, and P. Zoller, Low energy excitations of a bose-einstein condensate: A time-dependent variational analysis, Phys. Rev. Lett. **77**, 5320 (1996).

[163] V. M. Pérez-García, H. Michinel, J. I. Cirac, M. Lewenstein, and P. Zoller, Dynamics of bose-einstein condensates: Variational solutions of the gross-pitaevskii equations, Phys. Rev. A **56**, 1424 (1997).

[164] M. Wenzel, F. Böttcher, T. Langen, I. Ferrier-Barbut, and T. Pfau, Striped states in a many-body system of tilted dipoles, Phys. Rev. A **96**, 053630 (2017).

[165] A. Cappellaro, T. Macrı, G. F. Bertacco, and L. Salasnich, Equation of state and self-bound droplet in Rabi-coupled Bose mixtures, Scientific Reports **7**, 13358 (2017).

[166] E. Nicklas, H. Strobel, T. Zibold, C. Gross, B. A. Malomed, P. G. Kevrekidis, and M. K. Oberthaler, Rabi flopping induces spatial demixing dynamics, Phys. Rev. Lett. **107**, 193001 (2011).

[167] M. Baranov, Theoretical progress in many-body physics with ultracold dipolar gases, Physics Reports **464**, 71 (2008).

[168] M. A. Baranov, M. Dalmonte, G. Pupillo, and P. Zoller, Condensed matter theory of dipolar quantum gases, Chemical Reviews **112**, 5012 (2012).

[169] A. Griesmaier, J. Werner, S. Hensler, J. Stuhler, and T. Pfau, Bose-einstein condensation of chromium, Phys. Rev. Lett. **94**, 160401 (2005).

[170] K. Aikawa, A. Frisch, M. Mark, S. Baier, A. Rietzler, R. Grimm, and F. Ferlaino, Bose-einstein condensation of erbium, Phys. Rev. Lett. **108**, 210401 (2012).

[171] M. Lu, N. Q. Burdick, S. H. Youn, and B. L. Lev, Strongly dipolar bose-einstein condensate of dysprosium, Phys. Rev. Lett. **107**, 190401 (2011).

[172] H. Kadau, M. Schmitt, M. Wenzel, C. Wink, T. Maier, I. Ferrier-Barbut, and T. Pfau, Observing the Rosensweig instability of a quantum ferrofluid, Nature **530**, 194 (2016).

[173] L. De Marco, G. Valtolina, K. Matsuda, W. G. Tobias, J. P. Covey, and J. Ye, A Fermi Degenerate Gas of Polar Molecules, ArXiv:1808.00028 (2018).

[174] S. Giovanazzi, A. Görlitz, and T. Pfau, Tuning the dipolar interaction in quantum gases, Phys. Rev. Lett. **89**, 130401 (2002).

[175] S. Yi and L. You, Trapped atomic condensates with anisotropic interactions, Phys. Rev. A **61**, 041604 (2000).

[176] S. Yi and L. You, Trapped condensates of atoms with dipole interactions, Phys. Rev. A **63**, 053607 (2001).

[177] S. Ronen, D. C. E. Bortolotti, D. Blume, and J. L. Bohn, Dipolar bose-einstein condensates with dipole-dependent scattering length, Phys. Rev. A **74**, 033611 (2006).

[178] D. C. E. Bortolotti, S. Ronen, J. L. Bohn, and D. Blume, Scattering length instability in dipolar bose-einstein condensates, Phys. Rev. Lett. **97**, 160402 (2006).

[179] R. Ołdziejewski and K. Jachymski, Properties of strongly dipolar bose gases beyond the born approximation, Phys. Rev. A **94**, 063638 (2016).

[180] V. I. Yukalov and E. P. Yukalova, Bose-condensed atomic systems with nonlocal interaction potentials, Laser Physics **26**, 045501 (2016).

[181] T. Lahaye, J. Metz, B. Fröhlich, T. Koch, M. Meister, A. Griesmaier, T. Pfau, H. Saito, Y. Kawaguchi, and M. Ueda, *d*-wave collapse and explosion of a dipolar bose-einstein condensate, Phys. Rev. Lett. **101**, 080401 (2008).

[182] A. R. P. Lima and A. Pelster, Beyond mean-field low-lying excitations of dipolar bose gases, Phys. Rev. A **86**, 063609 (2012).

[183] I. Ferrier-Barbut, H. Kadau, M. Schmitt, M. Wenzel, and T. Pfau, Observation of quantum droplets in a strongly dipolar bose gas, Phys. Rev. Lett. **116**, 215301 (2016).

[184] I. Ferrier-Barbut, M. Schmitt, M. Wenzel, H. Kadau, and T. Pfau, Liquid quantum droplets of ultracold magnetic atoms, Journal of Physics B: Atomic, Molecular and Optical Physics **49**, 214004 (2016).

[185] R. N. Bisset, R. M. Wilson, D. Baillie, and P. B. Blakie, Ground-state phase diagram of a dipolar condensate with quantum fluctuations, Phys. Rev. A **94**, 033619 (2016).

[186] H. Saito, Path-integral monte carlo study on a droplet of a dipolar bose-einstein condensate stabilized by quantum fluctuations, Journal of the Physical Society of Japan **85**, 053001 (2016).

[187] F. Wächtler and L. Santos, Quantum filaments in dipolar bose-einstein condensates, Phys. Rev. A **93**, 061603 (2016).

[188] F. Cinti, A. Cappellaro, L. Salasnich, and T. Macrì, Superfluid filaments of dipolar bosons in free space, Phys. Rev. Lett. **119**, 215302 (2017).

[189] A. Macia, J. Sánchez-Baena, J. Boronat, and F. Mazzanti, Droplets of trapped quantum dipolar bosons, Phys. Rev. Lett. **117**, 205301 (2016).

[190] F. Cinti and M. Boninsegni, Classical and quantum filaments in the ground state of trapped dipolar bose gases, Phys. Rev. A **96**, 013627 (2017).

[191] M. Boninsegni, N. Prokof'ev, and B. Svistunov, Worm algorithm for continuous-space path integral monte carlo simulations, Phys. Rev. Lett. **96**, 070601 (2006).

[192] M. Boninsegni, N. V. Prokof'ev, and B. V. Svistunov, Worm algorithm and diagrammatic monte carlo: A new approach to continuous-space path integral monte carlo simulations, Phys. Rev. E **74**, 036701 (2006).

[193] Y. Tang, A. Sykes, N. Q. Burdick, J. L. Bohn, and B. L. Lev, s-wave scattering lengths of the strongly dipolar bosons ^{162}Dy and ^{164}Dy, Phys. Rev. A **92**, 022703 (2015).

[194] T. Maier, I. Ferrier-Barbut, H. Kadau, M. Schmitt, M. Wenzel, C. Wink, T. Pfau, K. Jachymski, and P. S. Julienne, Broad universal feshbach resonances in the chaotic spectrum of dysprosium atoms, Phys. Rev. A **92**, 060702 (2015).

[195] N. Burdick, A. Sykes, Y. Tang, and L. B, Anisotropic collisions of dipolar bose-einstein condensates in the universal regime, New Journal of Physics **18**, 113004 (2016).

[196] P. Chaikin and T. Lubensky, *Principles of Condensed Matter Physics* (Cambridge University Press 2000).

[197] M. Ghabour and A. Pelster, Bogoliubov theory of dipolar bose gas in a weak random potential, Phys. Rev. A **90**, 063636 (2014).

[198] D. Husmann, M. Lebrat, S. Häusler, J.-P. Brantut, L. Corman, and T. Esslinger, Breakdown of the Wiedemann-Franz law in a unitary Fermi gas, ArXiv:1803.00935 (2018).

[199] S. Krinner, T. Esslinger, and J.-P. Brantut, Two-terminal transport measurements with cold atoms, Journal of Physics: Condensed Matter **29**, 343003 (2017).

[200] D. J. Bishop and J. D. Reppy, Study of the superfluid transition in two-dimensional ^{4}He films, Phys. Rev. Lett. **40**, 1727 (1978).

[201] Z. Hadzibabic, P. Krüger, M. Cheneau, B. Battelier, and J. Dalibard, Berezinskii-Kosterlitz-Thouless crossover in a trapped atomic gas, Nature **441**, 1118 (2006).

[202] N. Defenu, A. Trombettoni, I. Nándori, and T. Enss, Nonperturbative renormalization group treatment of amplitude fluctuations for $|\varphi|^4$ topological phase transitions, Phys. Rev. B **96**, 174505 (2017).

[203] Y. V. Kartashov, B. A. Malomed, L. Tarruell, and L. Torner, Three-dimensional droplets of swirling superfluids, Phys. Rev. A **98**, 013612 (2018).

[204] A. Cidrim, F. E. A. dos Santos, E. A. L. Henn, and T. Macrì, Vortices in self-bound dipolar droplets, Phys. Rev. A **98**, 023618 (2018).

[205] D. Rakshit, T. Karpiuk, M. Brewczyk, and M. Gajda, Quantum Bose-Fermi droplets, ArXiv:1801.00346 (2018).

[206] D. Rakshit, T. Karpiuk, M. Brewczyk, M. Lewenstein, and M. Gajda, Self-bound Bose-Fermi liquids in lower dimensions, ArXiv e-prints (2018), 1808.04793.

[207] A. Boudjemâa, Quantum and thermal fluctuations in two-component bose gases, Phys. Rev. A **97**, 033627 (2018).

[208] A. Boudjemaa, Two-dimensional quantum droplets in dipolar Bose gases, ArXiv:1709.07088 (2017).

[209] L. Salasnich, A. Parola, and L. Reatto, Modulational instability and complex dynamics of confined matter-wave solitons, Phys. Rev. Lett. **91**, 080405 (2003).

[210] J. H. V. Nguyen, P. Dyke, D. Luo, B. A. Malomed, and R. G. Hulet, Collisions of matter-wave solitons, Nature Physics **10**, 918 (2014).

[211] J. H. V. Nguyen, D. Luo, and R. G. Hulet, Formation of matter-wave soliton trains by modulational instability, Science **356**, 422 (2017).

[212] A. Morales, P. Zupancic, J. Léonard, T. Esslinger, and T. Donner, Coupling two order parameters in a quantum gas, Nature Materials **17**, 686 (2018).

[213] P. D. Powell, G. Baym, and C. A. R. S. de Melo, Superfluid transition temperature of spin-orbit and Rabi coupled fermions with tunable interactions, ArXiv:1709.07042 (2017).

[214] J. Kapusta, *Finite-Temperature Field Theory*, Cambridge Monographs on Mathematical Physics (Cambridge University Press 1993).

[215] A. Schmitt, *Introduction to Superfluidity: Field-theoretical Approach and Applications*, Lecture Notes in Physics (Springer International Publishing 2014).